2018

Cell Type Specific Roles of Serotonin Receptor 4 in the Hippocampus and Neocortex in Emotion and Cognition

Remzi Karayol

CELL TYPE SPECIFIC ROLES OF SEROTONIN RECEPTOR 4

IN THE HIPPOCAMPUS AND NEOCORTEX IN EMOTION AND COGNITION

A Thesis Presented to the Faculty of

The Rockefeller University

in Partial Fulfillment of the Requirements for

the degree of Doctor of Philosophy

by

Remzi Karayol

June 2018

CELL TYPE SPECIFIC ROLES OF SEROTONIN RECEPTOR 4 IN THE HIPPOCAMPUS AND NEOCORTEX IN EMOTION AND COGNITION

Remzi Karayol, Ph.D.

The Rockefeller University 2018

Anxiety and mood disorders are the most prevalent classes of mental disorders. However, current treatments for these debilitating diseases are limited due to their delayed onset of action and numerous side effects, emphasizing the need for faster acting and more efficacious therapies. Preclinical studies indicate a critical role for Serotonin Receptor 4 (5-HT_4R, product of the *Htr4* gene) in this direction as drugs that activate this receptor show fast-acting antidepressant-like properties. Unfortunately, 5-HT_4R is widely expressed in the periphery, limiting its use as a direct therapeutic target due to various side effects. Understanding the cell type specific mechanisms of 5-HT_4R function in the brain will facilitate the development of novel therapies.

To dissect the function of 5-HT_4R in genetically defined cell types of the hippocampus and neocortex, two regions highly implicated in emotive and cognitive function, I generated a novel Cre-dependent *Htr4* knockout mouse line. Intriguingly, the loss of functional 5-HT_4R specifically in the mature excitatory neurons of the hippocampus led to robust antidepressant-like behavioral, cellular and molecular responses. These phenotypes were accompanied by elevated

innate anxiety levels and deficits in hippocampus-dependent memories. By slice electrophysiology, we showed that 5-HT_4R was necessary for the proper excitability of dentate gyrus granule cells. To identify molecular adaptations underlying the observed changes in behavior and neuronal activity, I used the translating ribosome affinity purification (TRAP) approach combined with next-generation RNA sequencing to measure hippocampal region- and cell type-specific differential gene expression in the presence and absence of 5-HT_4R. Analysis of these datasets revealed that the ventral and dorsal hippocampus underwent distinct molecular adaptations, and identified functionally relevant genes that may underlie these phenotypes and be potential therapeutic targets.

My graduate work identified unique roles for hippocampal 5-HT_4R in modulating mood, anxiety and memory. By regulating the excitability of individual neurons and relevant intracellular pathways, 5-HT_4R mediates functionally distinct hippocampal circuits. Our findings suggest divergent molecular and functional roles for 5-HT_4R along the dorsoventral axis of the hippocampus, and that specific cell type- or circuit-based strategies that target the 5-HT_4R pathway may yield more effective antidepressant therapies.

For my wife and my parents

ACKNOWLEDGEMENTS

There are a number of people without whom this journey would not be complete and as fun.

First of all, I would like to thank my thesis supervisor *Dr. Nathaniel Heintz*, for his guidance and continuous support. I am really grateful to Nat for allowing me to be a part his lab and giving me the freedom to pursue the project and experiments I wanted. He always provided me with great insights to see the bigger picture and ask the right scientific questions.

I would especially like to express my sincere gratitude to my thesis advisor *Dr. Eric Schmidt*. He truly has been a great mentor with his everyday support, guidance and discussions in my times of need. He personally guided me to develop as a scientist in the making. His door was always open for my never-ending questions, experimental and personal troubles. Without his patience and knowledge, this work would not be possible. I am especially honored to be the first PhD student to graduate under his guidance.

A special thanks to *Dr. Winrich Freiwald* who is the chair of my faculty advisory committee. From the beginning of my time at Rockefeller, he has been a genuine inspiration and motivation. His contagious passion for neuroscience and his sincere advice for my PhD work and my personal development have been truly invaluable and much appreciated. I would also like to thank *Dr. Paul Greengard*, for being a member of my committee, providing his expertise that I cherish deeply, and always challenging me with the right questions to guide me

to become a better scientist. He also provided his resources for a collaboration that filled an important gap in my research. I also thank *Dr. Scott Russo*, my external examiner, for bringing his expertise and support and helping me to understand my results further. In addition, I would like to thank *Dr. Leslie Vosshall* for her influential support when I was an undergraduate student from Turkey at the beginning of his scientific journey. I would also like to thank everyone in the *Dean's Office* for accommodating our every need, making us PhD students' lives easier, and assuring our success and comfort.

I would also like to thank my colleagues that have supported me and my research and provided constructive criticism and feedback: *Lucian Medrihan* for our collaboration and discussions, and providing his expertise in electrophysiology; *Jodi Gresack* for teaching me practically everything I know about mouse behavior; *Erika Andrade*, my bench neighbor, for her experimental help and scientific discussions; *Eva Holzner* for technical support; *Jennifer Warner-Schmidt*, for her constructive feedback; and The Rockefeller University *Transgenic Lab Services staff and Collaborative Research Center staff*, for their hard work and providing their indispensable expertise. I would also like to thank each and every one of the *Heinz Lab members*, for all their help and good company.

I would not have been able to accomplish any of these without the truly unconditional support of my mother *Zehra Karayol* and my father *Celalettin Karayol*. No matter how hard it was for them or me, they never failed to

encourage me to follow after what I wanted to do. I am very grateful to them for providing me with the best education ever since I was a kid who wanted to become a scientist and teaching me the values which I hold the dearest. I also would like to thank my brother *Emre* and my friend *Furkan*, who have been with me through every important part of my life, for their everlasting friendship and support.

Finally, I would like to thank my wife, my other half, *Nesibe*, for her boundless love and being my best friend. Her company helps me grow as a person and as a scientist every day. As a student of neuroscience herself, she also shared invaluable discussions with me for my research and this dissertation. Further, her curiosity, intelligence and passion drive me to continuously learn about life and science. I am very thankful for her irreplaceable support.

TABLE OF CONTENTS

LIST OF FIGURES

CHAPTER 1

CHAPTER 2

CHAPTER 3

CHAPTER 4

CHAPTER 5

LIST OF TABLES

CHAPTER 2

MATERIALS AND METHODS

CHAPTER 1.

INTRODUCTION

1.1. Anxiety and mood disorders

1.1.1. Burden of the disease

Mental disorders are commonly occurring and they are the leading cause of years lived with disability worldwide, presenting an enormous global burden from a societal perspective. Anxiety and mood disorders are two of the most prevalent classes of mental disorders in the general population, anxiety disorders with estimated lifetime prevalence averaging 16% and mood disorders with 11% (Kessler et al., 2009). In addition, the most recent World Health Organization (WHO) survey presents that, globally, depressive disorders are the first and anxiety disorders are the sixth largest contributor to the non-fatal health loss as of 2015. Yet, only a small minority of people with even seriously impairing mental disorders receives treatment in most countries (Wang et al., 2007). Moreover, the success in treating anxiety and mood disorders has been limited as current therapies are neither consistently ameliorating nor precise enough. Although the first-line pharmacological and psychological interventions are highly efficacious for some individuals, many experience significant residual symptoms or various side effects.

Mood disorders include major depressive disorder (MDD) and bipolar disorder (BD), while disorders that have anxiety as a central aspect of phenomenology are generalized anxiety disorder (GAD), obsessive compulsive disorder (OCD), panic disorder, posttraumatic stress disorder (PTSD), specific

phobia, and social anxiety disorder (SAD) (Ressler et al., 2015). Despite the wide range in nosology, the comorbidity in psychiatric disorders is common. For instance, the prevalence of comorbid anxiety with MDD is as frequent as % 60 in patients (Kessler et al., 2005). Notably, comorbid symptoms generally worsen or improve simultaneously with the severity of depressive symptoms. Comorbid symptoms include irritability, restlessness, fatigue, trouble sleeping and difficulty in concentrating. Depression symptoms also include anhedonia, loss of interest, change in appetite, psychomotor retardation and suicidality, while patients with anxiety also exhibit excessive worry, autonomic hyperactivity, increased startle response and muscle tension. Although the combinations of depressive and anxiety syndromes are classified as mood disorders with comorbid anxiety, functional imaging studies in patients and postmortem analyses suggest that they reflect dysfunction from a single etiology, which alters emotion regulation (Price and Drevets, 2012). Consistent with this, antidepressant drugs are the first-line treatments for both depressive and anxiety disorders (Gorman, 1996).

1.1.2. Basic neural circuitry of emotion

A variety of neuroanatomical, neurotransmitter and neuroendocrine disruptions have been linked to anxiety and mood disorders. Functional imaging studies that allow the characterization of anatomy, physiology and neurochemistry in patients, and postmortem neuropathological analyses indicate abnormalities in the brain regions that support emotive behavior (Drevets et al.,

2008). The neural network controlling emotion involves mainly the limbic system – including the hippocampus, amygdala, limbic cortices, basal ganglia, thalamus and hypothalamus, and also higher cognitive centers in the frontal lobe that extensively modulates the limbic system such as the subdivisions of prefrontal cortex (PFC). These brain regions together form an extended 'visceromotor' network, and the abnormalities in the anatomy and function in this network putatively account for the dysregulation of visceral, behavioral and cognitive responses to emotional or stressful stimuli, reward learning and certain emotional memory in anxiety and mood disorders (Price and Drevets, 2009). Notably, patients with mood disorders show various abnormalities of morphology or morphometry in the visceromotor network structures.

1.1.2.a. Hippocampus

The hippocampus is one of the most widely studied brain structure in relation to anxiety and depression, both in humans and animals (Campbell and Macqueen, 2004). First, it plays a central role in learning and memory, therefore, hippocampal dysfunction possibly leads to improper context-dependent emotional responses. Second, the hippocampus has modulatory effect on the hypothalamic stress-response system hypothalamic-pituitary-adrenal (HPA) axis (Herman et al., 2003; Rubin et al., 1966) and the amygdala (Phelps, 2004), a brain region that is central in the encoding and expression of fear. Moreover, it is one of the two brain areas where neurogenesis occurs in the adult mammalian

brain, posing high capacity for neuroplasticity (Doetsch, 2003). Notably, hippocampal volume has been observed to decrease in depressed patients (Videbech and Ravnkilde, 2004), and changes in adult hippocampal neurogenesis have been strongly implicated in anxiety and mood disorders and antidepressant treatments (Sahay and Hen, 2007).

1.1.2.b. Neocortex

The hippocampus has also direct connections to the prefrontal cortex (PFC) as wells as other limbic cortices (Ongür and Price, 2000). The PFC consists of many subcortical regions involving in its heteromodal functions. It is responsible for higher executive tasks involved in planning, decision making, impulse control, reward processing, visceral response to emotions and mood regulation (Price and Drevets, 2012). Although the frontal cortical regions, such as the medial prefrontal cortex (mPFC) and orbitofrontal cortex (OFC), mediate different aspects of emotionality and the extent of their link to anxiety and mood disorders differs, they essentially modulate limbic structures responsible for emotional processing. The limbic cortices include the cingulate and insular cortices and these regions integrate the external and internal sensory information regarding the environmental and emotional state of the organism. Abnormal activity and decreased volume in the PFC and other cortical regions have also been strongly associated with mood disorders in patients (Coryell et al., 2005; Treadway et al., 2009).

1.1.3. Neurobiology and neurochemistry of emotion

1.1.3.a. Neurotransmitters and neuropeptides

Although the precise mechanisms of how interconnected limbic regions mediate emotion, and generate various symptoms of anxiety and depression remain to be elucidated in more detail, data from human and animal studies implicate the neurotransmitters providing communication between these regions – such as glutamate (Glu) (Auer et al., 2000; Hashimoto et al., 2007), γ-amino-butyric-acid (GABA) (Sanacora et al., 2004), serotonin (5-hydroxytryptamine, 5-HT) (Mann, 1999), norepinephrine (NE) (Delgado and Moreno, 2000), and dopamine (DA) (Dunlop and Nemeroff, 2007) –; as well as the neuropeptides – such as cholecystokinin (CCK) (Bradwejn et al., 1991), oxytocin (OXT) (Neumann and Slattery, 2016), and corticotropin-releasing factor (CRF) (Laryea et al., 2012). The involvement of numerous neurotransmitter and neuromodulatory systems in emotive regulation emphasizes the complexity and diversity of the factors that may constitute the etiology of affective disorders, and strongly suggests their synergistic actions on different elements of the emotive circuitry that mediate the homeostasis of the activity. On the other hand, neurotransmitter systems provide an enormous range of targets for pharmacological agents by which discreet therapeutic manipulations have been attempted to ameliorate the pathophysiology and symptoms of affective disorders.

Anxiolytic and antidepressant drugs that act primarily on monoaminergic systems are major examples at this direction. The efficacy of these drugs has implicated serotonin (5-hydroxytryptamine, 5-HT), norepinephrine (NE), and dopamine (DA) in the pathogenesis of anxiety and mood disorders, giving rise to '*the monoamine hypothesis*' of mood disorders (Hirschfeld, 2000). These monoamines significantly modulate the limbic system via monoamine projections from the midbrain and brainstem nuclei (5-HT from the dorsal raphe nuclei (DRN), NE from the locus coeruleus (LC), and dopamine from the ventral tegmental area (VTA)), and significant evidence from human and animal studies has shown the dysregulation of these systems in anxiety and depression (Cowen, 2008; Ruhé et al., 2007).

The regulators of the monoaminergic signaling have been given more attention because they are critical for the mechanisms of action of the antidepressant drugs. For example, the most prescribed drugs for anxiety and depression, selective serotonin reuptake inhibitors (SSRI) and serotonin-norepinephrine reuptake inhibitors (SNRI), inhibit the reuptake of these monoamines by blocking the serotonin transporter (SERT) and/or the norepinephrine transporter (NET). However, the delayed onset of antidepressant effects in patients about three to four weeks strongly suggests that secondary mechanisms involving changes in gene expression and synaptic plasticity may

underlie the therapeutic mechanisms of these drugs (Krishnan and Nestler, 2008).

Neurotransmitters are usually co-released with neuropeptides, many of which are expressed in limbic regions where they can influence stress and emotion circuitry. Among many, corticotropin-releasing factor (CRF) is the primary secretagogue of the *hypothalamic-pituitary-adrenal (HPA) axis* in response to stress. Inappropriate stress responses and chronic exposure to stress have been associated with anxiety and depression; for example, the HPA axis is overactive in some patients with anxiety and depression with increased CRF and glucocorticoid levels such as cortisol being the main stress steroid in humans (Pariante and Lightman, 2008). Notably, HPA activity is under extensive control of limbic structures including the amygdala (excitatory) (Gray et al., 1989; Jankord and Herman, 2008) and the hippocampus (inhibitory) (Radley and Sawchenko, 2011).

1.1.3.b. Neurotropic factors and neurogenesis

The observations of decreased volume in the hippocampus and cortical structures in anxiety and depression patients have also led to the study of *neurotrophic factors* that regulate neurogenesis and neuroplasticity in the brain, mainly brain derived neurotrophic factor (BDNF) (Duman, 1997). Limbic regions, especially the hippocampus, is rich in BDNF, which regulates neuronal growth and survival as well as dendritic arborization and synaptic plasticity. In depressed

patients, BDNF levels were low (Karege et al., 2002; Shimizu et al., 2003) and it increased with successful treatments (Chen et al., 2001). Rodent studies recapitulate that BDNF signaling is involved in the changes in neuroplasticity in response to stress and antidepressants (Sairanen et al., 2005); however, the effects are both region and antidepressant specific (Dias et al., 2003).

A pronounced effect of several but not all antidepressant treatments is the enhanced *adult hippocampal neurogenesis* (Santarelli et al., 2003). In the hippocampus, new born cells in the subgranular zone of dentate gyrus (DG) migrate into granule cell (GC) layer to become new mature GCs through a mechanism involving proliferation, differentiation, migration and maturation. Chronic antidepressant treatments increase the rate of neurogenesis, possibly via several neurotropic factors, while several types of stress reduce it (Duman, 2004; Warner-Schmidt and Duman, 2006). Intriguingly, the ablation of hippocampal neurogenesis inhibits some therapeutic-like effects of antidepressant treatments in rodent models; however, it does not produce increased anxiety or depression-related behaviors (David et al., 2009). Comparably, while analysis of postmortem samples from depressed patients indicate a decrease in the number of DG GCs, the number of progenitor cells remains intact (Boldrini et al., 2013). Therefore, while increasing adult hippocampal neurogenesis may be necessary for the antidepressant response, it may not be sufficient to produce an antidepressant-like response (Sahay et al., 2011). Currently, the data is not sufficient to suggest that a decrease in adult

hippocampal neurogenesis may underlie the pathophysiology of depression. The exact mechanisms of antidepressant induced neurogenesis and how it may contribute to restore mood are yet to be detailed.

In summary, anxiety and mood disorders have a multifactorial etiopathogenesis, including genetic predisposition and stress, resulting in a number of pathophysiological changes. These possibly involve abnormalities in the monoaminergic transmission, the hyperactivity in HPA axis and the reduction in brain neurotropic signaling. Moreover, these pathologies are associated with functional dysregulation of the extended visceromotor network. While monoamine-based antidepressants remain the first line of therapy for anxiety and depression, their limited efficacy emphasizes the need for faster acting therapeutics with fewer side effects. Nevertheless, they have beneficial modulatory effects on limbic circuit by increasing monoaminergic neurotransmission and reversing some of the structural and physiological abnormalities in the limbic circuit, which may underlie the improvement in some of the debilitating symptoms of anxiety and depression in patients.

1.1.4. Rodent models of anxiety and mood disorders

Animal models have been crucial tools for understanding the etiology of anxiety and mood disorders as well as the progress towards the development of new therapeutic targets with improved efficacy and fewer side effects for their treatment. However, it is impossible to precisely recreate these diseases in

animal models due to the heterogeneous and unique nature of the symptoms in humans, and the weakness in our understanding of the underlying complex mechanisms. An acceptable animal model should have causative conditions, behavioral symptom profiles (face validity), neuropathological changes (construct validity) and treatment responses (predictive validity) that are similar to the human disease. Most current models do not express all the abnormalities of anxiety and depression related pathology, just as the symptoms in patients are highly heterogeneous.

Since stress is a major factor in anxiety and mood disorders, various rodent stress models have been used to induce anxiety and depression-like symptoms and to investigate the underlying neural and molecular mechanism (Krishnan and Nestler, 2011). Similar to the comorbidity of symptoms in anxiety and depression in humans, all stress models in rodents exhibit some of abnormalities related to both anxiety and depression. Thanks to these disease models and advances in transgenic strategies the effects of a genetic, pharmacological, or environmental manipulations can be studied mechanistically.

Genetically engineered mice also represent a powerful tool to study candidate genes as the manipulation of a specific gene (loss or gain of function) can result in anxiety and depression related pathology. These models have been used to study the roles of candidate proteins in the progression of these disorders and in the actions of classic and potential antidepressants as well as to understand the neural mechanisms underlying the pathophysiology. Although the

function of any gene in any part of the region or cell type in the brain can be investigated through targeted genetic approaches, most studies have focused on the models based on; 1) monoamine hypothesis, such as various monoamine transporters, receptors and their modulators; 2) neurotrophic factor-related hypothesis, such as BDNF the respective receptors, 3) HPA axis related alterations, such as CRF, glucocorticoids and respective receptors.

1.1.4.a. Assessment of anxiety and mood related behaviors in rodents

It is important to distinguish between animal models and behavioral tests. Behavioral tests are only the assays that are employed to assess the relevant phenotypes on established or candidate models as well as behavioral responses to antidepressant treatment. These tests use the animal's response to potentially threatening situations in the case of anxiety based assays, to stressful situations in the case of despair based assays and to reward in the case of anhedonia based assays.

Anxiety is normally inherent, protective and most of the time necessary for animals to survive, however, abnormal and excessive anxiety is the hallmark of the anxiety disorders and comorbid depression. Assays assessing anxiety-like phenotypes in mice are based on mice's exploratory tendencies towards novel environments versus the aversion of exposed and/or well-lit areas (Ramos, 2008). Other ethologically relevant measures such as social interaction (File and Hyde, 1979) and startle responses (Lee and Davis, 1997) have also been used.

Mice displaying excessive anxiety-like behaviors in these paradigms have often shown to successfully respond to acute or chronic administration of antidepressants (or anxiolytics with non-antidepressant properties).

It is a harder challenge to understand *mood related behaviors* in mice due to the uniqueness of the most depression phenotypes in human. However, despair based models gauge the animal's response to acute inescapable stress as the lack of active coping (despair-like) behavior. These tests still retain their popularity and utility since they are consistently responsive to acute antidepressant treatment, and can be easily used to screen potential drugs. Reward based assays assessing anhedonia like states in mice are regarded more relevant because of the lack of the desire or experience of pleasure in patients as well.

Since there is a lot of factors that may affect a rodent's behavior during testing, it is important to use multiple assays and internal controls, and to interpret the results with caution and based on their nature. These tests, in the end, are indispensable tools to understand the neurobiology of anxiety and mood disorders, and to find new antidepressant treatments with better therapeutic efficacy.

1.2. Serotonergic system in anxiety and mood regulation

Serotonin (5-HT) is a monoamine, acting as a neurotransmitter, a hormone and a mitogen, and is ubiquitous in all animals (Smythies, 2005). The study of serotonergic system has provided biological insights into virtually all brain functions, and the abnormalities in the serotonergic function have found to be a common factor in numerous psychiatric and neurological diseases (Berger et al., 2009). Serotonin modulates plethora of behaviors and neurophysiological processes, including anxiety and mood as well as aggression, sleep, appetite, memory and attention, even though less than one in a million of central nervous system (CNS) neurons are serotonergic in the human brain, and immense majority of serotonin in the body is outside the CNS. Nevertheless, brain stem serotonin neurons, mainly in the dorsal and medial raphe nuclei of midbrain, send ascending axonal projections throughout the brain. Where released, 5-HT targets 14 different serotonin receptor subtypes (5-HTRs) of 7 families (5-HT_{1-7} receptors) that are expressed in many distinct combinations in different neuronal types throughout the brain (Hannon and Hoyer, 2008).

1.2.1. Serotonin and its modulation in brain

In the CNS, upon neuronal depolarization of the 5-HT cells, serotonin is released into the synaptic cleft where it can bind to the postsynaptic 5-HT receptors or to the presynaptic 5-HT autoreceptors (somatodentridic $5HT_{1A}$ and

$5HT_{1B}$ receptors at axon terminals) (Hannon and Hoyer, 2008). As a modulatory neurotransmitter, the strength and duration of 5-HT action on the postsynaptic 5-HT receptor is crucial, and primarily dependent on the abundance of serotonin in the synaptic cleft. The amount of extracellular serotonin is determined by its binding to the autoreceptors and the activity of the selective serotonin transporter (SERT). The autoreceptors provide a negative feedback against further release of serotonin (Blier et al., 1998; Gardier et al., 2001) while SERT located on the presynaptic and soma membrane of serotonergic neurons is responsible for removing serotonin from the synaptic cleft into the presynaptic neuron (Rudnick and Clark, 1993). The activity of serotonergic neurons is also tightly controlled via glutamatergic inputs from forebrain areas (Zhou et al., 2017), inhibitory GABAergic inputs from local interneurons (Challis et al., 2013) and dopaminergic input from the midbrain dopaminergic nuclei (Ogawa et al., 2014).

One of the most clinically relevant functions of serotonin has been its role in mood and anxiety disorders. The serendipitous discovery of the antidepressant properties of tricyclics that elevate extracellular 5-HT levels, and later of selective serotonin reuptake inhibitors (SSRIs), has prompted scientists to investigate the role of the serotonergic system in anxiety and mood disorders and antidepressant medication. SSRIs are still the first line treatment for anxiety and mood disorders although they exert therapeutic effects only after chronic treatment in clinical settings along with considerable side effects (Nestler et al., 2002; Quitkin, 1984; Rush et al., 2006).

Consistent with the action of serotonergic antidepressants, numerous clinical and preclinical studies indicate that a disturbance in central serotonin activity is a key factor in the pathophysiology of anxiety and mood disorders. For example, abnormal levels of cerebrospinal fluid 5-HIAA, the main metabolite of 5-HT, has been indicated in some anxiety and mood disorders (Åsberg, 1976; Sullivan et al., 2006). Low levels of tryptophan, 5-HT precursor, have also been consistently linked to depression (Lindseth et al., 2015). Notably, a polymorphism in SERT causing low levels of the transporter in humans has been associated with the susceptibility to anxiety and depression (Katsuragi et al., 1999). Many recent studies have focused on studying the impact of SERT (mostly by blocking with SSRI's) and the serotonin receptors by using human brain imaging, pharmacological manipulations and genetic mouse models.

1.2.2. Serotonin receptors

In addition to the serotonin transporter, the majority of the serotonin receptors have been implicated in the neurobiology of anxiety, depression, and/or antidepressant treatments. Except the ionotropic 5-HT_3 receptor, all 5-HT receptors are metabotropic G-protein coupled receptors (GPCRs), and have either excitatory or inhibitory actions in distinct cell types (Bockaert et al., 2004). $5HT_3$ receptor is a ligand-gated Na+/K+ ion channel similar to GABA receptors and expressed in a subtype of interneurons. 5-HT_1 and 5-HT_5 receptors are negatively coupled to the adenylyl cyclase (G_i/o-coupled), meaning that the activation of these receptors downregulates intracellular cAMP. 5-HT_2 receptors,

G_q/11-coupled, upregulate the inositol triphosphate and diacylglycerol pathways increasing intracellular Ca^{2+} release and mediating excitatory transmission. 5-HT_4, 5-HT_6, and 5-HT_7 receptors are Gs-coupled increasing intracellular cAMP upon activation. Additional G-protein independent signal transduction pathways have also been described for some 5-HT receptors (Bockaert et al., 2010). The functions of 5-HTRs have been mostly studied using pharmacological and genetic manipulations in rodents to target each receptor subtype exclusively. This allowed to understand the specific roles of each receptor in various parts and cell types of the brain in anxiety and depression related behaviors as well as behavioral and cellular actions of antidepressants.

Widespread expression of 5-HTRs in limbic and cortical regions that mediates emotion justifies their involvement in anxiety and mood related behaviors. Indeed, analyses of 5-HT receptor binding and expression in patients and suicide victims from imaging and post mortem studies have revealed altered levels of 5-HTRs indicating their possible involvement in the etiology of anxiety and depression (Yohn et al., 2017). Pharmacological agents used in patients also showed the link between these receptors and mood; for example, a partial 5-HT_{1A}R agonist has been used for generalized anxiety disorder (Huang et al., 2017), and multimodal drugs targeting several 5-HTRs are used for major depression (Sanchez et al., 2015). However, several factors including the wide expression of serotonin receptors in CNS and periphery, and the presence of 5-HT_{1A}R and 5-HT_{1B}R receptors as both autoreceptors and heteroreceptors

complicates the use of these drugs. Hence, the discovery of new drugs that could target subpopulations of these receptors may be necessary.

More evidence for 5-HTRs role in mood disorders comes from preclinical studies. Pharmacological manipulation of most of the 5-HTRs via agonists or antagonists leads to changes in anxiety and depression related behaviors in mice, while these effects may not always be ideal. In this context, one of the most recent promising findings is that a 5-HT_4R partial agonist (RS67333) produces rapid anxiolytic and antidepressant effects in rodents (Lucas et al., 2007). Considering that the enhanced serotonergic tone after SSRI treatment acts practically on 5-HTRs, recent studies have aimed to decipher the role of these receptors in antidepressant responses to identify specific mechanisms that may harness better antidepressant targets (Medrihan et al., 2017; Samuels et al., 2015).

1.2.2.a. Serotonin receptors in selective serotonin reuptake inhibitor action

Our current understanding of SSRI action is limited; however, one of the main goals of the field is to understand, and ultimately, bypass the delayed onset of actions of SSRIs by three to four weeks. This delay may stem from the limiting actions of 5-HT_{1A} and 5-HT_{1B} autoreceptors on the serotonin release from the serotonergic cells in the raphe nuclei; among other possibilities such as establishment of gene expression changes and synaptic plasticity (Krishnan and Nestler, 2008). After chronic treatment, the negative feedback mechanism

ultimately inactivates, at least in part, due to the desensitization of the 5-HT_{1A} autoreceptors in the raphe nuclei, consequently, resulting in a greater 5-HT availability in the synapses (Artigas et al., 1996). Therefore, the identification of serotonin receptors and cell types that drive the actions of elevated 5-HT levels may present new targets that can be directly manipulated to mimic this process and provide more efficacy.

1.3. Serotonin receptor 4 (5-HT_4 receptor, 5-HT_4R)

1.3.1. Molecular biology, signal transduction and central expression

5-HT_4 receptor is an excitatory 5-HT receptor type that is coupled to Gs proteins. In humans, the *Htr4* gene is around 700kb with 38 exons in chromosome 5; in mice, it is in chromosome 18 with 7 exons. The receptor has several different isoforms, generated through alternative splicing of the gene, with distinct C-terminus sequences and functional properties. The longest isoform in mouse is 388 amino acids long and around 42 kD. In brain and peripheral tissues, humans have nine distinct variants of 5-HT_4R (a-i, n), whereas mice are currently thought to have only four (a, b, e, and f) (Bockaert et al., 2004). The exact functional roles of these distinct isoforms remain unresolved; however, numerous studies suggest that isoform-specific differences in 5-HT_4Rs and their distribution impact the overall coupling and regulation of the receptor (Claeysen et al., 1999; Mnie-Filali et al., 2010). 5-HT_4R is expressed in the heart, gastrointestinal tract, adrenal gland, urinary bladder and lung as well as in the CNS (Hegde and Eglen, 1996).

In situ hybridization, radioligand binding assays and transgenic *Htr4* reporter mice revealed that, in the CNS, 5-HT_4R is expressed in many limbic structures and more: the hippocampus, neocortex, amygdala, hypothalamus and many regions of the basal ganglia, although poorly expressed in the raphe nuclei (**Figure 1.1**).

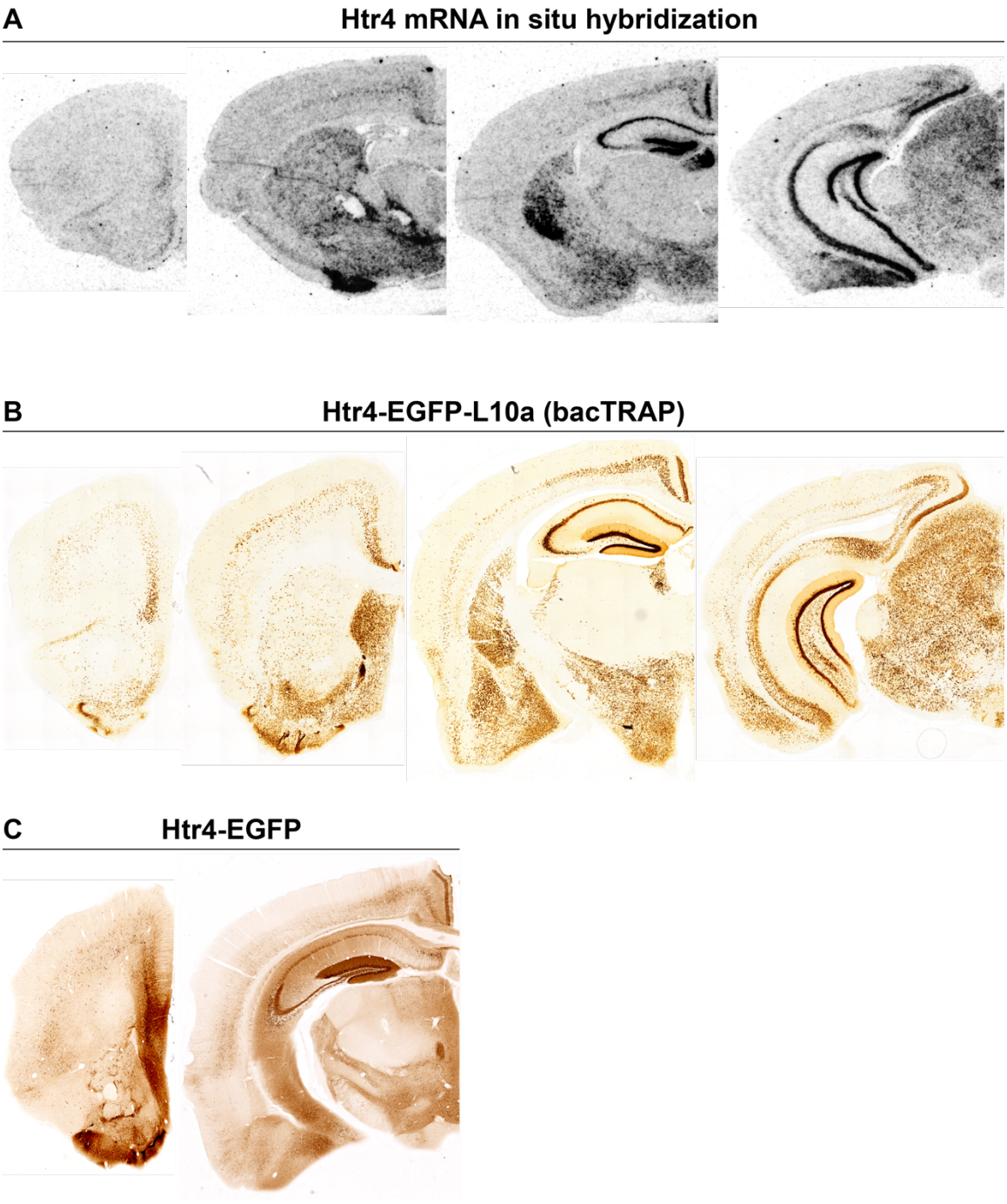

Figure 1.1. *Htr4* expression in the mouse brain
A. In situ hybridization (ISH) images showing *Htr4* mRNA expression in the mouse brain. Modified from BGEM ISH database (Magdaleno et al., 2006)
B. Anti-EGFP immunolabeling in *Htr4*-EGFP-L10a (bacTRAP) reporter mouse brain showing EGFP-L10a expression under *Htr4* regulatory elements.
C. Anti-EGFP immunolabeling in *Htr4*-EGFP reporter mouse brain showing EGFP expression under *Htr4* regulatory elements.
Images produced under GENSAT project (gensat.org).

In the hippocampus, it is expressed in the pyramidal cells of CA fields and the granule cells of dentate gyrus. In the neocortex, it is expressed in glutamatergic pyramidal neurons, mostly in deeper layers in a relatively laminar pattern.

1.3.2. 5-HT_4 receptor in anxiety and mood regulation

Postmortem analyses of the brains from depressed subjects and suicide victims showed changes in 5-HT_4R binding in several brain regions (Rosel et al., 2004). Moreover, imaging studies in humans demonstrated that an alteration in 5-HT_4R binding in the striatum is associated with major depression. (Marner et al., 2010). Moreover, some polymorphisms in *Htr4* were associated with the susceptibility to unipolar depression (Ohtsuki et al., 2002). Together these results indicate a role for 5-HT_4R in mood disorders in humans.

More understanding of the roles that 5-HT_4R plays in anxiety and mood disorders comes from the animal models of anxiety and depression. For example, the Flinders sensitive line of rats, olfactory bulbectomy model, glucocorticoid receptor heterozygous mice (GR+/–), and maternal prenatal stress model in mice, showed changes in 5-HT_4R receptor density in the limbic areas such as the hippocampus (Chen et al., 2012; Licht et al., 2010; 2009).

1.3.2.a. Evidence from pharmacological studies

Further studies investigated whether 5-HT_4R ligands can directly exert anxiolytic and antidepressant-like effects or modify the effects of monoaminergic

antidepressants. The most promising results have been achieved by an agonist of this receptor. In rats, continuous systemic administration of a 5-HT_4R agonist (RS67333) rapidly increased the firing of 5-HT neurons, reaching a maximum only after 3 days compared to similar effects of SSRIs that take up to several weeks (Lucas et al., 2005). Intriguingly, subchronic administration of 5-HT_4R agonists (3-7 days) has consistently shown fast acting anxiolytic and antidepressant-like properties, both in rats and mice (Lucas et al., 2007; Warner-Schmidt et al., 2009). In chronic mild stress (CMS) models, the 5-HT_4R agonist also reversed prolonged anxiety and depression-like behaviors in three days, much faster than SSRIs (two weeks) (Lucas et al., 2007). Intriguingly, subchronic 5-HT_4R activation also recapitulated the molecular and cellular effects of chronic SSRI treatment in the hippocampus, including desensitization of 5-HT_{1A} autoreceptors, enhanced hippocampal neurogenesis and neurotrophic factor expression. These evidences suggested that 5-HT_4R agonists represent the first putative fast-acting serotonergic antidepressants.

To study the loss of function of 5-HT_4R, an *Htr4* germline knockout mouse line was generated (Compan, 2004). Although these mice did not display a depressed-like phenotype, they showed an anxiety-like response to stress and novelty. Similarly, chronic inhibition of 5-HT_4R with an antagonist (GR125487) does not affect the anxiety- and depression-like phenotypes induced by chronic corticosterone treatment in mice (Mendez-David et al., 2014). However, inhibition

of 5-HT_4R attenuated the effects of an SSRI in this model, although there is conflicting evidence by other groups (Cryan and Lucki, 2000).

1.3.2.b. 5-HT_4 receptor and p11 in antidepressant response

Our lab also previously reported some evidence to support 5-HT_4R involvement in SSRI responses in the neocortex. In this study, p11-expressing cortical neurons that projects to striatum were identified as the cortical neurons that mediate the response to chronic SSRI treatment (Schmidt et al., 2012). This population was targeted because p11 was shown to be increased in the neocortex following chronic antidepressant treatment, and decreased in the neocortex of depressed patients, suicide victims, and a mouse model of depression. Moreover, p11 acts as an anchoring protein that binds to 5-HT_{1D}R and 5-HT_4R and stabilizes their localization at the cell surface. Notably, the fast acting anxiolytic and antidepressant-like effects of the 5-HT_4R agonist were dependent on p11 expression (Warner-Schmidt et al., 2009).

After chronic SSRI treatment, corticostriatal (CStr) p11 neurons showed a robust molecular response, compared to neighboring corticopontene (CPn) layer 5 population, including a striking 16-fold upregulation of *Htr4* expression in p11 neurons. Furthermore, the deletion of p11 specifically from the cortex resulted in abolished behavioral response to chronic SSRI treatment, while the upregulation of *Htr4* was significantly blunted. Whether 5-HT_4R in p11 cells is mediating the effects of SSRIs remains to be an intriguing question.

Accumulating evidence strongly suggests a role for 5-HT_4R in the modulation of anxiety and mood disorders both in the hippocampus and neocortex. However, the expression of 5-HT_4R in periphery and especially in the gastrointestinal track and heart complicates the use of 5-HT_4R agonists as an antidepressant in humans due to the possibility of major side effects. In fact, 5-HT_4R ligands are clinically used in the treatment of irritable bowel syndrome although there are some concerns over cardiovascular side effects as well (Tonini and Pace, 2006). Therefore, specific approaches targeting 5-HT_4R pathway in specific cell populations or circuits that are mediating its fast acting antidepressant properties will facilitate our understanding of its mechanism of action and may lead to more efficacious therapies.

1.4. Cell type specific experimental approaches in mouse

In order to investigate the mechanisms regulating 5-HT_4R function and for the discovery of new paths toward treatment of anxiety and mood disorders, it is essential to target experimental manipulations to specific CNS cell types of functional relevance. The Cre-recombinase approach and the intersectional strategy using Cre-dependent mutant mice or viral vectors allow for the investigation of the distinct contribution of each cell type and gene to anxiety and depression-related phenotypes and responses to antidepressant drugs.

1.4.1. Cre/loxP system

The development of the Cre/loxP system for mouse genetics expanded the possibilities for cell type specific manipulation of gene expression and function. Cre recombinase is a DNA recombinase enzyme that carries out 'Cre-dependent' site specific recombination between specific DNA target sequences, loxP sites (Kühn and Torres, 2002). In the presence of Cre recombinase, this recombination approach allows either for excision or reversal of the genomic sequence in between loxP sites depending on the orientation and the number of the loxP sequences. The Cre gene and loxP sites are typically integrated into the genome via genome targeting techniques during embryonic stage to generate transgenic lines. Cre and loxP transgenic mouse lines are generated separately and crossed to produce a specific Cre-loxP line. Alternatively, the Cre

recombinase coding sequence or the transgenes carrying loxP sites can be delivered via carrier viruses into the brain region of interest of the reciprocal transgenic line.

1.4.2. BAC Recombineering and transgenic targeting

The ability to genetically target specific cell types to understand their properties in the context of an intact organism is essential to biological research. The most efficient methodology devised for this purpose is the generation of BAC transgenic mice, which was invented in our lab (Schmidt et al., 2013). The use of modified BAC (bacterial artificial chromosome) vectors containing a specific reporter (Cre, GFP, etc.) under a cell type specific promoter has been systematically developed in our lab under GENSAT Project (gensat.org), which generated an extensive library of transgenic reporter mouse lines expressing the specific reporter (bacTRAP, Cre or EGFP) in distinct cell types in the CNS.

1.4.3. TRAP-Seq: genome-wide cell-type specific transcriptomics

The TRAP-Seq (Translating Ribosome Affinity Purification followed by next-gen RNA sequencing) strategy allows the identification of all proteins being translated in any genetically targeted cell population, and the alterations of this translational profile in response to pharmacological or genetic perturbations (Heiman et al., 2014). The basis of this technique is expressing EGFP-tagged ribosomal protein L10a (EGFP-RPL10a) in the cell type of interest by employing

abovementioned cell-type specific transgenic lines; followed by pulling down the polysomes with the mRNAs being translated and sequencing these mRNA to analyze changes in the gene expression upon genetic or pharmacological perturbations. TRAP combines coincident detection of all translated mRNAs with cell-type specificity and can be repeated easily for any experimental condition. The use of bacTRAP transgenic lines or Cre-mediated EGFP-RPL10a expression in Cre transgenic mice ensures that mRNA translational profiles can be reproducibly obtained and directly compared from the same cell population across experimental conditions. The extreme sensitivity of the technique is demonstrated by its ability to distinguish very subtle gene expression changes in response to drug administration between highly similar cell types, such as two populations of layer 5 projection neurons in the cortex (Schmidt et al., 2012).

1.5. Rationale

In the introduction, current understanding towards the etiology and the extensive involvement of the serotonergic system in anxiety and mood disorders is discussed. Strong evidence suggests that 5-HT_4 receptors in the hippocampus and neocortex are involved in the pathophysiology of these diseases, and may provide faster and more effective routes towards the enhancement of their symptoms. In this thesis, I investigate the role of 5-HT_4R in genetically defined cell populations in the hippocampus and neocortex to decipher its role in anxiety and mood related behaviors and antidepressant responses. Later, I use molecular, cellular and physiological approaches to discover underlying mechanisms through which 5-HT_4R mediates emotive behaviors. The identification of novel targets by studying cell type and circuit specific mechanisms of 5-HT_4R function will facilitate the development of efficacious therapies for affective disorders with fewer side effects.

CHAPTER 2.

THE ROLE OF 5-HT_4 RECEPTOR IN EXCITATORY NEURONS OF PALLIAL ORIGIN IN ANXIETY AND DEPRESSION

2.1. Introduction

The identification and targeting of the specific cell types and proteins underlying the pathophysiology of disease present a powerful approach for developing novel, more efficacious therapies with fewer side effects. There is a body of work suggesting that 5-HT_4 receptor (5-HT_4R) may be involved in the modulation of anxiety and mood, and the activation of this receptor may be a faster route to an antidepressant response. Recently, data from our lab suggested that 5-HT_4R in the cerebral cortex may be involved in the mechanism of chronic SSRI action (Schmidt et al., 2012). Therefore, we sought to investigate the role of 5-HT_4R in more defined brain regions and cell types. Teasing apart the function of 5-HT_4R in distinct elements of the anxiety and mood circuitry in the brain is essential to have a better understanding of its function and the disease due to the complexity of the emotion circuitry. Finding relevant cell types and molecular mechanisms may yield novel therapeutic candidates.

We sought to study the role of 5-HT_4R in the hippocampus and neocortex because of a variety of strong reasons. First, the hippocampus is one of the most implicated brain region in the modulation of anxiety, mood and antidepressant responses. Most of the pathophysiology in the disease and the plasticity upon treatment occur in the hippocampus. Second, our lab's finding has led to the hypothesis that an enhanced serotonergic tone acts on an upregulated pool of 5-HT_4R in p11 expressing cortical layer 5 neurons, thereby increasing the outflow

from the neocortex to the striatum and contributing to the efficacy of antidepressants. Third, the expression of *Htr4* in hippocampal neurons is high and almost ubiquitous especially in the dentate gyrus; and in the neocortex, it is relatively laminar and mostly in layer 5 neurons similar to p11. Finally, the partial 5-HT_4R agonist, RS67333, increases the DRN neuronal firing possibly via feedback from 5-HT_4R expressing neurons in the mPFC (Lucas et al., 2005), and it has antidepressant-like effects in the hippocampus either due to a direct activation or via indirect mechanisms (Lucas et al., 2007).

In Chapter 2, we achieved a conditional knockout strategy using our newly generated transgenic *Htr4* conditional knockout mice. We functionally ablated 5-HT_4R receptor from the excitatory neurons of the hippocampus and neocortex, including p11 neurons. This approach allowed us to investigate the role of 5-HT_4R in these neurons in mediating emotional behaviors and antidepressant efficacy.

2.2. Genetic targeting of *Htr4* gene

2.2.1. Conditional knockout strategy: generation of Htr4-floxed mouse line

To study cell type specific functions of 5-HT_4R, we targeted the *Htr4* gene to generate *Htr4* conditional KO (cKO) mouse line to drive deletion in genetically defined cell populations using the Cre/loxP system. **Figure 2.1** shows the gene targeting strategy. The exon 5 of *Htr4* wildtype (WT) allele in the mouse *chr18qE1* locus was targeted (**Figure 2.1A**). Targeting vector design is shown in **Figure 2.1B**, which includes: *Htr4* exon 5 (black bar); middle arm (MA, black), the intronic sequence surrounding exon 5; a 5' long arm (LA, green) and a 3' short arm (SA, blue), intronic sequences for homologous recombination; a Neomycin resistance cassette (Neo, yellow rectangle), between MA and SA; FRT (flippase recognition target) sites (grey half circle) flanking the Neo cassette, an analogous system to Cre/loxP; and loxP sites (red triangle), flanking exon 5 and Neo cassette.

After the introduction of the targeting vector into mouse embryonic stem (ES) cells, the homologous arms drove the homologous recombination inserting the targeting construct into the genome. Neo cassette was used to select for the ES cells with the recombination via the antibiotic neomycin. FRT sites were designed to excise the Neo cassette when the Htr4-floxed mice were generated and crossed with flippase (FLP, the recombinase for FRT site) expressing mouse line Rosa26::FLPe (R26FLP).

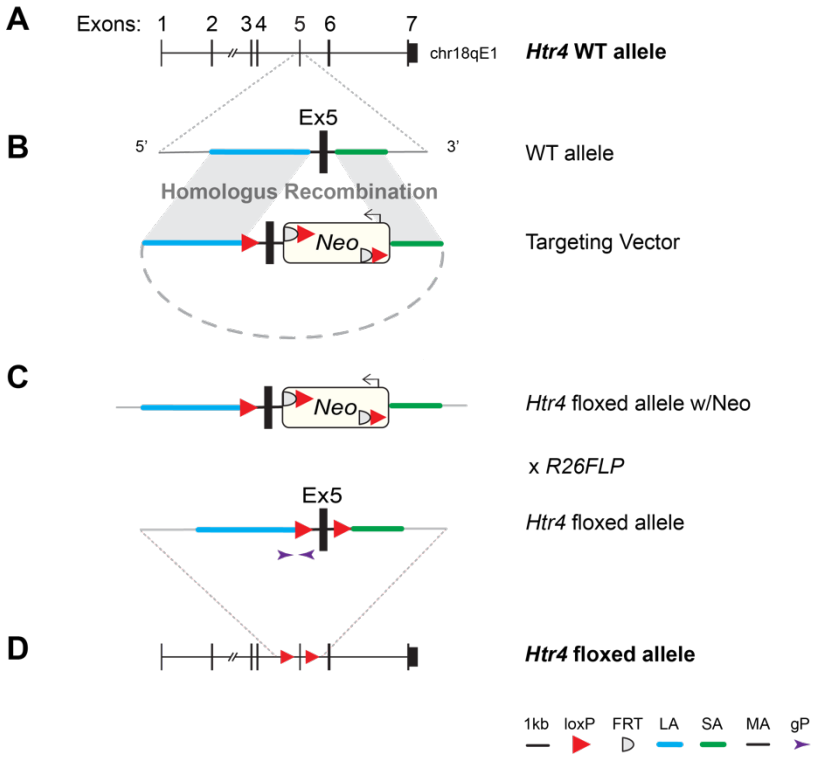

Figure 2.1. Gene targeting strategy of Htr4-floxed mouse line.
(A) Schematic of *Htr4* gene in mouse chr18qE1 locus.
(B) Gene targeting vector designed to drive the homologous recombination via LA and SA to insert the loxP-flanked exon 5 and Neo cassette. Targeting vector includes: *Htr4* exon 5 (black bar); middle arm (MA, black); 5' long arm (LA, green) and short arm (SA, blue); Neomycin resistance cassette (Neo, yellow rectangle); FRT (flippase recognition target) sites (grey half circle); loxP sites (red triangle).
(C) Neo cassette and FRT sites were designed to be excised by crossing the Htr4-floxed mice with Rosa26::FLP (R26FLP) mice. FLP-mediated recombination would lead to Htr4-floxed allele.
(D) Schematic of *Htr4* gene with exon 5 flanked with loxP sites (Htr4-floxed).
gP, genotyping primers (purple arrows). Scale bar for magnified schematics, 1kb.

In Htr4-floxed line, loxP sites were inserted to flank exon 5 of the mouse *Htr4* gene, which encodes for the fourth transmembrane domain. In silico translation analysis (via MacVector) predicted that deletion of exon 5 would result in a frame shift mutation and the introduction of potential stop codons downstream, including one right after the deletion site, six others before the endogenous stop codon site, and more in the 3'UTR region **(Figure 2.2A).**

Once the frame shift is created by Cre mediated excision, the resulting mRNA (*Htr4* mRNA exon 5 deleted) should be subject to nonsense-mediated decay or the translated protein would be truncated (green amino acid sequence), non-functional, and tagged for degradation. This would effectively result in animals null for this allele. Similar targeting of other seven transmembrane proteins has worked efficiently in the past (personal communication, inGenious Targeting Laboratory).

Three lines of chimeric mice were generated at the Janelia Research Campus Gene Targeting and Transgenic Facility; and one of these lines, ROXY Htr4 1G12, showed germline transmission of the mutation. We have established a colony of the mice from the 1G12 line in our laboratory. In **Figure 2.2B**, genotyping results show examples of PCR products in agarose gel electrophoresis, using genomic DNA samples from mice that are WT (+/+), heterozygous (loxP/+) and homozygous for the floxed *Htr4* allele (loxP/loxP).

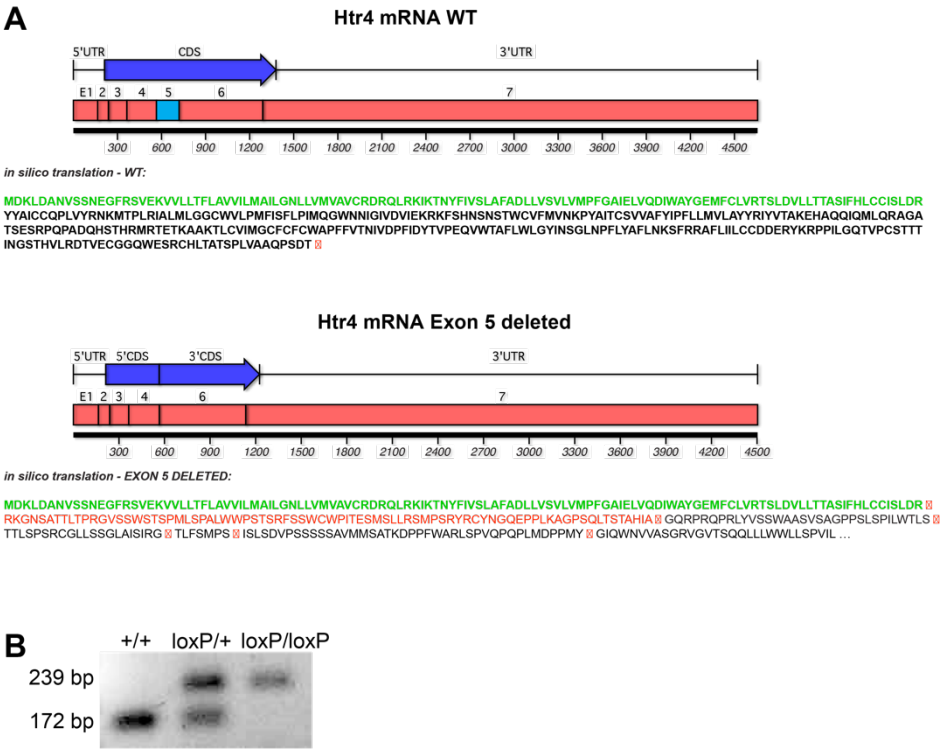

Figure 2.2. Analysis of the generation of Htr4-floxed line.
(A) In silico translation analysis predicting the loss of exon 5 from *Htr4* mRNA would lead to immediate early stop codons. Green amino acid sequence represents the translation up to exon 5. Red squared X represents the translation of the stop codons.
(B) Example genotyping results for mice that are WT (+/+), heterozygous (loxP/+) and homozygous for the floxed *Htr4* allele (loxP/loxP).

PCR primers were designed to amplify 172 basepair (bp) region in WT allele where 5' loxP was inserted in the floxed *Htr4* allele. Hence, genotyping from mice containing floxed *Htr4* allele results in longer, 239 bp, amplicons.

We crossed these mice to several Cre-driver lines to delete *Htr4* from specific cell populations in the mouse brain. Htr4-floxed mouse line is a novel tool that will enable us to better understand the contribution of 5-HT_4R signaling in many neurological processes, from mood regulation and antidepressant responses to cognition and memory, as well as any other biological processes in other systems, such as gastrointestinal system.

2.2.2. RNAi knockdown strategy: screening for shRNA's against *Htr4*.

Cre dependent knockout is a powerful approach to study cell specific functions of a gene. However, in the unlikely event that the protein function remains following the deletion of exon 5 in the *Htr4* conditional KO mice, we have generated small hairpin RNA (shRNA) expressing vectors to knock-down *Htr4* expression in spatially isolated brain regions by combining with AAV-mediated gene delivery.

RNA interference (RNAi) is an RNA-dependent gene silencing process controlled by the RNA-induced silencing complex (RISC) which uses the endogenous microRNAs in the cytoplasm to regulate mRNA translation (Sharp, 2001). miRNA's are processed from double-stranded RNAs (dsRNA) by Dicer, an endogenous cytoplasmic ribonuclease protein. By utilizing the RISC,

exogenous expression of small short hairpin RNAs (shRNA), can also be used to regulate transcription. shRNAs designed for a specific gene are cleaved and processed by Dicer into 20-25 bp double-stranded small interfering RNAs (siRNA). siRNAs are further processed into single stranded antisense RNAs, and RISC-mediated binding to the mRNA product of a gene of interest downregulates its translation.

RNAi has been used as a powerful tool to generate region-specific knockdowns in the brain (Raoul et al., 2005). AVV-mediated delivery of plasmid vectors capable of expressing a shRNA was one of the major advances in this field. These vectors use a PolIII promoter (e.g U6) to permit high level of expression of shRNA molecules with very specific start and stop sites, which is ultimately trimmed and resolved into siRNA. This can act to efficiently decrease the mRNA levels of targeted genes very efficiently in animal brains in vivo (Hommel et al., 2003).

To find a potent shRNA, we screened five shRNA constructs against mouse *Htr4* gene (designed by The RNAi Consortium, Broad Institute) in human embryonic kidney (HEK) cells. shRNA sequences were cloned into an AAV-expression vector pGFP-shRNA (Hommel et al., 2003) (**Figure 2.3A**). To determine the knockdown efficiencies of five shRNAs (sh249, sh261, sh270, sh284 and sh308), we cotransfected pGFP-shRNA vectors with a mouse *Htr4* overexpression vector into HEK cells; and performed quantitative RT-PCR (qRT-PCR) using a TaqMan assay for mouse *Htr4* gene. A scrambled shRNA

sequence, similar in length and base-pair constitute to other shRNAs, was used as a control shRNA (shControl).

Compared to shControl, three constructs significantly reduced the overexpression of mouse *Htr4* mRNA by at least 50%, and one of them, sh308, being the most potent and reducing to ~30% (31.01± 6.63%, p=0.009) (**Figure 2.3.B**). pGFP-sh308 construct showed a significant knockdown efficiency and can be packed into suitable AAV viral vectors to be delivered in vivo as a powerful alternative to the transgenic conditional KO approach.

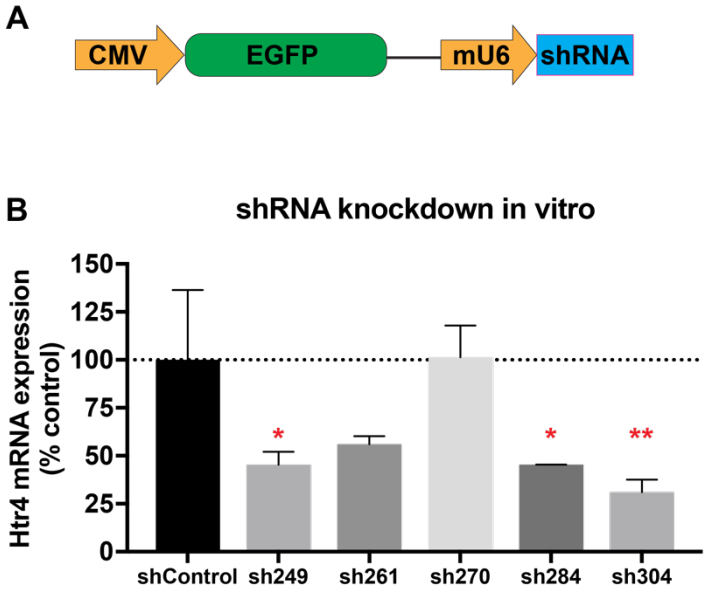

Figure 2.3. Screening for shRNAs against *Htr4*.
(A) Schematic of AAV-expression vector pGFP-shRNA. EGFP is expressed under CMV promoter and shRNA is under mU6 promoter.
(B) qPCR quantification of the *Htr4* mRNA expression in HEK cells transfected with different pGFP-shRNA constructs. Data are shown as percent (%) of control (black bar). Data are represented as mean ± SEM. Ordinary one-way ANOVA followed by post hoc Fisher's LSD test, n=4 per group, *p<0.05, **p<0.01.

2.3. Conditional loss of 5-HT_4R from excitatory neurons of pallial origin

Given the prominent expression of 5-HT_4R in the hippocampus and the neocortex, and the extensive literature documenting a role for the hippocampus and cortex in anxiety and mood regulation, we were particularly interested in the role of 5-HT_4R in these regions. In addition, our lab's previous work showing that the conditional deletion of p11 from the hippocampus and neocortex using Emx1-Cre driver line suggested that 5-HT_4R in these regions may be involved in behavioral antidepressant responses. Accordingly, we deleted *Htr4* specifically in hippocampal and neocortical excitatory neurons by crossing our newly generated Htr4-floxed line with Emx1-IRES-Cre (Emx1-Cre) driver line to investigate whether 5-HT_4R mediated behaviors related to anxiety, mood and antidepressant responses in the hippocampus and neocortex.

Heterozygous Emx1-Cre animals were crossed with Htr4-floxed animals homozygous for the floxed allele (*Htr4*$^{loxP/loxP}$) for two generations to obtain Emx1/Htr4 cKO mice (Emx1-Cre::*Htr4*$^{loxP/loxP}$). To maintain the colony, Emx1/Htr4 cKO animals were bred with homozygous Htr4-floxed animals. The litters from this breeding should be Emx1/Htr4 cKO in 1:2 ratio and Htr4-floxed in 1:2, referred as control or wildtype (WT) littermates.

2.3.1. Emx1-Cre driver line

The Emx1-Cre line expresses Cre recombinase specifically in the excitatory neurons of most brain structures of pallial origin, including the entire hippocampus and neocortex in the adult mouse brain (Gorski et al., 2002). This line was generated by homologous recombination of an internal ribosome entry site (IRES) and Cre recombinase coding region into the 3' untranslated region of the mouse *Emx1* gene. Due to the use of IRES for the translation of Cre, this strategy prevents reduction in *Emx1* expression in Emx1-Cre transgenic mice. *Emx1* encodes a homeodomain protein that is expressed primarily in the pallium, the cortical subdivisions of the telencephalon. The expression data is available as early as embryonic day 10.5 showing Cre expression dependent recombination of a reporter in the pallium. In adult mice, Cre expression was observed in ~88% of the neurons in the hippocampus and cortex while over 98% of the GABAergic interneurons did not express Cre. Overall, most pallial excitatory neurons, astrocytes and oligodendrocytes but not GABAergic neurons expressed the Cre reporter in the Emx1-Cre line.

To have our own reference and confirm that Emx1-Cre line in our lab did not go through under any other recombination events altering the expected expression pattern, we also crossed Emx1-Cre with Cre dependent EGFP-RPL10a (EGFP-L10a) expressing reporter mouse line, and Emx1-Cre expressing cells and brain regions were revealed using anti-EGFP DAB immunohistochemistry (**Figure 2.4**)

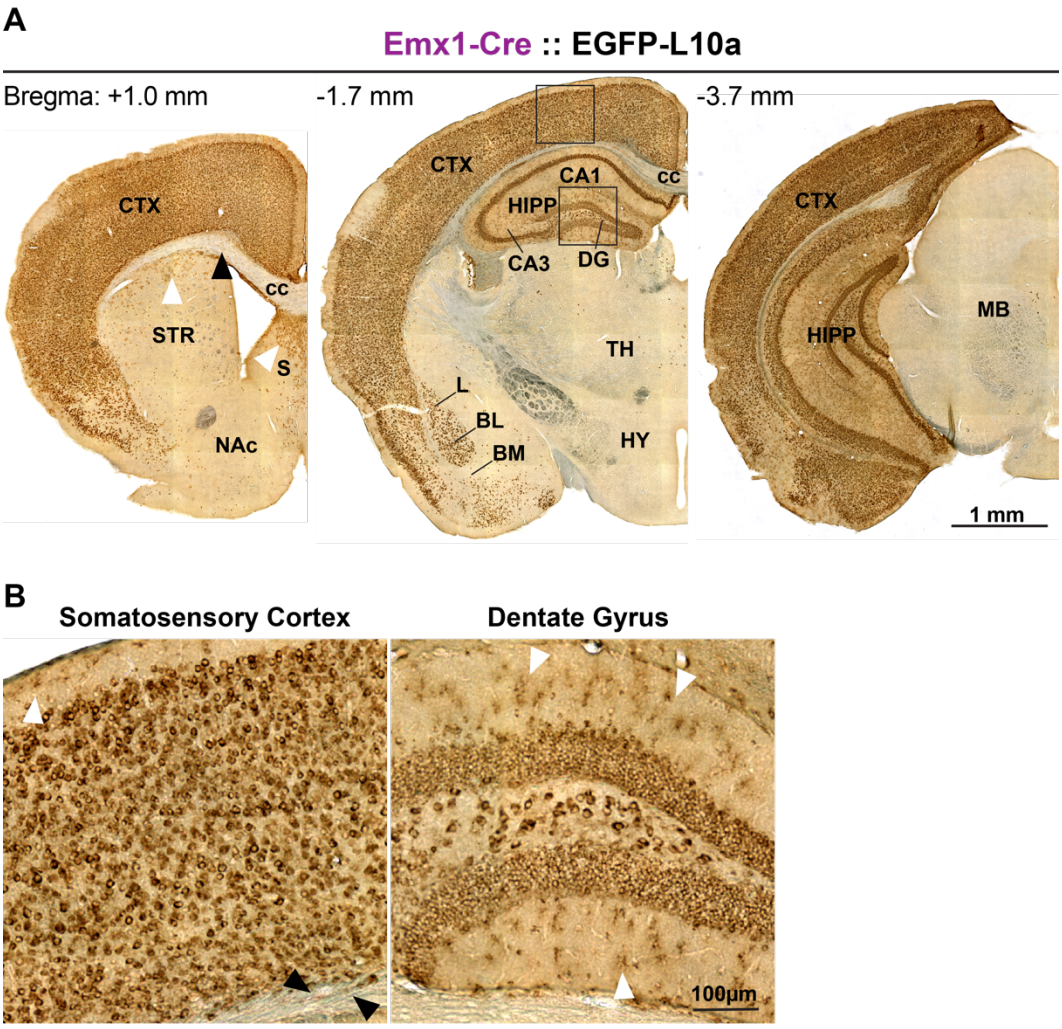

Figure 2.4. Emx1-Cre expression is restricted to pallial structures.
(A) Anti-EGFP immunohistochemistry images of the coronal sections of a Emx1-Cre::EGFP-L10a mouse brain exhibiting the expression pattern of Emx1-Cre driver line. (B) Higher magnification images of somatosensory cortex and dentate gyrus corresponding to the squares in Figure 2.4.A.
White arrowheads show labeled astrocytes and black arrowheads show labeled oligodendrocytes in cc. CTX: neocortex, STR: striatum, S: septum, NAc: nucleus accumbens, HIPP: hippocampus, DG: dentate gyrus, TH: thalamus, HY: hypothalamus, L: lateral amygdala, BL: basolateral amygdala, BM: basomedial amygdala, MB: midbrain, cc: corpus callosum. Section coordinates are displayed as from bregma.

Consistent with the literature, we saw the recombination of EGFP-L10a in virtually all projection neurons (e.g. pyramidal neurons), astrocytes (with spiny and cloudy morphology, white arrowheads) and oligodendrocytes (positively labeled cells in the corpus collosum, black arrowheads) in pallial structures such as the hippocampus and neocortex. These interpretations were made by the morphology of immunolabeled cells. Note that basomedial, basolateral and lateral amygdala cells also express, consistent with the literature documenting that excitatory neurons of most pallial regions showed Emx1-Cre recombination. Some small scattered populations of cells are also labeled especially in the striatum and septum. Although the astrocytes and oligodendrocytes of pallial structures expressed Emx1-Cre::EGFP-L10a, 5-HT_4R is expected not to be expressed in glia based on the expression profiles observed in the transgenic *Htr4* reporter mice.

2.3.2. qRT-PCR confirmation of the deletion of *Htr4* exon 5

The expected deletion of the exon 5 of *Htr4* from the hippocampus and neocortex in Emx1/Htr4 cKO mice was confirmed using qRT-PCR (qPCR). We selected TaqMan qPCR assays that uses probes amplifying on *Htr4* mRNA exons 3 and 4 (Probe 3-4) and exons 4 and 5 (Probe 4-5) (**Figure 2.5A**). Probe 4-5 failed to amplify the cDNA produced from the total RNA samples from the hippocampus (HIPP) and neocortex (CTX) of Emx1/Htr4 cKO mice (**Figure 2.5B**).

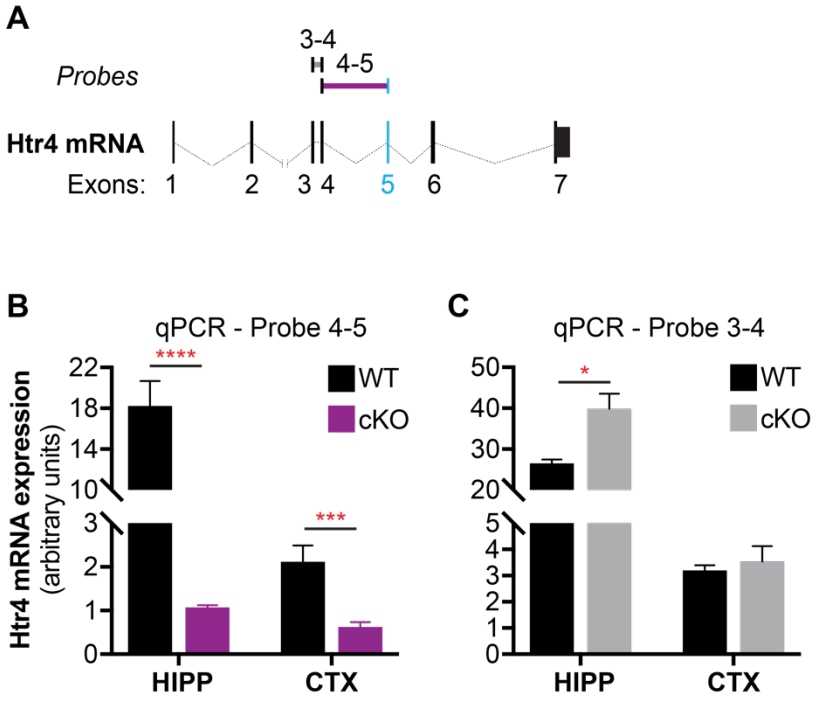

Figure 2.5. Exon 5 was deleted from *Htr4* mRNA in the hippocampus and neocortex in Emx1/Htr4 cKO mice.
(A) Schematic showing the TaqMan probes used to amplify on *Htr4* mRNA.
(B) qPCR quantification of the expression of *Htr4* in the hippocampus (HIPP) and neocortex (CTX) in Emx1/Htr4 cKO (purple bars) and WT (black bars) using Probe 4-5.
(C) qPCR quantification of the expression of *Htr4* in the hippocampus (HIPP) and cortex (CTX) in Emx1/Htr4 cKO (grey bars) and WT (black bars) by Probe 3-4.
Data are represented as mean ± SEM. n=4 per group. Two-tailed unpaired t-test.
*p<0.05, ***p<0.001, ****p<0.0001.

In contrast, this assay did amplify in the cDNA samples from their Cre-negative control littermates (WT). Moreover, Probe 3-4 amplified in samples from the hippocampus of cKO significantly higher compared to WT (**Figure 2.5C**). It also amplified cortex samples equally well both in cKO and WT. These data suggested that exon 5 was deleted from the *Htr4* mRNA transcripts in the hippocampus and neocortex of Emx1/Htr4 cKO mice while the exon 5 deleted mRNA was being made at higher (in the hippocampus) or similar (in the neocortex) levels.

2.3.3. Confirmation of the loss of function of 5-HT_4R

To confirm the loss of function of the mutant 5-HT_4R, we used a cell culture based cyclic AMP (cAMP) induction assay. 5-HT_4R is a Gs-coupled receptor and therefore induces cAMP signaling in cells upon activation. We cloned the exon 5 deleted mutant *Htr4* cDNA (cKO) and the intact floxed *Htr4* cDNA (control) from the total RNA samples obtained from the hippocampus of Emx1/Htr4 cKO and their control littermates, respectively. The cDNA constructs were then inserted into a mammalian expression vector (pCMV6-Entry) under the CMV promoter and to be tagged with MYC and DDK epitope sequences for further immmunodetection.

We expressed both cKO and control vectors in HEK cells and immunofluorescent staining using anti-MYC antibody confirmed the expression and cellular localization of both cKO and control 5-HT_4R (**Figure 2.6A**).

The cKO 5-HT_4R, the product of exon 5 deleted *Htr4*, showed significant difference in cellular sublocalization compared to the control 5-HT_4R. The low magnification images show that control 5-HT_4R were distributed relatively homogenously in the cell, resulting in cell images with sharp and uniform borders. On the other hand, the distribution of cKO 5-HT_4R were less homogenous producing punctate stained cells with vague edges. Imaging at a higher magnification revealed that the control 5-HT_4R was localized highly in the cellular membrane, seen as sharp and bright cellular borders (arrowheads). Note also that the control 5-HT_4R was localized in filopodia. However, the cKO 5-HT_4R seemed not to localize to the cellular membrane, failing to form uniform cellular borders. Furthermore, intracellular location of control 5-HT_4R was more homogenous compared to the highly punctate localization of cKO 5-HT_4R. These results suggested that overexpressed cKO 5-HT_4R was still translated but not integrated into the cellular membrane where it is supposed to function.

Next, to confirm that the cKO 5-HT_4R is not functional, we compared 5-HT_4R mediated cAMP induction using a 5-HT_4R agonist, zacopride, in HEK cells transfected with control and cKO *Htr4* cDNA. For the cAMP induction, we used a stimulation buffer supplemented with IBMX, a phosphodiesterase inhibitor, to prevent the inactivation of cAMP and promote its intracellular accumulation during stimulation. 30 min after the addition of either stimulation buffer (basal) or stimulation buffer with zacopride (100 μM), the cells were lysed in 0.1 M HCl to prevent cAMP degradation.

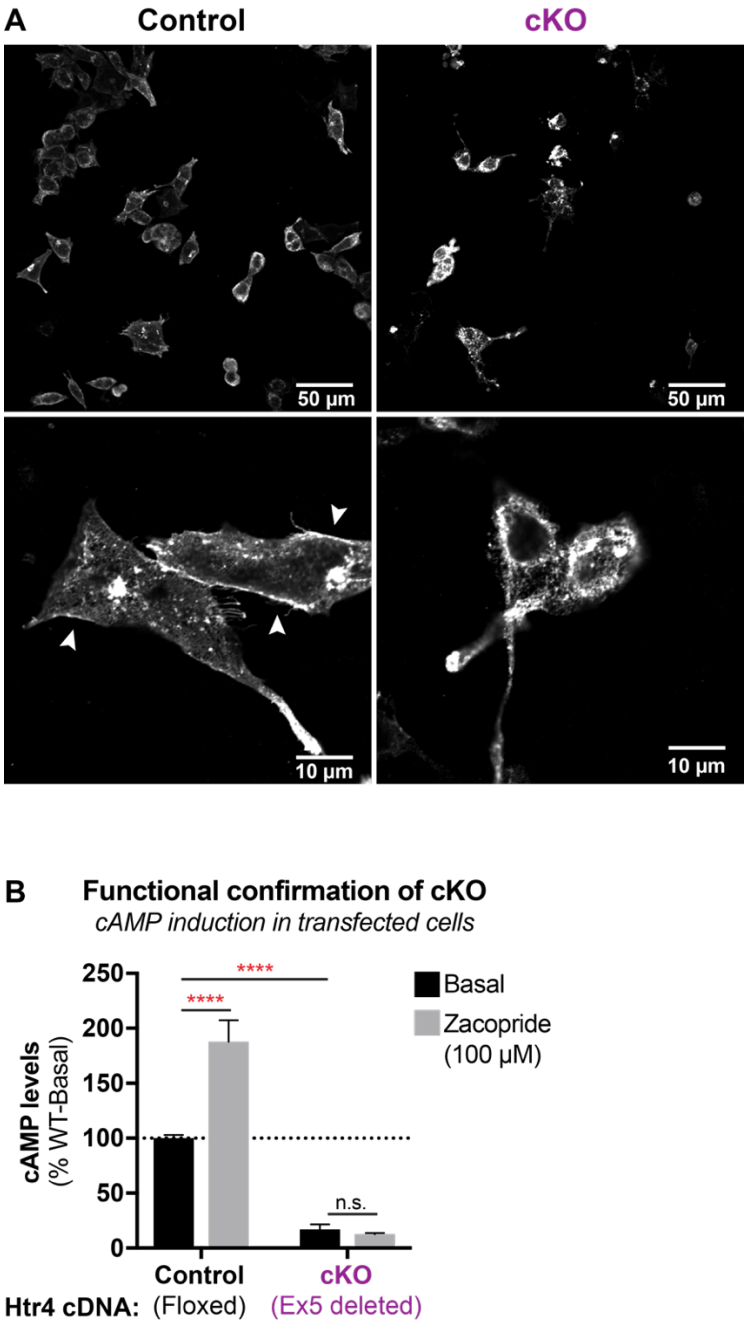

Figure 2.6. 5-HT$_4$R was non-functional after the deletion of *Htr4* exon 5.
(A) cKO 5-HT$_4$R did not localize on the cellular membrane in transfected HEK cells. Lower (above) and higher (below) magnification images of anti-MYC immunofluorescence of control and cKO 5-HT$_4$R-MYC transfected HEK cells. Arrowheads indicate the membrane localization of control 5-HT$_4$R.
(B) A 5-HT$_4$R agonist, zacopride, increased cAMP in HEK cells transfected with control (floxed) *Htr4* cDNA. Transfection with mutant cKO *Htr4* cDNA (exon 5 deleted) led to lower baseline levels of cAMP in HEK cells and zacopride did not induce cAMP in these cells. Data are represented as mean ± SEM. n=4 per group. Two-way ANOVA followed by post hoc Fisher's LSD test. ****p<0.0001, n.s. p>0.05.

cAMP concentrations in the lysates were measured using a monoclonal anti-cAMP antibody based ELISA and cAMP levels were normalized to the protein concentrations in each sample for accurate comparison.

As shown in **Figure 2.6B**, the basal cAMP levels in the control were significantly higher compared to the cKO (100 ± 2.9% versus 17.1 ± 4.9%, $p<0.0001$, n=4 per group). cKO 5-HT_4R expressing cells stimulated with zacopride did not show a difference in cAMP levels compared to their basal levels (Basal: 17.1 ± 4.9%, Zacopride: 12.6 ± 1.1%; $p=0.76$, n=4 per group). On the other hand, control cells stimulated with zacopride had a significant 88% increase in cAMP levels (Basal: 100 ± 2.9%, Zacopride: 188 ± 19.3 %; $p<0.0001$, n=4 per group). These results indicate that the cKO 5-HT_4R could not be activated with the 5-HT_4R agonist and therefore it is nonfunctional. On the other hand, the floxed *Htr4* allele could still produce a functional 5-HT_4R receptor.

2.3.4. Antibody screening against mouse 5-HT_4R

The exact subcellular localization of 5-HT_4R in the brain is not well established due to a lack of reliable antibodies. In situ hybridization (Peñas-Cazorla and Vilaró, 2014; Vilaro et al., 2005), and transgenic reporter mice (Warner-Schmidt et al., 2009) have helped to establish the cell types expressing 5-HT_4R. Much of our knowledge on the localization of 5-HT_4R is based on radioligand binding assays using antagonists against the receptor (Bonaventure et al., 2000; Varnäs et al., 2003). An attempt to use custom antibodies for the

immunolocalization of 5-HT_4R showed a somatodentridic localization in the rat brain and spinal cord (Manzke, 2003; Suwa et al., 2014). However, the data failed to show subcellular localization while overall distribution was similar to the expected expression pattern of 5-HT_4R. In mouse, another custom antibody was used for the immunostaining of myenteric and submucosal plexuses in mouse enteric nervous system (Liu, 2005), indicating 5-HT_4R may be expressed in axons terminals, at least in the peripheral nervous system. However, the antibody was not able to show immunolabeling in the mouse brain tissue (personal communication).

Showing the subcellular localization of 5-HT_4R in the mouse brain with a good antibody may bring novel insights regarding the function of the receptor in central synapses. Therefore, we systematically screened twelve of the commercially available antibodies by immunofluorescence on mouse 5-HT_4R-MYC expressing mammalian cells and on 4% PFA fixed mouse brain tissue with or without antigen retrieval. **Table 2.1** shows the results of the antibody screening. All commercial antibodies were generated against synthetic peptides of a part of human 5-HT_4R sequence. Human and mouse 5-HT_4R share >90% homology in their peptide sequence. Some of the antibodies, such as 1, 2 and 12 successfully immunolabeled the mouse 5-HT_4R when overexpressed in cell culture. On the mouse brain tissue, only antibody 1 and 2 achieved some specific staining, yet, with inconsistent results in between experiments. Antigen retrieval procedures did not improve the success of the staining for any antibodies tested.

Table 2.1. Summary of the antibody screening against mouse 5-HT_4R.

Antibody 1 and 2 achieved some specific immunofluorescent labeling on the mouse brain tissue, yet, with inconsistent results in between experiments. Some of the antibodies, such as 1, 2 and 12 successfully immunolabeled the mouse 5-HT_4R when overexpressed in cell culture. All commercial antibodies were generated against synthetic peptides of a part of human 5-HT_4R sequence (immunogen peptide).

No	Antibody Name	Clonality	Species	Immunogen Peptite	Cell Culture	Mouse brain tissue (4% PFA fixed)	w/ antigen retrieval
1	rb x 5-HT4R_C'	Poly	Rabbit	Human 5-HT4R, C-terminus	Colocalization w/ high background	Specific staining w/ high background (inconsistent results)	Non-specific staining
2	rb x 5-HT4R_N'	Poly	Rabbit	Human 5-HT4R, N-terminus	Colocalization w/ high background	Specific staining w/ high background (inconsistent results)	Non-specific staining
3	rbx5-HT4R_Ala361	Mono	Rabbit	Human 5-HT4R, surrounding Ala361	No staining	No staining	No staining
4	rb x 5-HT4R_3rdCYT	Poly	Rabbit	Human 5-HT4R, 3rd cytoplasmic loop	Non-specific staining	Non-specific staining	Non-specific
5	rb x 5-HT4R_31-70	Poly	Rabbit	Human 5HT4R, 1st cytoplasmic loop (31-70)	No staining	No staining	No staining
6	rb x 5-HT4R_333-401	Poly	Rabbit	Human 5HT4R, C-terminus (333-401)	Colocalization (Weak)	No staining	No staining
7	gt x SR-4 (C-18)	Poly	Goat	Human 5HT4R, C-terminus	Colocalization (Weak)	Non-specific staining of nuclei	Non-specific staining of nuclei
8	gt x SR-4 (K-19)	Poly	Goat	Human 5HT4R, a cytoplasmic domain	Colocalization (Weak)	No staining	No staining
9	gt x SR-4 (N-18)	Poly	Goat	Human 5HT4R, a cytoplasmic domain	Colocalization (Weak)	No staining	No staining
10	gt x SR-4 (N-16)	Poly	Goat	Human 5-HT4R, N-terminus	Non-specific binding	No staining	No staining
11	gt x SR-4 (G-3)	Mono	Mouse	Human 5-HT4R, (156-284)	Non-specific staining of EGFP expressing cells	Non-specific staining of EGFP expressing cells	Non-specific staining of EGFP expressing cells
12	rb x 5-HT4R_N'_2	Poly	Rabbit	Human 5-HT4R, N-terminus	Colocalization	No staining	No staining

2.3.5. Generation of a novel custom antibody against mouse 5-HT_4R

Due to the unavailability of a commercial antibody that successfully detect mouse 5-HT_4R, we have generated a custom rabbit polyclonal antibody in collaboration with Green Mountain Antibodies, Inc. (VT, USA) We selected the peptide sequence (GATSESRPQPADQHSTH) corresponding to the 233-249 amino acid sequence in the third cytoplasmic loop of 5-HT_4R (**Figure 2.7A**). CG was also added for conjugation to a carrier protein. This sequence was selected as the immunogen because it has more surface exposure in the predicted mouse 5-HT_4R structure and higher hydrophilicity due to the higher ratio of charged amino acids compared to other possible short sequences (**Figure 2.7B**). The hydrophilicity is necessary for the peptide to be soluble for the conjugation to the carrier proteins. In addition, the presence of two amino acid proline (P) would lead to the formation of secondary structures in the short peptide sequence rendering a more unique 3-D structure for a short peptide rather than a straight one. Theoretically, these would result in an immunogen with higher antigenicity.

The synthetic full length peptide was purified to >85% by HPLC and the net peptide content was 77.4% in the purified solution (New England Peptide Inc., MA, USA). The peptide was conjugated to a highly immunogenic and widely used carrier protein, KLH (keyhole limpet hemocyanin), before being injected into two rabbits systematically. We first tested the 5-HT_4R antibodies on HEK cells expressing intact (control) or exon 5 deleted (cKO) *Htr4* cDNA described earlier in section 2.3.3 (**Figure 2.7.C**).

A

Origin	Seq	Range	aa #	Location
m 5-HT4R	CGGATSESRPQPADQHSTH	233-249	17	CL-3

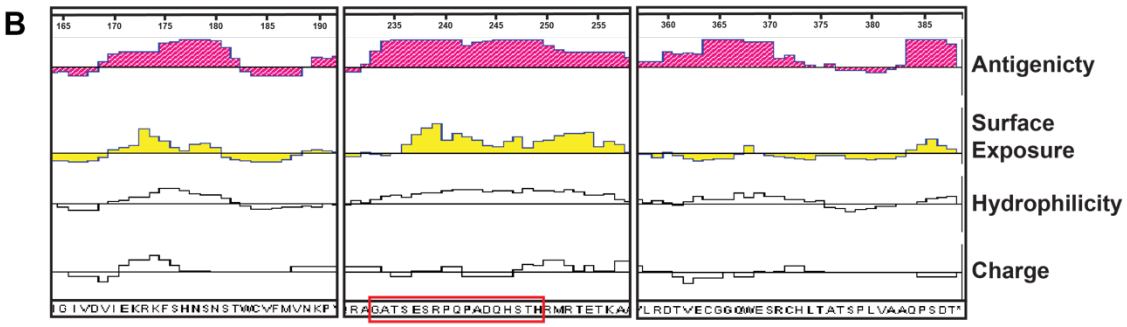

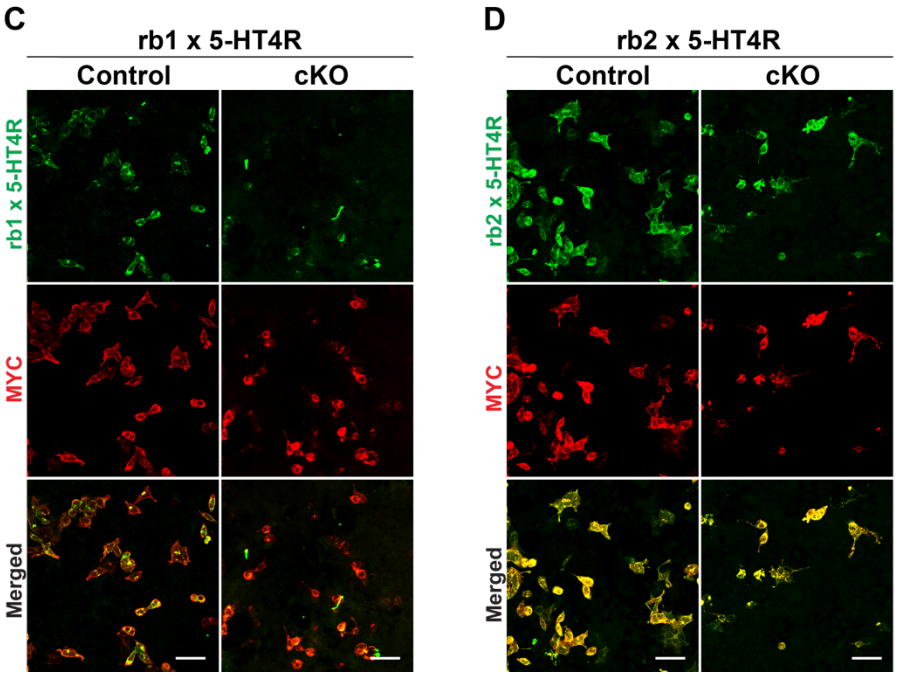

Figure 2.7. Custom antibody generation against mouse 5-HT$_4$R.
(A) Amino acid sequence and relevant information of custom immunogen peptide. CL-3: cytoplasmic loop 3. # aa: number of amino acids. Seq: sequence. m 5HT4R: mouse 5-HT$_4$ receptor.
(B) Predictive analysis of antigenicity of mouse 5-HT$_4$R sequence (Courtesy of Green Mountain Antibodies) Selected peptide (red rectangle) show antigenicity that other possible sequences (left and right panels).
(C, D) Polyclonal antibodies generated against custom m5-HT4R peptide from two rabbits, rb1 (C) and rb2 (D), were used for immunofluorescence (green) of HEK cells expressing either control or cKO 5-HT$_4$R. anti-MYC staining (red) was used as colabeling to detect 5-HT$_4$R. Note the colocalization of rb1 and rb2 x 5-HT4R with MYC in control panels. Also note the weaker labeling of rb1 x 5-HT4R in cKO panel. Scale bars, 50μm.

rb1 x 5-HT4R labeling colocalized with MYC staining in control while it did not detect cKO 5-HT_4R as efficiently, suggesting that it was able to detect intact 5-HT_4R better than cKO 5-HT_4R. rb2 x 5-HT4R labeling colocalized with MYC staining in control as well as in cKO, suggesting that although it specifically detects the mouse 5-HT_4R in HEK cells, it may not discriminate between intact 5-HT_4R and mutant 5-HT_4R. Together these data indicated that our custom polyclonal rabbit antibodies were able to detect overexpressed mouse 5-HT_4R in HEK cells, rb1x 5-HT4R displaying some selectivity towards the cKO 5-HT_4R.

Next, we tested the custom antibodies on the mouse brain tissue. Custom peptide was mixed with the antibodies as a negative control. DAPI was used as a counter stain to visualize all nuclei. In mouse brain tissue, rb1 x 5-HT4R antibody showed specific labeling in the hippocampus and neocortex. For example, in the dentate gyrus (DG) of a wildtype (WT) mouse, rb1 x 5-HT4R labeled the granule cells and some but not all cells in hilus (**Figure 2.8A**). When the peptide was added, the specific staining in DG was not observed. In somatosensory cortex (**Figure 2.8B**), rb1 x 5-HT4R labeling was mostly specific to layers 5 and 6 in WT mice with some staining in higher layers. Although there was some staining in the cortex of Emx1/Htr4 cKO mice, it was not as layer-specific and defined. Together, these results indicate that our custom rb1 x 5-HT4R antibody showed staining of 5-HT_4R in the hippocampus and neocortex in a similar pattern to the expected expression, and that it is a novel tool for specific immunolabeling of 5-HT_4R.

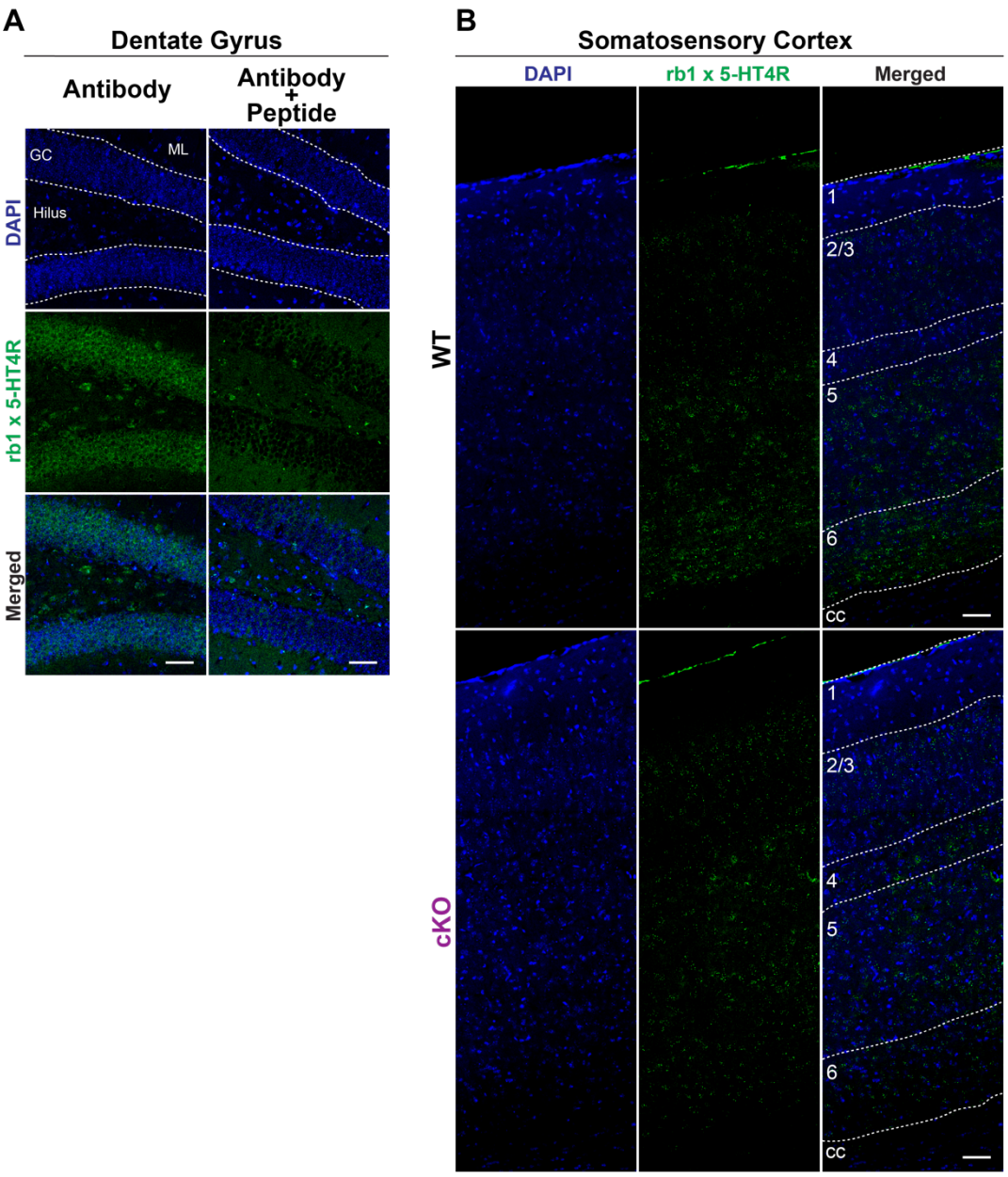

Figure 2.8. Custom rb1 x 5-HT$_4$R antibody showed specific immunostaining on mouse brain tissue.

(A) Fluorescent confocal images showing the immunolabeling of rb1 x 5-HT4R (left) and rb1 x 5-HT4R mixed with custom immunogen peptide (right) in dentate gyrus (DG) of a wildtype mouse (green). DAPI was used as a nuclear counterstain (blue). Note that the staining in granule cell layer (GC) was not observed when peptide was added. In addition, rb1 x 5-HT4R stained some but not all cells in hilus. ML: molecular layer. Scale bars 50 μm.

(B) Tiled fluorescent confocal images showing the immunolabeling of rb1 x 5-HT4R (green) in the somatosensory cortices of a wildtype (WT, above) and an Emx1/Htr4 cKO (cKO, below) mice. Note that the staining was localized in layer 5 and 6 in WT but not in cKO. Scale bars 50 μm.

2.4. Anxiety and depression related behaviors and behavioral antidepressant responses

After confirming the loss of functional 5-HT_4R following Cre-mediated recombination in the cKO mice, we next tested whether pallial 5-HT_4R is necessary for regulating anxiety, mood and behavioral responses to chronic SSRI treatment. To this end, Emx1/Htr4 cKO mice were put through a battery of behavioral assays assessing anxiety and depression related behaviors with or without chronic SSRI treatment.

Figure 2.9A shows the timeline for drug treatment and following behavioral assays. Briefly, 8-week-old Emx1/Htr4 cKO mice and their Cre negative Htr4-floxed littermates (WT, control) were either given 0.167 mg/ml fluoxetine (FLX) (~18 mg/kg/day) or vehicle (VEH) in drinking water for 18 days (Schmidt et al., 2012). For behavioral phenotyping, a battery of assays was performed with four groups (WT-VEH, WT-FLX, cKO-VEH, cKO-FLX; n= 33, 30, 28, 28, respectively), combining three cohorts, unless otherwise noted. The drug treatment continued until the end of behavioral assessments.

2.4.1. Thigmotaxis and locomotor activity in the open field test

Thigmotaxis is a measure of anxiety-like behavior which is the ratio of time a mouse spends near the walls of an open field (OF) arena. It measures the

balance between the innate tendency of mice to avoid well-lit, open areas and their drive to explore novel environments (Gould et al., 2009).

In the OF test, each mouse was placed in a high-walled square arena and tracked for 60 mins (**Figure 2.9B**). In the first 10 mins of the OF test, Emx1/Htr4 cKO and their control littermates (WT) did not show any significant difference in thigmotaxis (time spent in periphery/total time) compared to their control littermates (cKO-VEH: 0.751 ± 0.01, WT-VEH: 0.763 ± 0.01, p=0.55) (**Figure 2.9C**, left). Over 60 min, Emx1/Htr4 cKO mice showed slightly increased thigmotaxis compared to WT (**Figure 2.9C**, right) although this difference did not reach statistical significance (cKO-VEH: 0.724 ± 0.02, WT-VEH: 0.691 ± 0.02, p=0.26), indicating the loss of 5-HT_4R may be anxiogenic. When chronically treated with fluoxetine, control mice showed significantly increased thigmotaxis, both in first 10 mins (WT-VEH: 0.763 ± 0.01, WT-FLX: 0.879 ± 0.02, p<0.0001) and over 60 mins (0.691± 0.02 versus 0.764 ± 0.02, respectively, p=0.01), indicating that chronic fluoxetine treatment increased anxiety-like behaviors in the OF. This result is consistent with other studies showing that naïve mice of some strains, including C57B6J, when administered with fluoxetine chronically, exhibited increased anxiety-like behaviors in some tests (Baek et al., 2015). Although Emx1/Htr4 cKO displayed similar increase in thigmotaxis in the first 10 mins after fluoxetine treatment (cKO-VEH: 0.751 ± 0.02, cKO-FLX: 0.862 ± 0.02, p<0.0001), this anxiogenic effect was not observed in cKOs over 60 mins (cKO-VEH: 0.724 ± 0.02, cKO-FLX: 0.754 ± 0.03, p=0.33).

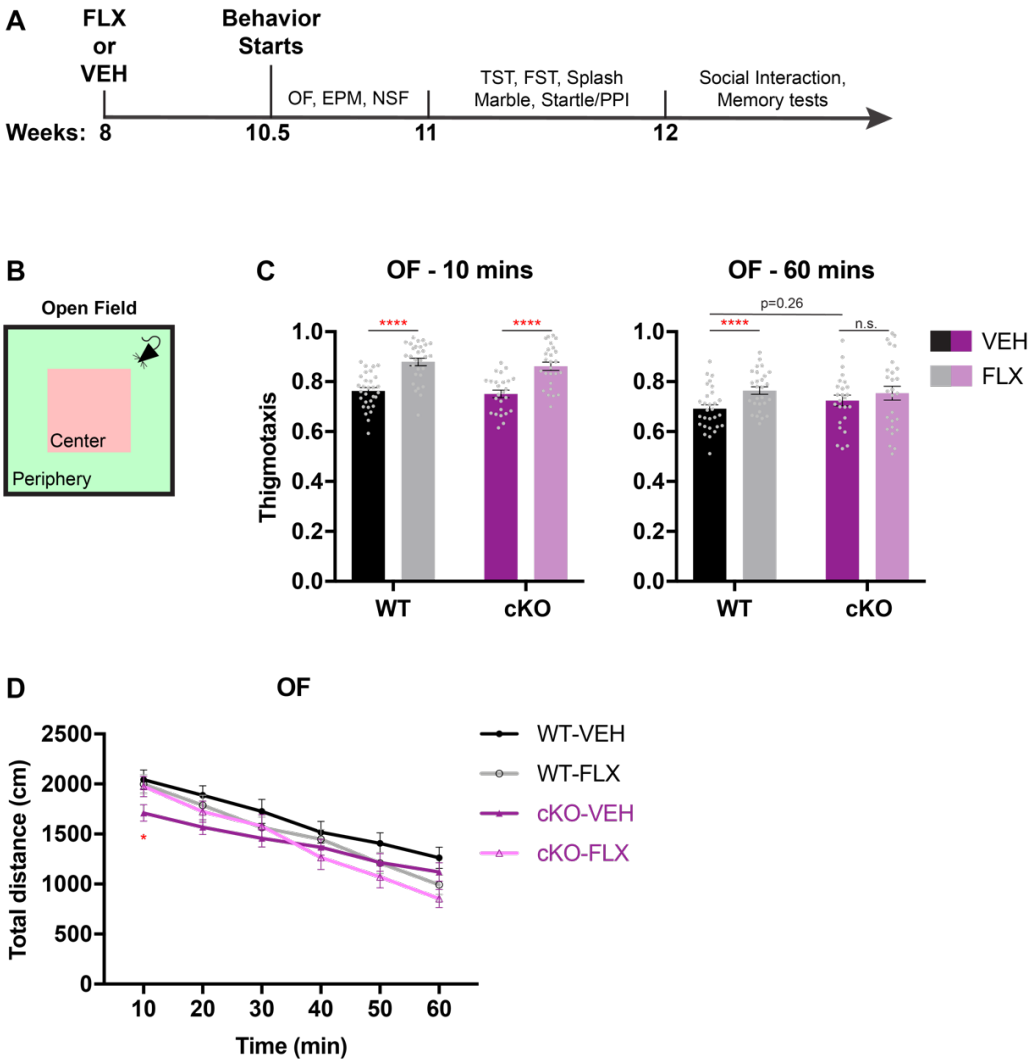

Figure 2.9. The loss of pallial 5-HT$_4$R resulted in slightly elevated anxiety-like behaviors in the open field.

(A) Schematic showing the timeline for the battery of behavioral assays.

(B) Schematic of the open field (OF) test. Mice with increased anxiety-like behaviors tend to spend more time in periphery (green) and less time in the center (red) compared to wildtype mice.

(C) Emx1 Htr4/cKO mice (cKO-VEH) showed slightly increased thigmotaxis (periphery/total time) in the OF in 60 min (right), compared to their control littermates (WT-VEH). Following chronic fluoxetine (FLX) treatment, both Emx1 Htr4/cKO and WT littermates showed significantly increased thigmotaxis in 10 mins (left) and 60 mins (right), compared to vehicle treated counterparts.

(D) Emx1 Htr4/cKO mice (cKO-VEH) showed less locomotor activity (total distance) in the first 10 mins of the OF test, compared to control littermates (WT-VEH). There was no significant effect of chronic fluoxetine on the locomotor activity. Data are represented as mean ± SEM. Two-way ANOVA followed by post hoc Fisher's LSD test. *p<0.05, ****p<0.0001.

Together, these results indicate that 5-HT_4R in the pallium may mediate anxiety-like behaviors and the anxiogenic responses to chronic fluoxetine treatment in mice.

Spontaneous locomotor activity is also measured in the open field as total distance traveled (cm). Since tests measuring anxiety-like behaviors rely on the locomotor activity, it should be taken into account while interpreting anxiety-like behaviors. The activity data is shown in 10 min bins in **Figure 2.9D**. In the first 10 min, Emx1/Htr4 cKO mice were less active compared to their WT littermates (WT-VEH: 2044 ± 96 cm, cKO-VEH: 1711 ± 81 cm, p=0.02). However, over 60 min, the difference in the spontaneous locomotor activity between groups was not statistically significant (p=0.17, Repeated measures two-way ANOVA). Therefore, either the loss of 5-HT_4R or fluoxetine treatment did not alter locomotor activity in the OF over 60 min.

2.4.2. Elevated-plus maze test

The elevated-plus maze (EPM) is a “plus” shaped maze with two open arms located at opposite sides connected by a neutral center to two perpendicular closed arms (**Figure 2.10A**). The mice were placed in the center, facing an open arm, and their time spent in open versus closed arms in 5 mins were calculated as a measure of anxiety. Similar to the thigmotaxis in the OF, the EPM employs the innate conflict between the tendency to explore versus the aversion from a well-lit open environment. The commonly used anxiety measures

in the EPM are the amount of time spent in the open arms, the amount of time spent in the closed arms and the ratio of time spent in open versus both arms (Walf and Frye, 2007).

Emx1/Htr4 cKO mice spent significantly less time spent in the open arms compared to their WT littermates (cKO-VEH: 26.3 ± 6.1 s, WT-VEH: 51.6 ± 6.9 s, p=0.0085) (**Figure 2.10B**), indicating that the loss of 5-HT_4R resulted in increased anxiety-like behaviors. Following chronic treatment with fluoxetine, control mice showed significantly less time in the open arms (WT-VEH: 51.6 ± 6.9 s, WT-FLX: 5.7 ± 2.2 s, p<0.0001), while chronic fluoxetine treated Emx1/Htr4 cKO mice did not display a significant difference in time spent in open arms compared to VEH treated cKO mice (cKO-VEH: 26.3 ± 6.1 s, cKO-FLX: 27.4 ± 9.4 s, p=0.91). These results indicated that while increasing anxiety-like behaviors in naïve mice, chronic fluoxetine treatment did not induce similar behaviors in the absence of 5-HT_4R in the EPM, a result similar to the OF.

Since the EPM also relies on locomotor responses, we also measured the velocity during the test. There were no significant differences between groups (WT-VEH-: 6.2 ± 0.5 cm/s, WT-FLX: 5.2 ± 0.4 cm/s, cKO-VEH: 5.3 ± 0.6 cm/s, cKO-FLX: 5.3 ± 0.5 cm/s, p=0.35, two-way ANOVA) (**Figure 2.10C**). Together, these results suggest that 5-HT_4R in the pallium mediates anxiety-like behaviors and the anxiogenic responses to chronic fluoxetine treatment in mice.

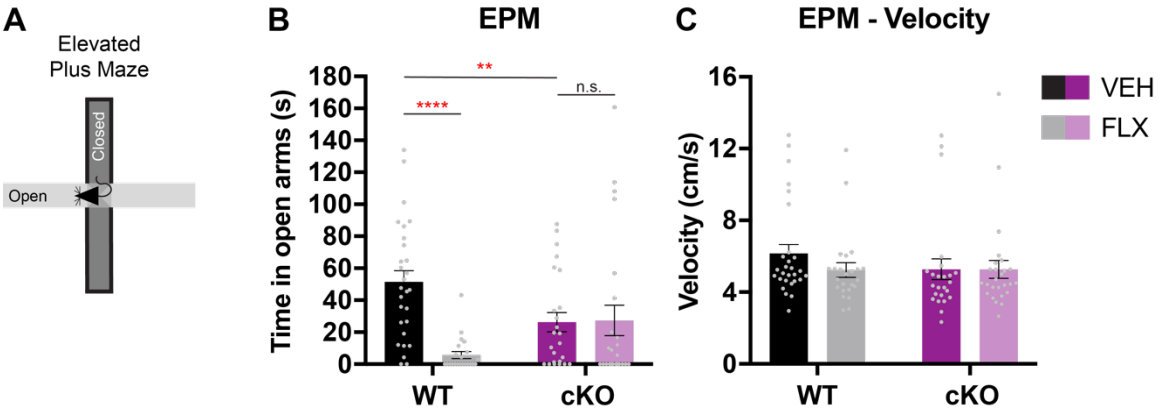

Figure 2.10. The loss of pallial 5-HT$_4$R led to increased anxiety-like behaviors in the elevated plus maze.
(A) Schematic representation of the elevated plus maze (EPM) test. Mice were placed in the center, facing an open arm, and the time they spent in the open versus closed arms in 5 mins were calculated as a measure of anxiety-like behavior.
(B) Emx1/Htr4 cKO (cKO-VEH) spent significantly less time in the open arms compared to their control littermates (WT-VEH). Following chronic treatment with fluoxetine (FLX), Emx1/Htr4 cKO mice (cKO-FLX) did not display a significant difference in time spent in open arms compared to vehicle (VEH) treated cKO mice (cKO-VEH) whereas control mice (WT-FLX) spent significantly less time in the open arms compared to WT-VEH.
(C) There were no significant differences between groups in the velocity in the EPM.
Data are represented as mean ± SEM. Two-way ANOVA followed by post hoc Fisher's LSD test. **p<0.01, ****p<0.0001, n.s. p>0.05.

2.4.3. Novelty suppressed feeding test

Hyponeophagia, the inhibition of feeding produced by novelty, provides a measure of anxiety-related behavior in rodents. It can be evoked by the novelty of the test environment compared to the housing environment. Hyponeophagia-based tests are also conflict tests in which animals face a choice between engaging in feeding and neophobic behaviors. While hyponeophagia-based tests offer strong predictive validity as anxiety measures, they have also found to predict the time-course of action of many therapeutic compounds including SSRIs. For example, the novelty suppressed feeding (NSF) test is one of the few tests that is responsive to chronic fluoxetine administration in mice (Dulawa and Hen, 2005). Therefore, the NSF is popularly used to study the mechanisms underlying therapeutic effects of chronic antidepressant treatment.

In the NSF, mice were food deprived for 24 h before the test to instigate feeding behavior. The efficiency of food deprivation was measured as decreased body weight (data not shown). Mice were then tested in a brightly lit arena where a food pellet was placed in the middle and the latency to bite the food was measured in 15 min-trials (**Figure 2.11A**). Since the NSF relies on feeding, each animal was put in a clean cage similar to their home cage for 30 min with food *ad libidum* after each trial to measure home cage feeding behavior.

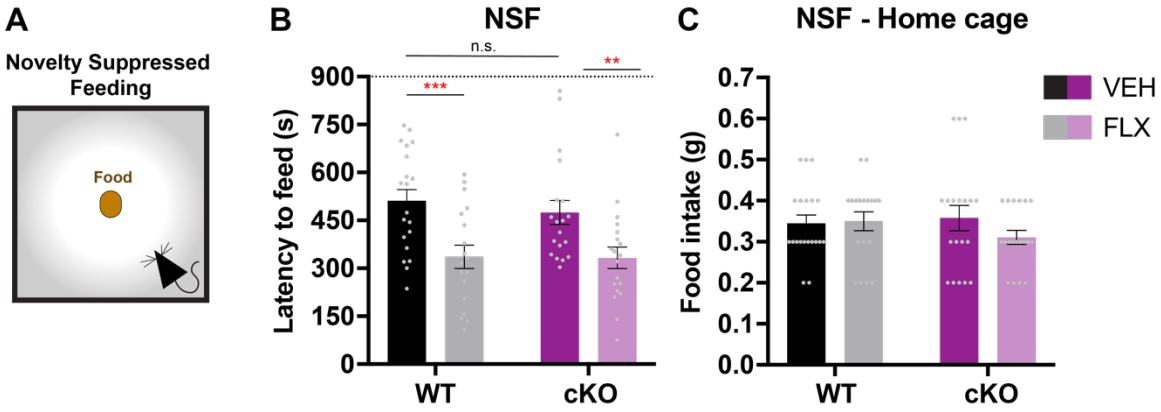

Figure 2.11. Emx1/Htr4 cKO mice did not show a difference in anxiety-like behaviors in the novelty suppressed feeding (NSF) test and responded to chronic fluoxetine treatment.

(A) Schematic representation of the novelty suppressed feeding (NSF) test. The latency to bite the food of 24-hour fasted mice in a novel environment was calculated as a measure of anxiety-like behavior.

(B) Emx1/Htr4 cKO mice (cKO-VEH) did not show any significant differences in the latency to bite the food compared to their control (WT-VEH) littermates. Following chronic treatment with fluoxetine, both Emx1/Htr4 cKO mice and WT littermates showed significant decrease in the latency to bite compared to vehicle treated counterparts.

(C) There were no significant differences between groups in their home cage food intake.

Data are represented as mean ± SEM. Two-way ANOVA followed by post hoc Fisher's LSD test. **p<0.01, ***p<0.001, n.s. p>0.05.

Emx1/Htr4 cKO mice did not show any significant differences in the latency to bite the food compared to their control littermates (cKO-VEH: 475 ± 37 s, WT-VEH: 511 ± 36 s, p=0.47, n=19, 20, respectively) (**Figure 2.11.B**), indicating that they did not display any difference in the levels of anxiety-like behaviors in the NSF. Following chronic treatment with fluoxetine, Emx1/Htr4 cKO mice and WT littermates showed similarly significant decrease in the latency to bite compared to vehicle treated counterparts (WT-VEH/FLX: 511 ± 36 / 336 ± 37 s, p=0.0009, n=20/19; cKO-VEH/FLX: 475 ± 37 / 333 ± 33 s, p=0.0066, n=19/19). None of the groups showed significant differences in their home cage feeding (WT-VEH: 0.35 ± 0.02 g, WT-FLX: 0.35 ± 0.03 g, cKO-VEH: 0.36 ± 0.03 g, cKO-FLX: 0.31 ± 0.02 g, p=0.26, Two-way ANOVA) (**Figure 2.11C**). Together, these results indicate that the loss of 5-HT_4R in the hippocampus and neocortex did not alter the chronic antidepressant responses in NSF.

2.4.4. Tail suspension test

The tail-suspension test (TST) is a widely-used assay for screening potential antidepressant drugs and behavioral characterization of genetically modified mice to identify novel targets mediating depression and antidepressant response. The test is based on the principle that mice subjected to inescapable stress of being suspended by their tail, will move and struggle in an attempt to escape. The amount of time they are not struggling (immobility) is used as an indication of the level of behavioral despair.

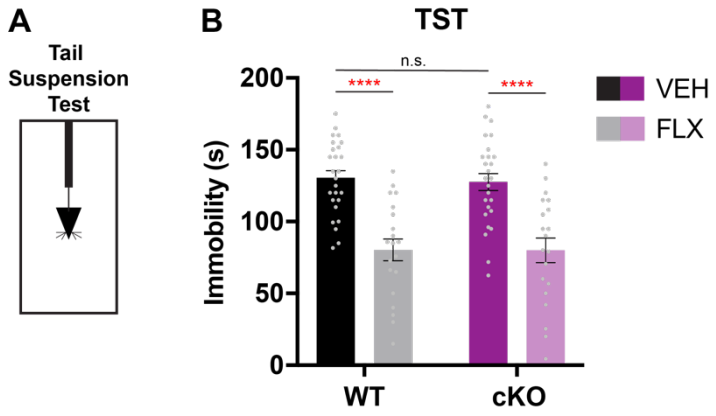

Figure 2.12. Emx1/Htr4 cKO mice did not display a difference in depression-like behaviors in the tail suspension test (TST) and responded to chronic fluoxetine treatment.

(A) Schematic representation of the tail suspension test (TST). Mice were suspended by the tip of their tails for 6 min, and the immobility time was measured in the last 4 min as an indication of the level of behavioral despair.

(B) Emx1/Htr4 cKO mice (cKO-VEH) did not exhibit any differences in immobility compared to their control (WT-VEH) littermates. Both Emx1/Htr4 cKOs and controls treated with chronic fluoxetine showed significantly decreased immobility compared to vehicle treated counterparts.

Data are represented as mean ± SEM. Two-way ANOVA followed by post hoc Fisher's LSD test. ****$p<0.0001$, n.s. $p>0.05$.

Acute and chronic treatments with variety of antidepressants including SSRIs have been reported to decrease the immobility in mice during the TST (O'Leary and Cryan, 2009).

In the TST, mice were suspended by the tip of their tails for 6 min, and the immobility time was measured in the last 4 min (**Figure 2.12A**). Emx1/Htr4 cKO did not exhibit any differences in immobility compared to their control (WT) littermates (cKO-VEH: 128 ± 6 s, WT-VEH: 131 ± 5 s, p=0.74) (**Figure 2.12B**), indicating that they do not show any difference in the levels of despair-like responses. In addition, both Emx1/Htr4 cKOs and controls treated with chronic fluoxetine showed significantly decreased immobility compared to vehicle treated counterparts (WT-VEH/FLX: 131 ± 5 / 80 ± 8 s, $p<0.0001$; cKO-VEH/FLX: 128 ± 6 / 80 ± 9 s, $p<0.0001$). Together, these results indicate that the loss of 5-HT_4R in the hippocampus and neocortex does not affect the depression-like behaviors and chronic antidepressant responses in the TST.

2.4.5. Forced swim test

The forced swim test (FST) is another most commonly used behavioral assay to screen depression-related and antidepressant behavior. It is also a despair based assay in which mice are subjected to inescapable stress of swimming and immobility is the measure of depressive-like behavior. Both acute and chronic treatments with variety of antidepressants including SSRIs have been reported to decrease the immobility in mice during the FST (Cryan and

Lucki, 2000). It has also been used for behavioral characterization of genetically modified mice to assess the levels of despair-like behavior and to identify targets for novel antidepressants (Nestler et al., 2002).

In the FST, mice were placed in a cylinder with water for 6 min, and the immobility time was measured in the last 4 min (**Figure 2.13A**). Emx1/Htr4 cKO mice did not display any significant difference in immobility compared to their control (WT) littermates (cKO-VEH: 132 ± 7 s, WT-VEH: 140 ± 6 s, p=0.38) (**Figure 2.13B**), indicating that they do not show any difference in the levels of despair-like responses. Emx1/Htr4 cKOs and controls treated with chronic fluoxetine showed significantly increased immobility compared to vehicle treated counterparts (WT-VEH/FLX: 140 ± 6 / 177 ± 5 s, p=0.0002; cKO-VEH/FLX: 132 ± 7 / 167 ± 9 s, p=0.0006), showing an opposite effect from the expected antidepressant-like response, leading to an inconclusive result. Other studies have also reported that the observation of antidepressant-like response in the FST depends on the strain of mice, the antidepressant and its dose (David et al., 2003; Dulawa et al., 2004; Lucki et al., 2001). Together with the TST, these data indicate that 5-HT_4R in the hippocampus and neocortex may not be necessary for mediating depressive-like and antidepressant behaviors in mice.

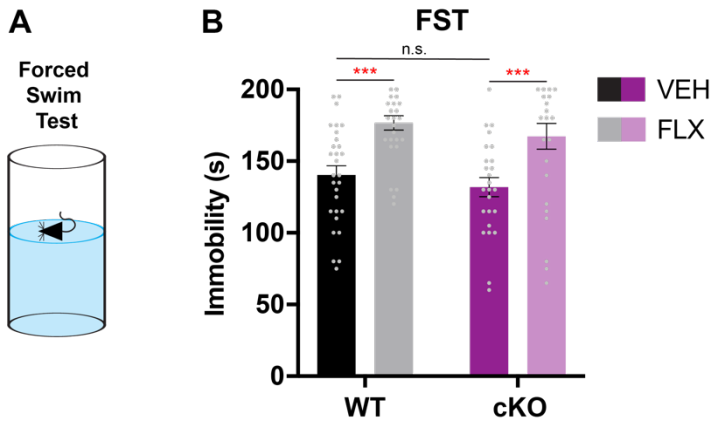

Figure 2.13. Emx1/Htr4 cKO mice did not show a difference in depression-related behaviors in the forced swim test (FST).
(A) Schematic representation of forced swim test (FST). Mice were placed in a cylinder with water for 6 mins, and the immobility time was measured in the last 4 mins as an indication of the level of behavioral despair.
(B) Emx1/Htr4 cKO mice (cKO-VEH) did not display any significant difference in immobility compared to their control (WT-VEH) littermates. Emx1/Htr4 cKOs and controls treated with chronic fluoxetine showed significantly increased immobility compared to vehicle treated counterparts.
Data are represented as mean ± SEM. Two-way ANOVA followed by post hoc Fisher's LSD test. ***$p<0.001$, n.s. $p>0.05$.

2.4.6. Splash test

In mice, grooming behavior serves the purpose of hygiene as well as other rewarding functions such as stress reduction and social interaction. It is sensitive to stress and various genetic and pharmacological manipulations. For example, mouse models with depression-like behaviors generally display poor coat status, such as matte, dirty, and unkempt coat, whereas antidepressant treatments tend to reverse this phenotype (David et al., 2009; Griebel et al., 2002).

To measure induced grooming, mice were sprayed with 10% sucrose on their lower back (**Figure 2.14A**). Grooming time was measured in 5 min trials and displayed as percent of control (WT-VEH). Emx1/Htr4 cKO mice groomed slightly more compared to their control littermates, although this difference did not reach statistical significance (cKO-VEH: 112.3 ± 6.3 %, WT-VEH: 100 ± 4.9 %, p=0.15, n= 20, 20 respectively) (**Figure 2.14B**), indicating that Emx1/Htr4 cKO mice may have displayed slightly enhanced hedonic behaviors. Following chronic treatment with fluoxetine, both Emx1/Htr4 cKO and control did not show a significant change in time spent grooming compared to vehicle treated counterparts (WT-VEH/FLX: 100 ± 4.9 / 108 ± 5.6 %, p=0.34, n=20/17; cKO-VEH/FLX: 112.3 ± 6.3 / 106 ± 9 %, p=0.48, n=20/17), indicating that chronic fluoxetine did not regulate hedonic behaviors in the splash test in these mice. Together, these results suggest that pallial 5-HT_4R may mediate hedonic behaviors.

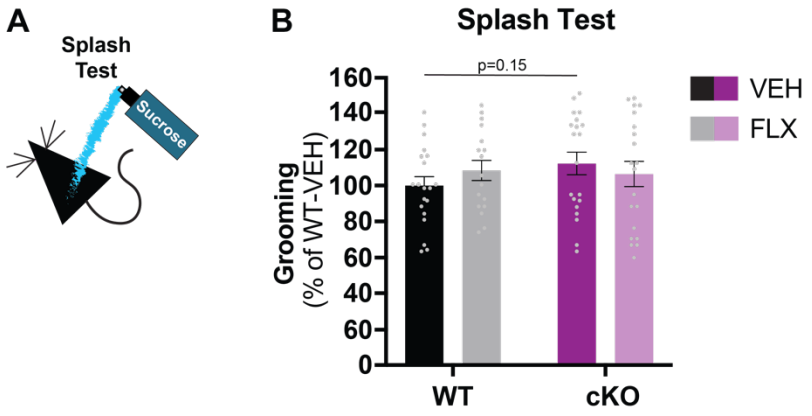

Figure 2.14. Emx1/Htr4 cKO mice showed slightly higher grooming in the splash test.
(A) Schematic representation of the splash test. Mice were squirted with 10% sucrose by a spray bottle on their back. Grooming time was measured in 5-min as a measure of hedonic behavior.
(B) Emx1/Htr4 cKO mice (cKO-VEH) groomed slight more compared to their control littermates (WT-VEH). Following chromic treatment with fluoxetine, Emx1/Htr4 cKO and control littermates did not show a significant change in time spent grooming compared to vehicle treated counterparts.
Data are represented as mean ± SEM. Two-way ANOVA followed by post hoc Fisher's LSD test. ***p<0.001, n.s. p>0.05.

2.4.7. Sucrose preference test

The sucrose preference test is another reward-based assay assessing anhedonia-like phenotype in mice. Sucrose has a natural hedonic value and given a choice between sucrose and water, mice prefer sucrose. A drop in the ratio of sucrose to water consumption below 65% is established as anhedonia-like behavior (Strekalova et al., 2004).

In the sucrose preference test, non-treated naïve mice were water deprived for 24 h to encourage more drinking during testing. Each mouse was then placed in a clean cage containing a 1% sucrose bottle and a water bottle (**Figure 2.15A**). Sucrose and water consumption for 6 hours was measured by the decrease in the weight of the bottles. At the 3-hour mark, bottles were switched places to avoid side preference. Sucrose preference was calculated for 6 h as the ratio of total 1% sucrose consumed (g) to total drinking. Since the sucrose preference test relies on drinking, we calculated total drinking amount to see whether water deprivation was effective. Mice without an enhanced drinking drive were excluded from analysis (Total drinking cutoff = 1 g)

There was not any significant difference in total drinking amount between Emx1/Htr4 cKO and control littermates (WT: 3.6 ± 0.3, cKO: 3.9 ± 0.5, p=0.59, n= 16, 11, respectively) (**Figure 2.15D**). Emx1/Htr4 cKO mice and control littermates showed similar over 85% preference for 1% sucrose over water (WT: 0.88 ± 0.02, cKO: 0.86 ± 0.03, p=0.62) (**Figure 2.15B**).

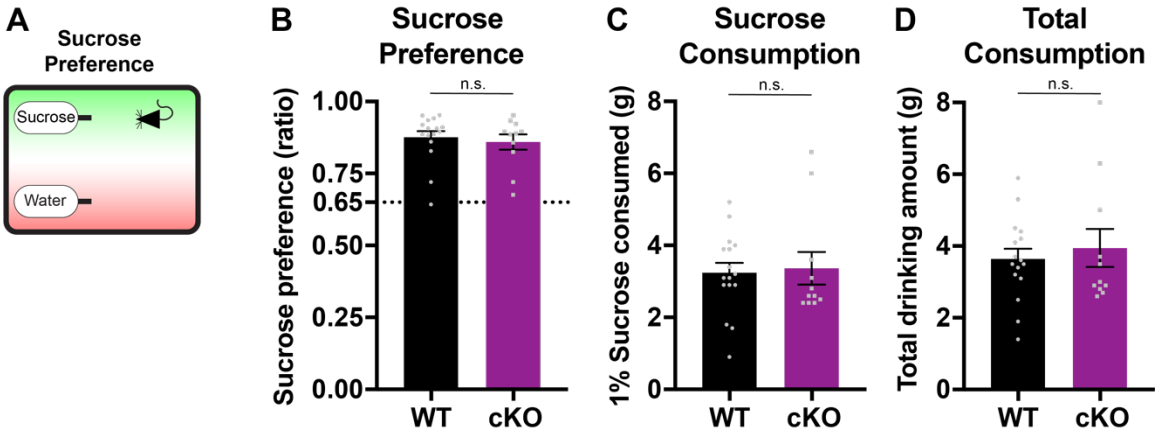

Figure 2.15. Emx1/Htr4 cKO mice did not exhibit a difference in hedonic behaviors in the sucrose preference test.
(A) Schematic representation of sucrose preference test. Each 24-hour water deprived mouse was placed in a cage containing a 1% sucrose bottle and a water bottle. Sucrose and water consumption for 6 hours was measured and sucrose preference was calculated as a measure of hedonic behavior.
(B) Both Emx1/Htr4 cKO mice and control littermates (WT) showed over 85% preference for 1% sucrose.
(C) There was not any difference in the amount of sucrose consumption between groups.
(D) There was not any significant difference in total drinking amount between groups. Data are represented as mean ± SEM. Two-tailed unpaired t-test. n.s. $p>0.05$.

There was also no difference in the amount of sucrose consumption between groups (WT: 3.2 ± 0.3 g, cKO: 3.4 ± 0.5, p=0.80) (**Figure 2.15C**). Together these data indicate that the loss of pallial 5-HT_4R did not alter hedonic behaviors in mice in the sucrose preference test.

2.4.8. Marble burying test

The animal models of anhedonia show decreased marble burying, and anxiolytics and SSRIs reduce the marble burying behavior in mice (Greene-Schloesser et al., 2011). Hence, marble burying has been associated with changes in anxiety and mood related behaviors. Mice spontaneously dig as an innate behavior when given a suitable substrate such as deep bedding. A way of measuring the digging behavior is the marble burying test in which a set of marbles is distributed on the surface of a bedding-filled cage. The number of marbles buried by displaced bedding due to digging after a set time is counted.

To measure digging, we placed equally spaced 12 marbles (4x3) on a deep woodchip bedding filled in a small mouse cage with open top (**Figure 2.16A**). The number of marbles buried in each 15 min trial per mouse was counted as a measure of spontaneous digging. Emx1/Htr4 cKO did not exhibit any differences in the number of marbles buried compared to their control littermates (cKO-VEH: 9.7 ± 0.6, WT-VEH: 10.7 ± 0.3, p=0.38, n=7, 11, respectively) (**Figure 2.16B**), indicating that they do not show any difference in the levels of spontaneous digging.

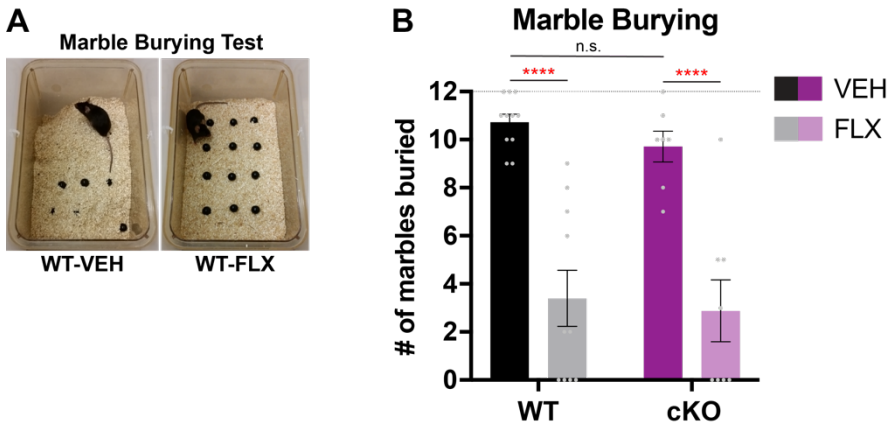

Figure 2.16. Emx1/Htr4 cKO mice did not show a difference in digging behavior and responded to chronic fluoxetine treatment in the marble burying test.
(A) Example images of mice tested in marble burying test for 15 min. Left, a control mice (WT-VEH) having buried 8 marbles. Right, a control mice treated with fluoxetine (WT-FLX) having buried zero marbles.
(B) Emx1/Htr4 cKO (cKO-VEH) did not exhibit any differences in the number of marbles buried compared to their control littermates (WT-VEH). Both Emx1/Htr4 cKOs and controls treated with chronic fluoxetine (FLX) buried significantly decreased number of marbles compared to vehicle (VEH) treated counterparts.
Data are represented as mean ± SEM. Two-way ANOVA followed by post hoc Fisher's LSD test. ****$p<0.0001$, n.s. $p>0.05$.

Emx1/Htr4 cKOs and controls treated with chronic fluoxetine buried significantly decreased numbers of marbles compared to vehicle treated counterparts (WT-VEH/FLX: 10.7 ± 0.3 / 3.4 ± 1.1, $p<0.0001$, n=11/10; cKO-VEH/FLX: 9.7 ± 0.6/ 2.9 ± 1.3, $p<0.0001$, n=7/8), showing a significant behavioral antidepressant effect independent of pallial 5-HT_4R. Together, these results indicate that the loss of pallial 5-HT_4R did not affect baseline digging behavior or chronic antidepressant-dependent changes.

2.4.9. Acoustic startle response and pre-pulse inhibition

The acoustic startle reflex is a defensive motor response to a sudden, intense auditory stimulus. The measurement of acoustic startle responses (ASR) can provide general information regarding sensorimotor processing (Geyer and Swerdlow, 2001), but it is also subjected to modulatory influences from higher cortical and limbic structures (Kaviani et al., 2004). Prepulse inhibition (PPI) of the ASR is the suppression of the startle response when a startling acoustic stimulus is preceded by an immediate, weaker pre-stimulus (**Figure 2.17A**). PPI is an operational measure of sensorimotor gating, and used as a clinical measure of schizophrenia (Valsamis and Schmid, 2011a). However, startle reactivity and inhibition of startle are altered in some anxiety and mood disorders, and associated animal models. Enhanced ASR was linked with increased anxiety and its physiological features (Miller and Gronfier, 2006), while decreased ASR was observed in patients with anhedonia (Giakoumaki et al., 2010).

To measure ASR, acoustic stimuli were presented in five different intensities (120, 110, 100, 90 and 80 dB), each for four trials in a pseudorandom order. Maximum startle responses (Vmax) were recorded for each trial and averaged for each stimulus intensity per subject. Emx1/Htr4 cKO mice showed significantly larger startle response at the 120 dB intensity of acoustic stimulus, compared to their control littermates (Vmax at 120 dB; cKO-VEH: 484 ± 38, WT-VEH: 404 ± 36, p=0.001, n= 21, 21, respectively) (**Figure 2.17B**), demonstrating that the loss of pallial 5-HT_4R led to increased startle responses. Following chronic treatment with fluoxetine, both Emx1/Htr4 cKO mice and control littermates showed significantly decreased startle responses overall (Two-way ANOVA, WT-VEH/FLX: p=0.0078, cKO-VEH/FLX: p=0.0004), indicating that chronic fluoxetine treatment in mice reduces ASR independent of pallial 5-HT_4R. There was not any significant difference in ASR between Emx1/Htr4 cKO and their control littermates treated with chronic fluoxetine, suggesting that the treatment was compensated for the effects of the loss of pallial 5-HT4R.

To measure PPI, 120 dB acoustic stimuli preceded by four different pre-pulse (PP) intensities (0, 3, 6, 12 dB) were presented, each for ten trials in a mixed order. Maximum startle responses (Vmax) were recorded for each trial and averaged for each pre-pulse intensity per subject. PPI was measured as percent (%) inhibition which is the percent decrease in startle response in PP3, PP6 and PP12 compared to PP0 per subject.

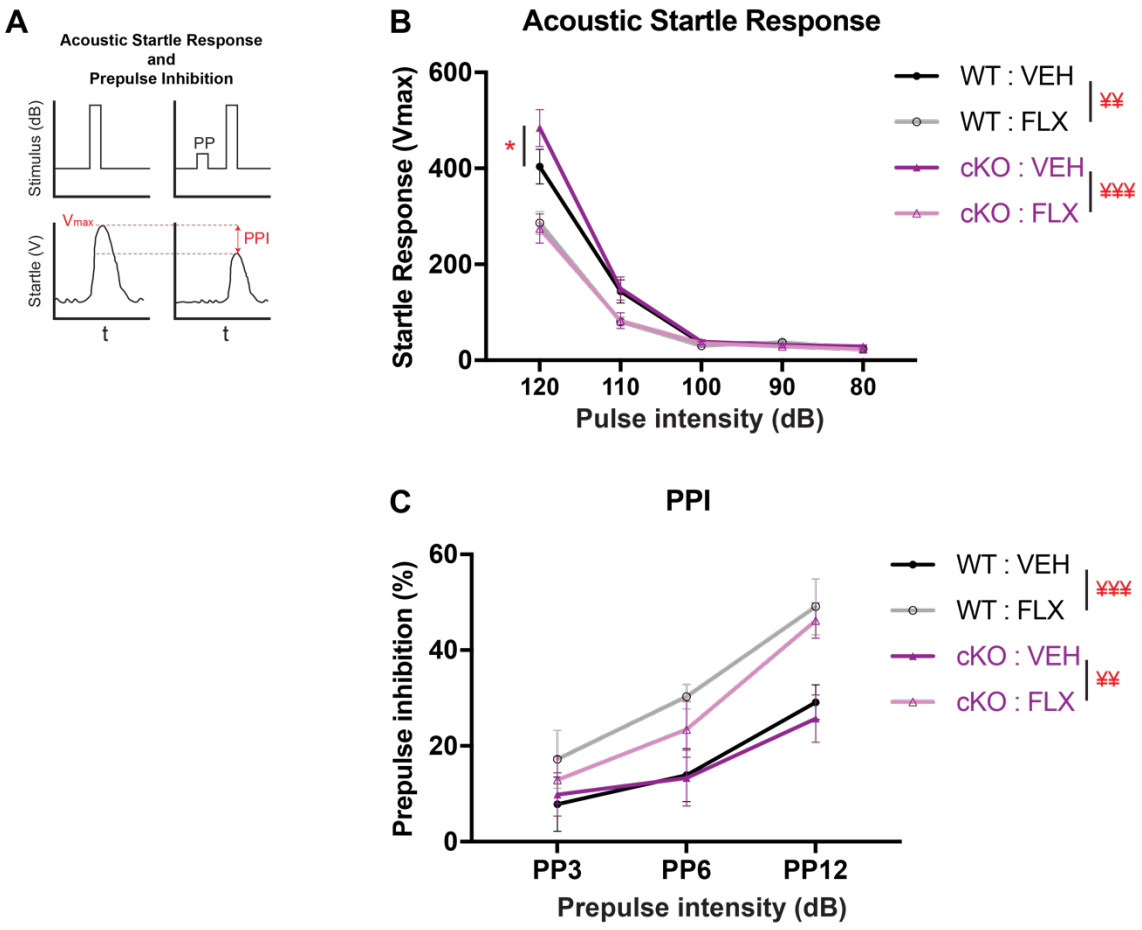

Figure 2.17. The loss of pallial 5-HT$_4$R led to increased acoustic startle responses.
(A) Schematic representation of the acoustic startle and prepulse inhibition paradigm. Mice that are subjected to a sudden, intense auditory stimulus exhibit startle responses. Prepulse inhibition (PPI) is the suppression of the startle response when a startling acoustic stimulus is preceded by an immediate, weaker pre-pulse (PP).
(B) Emx1/Htr4 cKO mice (cKO-VEH) showed significantly larger startle response at the 120 dB, compared to their control littermates (WT-VEH). Following chronic treatment with fluoxetine, both Emx1/Htr4 cKO mice and control littermates showed significantly decreased startle responses.
(C) Emx1/Htr4 cKO (cKO-VEH) did not show any changes in PPI, compared to control littermates (WT-VEH). Following chronic treatment with fluoxetine, both Emx1/Htr4 cKOs and controls exhibited significantly enhanced PPI.
Data are represented as mean ± SEM. Two-way ANOVA followed by post hoc Fisher's LSD test. *p<0.05, ¥¥p<0.01, ¥¥¥p<0.001.

Emx1/Htr4 cKO did not show any changes in the inhibition of the startle reflex with any pre-pulse stimuli and overall, compared to control littermates (Two-way ANOVA, p=0.88) (**Figure 2.17C**). Following chronic treatment with fluoxetine, both Emx1/Htr4 cKOs and controls exhibited significantly enhanced pre-pulse inhibition overall (Two-way ANOVA, WT-VEH/FLX: p=0.0004, cKO-VEH/FLX: p=0.0074), indicating that chronic fluoxetine treatment in mice enhances the PPI independent of pallial 5-HT_4R. Even though baseline startle responses were lower in Emx1/Htr4 cKO, the prepulse inhibition of startle was more significant with fluoxetine, indicating that the decrease in ASR in the cKO was not a confounding factor in PPI.

2.4.10. Social Interaction

Social withdrawal represents a common symptom in psychiatric conditions such as depression, social anxiety, and PTSD (Ressler et al., 2015). The three-chamber sociability test was developed as an ethologically relevant test for rodents to measure sociability and lower sociability may be associated with increased anxiety-like behaviors (File, 1985; Kaidanovich-Beilin et al., 2011). In this test, the subject is placed in the center chamber and allowed to freely explore the other two chambers, one of which contains a novel mouse while the other contains an unfamiliar inanimate object (Lego® piece) (**Figure 2.18A**). Decreased time spent in interacting with the novel mouse can be interpreted as social avoidance, an anxiety-related phenotype.

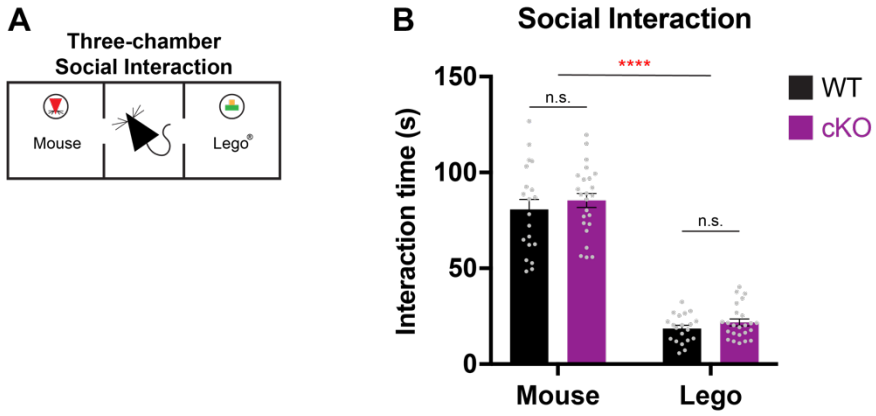

Figure 2.18. Emx1/Htr4 cKO mice showed normal social interaction.
(A) Schematic representation of the three-chamber social interaction test. Mice were placed in the center chamber and allowed to freely explore the other two chambers, one of which contains a strange mouse (red) while the other contains a Lego® piece (yellow and green), both inside identical wire containment cups. Time spent in interacting with the novel mouse is a measure of social interaction.
(B) Emx1/Htr4 cKO did not show any difference in time spent interacting the novel mouse in the three-chamber sociability test, compared to control littermates (WT-VEH). For both groups, social interaction time was significantly higher than time spent interacting with Lego®.
Data are represented as mean ± SEM. Two-way ANOVA followed by post hoc Fisher's LSD test. ****$p<0.0001$, n.s. $p>0.05$.

Emx1/Htr4 cKO did not show any difference in time spent interacting the novel mouse in the three-chamber sociability test, compared to control littermates (cKO: 85 ± 4 s, WT: 81 ± 5 s, p= 0.32, n=28, 25 respectively) (**Figure 2.18B**). For both groups, social interaction time was significantly higher than time spent interacting with Lego®. Together, these result show that Emx1/Htr4 cKO mice did not show any social anxiety-like phenotype in this paradigm.

2.4.11. Summary of the behavior analysis of Emx1/Htr4 cKO mice

The loss of functional 5-HT_4R from excitatory neurons in mouse pallial brain structures including the hippocampus and neocortex led to elevated anxiety-like behaviors in mice; significantly in the EPM and ASR, and slightly in the OF. This effect was not detected in other anxiety-based assays such as NSF and three-chamber social interaction. Chronic antidepressant treatment was anxiogenic in control mice in the OF and EPM. Interestingly, this response was not observed when the functional 5-HT_4R in the pallium was ablated. In addition, the loss of 5-HT_4R in the pallium did not alter depression-like behaviors and chronic antidepressant responses in the NSF, TST, FST, sucrose preference test and marble burying test. It only led to slightly enhanced basal hedonia levels in splash test. Finally, the ablation of pallial 5-HT_4R did not result in any changes in basal sensorimotor processing during the PPI assessment while chronic fluoxetine improved it independent of 5-HT_4R.

2.5. Discussion

2.5.1. Generation of new tools to study 5-HT_4R function in the brain

We have successfully generated a new tool, Htr4-floxed mice, to study the function of 5-HT_4R in specific cell types. By employing an intersectional strategy using Emx1-Cre and Htr4-floxed mice, we restricted the conditional knockout of the 5-HT_4R in the excitatory neurons in brain regions of pallial origin, such as the hippocampus and neocortex. This approach allowed us to analyze 5-HT_4R function in anxiety and mood related behaviors in a region and cell type specific manner. In addition, a conditional knockout strategy may circumvent compensatory neuroplastic changes in a constitutive knockout approach to some extent. Therefore, our *Htr4* conditional knockout mice is an invaluable tool for the investigation of the function of 5-HT_4R, not only in the emotion circuitry but also in other biological processes. We also identified an shRNA for the efficient knockdown of *Htr4* expression as a valuable tool for AAV-mediated gene knockdown experiments.

We initially crossed Htr4-floxed mice to Emx1-Cre reporter line and generated Emx1/Htr4 cKO mice to confirm the functional loss of 5-HT_4R in pallial structures and investigate its behavioral consequences. We showed the deletion of exon 5 in the mouse hippocampus and neocortex by qRT-PCR at the RNA level. While the exon 5 was deleted, exon 5 deleted *Htr4* mRNA was still being produced. The increase in the cKO mRNA expression in the hippocampus of

Emx1/Htr4 cKO was possibly due to a compensation mechanisms detecting the absence of wildtype 5-HT_4R and effectively increasing the *Htr4* transcription. Nonetheless, this would not have any effect on the efficiency of the cKOs.

We expected that the deletion of exon 5 in *Htr4* would result in a truncated protein due to immediate early stop codons generated right after exon 5. This was not the case, at least in a heterologous system, when we cloned the mutant *Htr4* cDNA and overexpressed in HEK cells. We detected the expression of the cKO 5-HT_4R protein tagged with MYC epitope using anti-MYC immunofluorescence. This could be due to the possibility that the overexpression may have led to some translational read through at the early stop codons. Nevertheless, the cKO 5-HT_4R seemed not to localize on the cellular membrane. Furthermore, we confirmed that the cKO 5-HT_4R was non-functional as it did not increase intracellular cAMP levels upon 5-HT_4R agonist stimulation in HEK cells.

As another tool to study 5-HT_4R in laboratory settings, we have successfully generated a novel custom polyclonal antibody that could detect the mouse 5-HT_4R protein in both a heterologous system and fixed mouse brain tissues. Our initial commercial antibody screening did not yield any reliable antibodies possibly due to the fact that they were generated against custom peptide sequences of human 5-HT_4R. Our custom antibody was generated against a custom peptide sequence in the third cytoplasmic domain of mouse 5-HT_4R. The difference in immunolabeling between two batches produced by two rabbits was possibly a result of the heterogeneity in the immune responses

between rabbits. Further studies using this antibody will help extend our knowledge in the cellular localization of 5-HT_4R in vivo.

2.5.2. 5-HT_4R in the excitatory neurons of pallial origin mediates anxiety-like behaviors

The behavioral analysis of Emx1/Htr4 cKO mice revealed decreased basal levels of anxiety-like behaviors in the cKO. These data suggest that 5-HT_4R may be necessary in the excitatory neurons of pallial origin to mediate the anxiety levels at appropriate levels.

The decrease in the locomotor activity in only the first 10 min of the open field test in Emx1/Htr4 cKO mice may be attributed to attenuated response to novelty as seen in the constitutive *Htr4* knockout line (Compan, 2004). This may be also interpreted as an anxiogenic response to the novel arena since the locomotor activity is at normal levels for the rest of the OF test as the animal habituates. In addition, the loss of 5-HT_4R did not alter locomotor activity in the EPM test. Therefore, we conclude that locomotor activity did not influence the anxiety-like behavioral measurements over 60 min in the OF and in the EPM. Moreover, enhanced acoustic startle responses seen following the ablation of pallial 5-HT_4R may be attributed to anxiogenic effects. On the other hand, other anxiety-related behaviors such as hyponeophagia and social interaction were not altered in Emx1/Htr4 cKO mice. This may be due to the differences in the nature of the assays, such as the sensitivity in the measurement parameters, or the

distinct factors inducing the anxiety-like behaviors. Furthermore, the expression of 5-HT_4R in the pallium was not necessary for the modulation of mood related behaviors in mice in the TST, FST, sucrose preference test and marble burying test. It is important to note that the slightly enhanced hedonic behaviors observed in the splash test may be relevant to regulation of mood.

Our findings suggest that 5-HT_4R mediates anxiety-like behavior through modulating hippocampal and/or neocortical excitatory circuits. Further studies using cell type specific driver lines in the hippocampus and cortex or spatially restricted conditional manipulations of 5-HT_4R expression is necessary to further dissect the role of 5-HT_4R in anxiety related behaviors.

2.5.3. Pallial 5-HT_4R is not necessary for behavioral responses to chronic SSRI treatment

We further investigated the involvement of pallial 5-HT_4R in the therapeutic actions of SSRIs. Our results suggest that 5-HT_4R in the pallial excitatory neurons is not necessary for antidepressant mediated behavioral effects in the NSF, TST, FST, marble burying, acoustic startle responses and PPI. Although chronic SSRI treatment increased the level of *Htr4* mRNA expression in p11 layer 5 pyramidal cells in neocortex, and the deletion of p11 from these cells blunted the responses to antidepressants, our results suggest that this increase was not necessary to mediate the p11 dependent antidepressant responses. *Htr4* upregulation may be a result of secondary

mechanisms and it may not play a critical role in the antidepressant response. On the other hand, it is possible that 5-HT_4R is mediating other characteristics of antidepressant response (efficacy, time-course etc.) for which current behavioral assays may not be sensitive enough to assess. An intriguing possibility supported by our data is that 5-HT_4R in the neocortex or hippocampus may regulate other antidepressant effects that are not related to anhedonia or despair-like behavior. In fact, our results showed that anxiogenic responses induced by chronic fluoxetine were not observed when the functional 5-HT_4R in the pallium was ablated. This suggests that 5-HT_4R may modulate anxiogenic side effects of SSRIs that are observed in clinical settings in some patients (Sinha et al., 2017), and in preclinical settings in naïve rodents (Baek et al., 2015). Another possibility to consider is that the anxiogenic effects of fluoxetine may have not been detectable in the OF and EPM due to the already anxiogenic profile seen after the genetic manipulation.

We also showed that the loss of pallial 5-HT_4R led to increased acoustic startle responses, an indication for enhanced anxiety-like behaviors. However, the effects of chronic fluoxetine, which was anxiogenic in the OF and EPM, on ASR was diminishing suggesting that ASR may be a measure discriminating between anxiogenic and antidepressant-like responses. On the other hand, PPI was enhanced following treatment with chronic fluoxetine, suggesting an enhancement in sensorimotor gating. This effect has also been documented in other rodent studies (Vorhees et al., 2011) and SSRIs were indicated to reduce

some symptoms of Schizophrenia patients (Singh et al., 2018). It is possible that enhanced serotonergic tone acts on various circuitries responsible for the execution and modulation of startle responses (emotion, sensorimotor gating etc.). The mechanism of action of enhanced central serotonin on the circuitry of startle reflex and the inhibition of startle via sensory gating is needed to be studied more in detail for a better understanding on how SSRIs may change these behaviors.

2.5.5. Caveats and future directions

We restricted the ablation of 5-HT_4R to the pallium, including almost all excitatory neurons in the hippocampus and neocortex, and some in basal and lateral amygdala. It is possible that this manipulation may not be specific enough to detect circuit or cell type specific roles of 5-HT_4R in distinct emotive behaviors. There may still have been adaptive changes compensating for the absence of 5-HT_4R in the pallium. Indeed, for example, neuroadaptations in cholinergic systems such as the hyperfunction of muscarinic receptors maintains memory processing in a constitutive *Htr4* KO mice (Segu et al., 2010). Moreover, 5-HT_4R expressing neurons in the hippocampus, neocortex and amygdala may have contradicting regulations on the same downstream circuits, shadowing its functional deficit in defined circuits.

The discrepancy in the response of naïve control mice to chronic fluoxetine (anxiogenic versus antidepressant-like) observed in anxiety-based

tests (EPM/OF versus NSF, respectively) may be due to the participation of distinct brain areas engaged in each test. The NSF relies on feeding and it was shown to respond to only chronic fluoxetine treatment. In addition, the daily drug dosage, the timing and means of drug administration (injection, drinking water, oral gauge etc.), and the mouse strain has been also shown as major sources of variation in behavioral responses (Võikar et al., 2001). The inconclusive response to chronic fluoxetine in the FST could also be ascribed to the mouse strain since many studies found the effects of acute or chronic SSRI treatments in C57Bl/6J mouse strain to be ineffective (Petit-Demouliere et al., 2005).

It remains to be investigated whether 5-HT_4R is involved in the development of the pathological anxiety and depression related behaviors upon chronic stress and whether the treatment of the pathological anxiety and depression in animal models of depression via SSRIs depend on the 5-HT_4R at any levels. Lastly, 5-HT_4R may regulate other behaviors beyond anxiety and mood in the hippocampus and cortex considering the involvement of these regions in cognition, learning and memory which will be investigated in Chapter 5.

2.5.6. Conclusion

Our findings show that 5-HT_4R in pallial excitatory neurons are necessary to modulate anxiety-like behaviors, but does not mediate the antidepressant-like behavioral responses to chronic SSRI administration. Following chapter will focus

on dissecting the role of 5-HT_4R in distinct cell populations in the hippocampus and neocortex to better understand these results.

CHAPTER 3.

DISSECTION OF CELL TYPE SPECIFIC 5-HT_4 RECEPTOR FUNCTION IN THE HIPPOCAMPUS AND NEOCORTEX IN ANXIETY AND DEPRESSION

3.1. Introduction

The hippocampus and neocortex has been two of the most highly implicated brain regions in the pathophysiology and treatment of anxiety and mood disorders due to their extensive involvement in emotive and cognitive circuitries. In Chapter 2, we investigated the consequences of the loss of function of 5-HT_4 Receptor in the excitatory circuits of pallium, including these two regions. However, pallial neurons are comprised of many cell types which may have opposing functions within the extended limbic circuit. Therefore, to tease apart the function of 5-HT_4R in more defined cell types and circuits, we investigated the behavioral consequences of the conditional loss of 5-HT_4R specifically from either the hippocampus or a subpopulation of cortical layer 5a projection neurons that express p11. Our results indicating a role for pallial 5-HT_4R in anxiety related behaviors and anxiogenic effects of antidepressants emphasize the need to selectively target distinct cell populations to further understand the underlying circuits mediating these behaviors.

3.1.1. Hippocampus in anxiety and depression

3.1.1.a. Hippocampal circuitry in the rodent brain

Understanding the function and modulation of hippocampal circuits within its own boundaries and among other limbic structures requires a perspective of

the physical and functional anatomy of hippocampal formation (for extended review (The Hippocampus Book, 2007)). The hippocampus is a medial temporal lobe structure that is crucially involved in episodic memory and spatial navigation as well as emotional memory and responses (Strange et al., 2014). In animal studies, the hippocampus describes dentate gyrus (DG) and *cornu ammonis* (CA) subfields. Hippocampal formation is a more comprehensive term that also includes subiculum complex and entorhinal cortex. It has a long, curved form that is present across all mammals, and that runs along a dorsal (septal) to ventral (temporal) axis in rodents, corresponding to a posterior-to-anterior axis in humans. The major intrinsic circuitry is maintained throughout the long axis and across species: a unidirectional circuit from the entorhinal cortex to the hippocampus, specifically to the dentate gyrus - to - CA3 - to - CA1 - to - the subiculum and back to the entorhinal cortex (Deng et al., 2010) (**Figure 3.1A**).

The dentate gyrus is comprised of three cell layers (**Figure 3.1A**). The principal cell layer (granule cell layer) is made up of a densely-packed granule cells. Superficial to this layer, the molecular layer is a relatively cell-free and where the dendrites of granule cells lie. The granule cell and molecular layers form the U-shaped structure that encloses the polymorphic cell layer, the third layer of the dentate gyrus, in the hilus of DG. In this layer, mossy cells and various types of interneurons are located (Freund and Buzsáki, 1996). The dentate gyrus receives major glutamatergic input from the entorhinal cortex via the perforant pathway that primarily innervates the molecular layer (van Groen et

al., 2003). Other brain regions also projects to the DG via serotonergic, norephinephrinergic, dopaminergic, cholinergic and GABAergic inputs. The dentate gyrus projects to CA3 region outside this structure. Other projections are made within DG amongst granule cells, interneurons, and hilar mossy cells.

The principal neuronal cell type of the CA fields is the pyramidal cell which makes up most of the neurons in the pyramidal cell layer. Pyramidal cells have basal dendrites that extends into the infrapyramidal region (stratum oriens) and an apical dentride that extends towards the hippocampal fissure to the suprapyramidal region (stratum radiatum) (**Figure 3.1A**). As in the dentate gyrus, there is a heterogeneous group of interneurons that are scattered through all layers (Freund and Buzsáki, 1996). Most of the synaptic input to CA fields arises from within its own boundaries. CA3 and CA2 are heavily innervated by collaterals of their own axons (i.e., associational connections), and from axons of the contralateral CA3 and CA2 (i.e., commissural connections). CA1, in turn, receives its heaviest input from collateral CA3 (via Schaffer collateral).

The hippocampus is connected to other brain regions through three major fiber systems. The angular bundle carries fibers between the entorhinal cortex and the other fields of the hippocampus (Deller et al., 1996). The fimbria-fornix pathway interconnects the hippocampus with the basal forebrain, hypothalamus, and brain stem (Daitz and Powell, 1954). Lastly, the dorsal and ventral commissures connect the hippocampal formation across hemispheres (Laurberg, 1979).

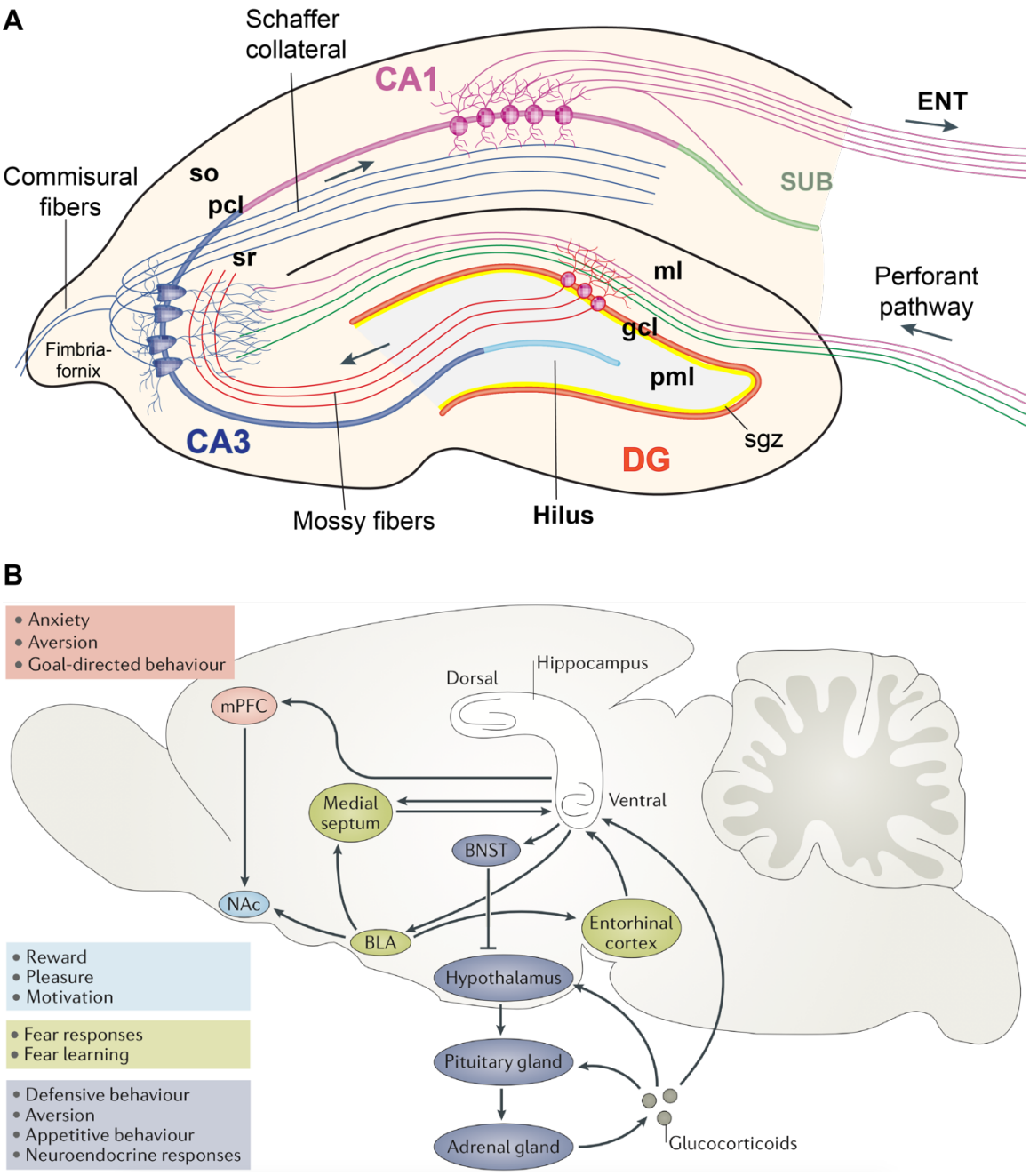

Figure 3.1. Hippocampal circuit and its role in anxiety and mood regulation.
A. An illustration of basic hippocampal circuitry. Modified from Deng et al. (2010). DG: dentate gyrus, SUB: subiculum, ENT: entorhinal cortex, mi: molecular layer, gcl: granule cell layer, pml: polymorph layer, sgz: subgranular zone, so: stratum oriens, pcl: pyramidal cell layer, sr: stratum radiatum.
B. The neural circuitry of anxiety and mood involving the ventral hippocampus. Adapted from Anacker et al. (20017). See text for details.

3.1.1.b. The neural circuitry of anxiety and mood along the dorsoventral axis of the hippocampus

Despite the conserved intrinsic circuitry, animal and human studies have shown that the hippocampus is functionally not uniform along the septotemporal (dorsoventral) axis (Strange et al., 2014). In rodents, lesion studies have been used to examine the differential functions of the dorsal and ventral hippocampus (dHIPP and vHIPP, respectively). These studies indicated that dorsal parts of the hippocampus mediate cognitive functions, particularly spatial memory (Morris et al., 1982) and contextual learning (Kheirbek et al., 2013). By contrast, the vHIPP has been implicated in emotional behavior, social interactions and stress resilience (Felix-Ortiz and Tye, 2014; Henke, 1990; Moser et al., 1993). Furthermore, the human anterior hippocampus, which is analogous to the ventral hippocampus in rodents, is smaller in patients with depression and larger in antidepressant-treated patients than in healthy individuals (Boldrini et al., 2014). Non-human primates with increased anxiety-like behavior and neuroendocrine activity also show an increase in metabolism in the anterior hippocampus (O'Leary and Cryan, 2014; Shackman et al., 2013).

The role of vHIPP in anxiety and mood regulation is also supported on the basis that ventral connectivity with the other limbic structures regulating emotion is heavier than those of dorsal. This circuit involves glutamatergic projections to several structures that are involved in anxiety regulation, stress responses and reward seeking (**Figure 3.1B**). For instance, the projections to the medial

prefrontal cortex (mPFC) promote anxiety and stress susceptibility (Padilla-Coreano et al., 2016), and are also involved in antidepressant actions (Bagot et al., 2015). Moreover, bidirectional connections between the vHIPP and the amygdala have been implicated in fear and anxiety responses (Tovote et al., 2015), social interaction (Felix-Ortiz and Tye, 2014), and the consolidation of emotive memories (Richardson et al., 2004). There are also glutamatergic projections from the vHIPP to the nucleus accumbens (NAc), promoting reward-seeking behavior in the absence of stress (Britt et al., 2012), while inducing anxiety-like and depressive-like behavior during stress (Bagot et al., 2015). Furthermore, glutamatergic projections from the vHIPP to bed nucleus of the stria terminalis (BNST) drive the inhibition of hypothalamus–pituitary–adrenal (HPA) axis activity and glucocorticoid release (Anacker et al., 2016).High levels of glucocorticoids during chronic stress have been linked with depression, reduced hippocampal neurogenesis and neuronal atrophy (David et al., 2009; Watanabe et al., 1992)

It should be noted that differences in the connectivity with cortical and subcortical structures along the dorsoventral axis of the hippocampus are gradual, which suggests that functional differences along this long axis may also exhibit a gradient-like organization (Amaral and Witter, 1989; Kjelstrup et al., 2008). Given the extensive evidence suggesting a role for the hippocampus in mediating emotive behaviors, it remains a central structure to identify specific

cellular or molecular targets for better therapeutics in anxiety and mood disorders.

3.1.1.c. Serotonergic modulation of the hippocampus

Consistent with the functional organization along the dorsoventral axis of the hippocampus, the more ventral parts receive stronger monoamine projections, such as serotonin (5-HT) (Gage and Thompson, 1980). The dorsal raphe nucleus (DRN) serotonergic neurons projects extensively along the long axis of the hippocampus whereas the projections from the median raphe nucleus (MRN) is limited to dorsal parts (McQuade and Sharp, 1997). The serotonergic terminals are primarily located in the subgranular zone of dentate gyrus (Swanson, 1987).

Majority 5-HT receptors are expressed in the hippocampus. They display expression patterns that varies along the dorsoventral axis, between the CA fields and DG and amongst cell-types (Tanaka et al., 2012). Due to this heterogeneous expression pattern and that many hippocampal neurons express a combination of both excitatory and inhibitory 5-HT receptors with varying affinity to 5-HT, the modulatory effect of 5-HT is under a complex regulation. For example, in dentate gyrus granule cells, the inhibitory 5-HT_{1A} heteroreceptors are the highest expressed serotonin receptor (Yohn et al., 2017) with the most affinity to 5-HT (Nichols and Nichols, 2008). Thus, the effect of 5-HT is overall inhibitory in these cells. However, the co-expression of other excitatory receptors, such as

5-HT_4R, has been shown to regulate the strength of this inhibitory action. For example, in CA1, the stimulation of 5-HT_4R has been shown to increase the excitability of the pyramidal cells (Torres et al., 1995; 1994).

It has been appreciated that antidepressant treatment increase adult hippocampal neurogenesis (Santarelli et al., 2003), some being preferentially in the ventral DG (Banasr et al., 2006; Jayatissa et al., 2006). Some evidence suggests that serotonin receptors in DG may mediate this action. For example, 5-HT_{1A}R in the DG was necessary for neurogenic effects of chronic fluoxetine administration and behavioral antidepressant responses (Samuels et al., 2015). Furthermore, a subchronic activation of 5-HT_4R by an agonist was sufficient to observe enhanced neurogenesis together with anxiolytic and antidepressant-like behavioral responses (Lucas et al., 2007). Whether the hippocampal 5-HT_4R mediates these behaviors remains to be investigated.

Given that most 5-HT receptors are expressed on both excitatory and inhibitory interneurons and can function in either a stimulatory or inhibitory manner depending on the receptor subtype, it would be expected that the net effect of 5-HT on hippocampal function depends on the local 5-HT concentration, and the ratio and level of expression of different 5-HT receptor subtypes in a particular population of cells. Thus, upon SSRI treatment, the change in local 5-HT concentrations in distinct brain regions would determine which 5-HT receptor subtypes become engaged. In addition, in disease conditions or after chronic SSRI treatment, the desensitization or chronic activation of 5-HT receptors may

lead to changes in 5-HTR expression. Therefore, understanding the functions of 5-HTRs in specific hippocampal cell types in mediating anxiety and mood may give novel insights for the development of optimized therapies.

3.1.2. Neocortex in anxiety and depression

The neocortex has been implicated in mediating key symptoms in anxiety and mood disorders, due to its executive role in the limbic system and extensive connections with the hippocampus, amygdala, striatum, nucleus accumbens and raphe nuclei (Price and Drevets, 2012). For example, altered cortical feedback to amygdala was correlated with dysphoric emotions in humans (Drevets et al., 2008) and heightened anxiety in both humans and monkeys (Birn et al., 2014). The antidepressant effects of deep brain stimulation of the medial prefrontal cortex (mPFC) are associated with restoration of both cortical and subcortical brain activity to normal levels (Mayberg et al., 2005; Nahas et al., 2010). In rodents, the mPFC-amygdala connections were also indicated to signal safety and regulate anxiety (Likhtik et al., 2014). Additionally, chronic stress impairs the structure and function of neurons in the mPFC (Radley et al., 2006), while optogenetic stimulation of the mPFC reverses these deficits and exerts antidepressant-like effects (Covington et al., 2010). In addition, surrounding cortical structures such as the orbitofrontal cortex, anterior cingulate cortex, and sensory-motor cortices have been associated with the pathological symptoms of anxiety and mood disorders (Drevets et al., 2008). Nevertheless, the specific cell

types and molecular mechanisms that mediate the role of different cortical regions in anxiety and mood regulation remain largely unknown.

3.1.2.a. Cortical circuitry in the rodent brain

The mammalian neocortex is divided into six major layers. The layer 4 defines the major input layer from thalamus and layer 5 defines the major output layer that sends long distance subcortical and callosal projections. The superficial layers 2 and 3 are involved in corticocortical connectivity and provide two-thirds of the input to all neurons in the neocortex, while the deepest layer 6 is primarily important for sending feedback to the thalamus. In addition to the laminar structure of the neocortex, there are distinct functionally defined regions parceled along the tangential axis. The cortical areas can be divided into three general functional modalities: sensory cortices (including the primary somatosensory, auditory and visual cortices), motor cortices (including the primary motor cortex), and association cortices (including the prefrontal and secondary motor cortices).

The neocortex, basal ganglia and thalamus are interconnected and closely involved in the forebrain function (Alexander et al., 1986). There are three major types of excitatory cortical neurons mainly classified by axonal anatomy: intratelencephalic (IT), pyramidal tract (PT) and corticothalamic (CT) neurons (Shepherd, 2013) (**Figure 3.2A**). IT neurons project ipsi- or bilaterally within the neocortex and striatum (telencephalon), yet not to outside the telencephalon

such as the thalamus or brainstem. Layer 2/3 neurons only have corticocortical (CCor) projections while layer 4 neurons (stellate cells) have only local axonal connections. IT neurons in layer 5 have both corticocortical (CCor) and corticostriatal (CStr) projections. PT neurons are restricted to layer 5b. Their final projections are in the brain stem structures such as the pons (corticopontene – CPn neurons), or in the spinal cord (corticospinal – CSpi neurons). They also send collateral branches off the pyramidal tract to innervate ipsilateral cortex and other subcortical regions such as the striatum, thalamus, midbrain, etc. Notably, the striatum is unique among all subcortical areas in receiving both IT and PT inputs. CT neurons form a third class of cortical projection neurons located in layer 6 and innervating the thalamus, but not the striatum.

3.1.2.b. Serotonergic modulation of the neocortex

The cortical circuits undergo extensive modulation by monoaminergic systems, including serotonin. Serotonin has heterogeneous effects on cortical neurons mostly due to the differential distribution of the serotonin receptors in distinct cell types. For example, the expression of 5-HT_{2A} receptors is the highest in layer 5a, which is enriched in IT-CStr neurons (Weber and Andrade, 2010). Consequently, 5-HT seems to biphasically inhibit (via 5-HT_{1A} receptors) and excite (via 5-HT_{2A} receptors) IT neurons while mostly inhibiting (via 5-HT_{1A} receptors) PT neurons (Avesar and Gulledge, 2012). In addition, IT-CStr neurons have higher expression of 5-HT_{1B}R and 5-HT_4R than PT neurons (Egeland et al., 2011a).

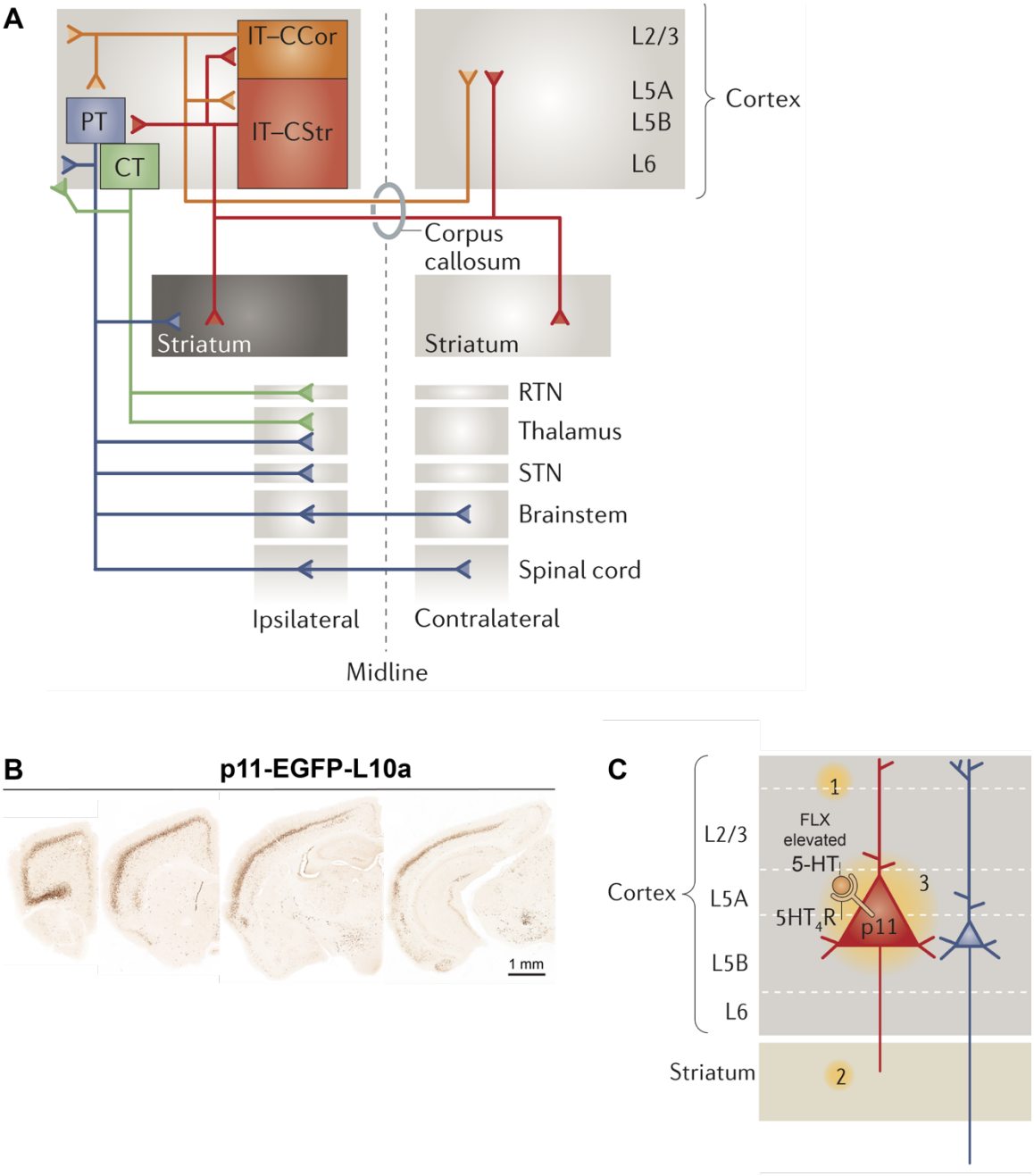

Figure 3.2. Corticostriatal circuit and its role in mood regulation.
A. Three major groups of excitatory cortical neurons and their axonal projections. IT: inratelencephalic (CStr: corticostriatal, CCor: corticocortical), PT: pyramidal track, CT: corticothalamic. Adapted from Shepherd (2013).
B. p11 expressing cells in p11-EGFP-L10a (bacTRAP) mouse line, detected by anti-EGFP immunohistochemistry. Modified from gensat.org.
C. IT-CStr-related changes in major depressive disorder (MDD). Changes affecting the CStr projection in MDD include abnormal activity in (1) neocortex and (2) striatum in human imaging studies, and (3) IT-CStr p11 cell specific upregulation of 5-HT_4R by chronic treatment with fluoxetine (FLX). There were no observed effects on PT neurons (blue). Modified from Shepherd (2013).

A recent study from our lab also indicated that a population of IT-CStr neurons mediate behavioral responses to chronic antidepressant administration (Schmidt et al., 2012). These cells are p11 expressing pyramidal cells, located in the upper layer 5 (5a) and projecting primarily to dorsal striatum and contralateral neocortex (**Figure 3.2B**). These neurons showed a robust molecular response upon chronic fluoxetine treatment including a significant increase in the expression of *Htr4*, compared to non-responsive neighboring PT-CPn neurons (**Figure 3.2C**). These results combined with the growing body of evidence indicating a role for the dorsal striatum in reward processing, motivated behavior and MDD pathology suggests that p11 CStr cells may underlie the antidepressant responses (Delgado, 2007; Pizzagalli et al., 2009). However, whether the CStr 5-HT_4R mediates the behavioral consequences of SSRI action had yet to be investigated.

Our findings by ablating 5-HT_4R from pallial excitatory neurons indicated that the antidepressant-like effects of chronic fluoxetine were not dependent on 5-HT_4R. However, it is still possible that the loss of 5-HT_4R from all cells in the neocortex including IT and PT projection neurons may have triggered compensation mechanisms during development or affected pallial circuits in opposing ways, shadowing the possible roles of 5-HT_4R in antidepressant response in CStr p11 pyramidal cells. Therefore, a more specific and powerful approach was essential to genetically manipulate the expression of 5-HT_4R only in p11 cells.

3.2. Cell type specific dissection of the role of 5-HT_4R in the hippocampus and neocortex in anxiety and depression related behaviors

3.2.1. Drd3-Cre driver line to target the hippocampus

Although Emx1-Cre line comprehensively targets the excitatory neurons in the hippocampus and neocortex, it is important to have a driver line that exclusively targets the hippocampus to study hippocampus-specific effects of a conditional genetic manipulation. We selected Drd3-Cre KI198 line (Drd3-Cre, generated by GENSAT Project) because it expresses Cre in the hippocampus the most exclusively and comprehensively among the available driver lines. This transgenic line was generated by using a BAC clone, which was constructed by inserting a Cre recombinase gene at the initiating ATG codon of the first coding exon of the *Drd3* gene in the BAC. Hence, Cre expression is driven by the regulatory sequences of *Drd3* in the BAC.

To reveal the Cre expressing cells, we crossed Drd3-Cre line with Cre-dependent transgenic reporter expressing ribosomal protein L10a (RPL10a) fused with EGFP (EGFP-L10a). **Figure 3.3** shows the anti-EGFP immunohistochemistry in coronal sections from the most rostral (top left) to the most caudal (bottom right) of a Drd3-Cre::EGFP-L10a mouse brain. Cre was expressed in the dentate gyrus in the granule cells layer, and some cells in the polymorph layer in the hilus throughout the dorsoventral axis (dorsal DG (dDG), intermediate DG (iDG) and ventral DG (vDG)). In the CA3 field of the

hippocampus, Cre mediated EGFP expression was observed in the pyramidal cell layer consistently along the dorsoventral axis (in dCA3 iCA3 and vCA3). Finally, in the CA1 field, Cre targets many pyramidal cells of dorsal parts (dCA1). Notably, the number of Cre expressing cells decreases as a gradient towards the ventral CA1 region, leaving only a scatter of Cre positive cells in the pyramidal layer of the vCA1. Outside the hippocampus, Cre expressing cells were observed in a small cell population in the very rostral part of the lateral septum (LS), in the islands of Calleja (ICj) as well as a few scattered cells in the dorsal nucleus accumbens (NAc) and the medial mammillary nucleus (MM) of the hypothalamus (HY).

Although, the CA1 is not fully targeted, we selected this driver line since it targets most of the cells in the excitatory neuron layers in hippocampus in which hippocampal *Htr4* is primarily expressed. In addition, among the available Cre driver lines, it has the least number of Cre-expressing cells outside the hippocampus, making it a highly specific line for targeting the whole hippocampus. Also note that, since endogenous *Drd3* gene (Dopamine Receptor D3) is expressed in other brain cells in regions such as neocortex and striatum, this BAC transgenic Drd3-Cre line did not fully recapitulate the *Drd3* expression pattern. Nevertheless, it is useful as a tool to drive Cre-mediated genetic manipulations specific to the hippocampus. Therefore, we crossed this line to our Htr4-floxed line to investigate hippocampus specific functions of 5-HT_4R in emotion and cognition.

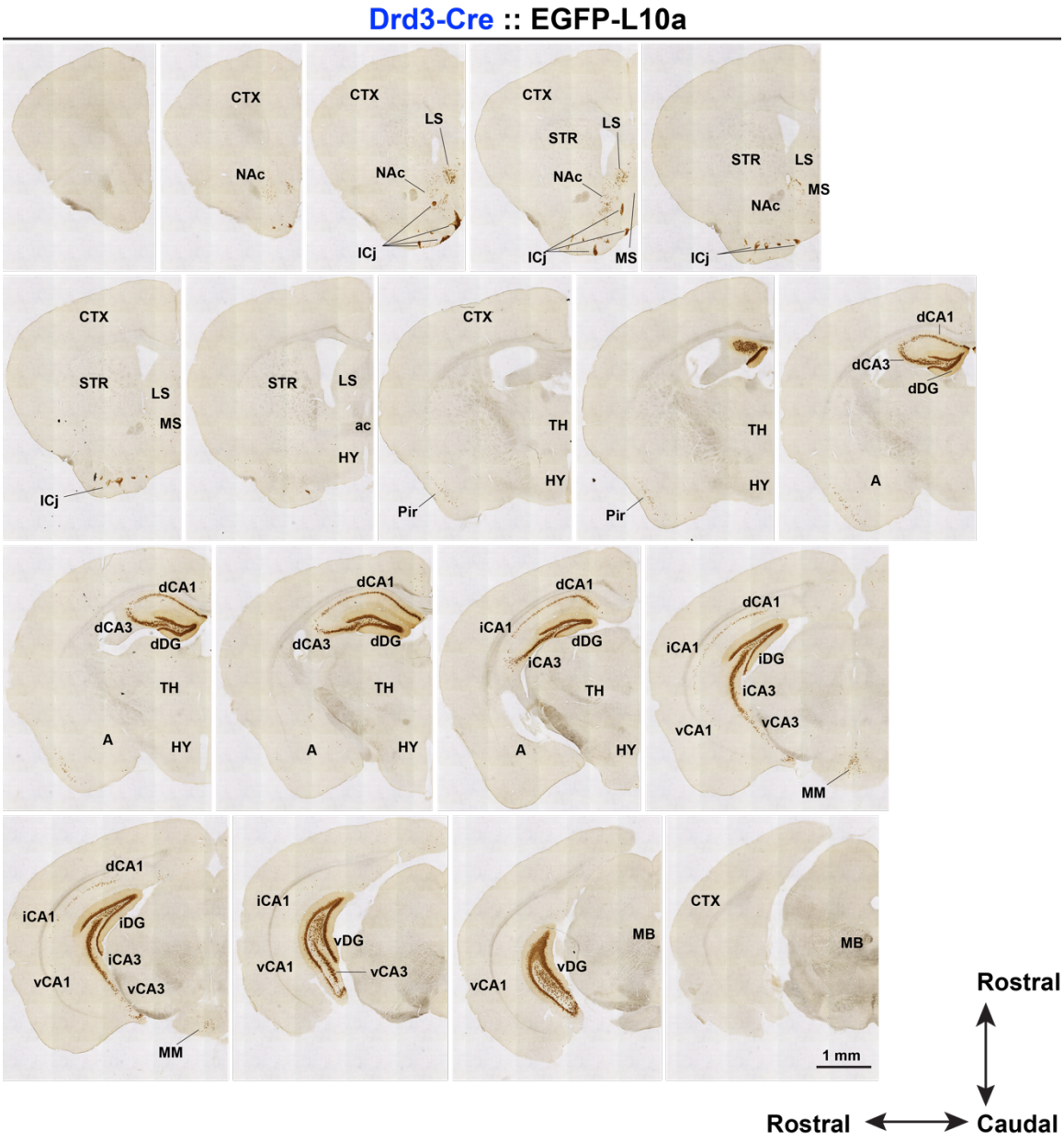

Figure 3.3. Drd3-Cre reporter line specifically targets the hippocampus. Anti-EGFP immunohistochemistry images of the coronal sections of a Drd3-Cre::EGFP-L10a mouse brain showing the expression pattern of Drd3-Cre driver line. From the most rostral (top left), to the most caudal (bottom right). Drd3-Cre is specifically expressed in hippocampus. Note the small number of Cre positive cells scattered in other regions such as rostral LS, NAc, ICj, Pir and MM. CTX: cortex, NAc: nucleus accumbens, LS: lateral septum, MS: medial septum, ICj: islands of Calleja, STR: striatum, TH: thalamaus, HY: hypothalamus, A: amygdala, Pir: piriform cortex, MM: mammillary nucleus of hypothalamus, MB: midbrain; dDG, iDG, vDG: dorsal, intermediate, ventral dentate gyrus, respectively; dCA, iCA, vCA1/3: (dorsal, intermediate, ventral CA1/3 fields, respectively.

3.2.2. Tlx3-Cre line to target CStr p11 pyramidal cells

We sought to find a Cre driver line that could achieve CStr p11 cell type specific conditional genetic manipulations. Although p11-Cre mouse line has been successfully generated, Cre expression was not restricted to p11 cells in adult mouse brain since it is expressed in progenitor cells during development (personal communication). To target the p11 neurons, we selected Tlx3-Cre line that expresses Cre exclusively in a cortical layer 5a population.

We crossed Tlx3-Cre line with the Cre dependent EGFP-L10a reporter mice to (Tlx3-Cre::EGFP-L10a) to reveal Cre expressing cells via anti-EGFP immunohistochemistry. Tlx3-Cre cells were pyramidal neurons located mainly in layer 5a in the neocortex in a laminar pattern (**Figure 3.4A**). Note that Cre-positive cells were sparse in the most medial and lateral regions of the cortex such as the prelimbic (PL), infralimbic (IL), retrosplenial (RSC), perirhinal (PRh), entorhinal (Ent) and piriform cortices. To confirm whether Tlx3-Cre expression is specific to p11 neurons, we performed TRAP followed by qRT-PCR gene expression analysis. Shortly, translating mRNAs from Tlx3-Cre neurons were isolated by anti-EGFP immunoprecipitation (IP) from the cortices of Tlx3-Cre::EGFP-L10a mice. mRNA isolated from whole cortex was used as the 'input' sample. Differential gene expression of actin beta (*ActB* - control), p11 (*S100a10*) and *Colgalt2* (a marker gene for CPn pyramidal neurons in layer 5b) was obtained between IP and input by qRT-PCR (**Figure 3.4B**).

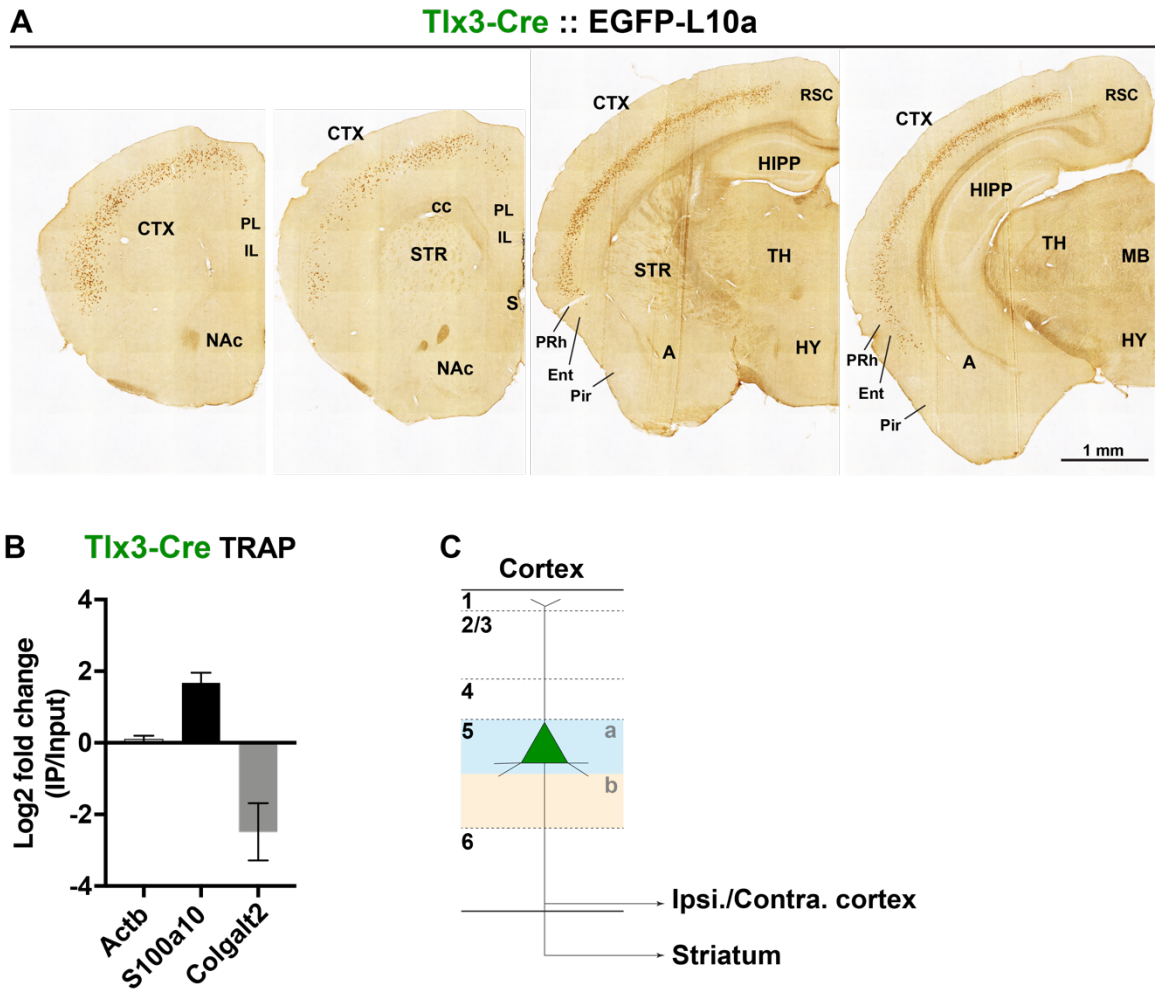

Figure 3.4. Tlx3-Cre reporter line targets corticostriatal (CStr) layer 5a pyramidal neurons.

(A) Anti-EGFP immunohistochemistry images of the coronal sections of a Tlx3-Cre::EGFP-L10a mouse brain showing the expression pattern of Tlx3-Cre driver line. Tlx3-Cre was expressed in a laminar pattern in the neocortex primarily in layer 5a. Note that Cre-positive cells were sparse in the most medial and lateral regions of the neocortex such as PL, IL and RSC as well as PRh, Ent and Pir.

(B) qRT-PCR quantification of the expression of actin beta (*ActB* - control), p11 (*S100a10*) and *Colgalt2* (a marker gene for CPn layer 5b neurons) in TRAP IP versus input samples in the neocortex of Tlx3-Cre::EGFP-L10a mice. Note that S100a10 was enriched in IP versus Colgalt2 in input. Data are represented as mean ± SEM. n=4 per group.

(C) Schematic depicting the layer localization and projection of Tlx3-Cre neurons in the cortex. Adapted by combining unpublished data from our lab and (Kim et al., 2015).

S100a10 expression was significantly enriched in IP (3.2-fold) while *Colgalt2* was significantly enriched in the input (5.6-fold). *ActB* expression was similar in both samples. These data suggested that Tlx3-Cre pyramidal cell population is enriched in p11 and depleted in CPn neuron marker.

Together with the previous findings that Tlx3-Cre neurons projects to dorsal striatum (CStr), and other ipsi- and contralateral cortical regions (CCor)(Kim et al., 2015), these results indicated that Tlx3-Cre targets the IT-CStr p11 expressing pyramidal neurons (**Figure 3.4C**). Therefore, Tlx3-Cre mouse line can be a specific and useful tool to further investigate p11 neurons in the neocortex. We crossed this line to our Htr4-floxed line to investigate the CStr layer 5a neuron specific functions of 5-HT_4R in emotion and cognition.

3.2.3. Hippocampus specific roles of 5-HT_4R in anxiety and depression related behaviors

To investigate the consequences of hippocampus specific deletion of 5-HT_4R, we crossed Htr4-floxed mice with the Drd3-Cre line. Heterozygous Drd3-Cre animals were crossed with Htr4-floxed animals homozygous for the floxed allele ($Htr4^{loxP/loxP}$) for two generations to obtain Drd3/Htr4 cKO mice (Drd3-Cre::$Htr4^{loxP/loxP}$). To maintain the colony, Drd3/Htr4 cKO animals were bred with homozygous Htr4-floxed animals. The litters from this breeding should be Drd3/Htr4 cKO in 1:2 ratio, and Htr4-floxed in 1:2, referred as control or wildtype (WT) littermates. Behavioral analysis was performed in two cohorts, comparing

Drd3/Htr4 cKO and their control littermates (cKO versus WT, n=20, 18, respectively), unless otherwise is noted.

3.2.3.a. Anxiety related behaviors in hippocampus specific *Htr4* conditional knockout mice

To assess whether hippocampal 5-HT_4R modulates anxiety related behaviors, and the ablation of 5-HT_4R specifically in Drd3-Cre cells leads to changes in anxiety-like behaviors, we tested Drd3/Htr4 cKO animals and control littermates in anxiety related behavioral paradigms, including conflict-based open field (OF), elevated plus maze (EPM) and novelty suppressed feeding (NSF), sociability based three-chamber social interaction, and finally, the acoustic startle responses (ASR) measuring motor defensive reflexes linked with anxiety-like behaviors (detailed in Chapter 2).

In the OF, Drd3/Htr4 cKO mice showed significantly higher levels of thigmotaxis both in the first 10 mins (**Figure 3.5A**) and over 60 mins (**Figure 3.5B**), compared to controls (10 mins – cKO: 0.82 ± 0.02 versus WT: 0.77 ± 0.01, p=0.04; 60 mins – cKO: 0.75 ± 0.03 versus WT: 0.68 ± 0.02, p=0.04). There was no significant difference in the locomotor activity between genotypes (p=0.45, Two-way ANOVA) (**Figure 3.5C**). These results indicated that Drd3/Htr4 cKO mice exhibited increased anxiety-like behaviors in the OF.

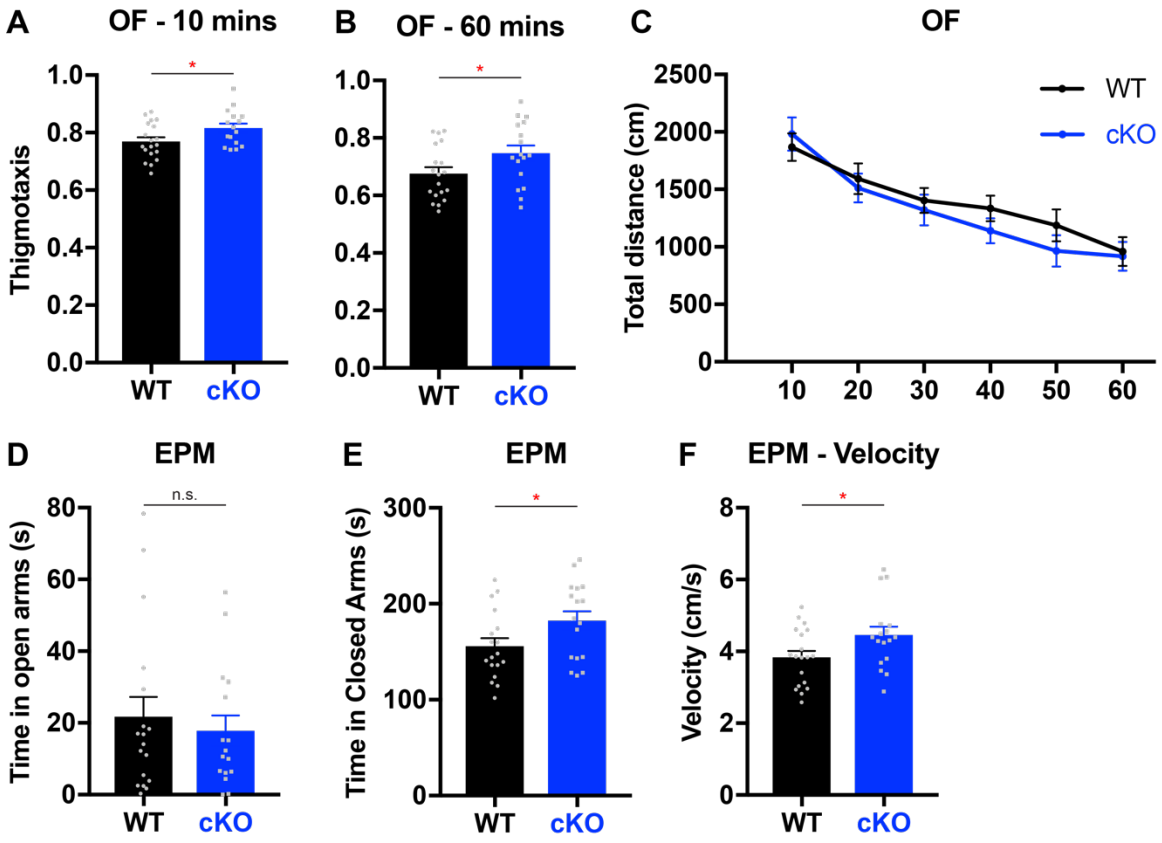

Figure 3.5. Hippocampus specific loss of 5-HT$_4$R led to increased anxiety-like behaviors in the open field and elevated plus maze.
(A) Drd3 Htr4/cKO mice (cKO, blue) showed significantly increased thigmotaxis (periphery/total time) in first 10 mins in the OF, compared to their control littermates (WT, black).
(B) Drd3 Htr4/cKO mice (cKO) exhibited a significant increase in thigmotaxis over 60 mins in the OF, compared to their controls (WT).
(C) There was not any significant difference between genotypes (cKO versus WT) in locomotor activity (total distance in cm) in OF.
(D) In the EPM, Drd3/Htr4 cKO and control (WT) did not exhibit a significant difference in the time spent in the open arms.
(E) Drd3/Htr4 cKO mice spent significantly more time in the closed arms compared to controls (WT).
(F) Drd3/Htr4 cKO mice showed significantly elevated locomotor activity as higher velocity (cm/s) in EPM compared to controls (WT).
Data are represented as mean ± SEM. Two-tailed unpaired t-test. *p<0.05, n.s. p>0.05.

In the EPM, Drd3/Htr4 cKO mice spent significantly more time in the closed arms, compared to control (cKO: 182.5 ± 9.8 s versus WT: 155.8 ± 8.3 s, p=0.046) (**Figure 3.5E**), demonstrating that the cKO mice exhibited elevated levels of anxiety-like behaviors in the EPM as well.

Although the time spent in the open arms was not significantly different between groups (p=0.58) (**Figure 3.5D**), Drd3/Htr4 cKO mice displayed significantly increased velocity in EPM, compared to controls (cKO: 4.5 ± 0.2 cm/s versus WT: 3.8 ± 0.2 cm/s, p=0.04) (**Figure 3.5F**). This suggested that higher locomotor activity in cKO mice was not accompanied by an increase in the time spent in the open arms, supporting the findings that Drd3/Htr4 cKO mice has elevated levels of anxiety-like behaviors.

In the NSF paradigm, Drd3/Htr4 cKO displayed a significant increase in latency to feed compared to controls (cKO: 740.7 ± 54.9 s versus WT: 523 ± 37.3 s, p=0.002) (**Figure 3.6A**), indicating a strong elevation in anxiety-like behaviors in the cKO mice. Drd3/Htr4 cKO also showed a significant increase in home cage feeding (cKO: 0.43 ± 0.04 g versus WT: 0.29 ± 0.03 g, p=0.01) (**Figure 3.6B**). Together, these results suggested that even though the cKO mice were more motivated in feeding in a less stressful environment, they did not approach the food as fast as WT in the NSF arena, conveying even more significant suppression of feeding in a novel environment. We also tested whether the increase in home cage feeding had long term effects on the physiology of the animals.

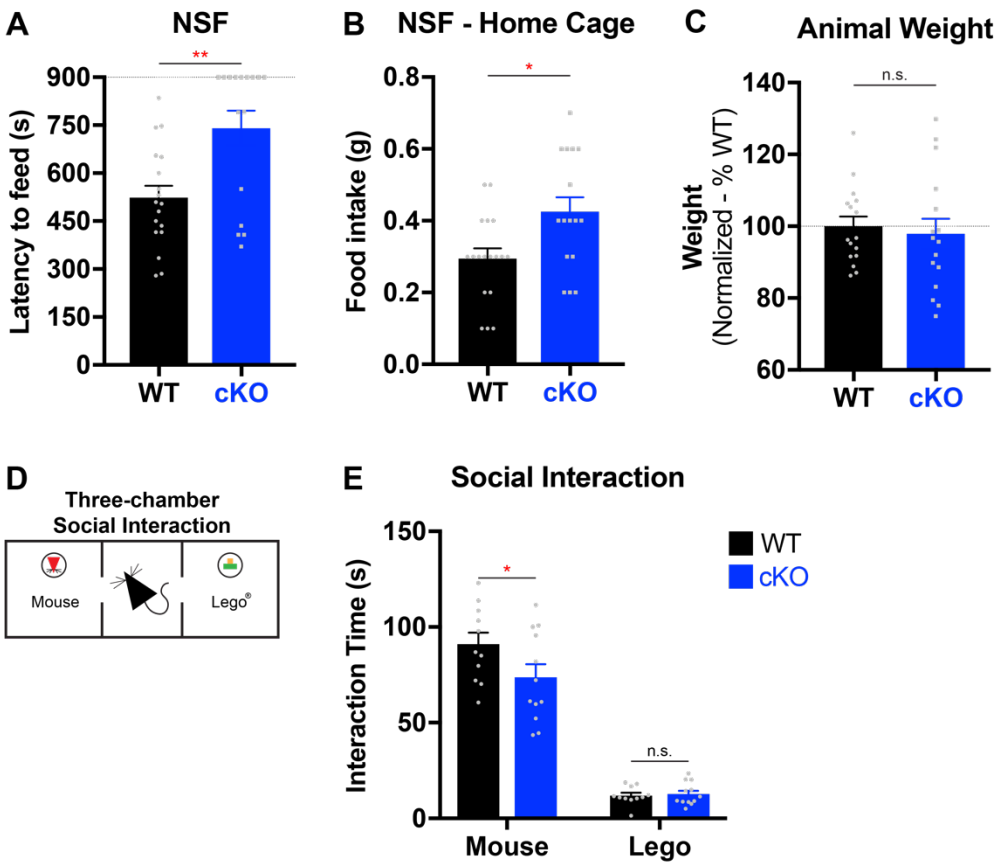

Figure 3.6. The loss of hippocampal 5-HT$_4$R resulted in elevated anxiety-like behaviors in the novelty suppressed feeding and social interaction tests.
(A) Drd3 Htr4/cKO mice (cKO, blue) displayed a significant increase in latency to feed compared to controls (WT, black) in the NSF.
(B) Drd3/Htr4 cKO mice showed a significant increase in feeding in home cage following NSF, compared to controls (WT).
(C)There was not any significant difference between groups in animal weight.
(D) Schematic representation of the three-chamber social interaction test.
(E) Drd3/Htr4 cKO mice spent significantly less time interacting with unfamiliar mouse in the three-chamber social interaction test, compared to controls (WT). Interaction with the Lego was not significantly different between groups.
Data are represented as mean ± SEM. Two-tailed unpaired t-test (A-C), two-way ANOVA followed by post hoc Fisher's LSD test (E). *p<0.05, **p<0.01, n.s. p>0.05.

There was not any significant difference in the animal weights between groups (p=0.68) (**Figure 3.6.C**). This suggested that the increase in home cage feeding in the cKO mice was acute, possibly due to prolonged fasting in the cKO mice compared to WT that had accessed the food much earlier in the NSF arena.

In the three-chamber social interaction test (**Figure 3.6D**), Drd3/Htr4 cKO mice interacted significantly less with the novel mice compared to controls (cKO: 73.7 ± 6.8 s, versus WT: 91 ± 6 s, p=0.01, n=12 per group), whereas the interaction with the novel inanimate object was not significantly different between groups (p=0.90) (**Figure 3.6E**). These data suggest an elevated anxiety-like behavior in social interaction in the cKO mice, supporting our previous behavioral findings.

Finally, we assessed the acoustic startle response (ASR) and pre-pulse inhibition (PPI) in Drd3/Htr4 cKO mice and their control littermates. The measurement was performed in four blocks. In the first block (pre-test), mice were presented with 120 dB acoustic stimuli for five trials for familiarization to the test. Maximum startle responses (Vmax) were recorded per trial and averaged per subject. In the second block (ASR), acoustic stimuli were presented in five different intensities (120, 110, 100, 90 and 80 dB), each for four trials in a pseudorandom order. Maximum startle responses (Vmax) were recorded for each trial and averaged for each stimulus intensity per subject. In the third block (PPI), 120 dB acoustic stimuli preceded by four different pre-pulse (PP) intensities (0, 3, 6, 12 dB) were presented, each for ten trials in a pseudorandom

order. Maximum startle responses (Vmax) were recorded for each trial and averaged for each prepulse intensity per subject. PPI was calculated as the percent decrease in the startle response in PP3, PP6 and PP12 compared to PP0 per subject. Lastly, in the fourth block (post-test), 120 dB stimuli were presented for five trials. Maximum startle responses (Vmax) were recorded per trial and averaged per subject to compare to the pre-test responses to assess the habituation of ASR during the testing. Habituation is a form of non-associative learning as the subject learns the repeated stimuli is non-threatening. It can also be viewed as a form of sensory filtering, since it desensitizes the organism to the stimuli. Disrupted habituation and PPI of ASR indicate cognitive dysfunction and observed in schizophrenia patients, while other mental and neurodegenerative disorders may also be accompanied by problems in the habituation and PPI (Geyer and Swerdlow, 2001; Valsamis and Schmid, 2011b).

In the ASR test, Drd3/Htr4 cKO mice exhibited enhanced startle response at 120 dB, compared to controls (cKO: 287.1 ± 32.8, versus WT: 212.8 ± 43.7, p=0.008, n=12 per group) (**Figure 3.7A**). At 110 dB, the cKOs also startled more that WT however this difference did not reach statistical significance (p=0.17). At lower dBs, the difference in the startle response between groups were not detectable, possibly due to a floor effect. Together, these data indicate that Drd3/Htr4 cKO mice showed elevated levels of anxiety-like responses to the acoustic startling stimuli.

Consistently, the cKO mice showed significantly increased startle responses during the pre-test (cKO: 277.4 ± 22.7, versus WT: 184.9 ± 33.3, p=0.03) and post-test blocks (cKO: 215.1 ± 27, versus WT: 132 ± 33.1, p=0.05) (**Figure 3.7B**). In addition, startle responses were significantly decreased in the post-test compared to the pre-test for both groups (cKO: -62.2 ± 23.1, p=0.01; WT: -52.9 ± 24, p=0,04), indicating a prominent habituation of ASR, independent of genotype. We also measured percent habituation per animal between the pre- and post-test to assess whether there was any effect of the conditional loss of 5-HT_4R on the extent of habituation. Both cKO and control mice habituated to 120 dB stimuli around 30% without any significant difference between genotypes (cKO: 27.9 ± 7.6, versus WT: 35.7 ± 10.8, p=0.55) (**Figure 3.7C**).

When PPI was measured, there was not any significant difference between Drd3/Htr4 cKO and control mice in the inhibition of startle at any pre-pulse intensities and overall (p=0.65, Two-way ANOVA) (**Figure 3.7D**). During the PPI block, consistent with the measurements in other blocks, Drd3/Htr4 cKO mice exhibited significantly higher startle responses to 120dB stimulus preceded by any pre-pulse (PP0, PP3, PP6 and PP12; p=0.01, 0.02, 0.02, 0.01, respectively), and overall (p=0.008, Two-way ANOVA) (**Figure 3.7E**). Together, these results suggested that, compared to controls, Drd3/Htr4 cKO mice displayed increased ASR throughout the test although they showed similar habituation and PPI of ASR.

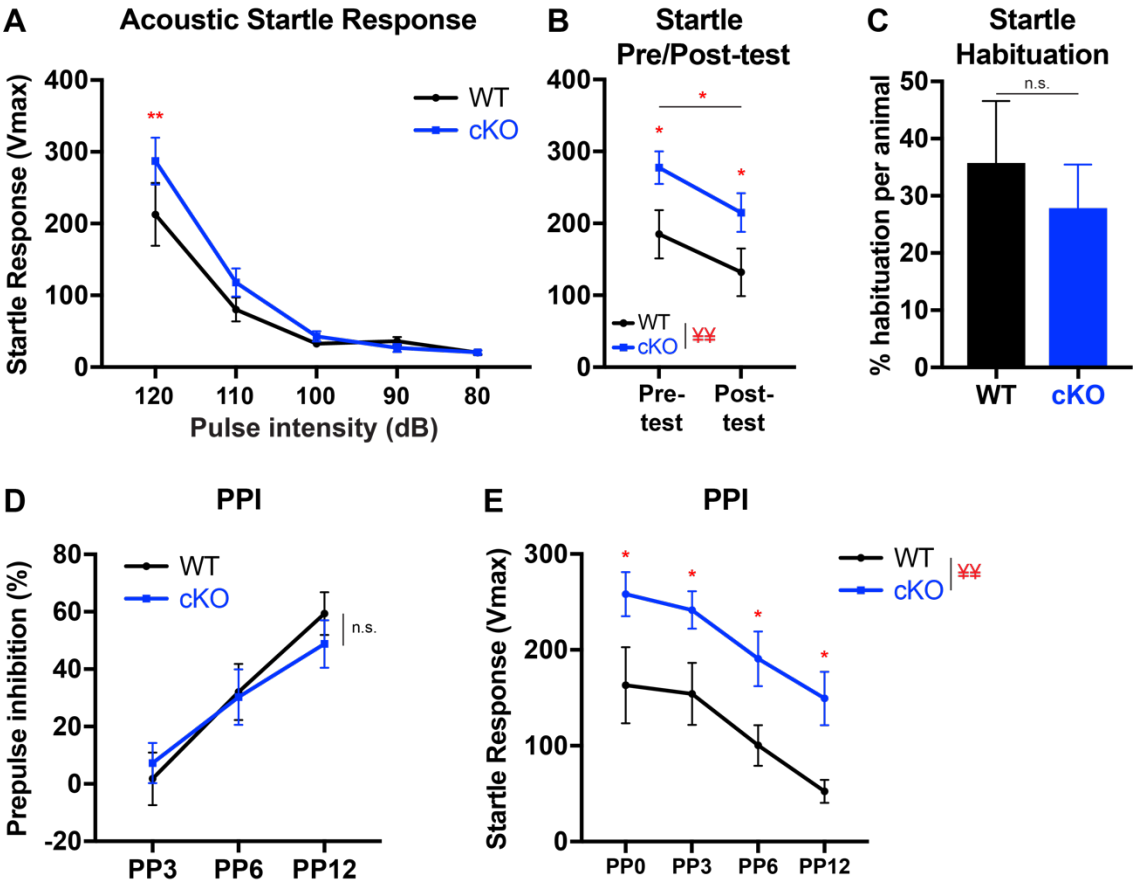

Figure 3.7. Drd3/Htr4 cKO mice exhibited increased anxiety-like behaviors as elevated acoustic startle responses.
(A) Drd3 Htr4/cKO mice (cKO, blue) displayed significantly larger startle responses to the 120dB acoustic pulse, compared to controls (WT, black). At 110 dB, the cKOs also startled more that WT however this difference did not reach statistical significance.
(B) Drd3/Htr4 cKO mice showed significantly elevated startle responses during the pre- and post-test blocks, compared to controls (WT). Note also that the startle responses were decreased significantly in the post-test compared to the pre-test for both groups.
(C) Percent habituation per animal between the pre- and post-test to 120 dB stimuli was not significantly different between groups.
(D) Prepulse inhibition (PPI) was not significantly different between groups.
(E) During the PPI measurements, Drd3/Htr4 cKO mice exhibited significantly higher startle responses to 120dB stimulus preceded by any pre-pulse and overall.
Data are represented as mean ± SEM. Two-way ANOVA followed by post hoc Fisher's LSD test (A, B, D, E), two-tailed unpaired t-test (C). ¥¥ $p<0.01$, *$p<0.05$, **$p<0.01$, n.s. $p>0.05$.

Anxiety-like behavioral measures in the OF, EPM, NSF, social interaction and ASR taken together, our data strongly suggest that the ablation of functional 5-HT_4R specifically from the hippocampus led to a prominent increase in anxiety-like behaviors.

3.2.3.b. Depression related behaviors in hippocampus specific Htr4 conditional knockout mice

Serotonergic neuromodulation in the hippocampus has been extensively implicated in anxiety and depression, and the hippocampus is one of the main structures responding to SSRI treatments including changes in the molecular and physiological properties in this area. Although the loss of 5-HT_4R from the excitatory neurons of pallium including the hippocampus in Emx1/Htr4 cKO mice did not result in a change in depression-related behaviors, there may be compensation mechanisms shadowing any depression-related effects. Perhaps, the slight increase in hedonia levels when pallial 5-HT_4R was ablated (Chapter 2.4.6) is an indication of the modulation of depression-like behaviors via 5-HT_4R in this area. To investigate whether 5-HT_4R in the hippocampus modulates depression related behaviors, we tested Drd3/Htr4 cKO animals and control littermates in several behavioral paradigms including despair-based tail suspension test (TST) and forced swim test (FST), and anhedonia-based splash test and sucrose consumption test.

Intriguingly, Drd3/Htr4 cKO exhibited significantly lower immobility compared to controls in both TST (cKO: 80.6 ± 7.4 %, versus WT: 100 ± "100 ± 4.2 %, p=0.02) (**Figure 3.8A**), and FST (cKO: 57.8 ± 10.1 s, versus WT: 115.6 ± 7.9 s, p<0.0001) (**Figure 3.8B**), revealing diminished despair-like behaviors (antidepressant-like). In splash test, Drd3/Htr4 cKO mice showed significant increase in grooming compared to controls (cKO: 73 ± 4.7 s, versus WT: 45.5 ± 3.2 s, p<0.0001) (**Figure 3.8C**), indicating enhanced hedonic behaviors in the cKO mice.

In addition, the sucrose consumption test was employed to evaluate the hedonic phenotype in the cKOs. In this test, each mouse was placed in a clean cage containing a 1% sucrose bottle and a water bottle. Sucrose and water consumption was measured for 72 hours. At each 12 hour-mark, bottles were switched places to avoid side preference. Sucrose and water consumption was measured per animal weight to normalize for the drinking needs of differently sized animals. The decrease in sucrose consumption is a measure of anhedonia. While animal models of depression have been established to consume less sucrose over time, antidepressant treatments tend to reverse this phenotype and increase sucrose consumption (Strekalova et al., 2011). This test was chosen instead of sucrose preference test since the enhanced hedonic behaviors in Drd3/Htr4 cKO mice would not have been evaluated by merely comparing the already-high levels of preference of sucrose in mice.

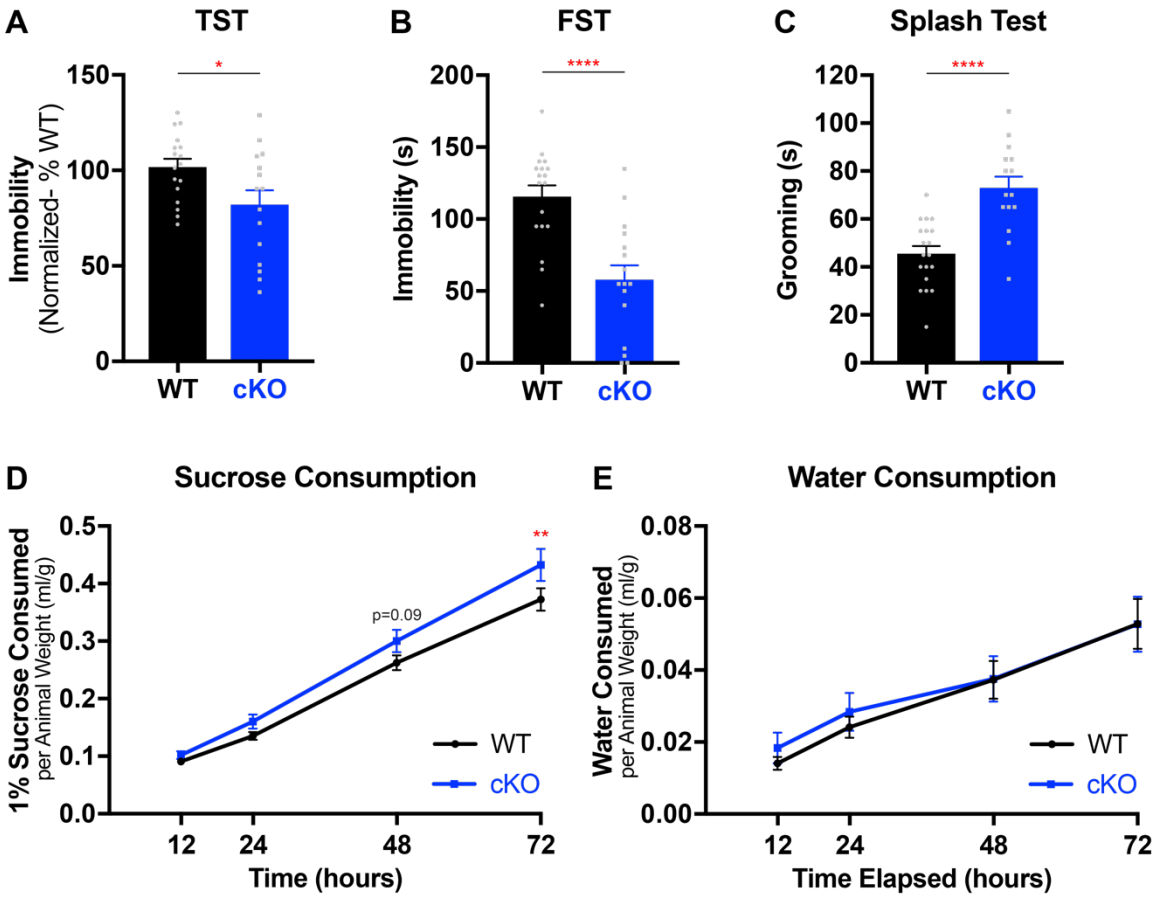

Figure 3.8. The loss of hippocampal 5-HT$_4$R led to antidepressant-like behavioral responses in the tail suspension, forced swim, splash and sucrose consumption tests.

(A) Drd3/Htr4 cKO mice (cKO, blue) showed significantly lower immobility in the TST, compared to controls (WT, black).

(B) Drd3/Htr4 cKO mice spent significantly less time immobile in the FST compared to controls (WT).

(C) Drd3/Htr4 cKO mice spent significantly more time grooming in the splash test.

(D) Drd3/Htr4 cKO mice consumed significantly more 1% sucrose over 72 hours.

(E) Water consumption during the sucrose consumption test was not significantly different between groups.

Data are represented as mean ± SEM. Two-tailed unpaired t-test (A-C), two-way ANOVA followed by post hoc Fisher's LSD test (D, E). *p<0.05, **p<0.01, ****p<0.0001, n.s. p>0.05.

Compared to control littermates, Drd3/Htr4 cKO mice consumed more sucrose throughout the test reaching statistical significance in difference over 72 hours (72 hours; cKO: 0.43 ± 0.03 ml/g, versus WT: 0.37 ± 0.02 ml/g, p=0.008) (**Figure 3.8D**). There was not any significant difference in water consumption between groups (**Figure 3.8E**). These results indicate that Drd3/Htr4 cKO mice showed enhanced hedonic behaviors in the sucrose consumption test.

In conclusion, Drd3/Htr4 cKO mice showed antidepressant-like behaviors in the TST and FST as well as in the splash and sucrose consumption tests. Hence, hippocampus specific loss of 5-HT_4R resulted in comprehensive antidepressant-like responses, implicating that 5-HT_4R modulates depression-related behaviors in Drd3-Cre positive cells in the hippocampus in addition to anxiety-related behaviors.

3.2.4. CStr layer 5a cell specific roles of 5-HT_4R in anxiety and depression

To investigate the consequences of the loss of 5-HT_4R specifically from the CStr layer 5a pyramidal neurons on anxiety and depression related behaviors as well as antidepressant-like responses, we crossed Htr4-floxed mice with the Tlx3-Cre line. Heterozygous Tlx3-Cre animals were crossed with Htr4-floxed animals homozygous for the floxed allele (*Htr4*$^{loxP/loxP}$) for two generations to obtain Tlx3/Htr4 cKO mice (Tlx3-Cre::*Htr4*$^{loxP/loxP}$). To maintain the colony, Tlx3/Htr4 cKO animals were bred with homozygous Htr4-floxed animals. The litters from this breeding should be Tlx3/Htr4 cKO in 1:2 ratio, and Htr4-floxed in

1:2, referred as control or wildtype (WT) littermates. To asses antidepressant-like behavioral responses, 8-week-old Tlx3/Htr4 cKO mice and control littermates were either given 0.167 mg/ml fluoxetine (~18 mg/kg/day) (FLX) or vehicle (VEH) in drinking water for 18 days (Schmidt et al., 2012). Behavioral analysis was performed in one cohort divided in four groups (WT-VEH, WT-FLX, cKO-VEH, cKO-FLX; n= 12, 12, 12, 11, respectively). The drug treatment continued until the end of behavioral assessments.

In the OF, Tlx3/Htr4 cKO mice and their control littermates showed similar thigmotaxis levels in first 10 mins (cKO-VEH: 0.87 ± 0.02, WT-VEH: 0.85 ± 0.01 p=0.38) (**Figure 3.9A**), and over 60 mins (cKO-VEH: 0.82 ± 0.02, WT-VEH: 0.81 ± 0.02 p=0.88) (**Figure 3.9B**). Following chronic treatment with fluoxetine, both the cKO and control mice showed significant increase in thigmotaxis both in 10 mins (cKO-VEH/FLX: 0.87 ± 0.02 / 0.97 ± 0.01 p=0.0003; WT-VEH/FLX: 0.85 ± 0.01 / 0.95 ± 0.02, p=0.0003), and 60 mins (cKO-VEH/FLX: 0.82 ± 0.02 / 0.94 ± 0.02, WT-VEH/FLX: 0.81 ± 0.02 / 0.91 ± 0.02, p<0.001). There was not any significant difference in the locomotor activity amongst groups (**Figure 3.9C**). Together, these data indicated that Tlx3/Htr4 cKO mice did not show any difference in anxiety-like behaviors, and that the anxiogenic effects of chronic fluoxetine was independent of genotype in the OF.

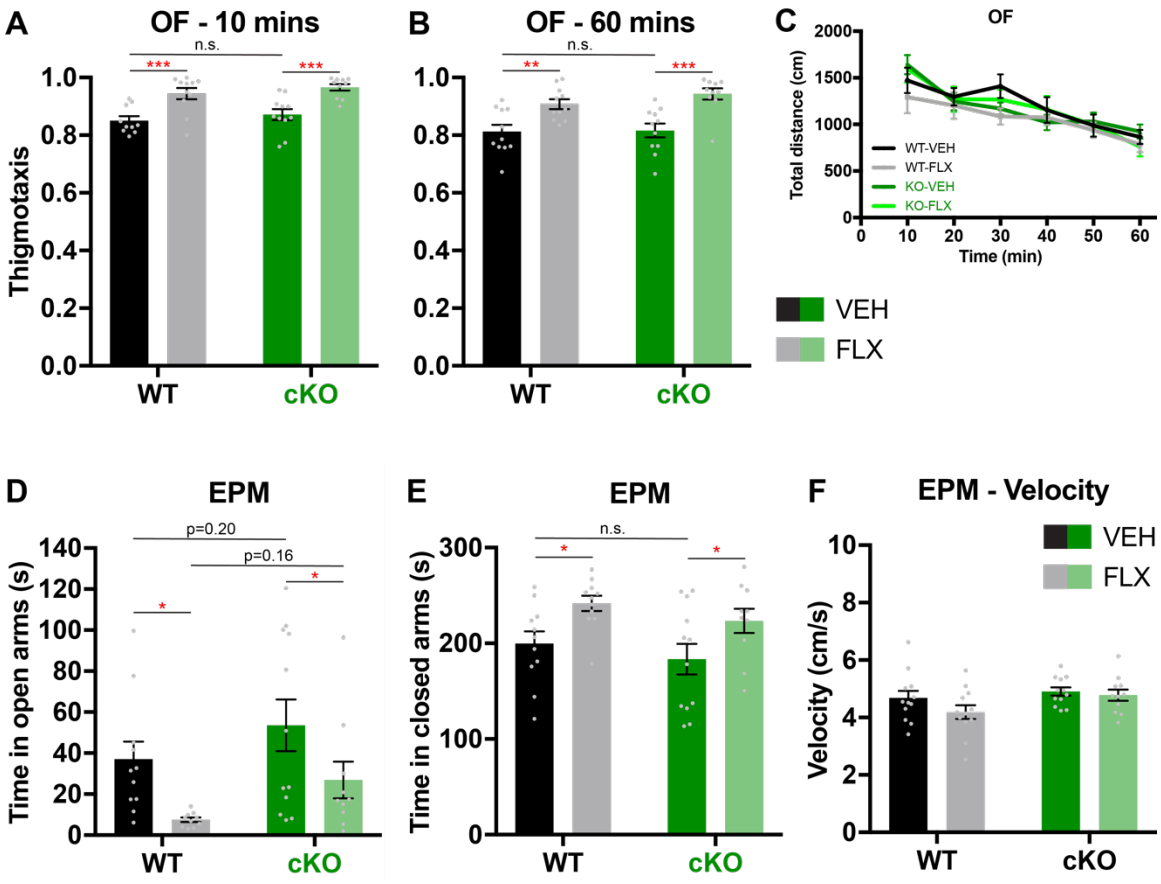

Figure 3.9. The loss of 5-HT$_4$R specifically from CStr layer 5a neurons led to slightly decreased anxiety-like behaviors in the EPM.
(A) Tlx3/Htr4 cKO mice (cKO-VEH) and controls (WT-VEH) showed similar thigmotaxis in the first 10 mins in the open field (OF). Following chronic fluoxetine (FLX) treatment, both cKO and WT showed significantly increased thigmotaxis in 10 mins, compared to vehicle treated counterparts.
(B) There was not any significant difference in thigmotaxis between genotypes (cKO-VEH versus WT-VEH) in OF over 60 mins. Following FLX treatment, both cKO and WT had significantly increased thigmotaxis in 60 mins, compared to vehicle treated counterparts.
(C) Locomotor activity (total distance traveled) in the OF was not significantly different amongst groups.
(D) Tlx3/Htr4 cKO mice (cKO-VEH) spent slightly longer time in open arms in EPM compared to controls (WT-VEH). Following chronic treatment with fluoxetine, both cKO and control mice showed significant decrease in the time spent in the open arms. Note that cKO-FLX spent slightly more time in open arms than WT-FLX. Two-way ANOVA, p=0.06 for genotype factor.
(E) Time in closed arms in the EPM were similar for both genotypes. Following FLX treatment, both cKO and WT spent significantly more time in closed arms in the EPM, compared to their vehicle treated counterparts.
(F) Locomotor activity (velocity) during the EPM was similar amongst groups.
Data are represented as mean ± SEM. Two-way ANOVA followed by post hoc Fisher's LSD test. *p<0.05, **p<0.01, ***p<0.001.

In the EPM, Tlx3/Htr4 cKO mice spent slightly higher amount of time in open arms, compared to controls, although this difference did not reach statistical significance (cKO-VEH: 53.6 ± 12.6 s, WT-VEH: 37 ± 8.6 s, p=0.20) (**Figure 3.9.D**), suggesting that the cKO mice may have had slightly lower levels of anxiety. Following chronic treatment with fluoxetine, both cKO and control mice showed significant decrease in the time spent in the open arms (cKO-VEH/FLX: 53.6 ± 12.6 / 26.9 ± 9 s, p=0.049; WT-VEH/FLX: 37 ± 8.6 / 7.5 ± 1.1 s, p=0.033). Note that cKO-FLX mice spent slightly more time in open arms than WT-FLX which was also not statistically significant (26.9 ± 9 s versus 7.5 ± 1.1 s, p=0.16). This trend may be attributed to a marginally anxiolytic phenotype of the cKO (p=0.06 for genotype factor, Two-way ANOVA). Furthermore, Tlx3/Htr4 cKOs and controls treated with chronic fluoxetine spent significantly more time in the closed arms in the EPM compared to their vehicle treated counterparts (p=0.03 for both comparisons) (**Figure 3.9E)**, detecting similar anxiogenic effects of the drug for both genotypes. There was not any significant difference in the velocity in the EPM amongst groups, indicating similar locomotor activity regardless of genotype and drug treatment (**Figure 3.9F**).

In the NSF, Tlx3/Htr4 cKO mice showed a slight decrease in latency to feed compared to controls while the difference did not reach statistical significance (cKO-VEH: 372 ± 96 s, WT-VEH: 550 ± 58 s, p=0.06) (**Figure 3.10A**).

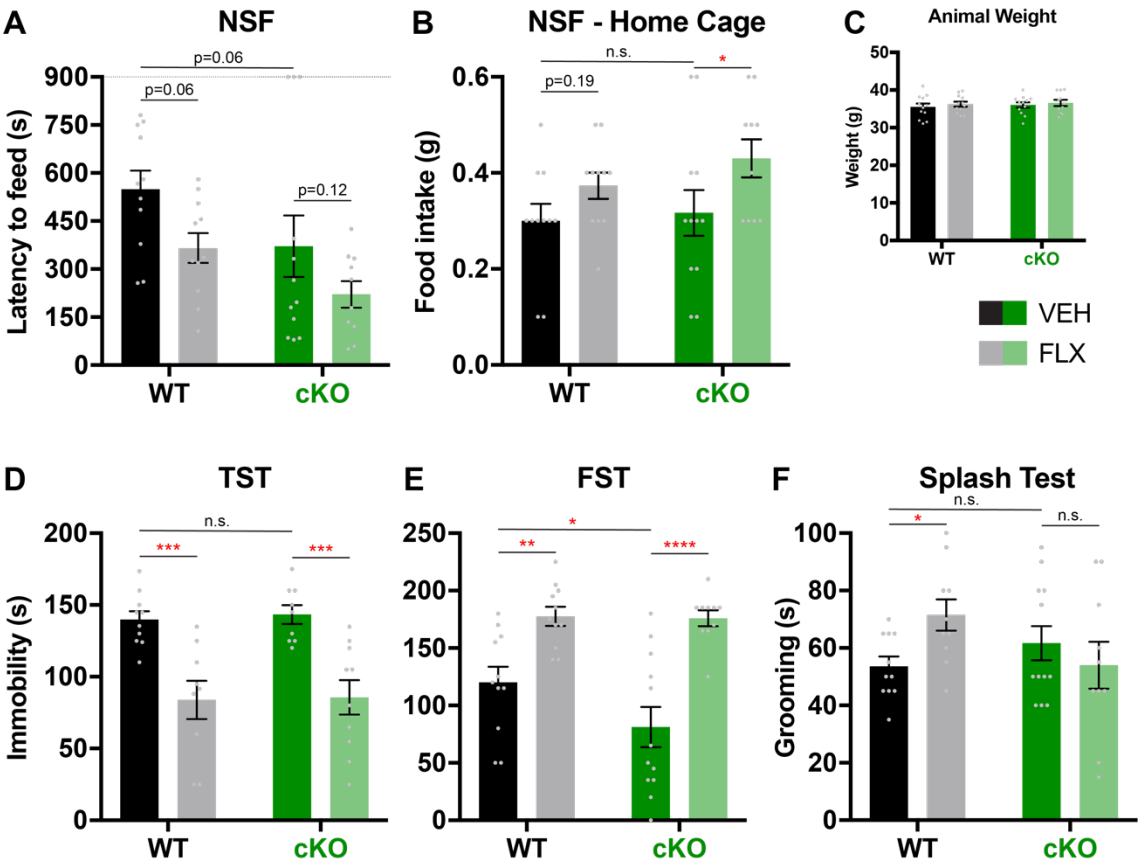

Figure 3.10. The loss of CStr 5-HT$_4$R led to slightly decreased anxiety-like behaviors in the NSF and anti-depressant-like behavioral responses in the FST.
(A) Tlx3/Htr4 cKO mice (cKO-VEH) showed slightly decreased in latency to feed in NSF, compared to control (WT-VEH). Following chronic treatment with fluoxetine (FLX), both cKO and WT exhibited slightly lower latency to feed. Overall effects of genotype and FLX treatment were significant. Two-way ANOVA, p=0.021 for genotype factor, p=0.017 for treatment factor.
(B) There was not any significant difference in food intake between genotypes in home cage following NSF. FLX treatment led to an increase in the food intake in home cage, significantly in cKO and slightly in WT.
(C) There was not any significant difference in animal weights between groups.
(D) cKO-VEH and WT-VEH groups displayed similar immobility in TST. Following FLX treatment, both cKO and WT showed a significant decrease in immobility compared to their VEH treated counterparts.
(E) cKO-VEH exhibited significantly lower immobility compared to WT-VEH in FST. Immobility was significantly increased in both genotypes treated with FLX.
(F) In splash test, there was not any significant difference in grooming between cKO-VEH and WT-VEH. FLX treatment led to more grooming in WT while it did not alter grooming in cKO. Data are represented as mean ± SEM. Two-way ANOVA followed by post hoc Fisher's LSD test. *p<0.05, **p<0.01, ***p<0.001, ****p<0.0001.

In addition, Tlx3/Htr4 cKO and control mice treated with fluoxetine showed a trend towards a decrease in the latency to feed compared to their vehicle treated equivalents (cKO-VEH/FLX: 372 ± 96 / 221 ± 41 s, p=0.12; WT-VEH/FLX: 550 ± 58 / 366 ± 47 s; p=0.06). Interestingly, two-way ANOVA analysis on the effect of genotype and drug treatment on the latency to feed in the NSF suggest that, overall, the cKO mice showed significantly less latency to feed compared to WT (p=0.021), and fluoxetine treatment significantly decreased the latency to feed (p=0.017), independent of genotype factor (genotype-drug interaction, p=0.81). Since NSF relies on feeding, we also measured home cage feeding immediately after the test. There was not any significant difference in food intake between genotypes in home cage following NSF (cKO-VEH: 0.31 ± 0.05 g, WT-VEH: 0.30 ± 0.04 g, p=0.76) (**Figure 3.10B**). Chronic fluoxetine administration significantly increased the food intake in in the cKO mice (p=0.049), and slightly in the controls, which did not reach statistical significance (p=0.19). However, overall, fluoxetine significantly elevated food intake in home cage independent of genotype (p=0.02, Two-way ANOVA). Finally, we measured the weight of animals to acquire whether the increase in food intake observed after the NSF had any effects of the physiology of the animals in the long term. There was not any significant difference between the animal weights among groups (**Figure 3.10C**). The NSF offers a strong predictive power for alterations in anxiety-like behaviors while it is also sensitive for detecting the behavioral responses to chronic antidepressant administration in mice. Our data suggest that, in the NSF,

Tlx3/Htr4 cKO mice showed anxiolytic behaviors compared to controls, while both cKO and control mice exhibited antidepressant-like behavioral responses to chronic fluoxetine.

In the TST, there was not any significant difference in immobility between Tlx3/Htr4 cKO and their control littermates (cKO-VEH: 143 ± 7 s, WT-VEH: 140 ± 6 s, p=0.80) (**Figure 3.10D**). Following chronic treatment with fluoxetine, immobility was significantly decreased in both genotypes (cKO-VEH/FLX: 143 ± 7 / 86 ± 12 s, p=0.0003; WT-VEH/FLX: 140 ± 6 / 84 ± 13 s; p=0.0002). Together, these results indicate that Tlx3/Htr4 cKO mice did not display an alteration in depression-like behaviors in the TST, and that chronic fluoxetine resulted in antidepressant-like behavioral responses independent of genotype.

In the FST, Tlx3/Htr4 cKO mice exhibited significantly lower immobility compared to controls (cKO-VEH: 81 ± 17 s, WT-VEH: 120 ± 14 s, p=0.80) (**Figure 3.10E**), indicating reduced despair-like behaviors in the cKO. Following chronic treatment with fluoxetine, immobility was significantly increased in both genotypes (cKO-VEH/FLX: 81 ± 17/ 176 ± 7 s, p<0.0001; WT-VEH/FLX: 120 ± 14 / 177 ± 8 s; p=0.003), showing an opposite effect from the expected antidepressant-like response, leading to an inconclusive result. Similar results were observed in some mouse strains and in our previous experiments (Chapter 2.4.5), rendering the FST inconclusive in determining chronic antidepressant effects in our model as well. The FST in this cohort only suggested that Tlx3/Htr4 cKO mice displayed antidepressant-like behaviors.

In the splash test, there was not any significant difference in grooming between genotypes (cKO-VEH: 61 ± 6 s, WT-VEH: 53 ± 3 s, p=0.33) (**Figure 3.10F**). Control mice treated with fluoxetine groomed longer compared to vehicle treated counterparts (WT-VEH/FLX: 53 ± 3 / 72 ± 5 s, p=0.04), while there was not any difference in grooming between fluoxetine and vehicle treated cKO mice (cKO-VEH/FLX: 61 ± 6 / 54 ± 8 s, p=0.36). Together, these data indicated that hedonic behaviors in Tlx3/Htr4 cKO was not altered in the splash test, however that the antidepressant-like behavioral responses observed in control mice were not evident in the cKO. This suggested that the loss of CStr 5-HT_4R may have diminished the hedonic behavioral effects of fluoxetine in Tlx3/Htr4 cKO mice.

In conclusion, Tlx3/Htr4 cKO mice showed anxiolytic phenotype, slightly in the EPM and significantly in the NSF, as well as an antidepressant-like behavioral response in the FST, implying that the loss of 5-HT_4R in CStr layer 5a neurons led to improvements in some anxiety and mood related behaviors. The anxiogenic effect of fluoxetine in the OF and EPM, and the antidepressant-like in the NSF and TST were observed in both genotypes. Only in the splash test, Tlx3/Htr4 cKO did not respond to chronic fluoxetine as increased grooming observed in the control group. This indicates that CStr 5-HT_4R was not necessary for most of the chronic antidepressant-like behavioral responses.

3.3. Spatial dissection of the role of 5-HT_4R in the hippocampus and neocortex in anxiety and depression related behaviors

3.3.1. The role of 5-HT_4R along the dorsoventral axis of the hippocampus

To gain insights into whether the function of 5-HT_4R in Drd3-Cre expressing neurons in spatially distinct parts of DG along the dorsoventral axis mediate the behavioral changes in Drd3/Htr4 cKO, we devised a rescue experiment such that functional 5-HT_4R would be conditionally re-expressed via AAV-mediated gene delivery in Drd3/Htr4 cKO mice either in the ventral or dorsal DG. We generated an expression construct (pAAV.Ef1a.DIO.Htr4-Myc-DDK.WPRE.hGH) that, in the presence of Cre, would recombine to express mouse *Htr4* mRNA under the EF1a promoter, a constitutive promoter of human origin that is standard for use to drive ectopic gene expression (**Figure 3.11A**). Htr4-Myc-DDK was cloned in the reverse orientation into the Cre-dependent pAAV.EF1a.DIO.EGFP plasmid, replacing EGFP. The presence of flanking loxP and lox2272 sites resulted in a construct that had a ‘‘double-floxed’’ inverted open reading frame (DIO) (Atasoy et al., 2008), to allow for cell type specific expression of 5-HT_4R tagged with MYC-DDK. This construct is hereafter referred to as pAAV-DIO-Htr4-Myc. In the presence of Cre recombinase, Htr4-Myc sequence would be reverted back, allowing for conditional expression of a functional protein.

To confirm Cre-dependent expression of the 5-HT_4R-MYC, HEK cells were both transfected by the pAAV-DIO-Htr4-Myc construct and transduced with AAV-Cre-EGFP, for AAV mediated Cre-EGFP expression. Immunofluorescent labeling with anti-MYC antibody revealed the Cre dependent expression of 5-HT_4R-MYC (**Figure 3.11B**). The expression of 5-HT_4R was restricted to Cre-EGFP expressing cells (above). There was not any 5-HT_4R-MYC expression in HEK cells transfected with our construct but negative for Cre (control, below). These results indicated that our pAAV-DIO-Htr4-Myc construct showed efficient Cre dependence.

For in vivo gene delivery, we generated AAV-DIO-Htr4-Myc, AAV2.9 virus packaging our rescue construct (UPenn Vector Core). To confirm the Cre dependent expression of viral construct in vivo, AAV-DIO-Htr4-Myc was stereotaxically injected into the dentate gyrus (DG) of Drd3-Cre::EGFP-L10a mice. The expression was checked three weeks later by immunofluorescent labeling in the coronal brain sections. Anti-MYC antibody was used to detect 5-HT_4R-MYC expression and EGFP was used to label EGFP-L10a in Drd3-Cre positive cells (**Figure 3.11C**). AAV-DIO-Htr4-Myc injected DG (below) was highly labeled with anti-MYC antibody, compared to control DG without AAV injection. However, EGFP expressing Drd3-Cre positive DG granule cells (DG), hilar cells, and CA3 pyramidal neurons were not observed in AAV injected hippocampus, compared to intact expression in control (arrowheads in EGFP panel).

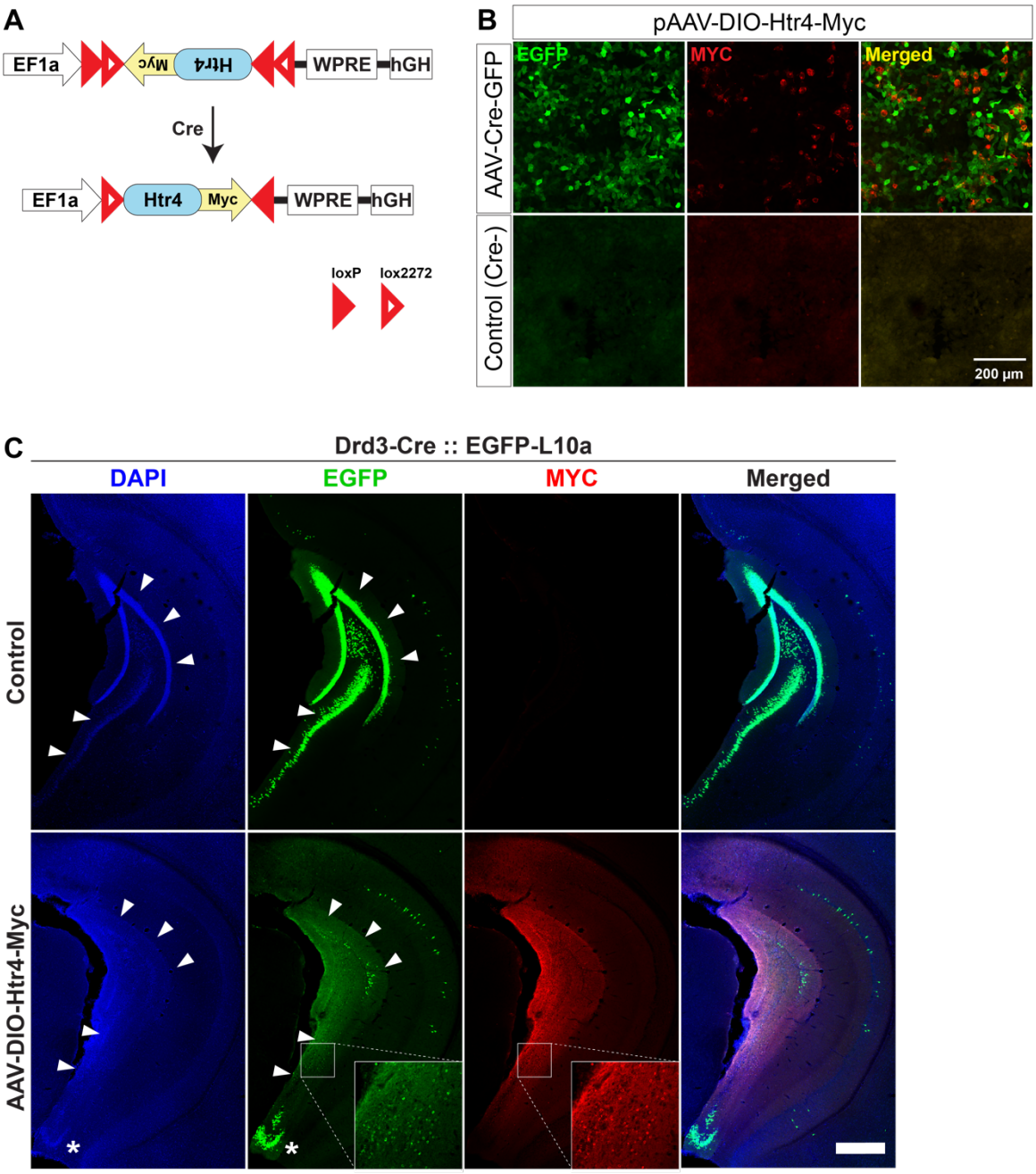

Figure 3.11. AAV-mediated Cre-dependent overexpression of 5-HT$_4$R in the hippocampus of Drd3-Cre mice led to neurotoxicity.
(A) Schematic of the design of the Cre-dependent pAAV-DIO-Htr4-Myc vector.
(B) Anti-MYC immunofluorescent staining of HEK cells transfected with pAAV-DIO-Htr4-Myc (red). 5-HT$_4$R-MYC was only detected in cells transduced with AAV-Cre-EGFP (above), but not in control cells negative for Cre (below).
(C) Anti-MYC immunofluorescent staining (red) of the Cre-dependent AAV-DIO-Htr4-Myc delivery in the hippocampus in a Drd3-Cre::EGFP-L10a mouse. 5-HT$_4$R-MYC was detected at the injection site, however, EGFP-L10a expressing cell layer in DG and CA3 were lost (arrowheads). Note the intact GC layer in MYC negative area (asterisk). Scale bar, 500 μm.

DAPI staining clearly showed granule cell and CA3 pyramidal cell layer in control while these layers were absent in the AAV injected site (arrowheads in DAPI panel). Note that, at the most ventral part of AAV injected DG, there were still EGFP expressing DG GCs (asterisk).

At a higher magnification, there were numerous small round cells stained with anti-MYC, scattered around the DG and CA3 in AAV injected hippocampus (MYC panel, below). These cells were also detected in green channel (EGFP panel, below). This suggests that they are Drd3-Cre::EGFP-L10a expressing, AAV-infected dying cells which were disintegrated from the layer. Also note that the injection area has a higher autofluorescence than the rest of the tissue in all three channels, which is an indication of damaged cells and tissues (Je et al., 2017). These data suggest that, at the AAV injection site, the DG GC and CA3 pyramidal neuron layers were disintegrated and EGFP expressing cells were lost, possibly due to the death of neurons overexpressing 5-HT_4R-MYC which was still detected in the tissue. Due to this neurotoxicity of AAV-DIO-Htr4-Myc, we did not pursue these rescue experiments further.

3.4. Discussion

In this chapter, we investigated the role of 5-HT_4R in emotive behavior in specific cell types and brain regions. As discussed in Chapter 2, the loss of 5-HT_4R from excitatory neurons of pallial origin resulted in increased anxiety-like behaviors suggesting that hippocampal and/or cortical 5-HT_4R may play a role in mediating anxiety and mood related behaviors. To target 5-HT_4R specifically in the hippocampus or neocortex, we used two Cre-driver lines, Drd3-Cre and Tlx3-Cre, that expresses Cre in non-overlapping cell populations, and that selectively target two of the most relevant population in each region in terms of serotonergic neuromodulation.

3.4.1. Hippocampal 5-HT_4R mediates anxiety and depression related behaviors

We found that the loss of 5-HT_4R specifically from the hippocampus resulted in a significant and comprehensive anxiogenic phenotype, measured by variety of assays that assess innate anxiety-like behaviors. These phenotypes included increased thigmotaxis, avoidance of open arms in EPM, hyponeophagia and startle responses as well as decreased social interaction. These finding suggest that 5-HT_4R mediates innate anxiety through a hippocampal pathway.

Remarkably, the ablation of 5-HT_4R from the hippocampus induced a significant antidepressant-like behavioral effect observed both in despair-based

task as decreased immobility, and hedonic/reward-based tasks as enhanced sucrose intake and grooming. Hereby, our findings implicate a unique role for hippocampal 5-HT_4R in modulating anxiety and mood, by showing that, in the hippocampus, 5-HT_4R modulates anxiety and depression related symptoms in opposite directions.

Growing evidence supports that especially the ventral hippocampus (vHIPP) mediates anxiety and depression related behaviors through various glutamatergic projections. For example, elevating the activity of GCs in the vDG via optogenetic stimulation suppresses innate anxiety in mice (Kheirbek et al., 2013). This supports our findings showing the anxiogenic consequences of the loss of an excitatory 5-HT receptor from DG GCs. However, the hippocampus regulates downstream neural pathways distinctly due to different circuit connections and dynamics. For instance, the inhibition of specific vHIPP-mPFC afferents via optogenetics were anxiolytic (Padilla-Coreano et al., 2016), while these connections promoted antidepressant-like properties via both optogenetic (Bagot et al., 2015) and chemogenetic activation (Carreno et al., 2015). Similarly, connections to the amygdala, BNST and NAc either enhance or inhibit different aspects of these behaviors. Considering the overall effect of serotonin is inhibitory in hippocampal neurons, how an excitatory 5-HT receptor subtype could regulate each component of the extended anxiety and mood circuit remains to be investigated. Our behavioral findings suggest that 5-HT_4R within

the hippocampus was necessary to sustain normal levels of anxiety while its absence resulted in the improvement of depression related behaviors.

As Drd3-Cre targeted cells in both the dorsal and ventral hippocampus, it still remains to be investigated whether the anxiogenic and antidepressant-like consequences of the deletion of 5-HT_4R from these cells were originated from the ventral or dorsal hippocampus. To dissect the function of 5-HT_4R in the dorsoventral axis of the hippocampus and to understand whether 5-HT_4R was sufficient to mediate these behaviors transiently, we designed rescue experiments using AAV-mediated cell type specific gene expression. However, we found that the overexpression of 5-HT_4R was neurotoxic in the hippocampus. Further studies should consider using other promoters to drive an optimal expression of 5-HT_4R. For example, another study used human synapsin (hSyn) promoter for successful AAV-mediated overexpression of 5-HT_4R in the mPFC (Castello et al., 2017), although mPFC neurons could be more resilient for 5-HT_4R overexpression.

3.4.2. 5-HT_4R in corticostriatal circuit mediates some anxiety and depression related behaviors

In contrast to the hippocampal 5-HT_4R function, the ablation of 5-HT_4R from CStr layer 5a p11 expressing neurons led to a slightly anxiolytic phenotype suggesting that CStr 5-HT_4R may regulate competing circuit elements against the hippocampus in mediating anxiety-like behaviors. In addition, our results imply

that CStr 5-HT_4R may be necessary for regulating mood related behaviors since the loss of CStr 5-HT_4R was antidepressant-like in a despair based assay, FST. In this context, the anxiolytic phenotype observed in NSF in CStr 5-HT4R cKO mice could be also interpreted as antidepressant-like since NSF paradigm has predictive validity for chronic antidepressant responses. Taken together, the loss of 5-HT_4R form CStr layer 5a pyramidal neurons had some anxiolytic and antidepressant-like behavioral consequences.

3.4.3. 5-HT_4R in corticostriatal circuit may regulate hedonic effects of SSRIs

We also tested the specific hypothesis that 5-HT_4R in CStr p11 neurons may be mediating the behavioral antidepressant-like responses to chronic SSRI treatment. Our results suggested that CStr 5-HT_4R was not necessary for the antidepressant-like behavioral effects of SSRI fluoxetine in the NSF and TST. However, the expected antidepressant-like effects of the SSRI in the splash test were blocked when CStr 5-HT_4R was ablated, suggesting a role for 5-HT_4R in CStr neurons in mediating hedonic effects of SSRI treatment. In fact, the dorsomedial striatum (DMS) plays a significant role in reward learning and motivated behavior (Voorn et al., 2004). Since the splash test is based on rewarding properties of grooming and sucrose, it is possible that 5-HT_4R mediates the effects of enhanced serotonergic tone by increasing the output from p11 CStr cells to the DMS upon chronic SSRI treatment and ultimately driving the hedonic antidepressant responses. These results provide an evidence that the

SSRI mediated enhancement of various mood related behaviors may be differentially mediated via distinct circuits and serotonin receptors. Another possibility may involve the well-described role of CStr system in repetitive behavior (Langen et al., 2012). Since grooming can also be considered as a type of repetitive behavior in rodents, 5-HT_4R may be necessary for the effects of SSRI on the CStr connections mediating this behavior.

Lastly, it should be also considered that CStr layer 5a neurons targeted by Tlx3-Cre are spanned across various functionally distinct cortical areas, and have extensive local and long range CCor connections. It is a possibility that CStr 5-HT_4R may regulate any part of the cortical circuits that could lead to the observed effects after the ablation of this receptor. Further studies that selectively target 5-HT_4R in functionally distinct subpopulations of CStr neurons will be necessary to tease apart the neuromodulatory roles of this receptor in specific behaviors.

3.4.4. Conclusion

In Chapter 2, the loss of 5-HT_4R from all excitatory neurons in the hippocampus and neocortex elevated anxiety levels to some extent. Further cell type specific analysis in Chapter 3 revealed some evidence for competing circuit elements that possibly have diluted the robust anxiety-like behaviors observed in hippocampal 5-HT_4R cKO mice. In addition, the extensive enhancements in mood related behaviors observed following the loss of 5-HT_4R specifically from the hippocampus support the idea that there could be neural adaptations

compensating for these behavioral changes to surface when all pallial excitatory neurons were missing 5-HT_4R. These findings point out the importance of cell type specific studies in the investigation of neuromodulation of emotive behaviors regulated by a complex network. The molecular and physiological mechanisms though which hippocampal 5-HT_4R mediates these behaviors will be investigated in the next chapter.

CHAPTER 4.

CELLULAR AND MOLECULAR FUNCTIONS OF 5-HT_4 RECEPTOR IN THE HIPPOCAMPUS

4.1. Introduction

The hippocampus accommodates various cell types with distinct contributions to its circuitry. In Chapter 3, we have established that 5-HT_4R in Drd3-Cre cells mediates anxiety and depression related behaviors. Although we gained insights into hippocampal cell types targeted in Drd3-Cre line by morphology, that is, they target cells in granule cell layer and polymorph layer in the dentate gyrus (DG), and pyramidal cell layer in the CA fields, within these fields, cells vary in molecular and functional identity. To pinpoint cell types in which 5-HT_4R may modulate neuronal function regulating anxiety and mood related behaviors, we sought to investigate the molecular identity of cells in which Drd3-Cre is expressed to conditionally abolish 5-HT_4R in Drd3/Htr4 cKO, consequently resulting in anxiogenic and antidepressant-like behavioral responses. This characterization will help us understand the function of 5-HT_4R within hippocampal circuits, and further electrophysiological and molecular investigation will shed light into cellular and molecular roles of 5-HT_4R.

4.1.1. Neuron types and the intrinsic connections of the hippocampus

As discussed in detail in Chapter 3.1.1, the hippocampus is extensively connected to other brain regions especially within the limbic system. While hippocampal afferents and efferents vary in topographical organization along the dorsoventral axis of the hippocampus, the intrinsic hippocampal circuitry

involving various cell types is well preserved and extensively studied (**Figure 4.1**). Here, we will discuss the basic properties of major cell types in the hippocampus to help us understand the consequences of our genetic perturbation within distinct cell types (for extended review (The Hippocampus Book, 2007)).

4.1.1.a. Granule cells of the dentate gyrus

The principal cell type of the dentate gyrus (DG) is the granule cell (GC). GCs have canonical spiny dendrites that extend into the molecular layer (**Figure 4.1**). They receive spatially isolated synaptic inputs on different parts of their dendrites: the proximal third (closest to the cell body), from the commissural/associational fibers arising from the mossy cells of hilus; middle third, from the medial entorhinal cortex (EC); and the distal, from the lateral EC (Amaral et al., 2007). In addition, GCs also receive neuromodulatory and inhibitory input from several external sources and local interneurons either on their dendrites or their cell bodies.

The resting membrane potential of a GC is more hyperpolarized than that of a pyramidal neuron in the CA fields although both cell types have similar action potential thresholds (Penttonen et al., 1997). Therefore, larger depolarizations are required to bring a GC to threshold for action potential generation. As the major excitatory input to the rest of the hippocampus, this characteristic may provide a wider range for neuromodulatory signals.

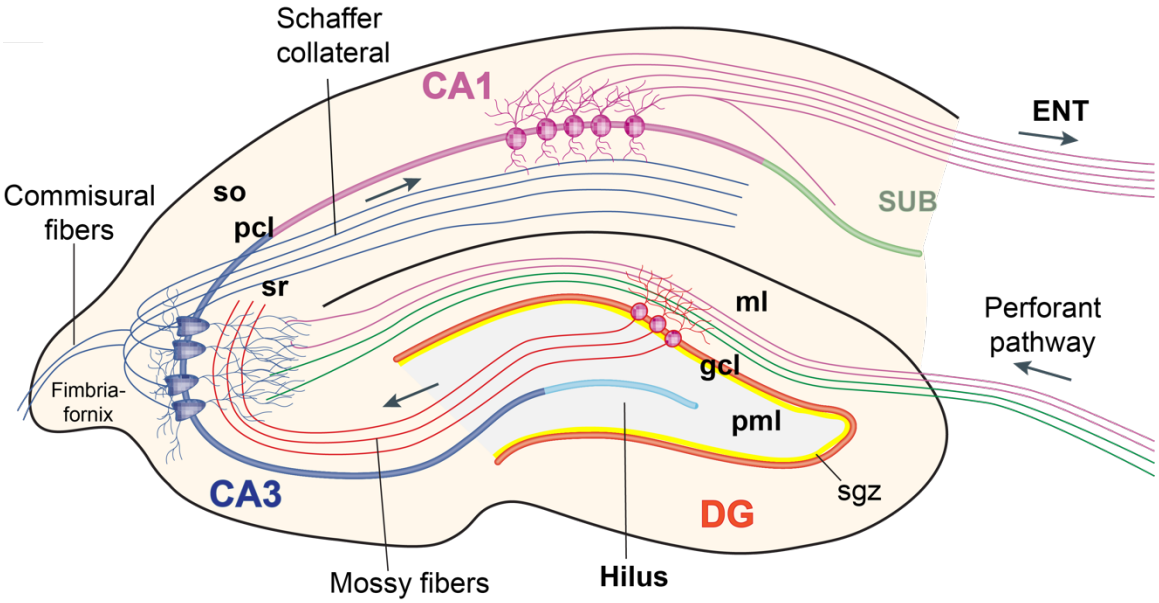

Figure 4.1. Hippocampal regions and intrinsic circuitry.
An illustration of basic hippocampal circuitry. Modified from Deng et al. (2010).
DG: dentate gyrus, SUB: subiculum, ENT: entorhinal cortex, mi: molecular layer, gcl: granule cell layer, pml: polymorph layer, sgz: subgranular zone, so: stratum oriens, pcl: pyramidal cell layer, sr: stratum radiatum.

Upon reaching the threshold in response to long depolarizing input, granule cells fire trains of action potentials demonstrating marked accommodation (Penttonen et al., 1997). On the other hand, young adult-born GCs risen from the subgranular zone (SGZ) have distinct electrophysiological properties, including high input resistance and a lack of GABAergic inhibition. This results in lower activation thresholds and higher excitability compared to mature GCs (Toni and Schinder, 2015). Notably, young adult-born GCs inhibit the overall activity of the mature GCs by recruiting local interneurons.

4.1.1.b. Mossy cells of the hilus

Another major excitatory neuron of the DG is the mossy cell in the polymorphic layer (the hilus) (**Figure 4.1**). Mossy cells receive direct excitatory input from the granule cell mossy fibers (Scharfman, 2013). Mossy cells exhibit frequent and large excitatory postsynaptic potentials (EPSPs), that can trigger bursts of action potentials (Scharfman and Schwartzkroin, 1988). The axons of mossy cells form the majority of excitatory projections on to the proximal dendrites of granule cells (Buckmaster et al., 1992). Indeed, individual mossy cells contribute to both the ipsilateral and contralateral projections. The projections from mossy cells located at any particular level of the dentate gyrus are distributed widely to both septal and temporal regions of the DG from the point of origin (Amaral and Witter, 1989). One of the most outstanding characteristics of these projections regarding their contribution to the

hippocampal circuit is that they are extremely weak at the level of the cells of origin while becoming increasingly stronger at levels that are progressively more distant. This indicates that the mossy cells transmit the collective output of GCs from one septotemporal region to GCs located at distant levels of the DG.

4.1.1.c. Interneurons of the dentate gyrus

There is an extreme diversity of interneurons in dentate gyrus. Some have axons that terminate on cell bodies, whereas others on the initial segments of the axons of different DG neurons executing distinct functions in the local circuit (Freund and Buzsáki, 1996). They are all GABAergic although can be distinguished on the basis of their location in a specific layer, morphology, inputs, electrophysiological properties or immunoreactivity to certain marker proteins and peptides such as parvalbumin (PV), somatostatin (SST), cholecystokinin (CCK) and vasoactive intestinal peptide (VIP).

One of the most widely studied interneuron classes is the basket cells due to their extensive direct innervation of granule cells. They are generally located along the hilar surface of the granule cells. Their axonal terminals form a basket shaped axonal plexus surrounding the granule cells, with inhibitory synapses located primarily on the cell bodies and proximal dendritic shafts of the granule cells (Freund and Buzsáki, 1996; Hu et al., 2014). Within the subgranular region, polymorphic and molecular layers of the DG, there are several other interneuron types with distinct forms and molecular profiles. GABAergic neurons in the

polymorphic layer are innervated by other extrinsic and local GABAergic terminals. These polysynaptic inhibitory interconnections provide intricate inhibitory and disinhibitory control of granule cell excitability. This inhibitory circuit is also differentially modulated by monoaminergic neuromodulators based on the specific receptors expressed in different cell types (Medrihan et al., 2017).

4.1.1.d. Neurons of the CA fields

The principal neuronal cell type of the CA fields is the pyramidal cell. As in the dentate gyrus, there is also a heterogeneous population of GABAergic interneurons scattered through all layers (Freund and Buzsáki, 1996). The inputs to infrapyramidal parts of CA fields (between pyramidal cell layer and hippocampal fissure) are relatively layer specific (The Hippocampus Book, 2007). From distal (closer to subiculum) to proximal (closer to DG), these projections consist of entorhinal afferents, Schaffer collaterals (from CA3 to CA1), recurrent and commissural collaterals (CA3 to CA3), mossy fibers (DG to CA3) (**Figure 4.1**). Suprapyramidal parts of the CA fields (between pyramidal cell layer and alveus) receive mostly recurrent connections. The CA3 to CA1 projection, the major input to CA1 pyramidal cells, terminates on the basal and the apical dendrites.

The connection from a particular CA3 pyramidal neuron to a CA1 pyramidal neuron depends on the septotemporal positions of the two cell bodies. At one particular septotemporal level, a distal CA3 cell (closer to CA1) is more

likely to interact with a proximal CA1 cell (closer to CA3), whereas a proximal CA3 cell (closer to DG) is more likely to interact with a distal CA1 cell (closer to subiculum).

4.1.2. Serotonergic modulation of hippocampal neurons

In the hippocampus, serotonergic input from the raphe nuclei terminates primarily in the hilus where it differentially modulates the activity of distinct cell types depending on the serotonin receptor composition (Swanson, 1987). 5-HT induces a hyperpolarization in isolated GCs in rodent slice preparations, at least in part, due to the expression of 5-HT_{1A} heteroreceptors (Piguet and Galvan, 1994). Other serotonin receptors coexpressed within GCs may mediate this inhibitory effect of 5-HT. For example, 5-HT_4R has been shown to decrease the afterhyperpolarization (AHP) following an action potential in the presence of 5-HT mediating the excitability (Andrade, 2006; Fagni et al., 1992; Torres et al., 1995). Moreover, in vivo, enhanced serotonergic tone in the DG after chronic SSRI treatment inhibits the activity of GCs through 5-HT_{1A}R which is necessary for behavioral responses to SSRIs (Samuels et al., 2015). Interestingly, optogenetic activation specific to the ventral dentate gyrus granule cells decreases innate anxiety-like behaviors (Kheirbek et al., 2013).

In addition to the direct modulation of GCs, interneuron activity has shown to be regulated via 5-HT by various 5-HTRs, and consequently, the activity of GC. For instance, enhanced serotonergic tone after acute SSRI treatment leads

to the inhibition of CCK-positive basket cells through 5-HT_{1B}R, in turn, disinhibiting PV-positive basket cells. As a result, the increased GABAergic input to GCs decreases the excitability of GCs (Medrihan et al., 2017). Since SSRI treatment leads to elevated neurogenesis in DG (David et al., 2009), and stress and glucocorticoids increase dentate gyrus activity (Schoenfeld et al., 2013), the neurogenic inhibition via young adult born GCs of the dentate gyrus may also be relevant for anxiety and depression. Modulating the dentate gyrus activity may direct the output strength from the hippocampus to downstream limbic centers and moderate the extended anxiety and mood network.

A number of features of pyramidal cell physiology are also under modulatory control by 5-HT. For example, serotonin has biphasic effects on CA1 pyramidal neurons, initially causing hyperpolarization due to the activation of a potassium (K+) current possibly through 5-HT_{1A}R, yet later leading to depolarization and inhibition of the AHP, possibly via some excitatory 5-HTRs, such as 5-HT_4R (Tokarski et al., 2002). Numerous other modulatory effects have been reported in pyramidal neurons of the CA fields, indicating that the resting and active properties of these neurons in vivo are likely to regulate behavioral states.

Serotonin has neuromodulatory effects depending on the serotonergic receptor profile of a specific neuron. As an excitatory GPCR, 5-HT_4R has been indicated to play a role in the activity of the neurons, increasing the excitability in the presence of 5-HT and 5-HT_4R agonist. In addition, increased serotonergic

tone via SSRI's has shown to decrease the excitability of the granule cells in DG. Thus, the investigation of neuronal activity and physiological properties in the absence of 5-HT_4R will provide more insights into both intracellular and circuit functions of this receptor.

4.1.3. Differential gene expression along the dorsoventral axis of the hippocampus

The development of a transcriptional map of the mouse hippocampus, using genome-scale in situ hybridization, has provided more detailed molecular evidence for distinct patterns of gene expression in mouse brain including hippocampus (Allen Brain Atlas)(Lein et al., 2007). Using robust gene markers, it has been proposed that the dentate gyrus, the CA3 and CA1 are segregated into three major molecular domains: dorsal, intermediate and ventral (Strange et al., 2014). Furthermore, the advancement in next generation genome-wide RNA sequencing has allowed for the analysis of the transcriptome of the principle excitatory neurons in the hippocampus, providing further evidence for the molecular diversity of neurons within the same layer at spatially distinct regions (Cembrowski et al., 2016).

Notably, four serotonin receptors, Htr1a, Htr2a, Htr2c and Htr7, also display an expression pattern that varies along the dorsoventral axis (Tanaka et al., 2012). The differential gene expression among discreet subpopulations of hippocampal neurons may also underlie physiological differences in neuronal

excitability (Dougherty et al., 2012) and synaptic plasticity (Dougherty et al., 2013; Maggio and Segal, 2007).

In this chapter, we investigated the underlying cellular and molecular mechanisms of the mediating function 5-HT_4R in anxiety and depression related behaviors. The identification of the cell types targeted by our genetic perturbation, and the investigation of cellular and molecular responses to 5-HT_4R ablation (such as changes in gene expression along hippocampal long axis and in electrophysiological properties of the neurons) will help us understand the function of this receptor at the cellular level.

4.2. Drd3-Cre and Htr4 expression in distinct cell types of the hippocampus

4.2.1. Cell type specific Drd3-Cre expression

To visualize the Cre expressing cells in Drd3-Cre mice, we used immunofluorescent labeling of EGFP in coronal sections of whole brain samples Drd3-Cre::EGFP-L10a mice. Drd3-Cre mice were crossed with a Cre dependent EGFP-RPL10a (EGFP-L10a) expressing reporter mouse line to generate the Drd3-Cre::EGFP-L10a line. Since EGFP is fused with the RPL10a (ribosomal protein subunit L10a), it would primarily localize to the soma of Drd3-Cre expressing neurons for an ideal identification without labeling the projections.

We first investigated the dorsal and ventral hippocampus expression pattern of Drd3-Cre::EGFP-L10a by co-labeling the hippocampal sections with anti-EGFP and anti-neuronal nuclei (NeuN) antibodies. NeuN is a neuronal nuclear protein synthesized by feminizing locus on X-3 gene, *Fox-3*, and commonly used as a histological marker for most neurons. In dorsal parts of the hippocampus, most of the CA1 and CA3 pyramidal neurons expressed EGFP-L10a and all of them co-localized with NeuN showing that all Cre expressing cells are neuronal (**Figure 4.2A,** left). However, as also discussed previously, EGFP-L10a expressing cells were not detectable more ventrally in CA1 (**Figure 4.2A,** right). Notably, there was a consistent expression of EGFP-L10a in the granule cell layer and some of the cells in the hilus of DG.

To determine whether any Drd3-Cre neurons in CA field were inhibitory interneurons, we colabeled the Drd3-Cre::EGFP-L10a brain sections with an anti-GAD67 antibody. GAD67 is a glutamic acid decarboxylase (GAD) enzyme that catalyzes the production of GABA, the primary neurotransmitter of the inhibitory interneurons, and can be used as a histological marker for all GABAergic interneurons. Both in the CA1 and CA3, none of the EGFP expressing cells were positive for GAD67 (**Figure 4.2B**), indicating that all Drd3-Cre expressing neurons are excitatory pyramidal cells in these regions.

To identify neuronal cell types of the Drd3-Cre expressing neurons in DG, hippocampal sections from Drd3-Cre::EGFP-L10a mice were double-labeled with antibodies for EGFP and neuronal-type markers (**Figure 4.3**). All EGFP expressing cells in DG were neurons marked by NeuN. Moreover, EGFP expressing cells were colabeled with calbindin (CBD) antibody, a marker for mature granule neurons. Note that some CBD positive cells in the edge of GC layer did not express EGFP (arrowheads), which are possibly the CBD-positive interneurons. In the hilus, EGFP was detected in calretinin (CRT)-expressing mossy cells. On the other hand, it was absent from CRT and doublecortin (DCX)-expressing immature neurons, and GAD67-expressing GABAergic interneurons), including the parvalbumin (PV)-expressing basket cells (asterisk in each corresponding panel).

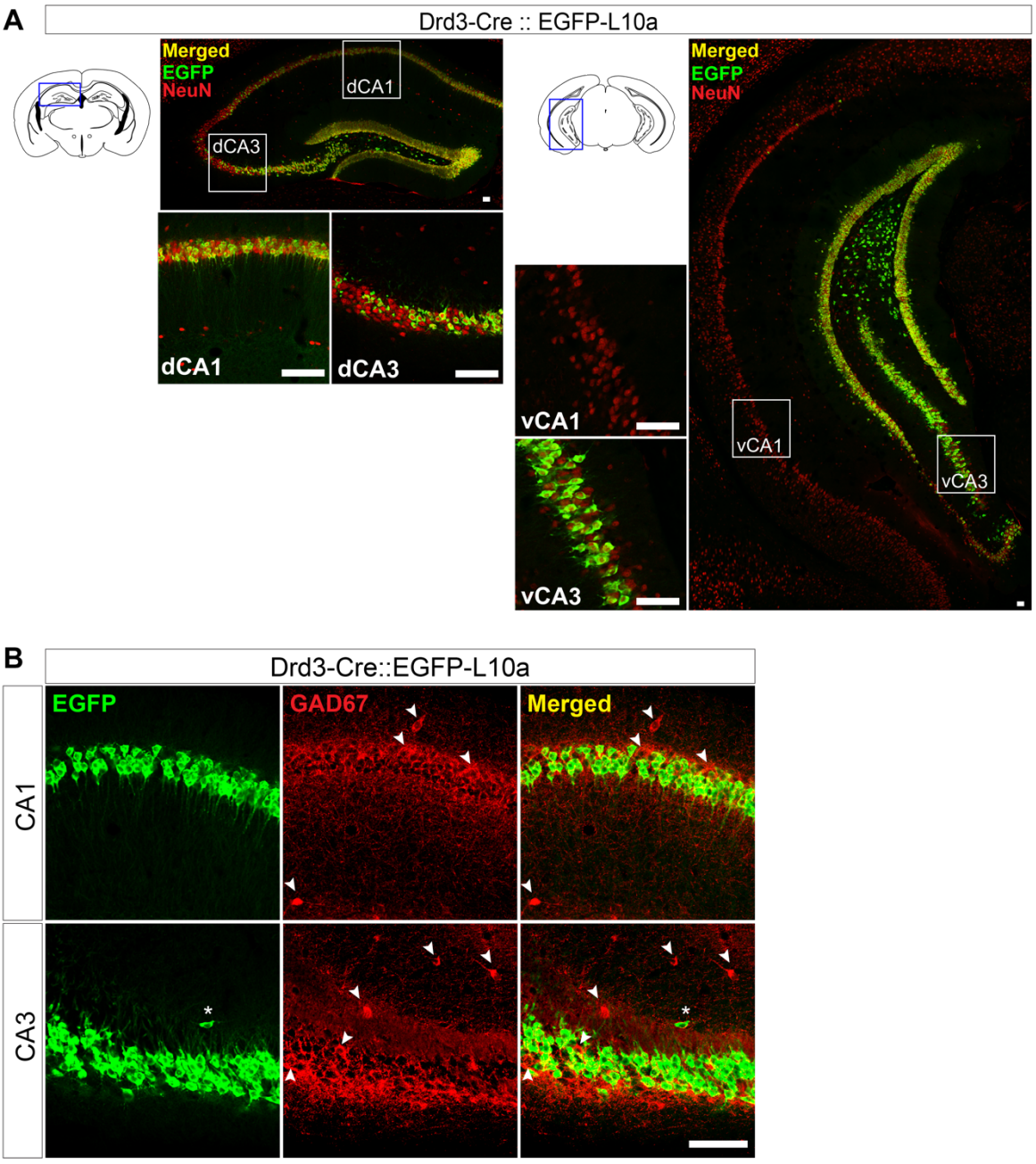

Figure 4.2. Drd3-Cre targets excitatory neurons of the hippocampus.
A. Anti-EGFP (green) and anti-NeuN (red) immunofluorescent images showing Drd3-Cre driven EGFP-L10a expression in the dorsal and ventral hippocampus. Note that EGFP staining was not detected in vCA1.
B. Anti-EGFP (green) and anti-GAD67 (red) immunofluorescent images depicting that none of the Drd3-Cre driven EGFP expressing cells were GAD67-positive GABAergic interneurons, both in the CA1, and CA3 fields. Arrowheads, GAD67-postive cells. Asterisks, GAD67-negative.
Scale bars, 100 μm.

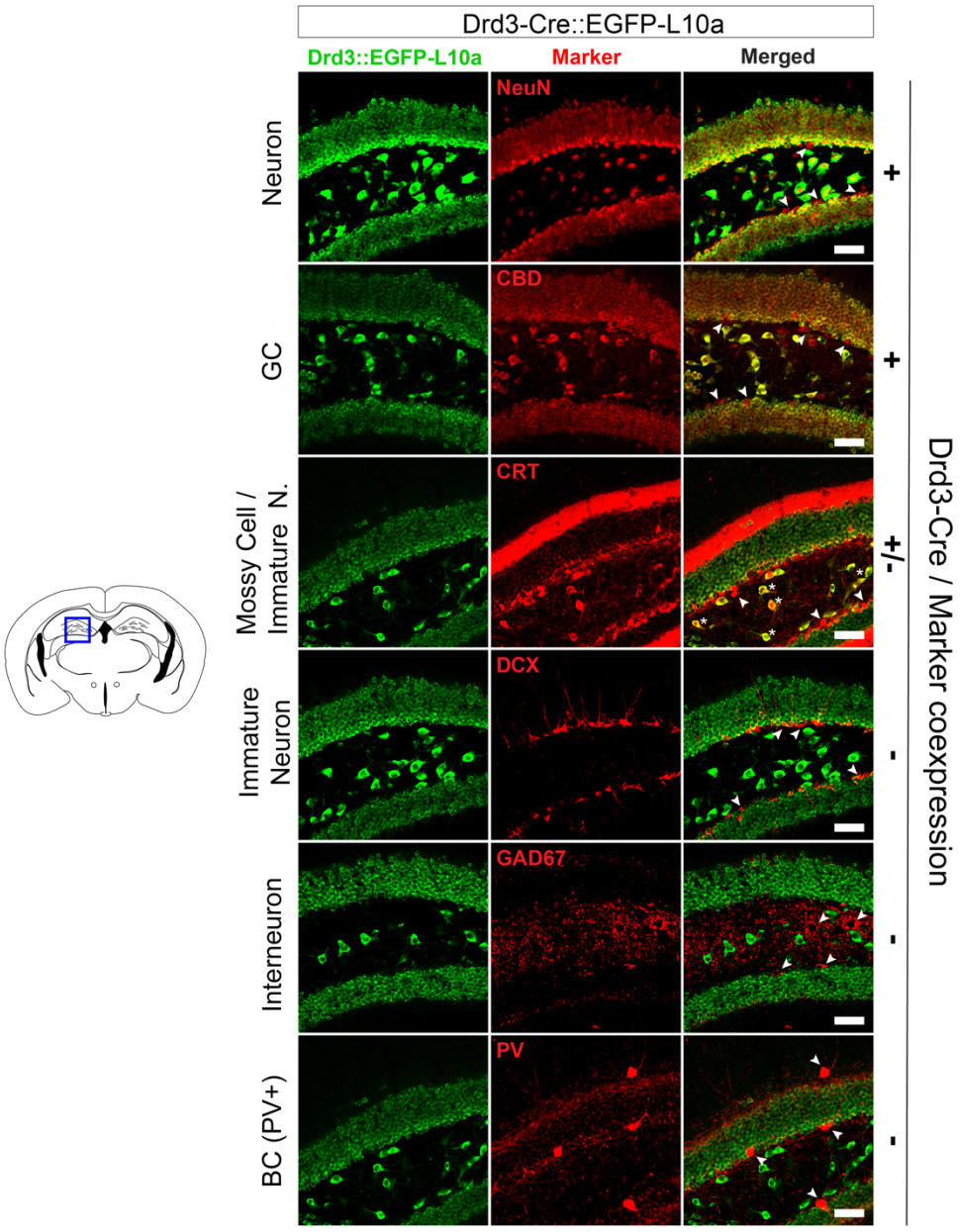

Figure 4.3. Drd3-Cre targets mature excitatory neurons in the dentate gyrus. Immunofluorescent images showing neuronal-type specific marker expression (red) in Drd3-Cre driven EGFP-L10 expressing neurons in dentate gyrus (DG). Arrowheads, cells expressing a specific neuron-type marker but not EGFP. Asterisks, cells coexpressing hilar mossy cell marker CRT and EGFP.
Scale bars, 50 μm.

Together, we conclude that, in the DG, Drd3-Cre exclusively targets mature excitatory neurons – mature granule cells and hilar mossy cells but not immature neurons, interneurons and non-neuronal cells (such as glia). In the CA fields, Drd3-Cre also only targets the excitatory pyramidal cells. This suggests that using Drd3-Cre to genetically ablate 5-HT_4R leads to its absence in the mature excitatory neurons of the hippocampus.

4.2.2. Cell type specific expression of Htr4-EGFP-L10a

In order to determine whether Drd3-Cre targets all 5-HT_4R expressing cells in the hippocampus, we wanted to identify 5-HT_4R expressing cell types. Due to its recapitulation of Htr4 expression pattern, we used Htr4-bacTRAP mice (Htr4-EGFP-L10a), which express EGFP-L10a under the regulatory elements and promoter of the *Htr4* gene. We investigated the distribution of EGFP-L10a along the dorsoventral axis by colabeling the hippocampal sections with anti-EGFP and anti-NeuN (**Figure 4.4A**). Throughout the hippocampus, Htr4-EGFP-L10a was expressed in most of the pyramidal cells of CA regions, and most of the cells in the granule cell layer and some cells in the hilus of DG. Notably, all EGFP labeled cells were NeuN-positive showing that Htr4-EGFP-L10a expressing cells are neuronal. In addition, anti-GAD67 immunofluorescent labeling in CA fields revealed that Htr4-EGFP-L10a neuron population did not include any GABAergic interneurons (**Figure 4.4B**), suggesting that *Htr4* is expressed only in excitatory neurons in the CA field.

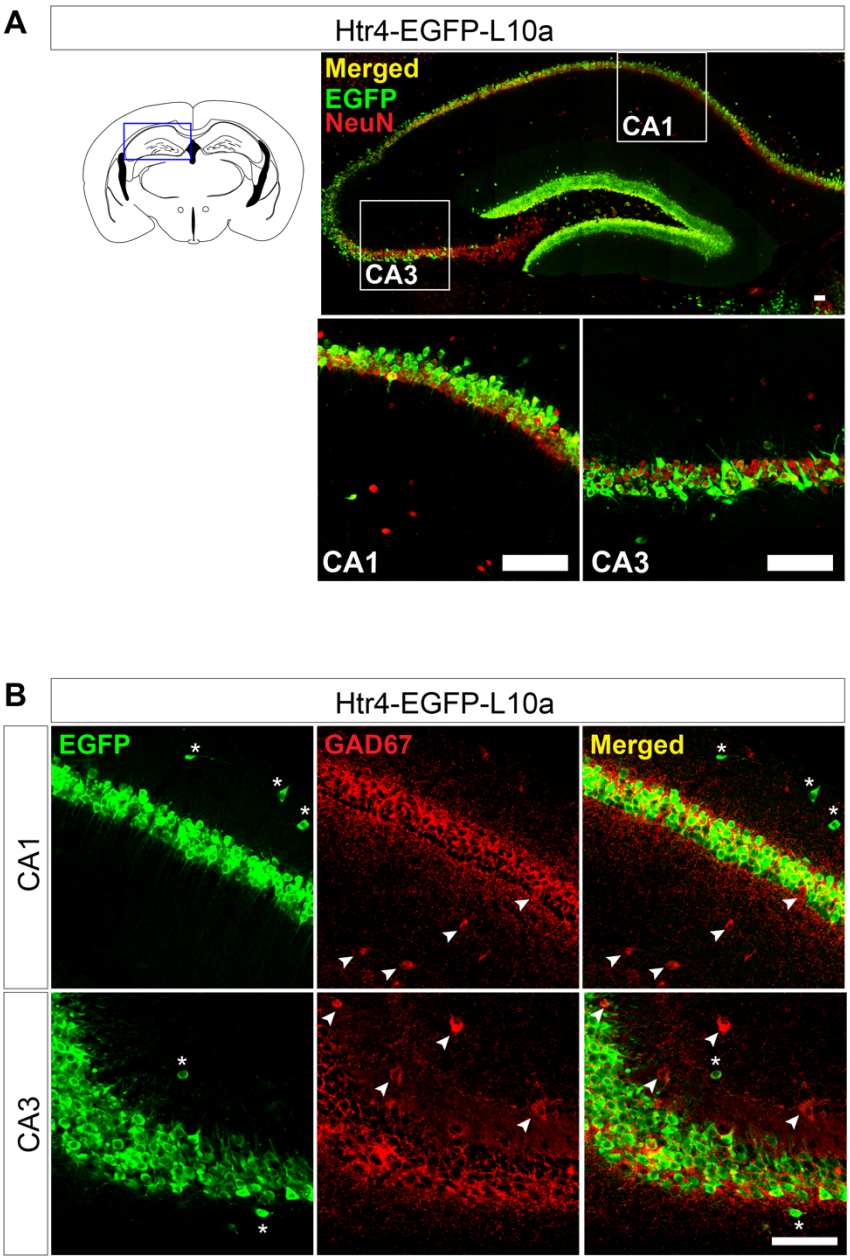

Figure 4.4. Htr4-EGFP-L10a is expressed in excitatory neurons of the hippocampus.
A. Anti-EGFP (green) and anti-NeuN (red) immunofluorescent images showing Htr4-EGFP-L10a expression in hippocampus (above). Higher magnification images showing coexpression of Htr4-EGFP-L10a and NeuN in CA1 and CA3 pyramidal cell layer (below).
B. Anti-EGFP (green) and anti-GAD67 (red) immunofluorescent images depicting that none of the Htr4-EGFP-L10a driven EGFP expressing cells were GAD67-positive GABAergic interneurons, both in the CA1, and CA3 fields. Arrowheads, GAD67-postive cells. Asterisks, GAD67-negative. Scale bars, 100 μm.

To identify which neuronal cell types express 5-HT_4R in the DG, hippocampal sections from Htr4-EGFP-L10a mice were double-labeled with antibodies for EGFP and neuronal-type markers (**Figure 4.5**). Similar to the Drd3-Cre line, Htr4-EGFP-L10a expressing cells were all neurons positive for NeuN in DG. Moreover, Htr4-EGFP-L10a was detected in CBD-expressing mature granule neurons and CRT-expressing mossy cells in hilus; whereas, it was absent in DCX- and CRT-expressing immature neurons and GAD67-expressing GABAergic interneurons, including PV-expressing basket cells. Together, the expression pattern of transgenic Htr4-bacTRAP line suggests that, in the DG, 5-HT_4R is expressed in mature excitatory neurons – mature granule cells and hilar mossy cells, similar to Drd3-Cre expression pattern. Therefore, in the DG, Drd3-Cre possibly targets almost all of the *Htr4* expressing cells. In CA fields, most of the *Htr4* expressing pyramidal cells were also targeted by Drd3-Cre except in the ventral parts of CA1 where Drd3-Cre expression is absent.

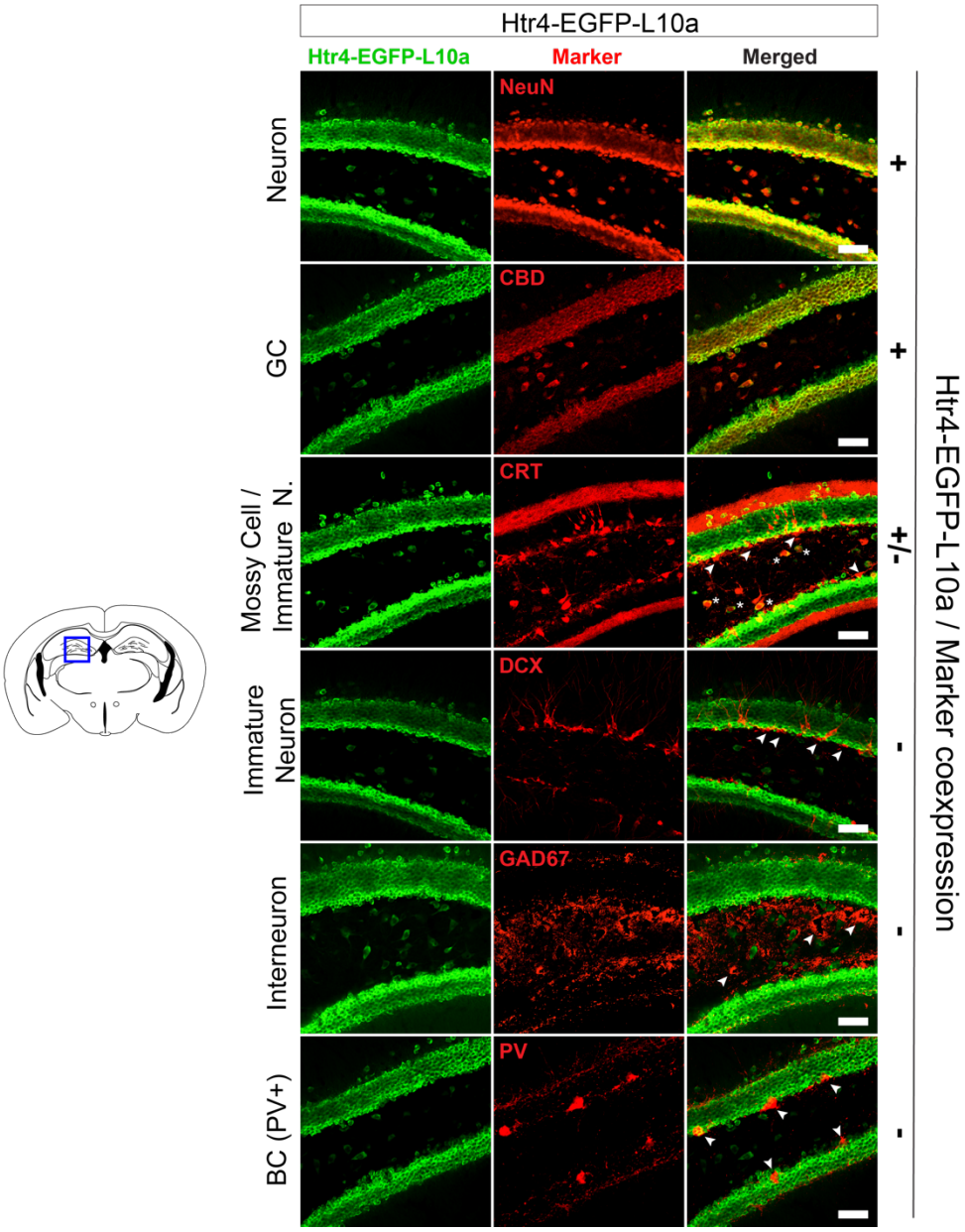

Figure 4.5. Htr4-EGFP-L10a is expressed in mature excitatory neurons in the dentate gyrus.
Immunofluorescent images showing neuronal-type specific marker expression (red) in Htr4-EGFP-L10a expressing neurons in dentate gyrus (DG). Arrowheads, cells expressing a specific neuron-type marker but not EGFP. Asterisks, cells coexpressing hilar mossy cell marker CRT and EGFP.
Scale bars, 50 μm.

4.3. Cellular and molecular adaptations in hippocampus specific *Htr4* knockout mice

As we identified the cell types in which 5-HT_4R was ablated in the Drd3/Htr4 cKO mice, we next sought to examine the cellular and molecular neuroadaptations that may underlie the behavioral phenotype observed. Specifically, since the absence of hippocampal 5-HT_4R led to behavioral antidepressant-like responses, we wanted to examine whether it also resulted in any antidepressant-like responses at cellular and molecular levels, such as enhanced adult hippocampal neurogenesis and increased expression of neurotrophic factors.

4.3.1. The effect of hippocampus specific loss of 5-HT_4R on neurogenesis

4.3.1.a. Changes in the number of young adult born granule cells

One of the hallmarks of antidepressant-like responses in the hippocampus is increased adult hippocampal neurogenesis. SSRIs and other antidepressant treatments boost neurogenesis in DG and neurogenesis is necessary for some of the behavioral responses to antidepressant treatment. To determine whether the loss of 5-HT_4R from the hippocampus altered adult hippocampal neurogenesis, we examined brains from the Drd3/Htr4 cKO mice and their control littermates from which the behavioral measures were previously assessed. To measure any

differences in adult hippocampal neurogenesis between groups, we measured the number of immature adult born granule cells (abGC) which are neurons that have recently been born in the SGZ of the DG, become post-mitotic, yet not fully incorporated in GC layer. Briefly, we immunolabeled abGCs with anti-doublecortin (DCX), a marker for immature neurons, in coronal brain sections of Drd3/Htr4 cKO mice and their control littermates. Under a fluorescent microscope, the number of DCX-positive cells was measured in the SGZ in every sixth 40 μm section, counting the cells at any depth in a section while blinded for genotype (**Figure 4.6A**). The hippocampus was divided into three subdivisions depending on the position of the coronal sections according to bregma – dorsal, intermediate and ventral (4 sections per subdivision) – to get a better estimate of the number of immature abGCs in the dorsoventral axis. Neurogenesis was calculated as the number of DCX+ neurons per granule cell layer area per section (**Figure 4.6B**) and averaged per region for normalization between sections and regions. We observed that there were more DCX+ neurons in the ventral DG of Drd3/Htr4 cKO mice compared to the controls (WT) (**Figure 4.6C**). Indeed, DCX+ neurons per area was significantly higher (67%) specifically in the ventral DG in the cKO compared to WT ($p=0.002$, $n=5$ animals per group) (**Figure 4.6D**). There was not any significant difference in the dorsal or intermediate DG between genotypes. These results indicated that Drd3/Htr4 cKO mice had increased number of immature abGC in the ventral DG, implying the loss of 5-HT_4R led to increased ventral hippocampal neurogenesis.

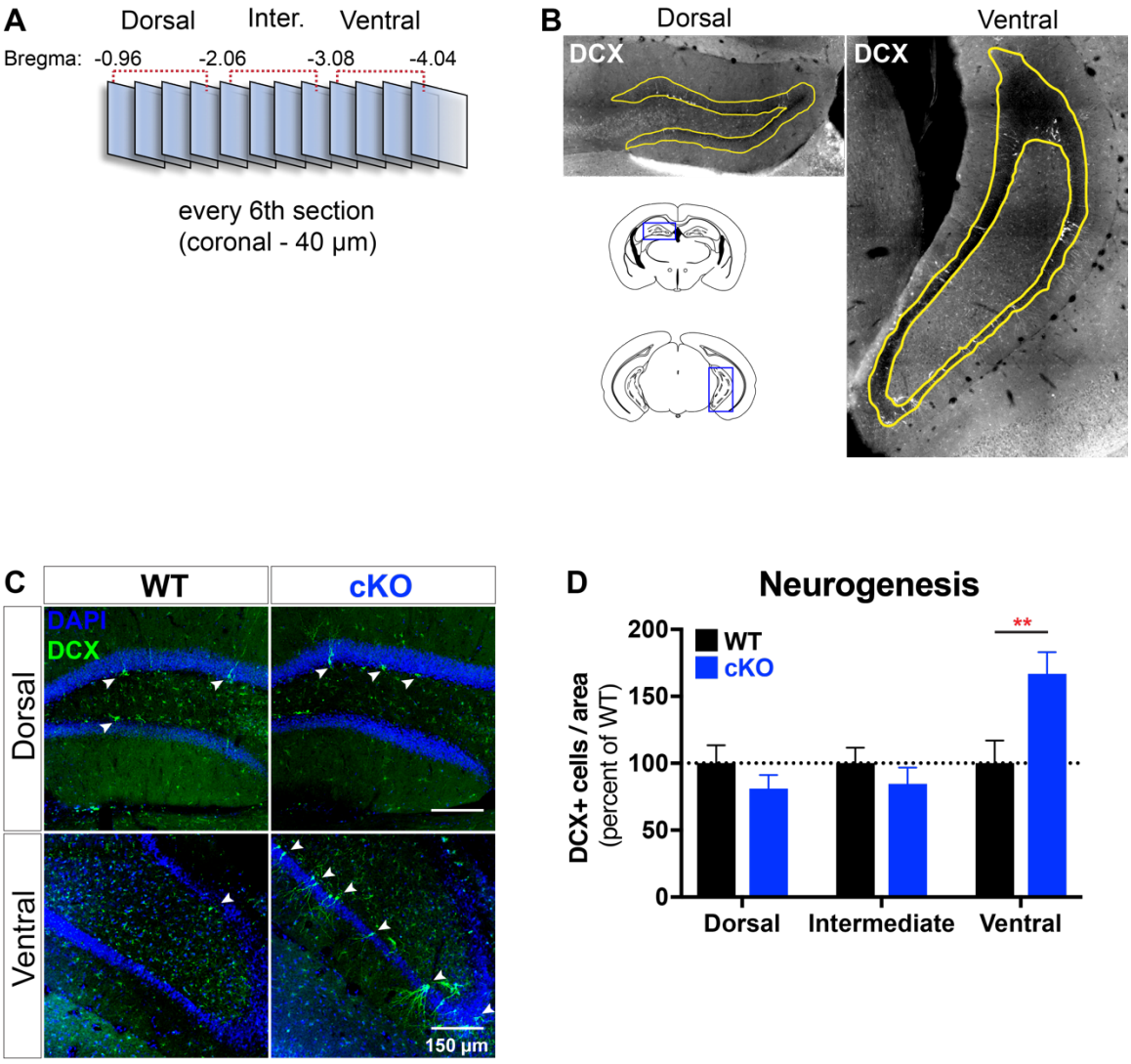

Figure 4.6. Drd3/Htr4 cKO mice showed increased neurogenesis specifically in the ventral dentate gyrus.

A. A schematic of the experimental approach. The hippocampus was divided into three subdivisions depending on the position of the coronal sections according to bregma – dorsal, intermediate and ventral (4 sections per region). The number of DCX-positive cells was measured in every sixth 40 μm section.

B. A depiction of granule cell layer area calculation in Image J in sections from which DCX+ neurons were counted.

C. Examples of immunofluorescent confocal microscopy images showing increased number of DCX+ cells (green) in the ventral DG.

D. DCX+ cells per area was significantly higher (67%) in the ventral DG in the cKO compared to WT. Data are represented as mean ± SEM. Two-way ANOVA followed by post hoc Fisher's LSD test. n=5 animals per group, **p<0.01.

4.3.1.b. Changes in the expression of neurotrophic factors

Increase in the levels of neurotrophic factors in the hippocampus have been associated with increased neurogenesis and the action of serotonergic antidepressants. To gain insight into the underlying molecular mechanism that may lead to enhanced adult hippocampal neurogenesis, we measured the gene expression levels of the neurotrophic factors, BDNF and VEGF, in the hippocampus (*Bdnf* and *Vegfa* genes, respectively). Dorsal and ventral parts of the DG and CA fields were dissected from the brains of the Drd3/Htr4 cKO mice and their control littermates from which the behavioral measures were previously assessed (**Figure 4.7A**). Total RNA samples from these four parts of the hippocampus were isolated, and the microdissection quality was checked by qRT-PCR measurements of the expression of region enriched genes: *Dsp* (desmoplakin, specific for DG), *Tyro3* (TYRO3 protein tyrosine kinase 3, specific for CA), *Lct* (lactase, specific for dDG) and *Trhr* (thyrotropin releasing hormone receptor, specific for vDG). All of our hippocampal regions were enriched for their respective region-specific gene expression, confirming the quality of the dissection (**Figure 4.7B**). In all four regions, *Bdnf* and *Vegfa* expression were consistently and significantly increased in Drd3/Htr4 cKO samples compared to control throughout the hippocampal regions (BDNF, $p=0.0007$; VEGF, $p=0.0034$; Two-way ANOVA) (**Figure 4.7C**).

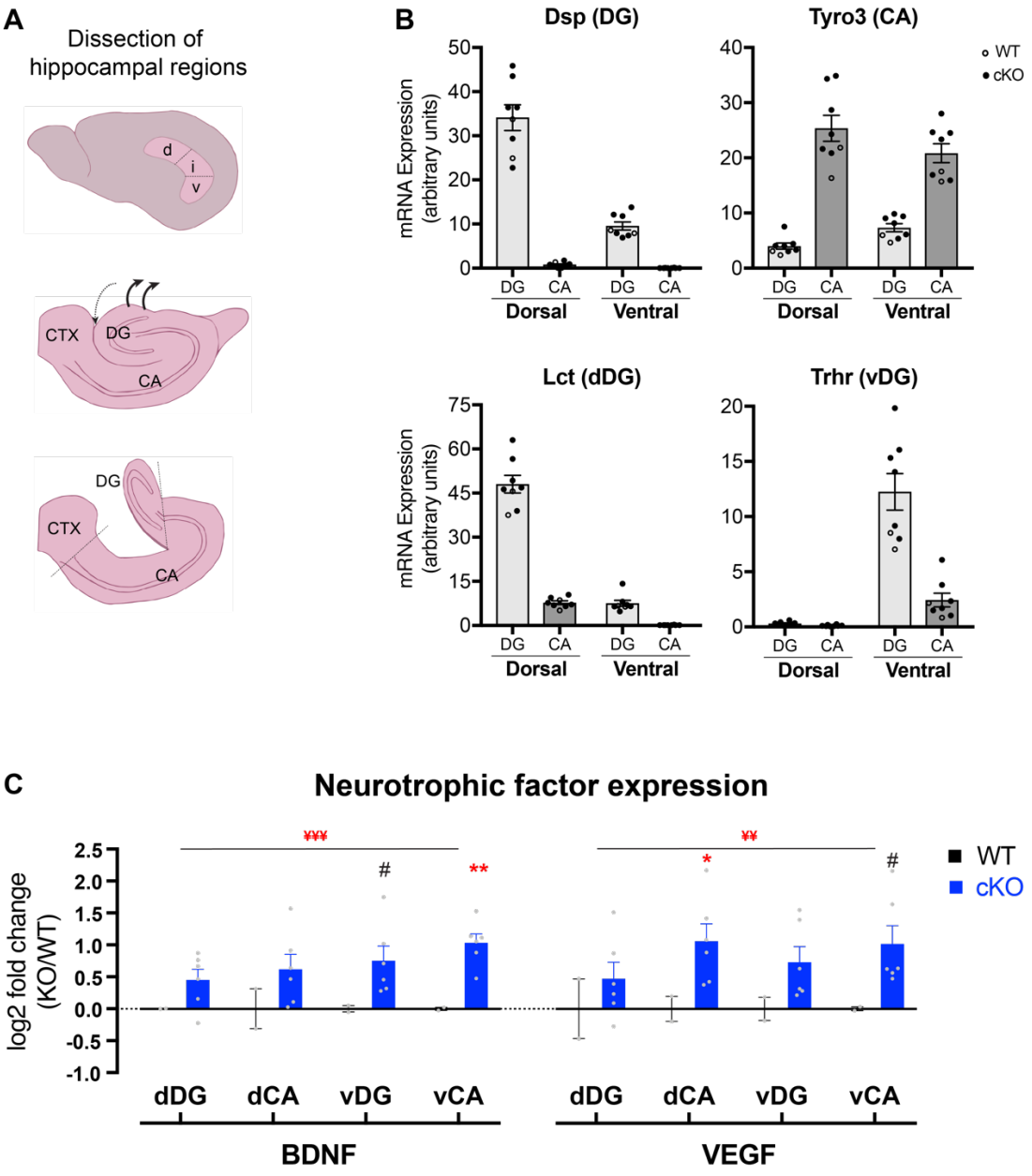

Figure 4.7. Drd3/Htr4 cKO mice showed elevated expression of neurotrophic factors in the hippocampus.

A. A schematic of the microdissection of different regions in hippocampus.

B. qRT-PCR measurements of the expression of region enriched genes in all samples: *Dsp* (desmoplakin, specific for DG), *Tyro3* (TYRO3 protein tyrosine kinase 3, specific for CA), *Lct* (lactase, specific for dDG) and *Trhr* (thyrotropin releasing hormone receptor, specific for vDG). Each hippocampal region was enriched for its respective region-specific gene expression. Data points represent WT and cKO sample replicates.

C. qRT-PCR measurements of the expression of neurotropic factors BDNF and VEGF showed significantly higher expression of both factors in Drd3/Htr4 cKO compared to WT throughout the hippocampal regions. Two-way ANOVA, ¥¥p<0.01, ¥¥¥p<0.001. Post hoc Fisher's LSD test, **p<0.01, *p<0.05, #p<0.10. WT: n=2, cKO: n=5.

4.3.2. Neuroadaptations in the serotonergic system in the hippocampus upon the loss of hippocampal 5-HT_4R

Serotonin receptors are expressed in various cell types in distinct combinations and act synergistically to mediate the effects of 5-HT on gene expression and cellular function. To determine whether there are neuroadaptations in the cellular serotonergic system in response to the loss of 5-HT_4R specifically from hippocampal mature excitatory neurons, the gene expression levels of different 5-HT receptors were measured in the total RNA samples from dorsal and ventral parts of DG and CA fields of the hippocampus by qRT-PCR, and compared between Drd3/Htr4 cKO mice and their control littermates (WT). Here, we report the differential expression of five serotonin receptors – *Htr1a, Htr1b, Htr2a, Htr2c and Htr6* – and *S100a10* (p11), as a known regulator of 5-HTR expression. In situ hybridization data from Allen brain atlas (**Figure 4.7A**) and other studies have shown the expression pattern of Htrs in the hippocampal regions and cell types (Tanaka et al., 2012). Briefly, *Htr1a* is expressed in all regions including GC in the DG, pyramidal cells in the CA fields and interneurons. *Htr1b* is expressed mainly expressed in CA1 pyramidal cells and some interneurons in the DG, while its expression in GCs and CA3 pyramidal cells are observed in lower levels. *Htr2a* is enriched in vCA3 pyramidal cells proximal to the DG, and hilar mossy cells, retaining lower expression in other cell types. On the other hand, *Htr2c* is more enriched in CA3 pyramidal cells distal to the DG, especially in the ventral hippocampus. *Htr6* have a

ubiquitous expression pattern throughout the hippocampus. *S100a10* is expressed in some CA pyramidal cells and interneurons, and some interneurons in the DG (Egeland et al., 2011b). *Htr1d*, *Htr1f*, *Htr2b*, and *Htr7* expression were too low to detect in our hippocampal samples by qRT-PCR. We did not measure *Htr5a* and *Htr5b* expression in this experiment.

We first showed that mRNA expression levels in our samples from each region, dDG, dCA, vDG and vCA, corresponded to observed expression in ISH data previously reported (**Figure 4.7B**). To better analyze the difference in Htr expression between Drd3/Htr4 cKO and WT, we plotted $\log_2$ fold change of each gene in cKO compared to WT, per region (**Figure 4.7C**).

Overall, the most significant differential expression of Htrs between genotypes was observed in the vDG. In the vDG, *Htr1a* expression was significantly depleted in the cKO (1.35 fold), while *Htr1b*, *Htr2c* and *Htr6* were significantly enriched (1.93, 1.66, and 5.30 folds, respectively). Although the differential expression pattern for these vDG significant genes was similar in the dDG, it was subtle and not significant.

Similar to the DG, the differential gene expression of Htrs between genotypes were more significant in the vCA compared to the dCA. In the vCA, *Htr1a* expression was slightly diminished in the cKO (1.28 fold, p=0.07), while *Htr1b* was significantly enriched (1.95 fold). In addition, *Htr2c* and *Htr6* expression were also slightly enriched in the cKO in the vCA (2.83 fold, p=0.08; 2.22 fold, p=0.08; respectively).

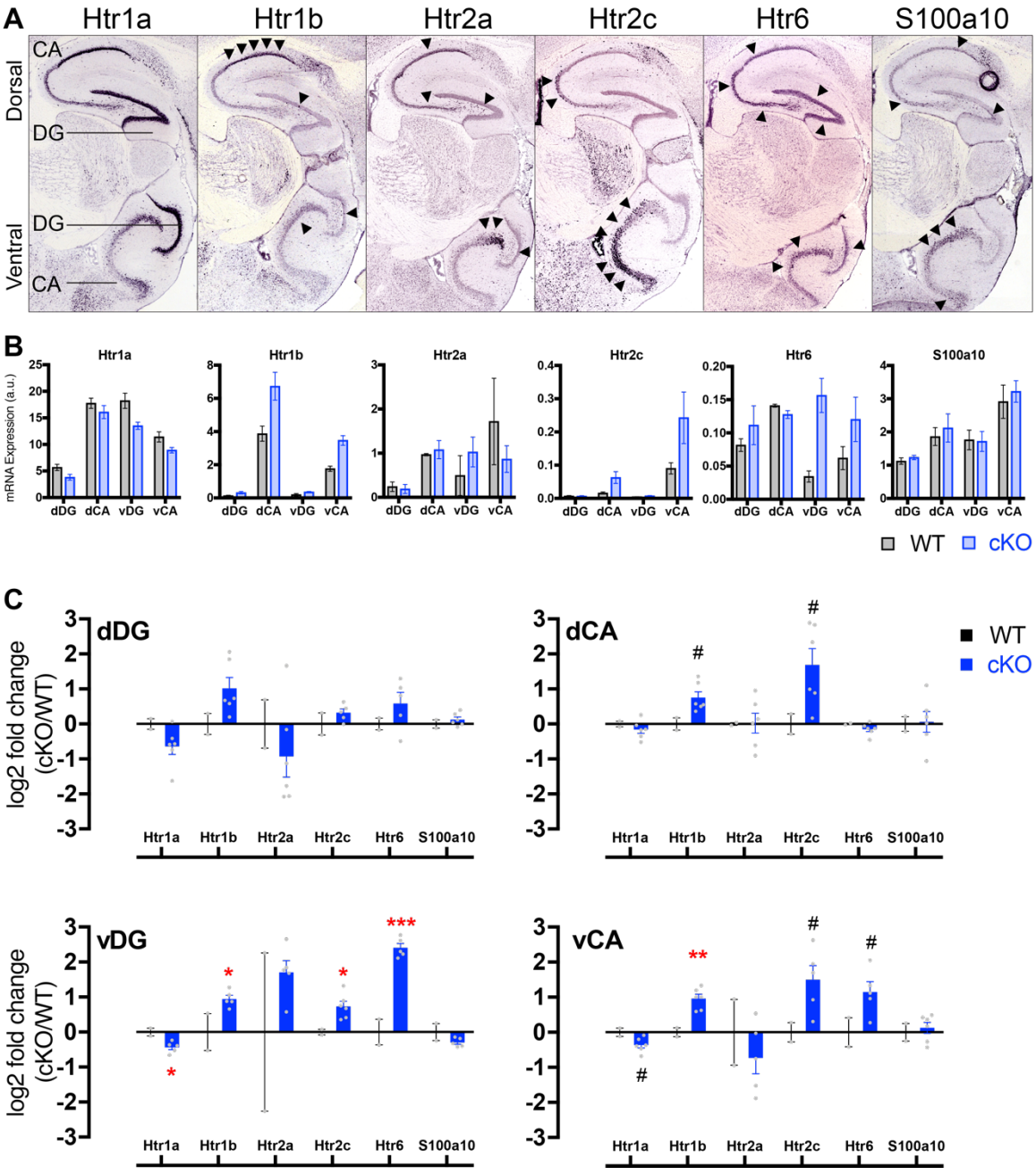

Figure 4.8. Region- and subtype specific-serotonin receptor expression changes in the hippocampus were observed in Drd3/Htr4 cKO mice.

A. Different serotonin receptor (*Htr*) expression profiles by ISH. Images from Allen Brain Atlas.

B. qRT-PCR quantification of each *Htr* expression in our hippocampal region samples. Arbitrary units (a.u.).

C. qRT-PCR quantification of *Htr* expression in Drd3/Htr4 cKO compared to controls (WT) in each hippocampal region.

Data are represented as mean ± SEM. Two-tailed unpaired t-test. WT: n=2, cKO: n=5, ***p<0.001, **p<0.01, *p<0.05, #p<0.10.

Similar to the vCA, *Htr1b* and *Htr2c* also showed slight enrichment in the cKO in the dCA (1.69 fold, p=0.05; 3.22 fold, p=0.10; respectively). There were not any significant differences in the expression levels of *Htr2c* and *S100a10* between genotypes throughout the hippocampal regions.

Together these results showed that, in the Drd3/Htr4 cKO mice compared to controls, *Htr1a* was depleted in the ventral DG and CA fields. *Htr1b* and *Htr2c* were consistently enriched in all regions, more significantly in the ventral hippocampus. Lastly, *Htr6* was preferentially enriched in the ventral hippocampus. Our data revealed that the loss of 5-HT_4R from the mature excitatory neurons of the hippocampus led to neuroadaptations in the serotonergic system in a receptor type- and region-specific manner in the hippocampus.

4.3.3. The role of 5-HT_4R in mediating the electrophysiological properties of dentate gyrus granule cells

To investigate if the specific loss of 5-HT_4R from hippocampal neurons has any electrophysiological consequences, we performed whole-cell patch recordings in dentate gyrus (DG) granule cells (GCs) in acute hippocampal slices from Drd3/Htr4 cKO mice and their control littermates (WT). First, we employed a potent 5-HT_4R agonist, BIMU-8, to test the effect of 5-HT_4R activation in DG GCs. **Figure 4.9A** shows representative traces of whole-cell recordings in the voltage clamp configuration from DG GCs in WT and Drd3-Cre/Htr4 cKO mice.

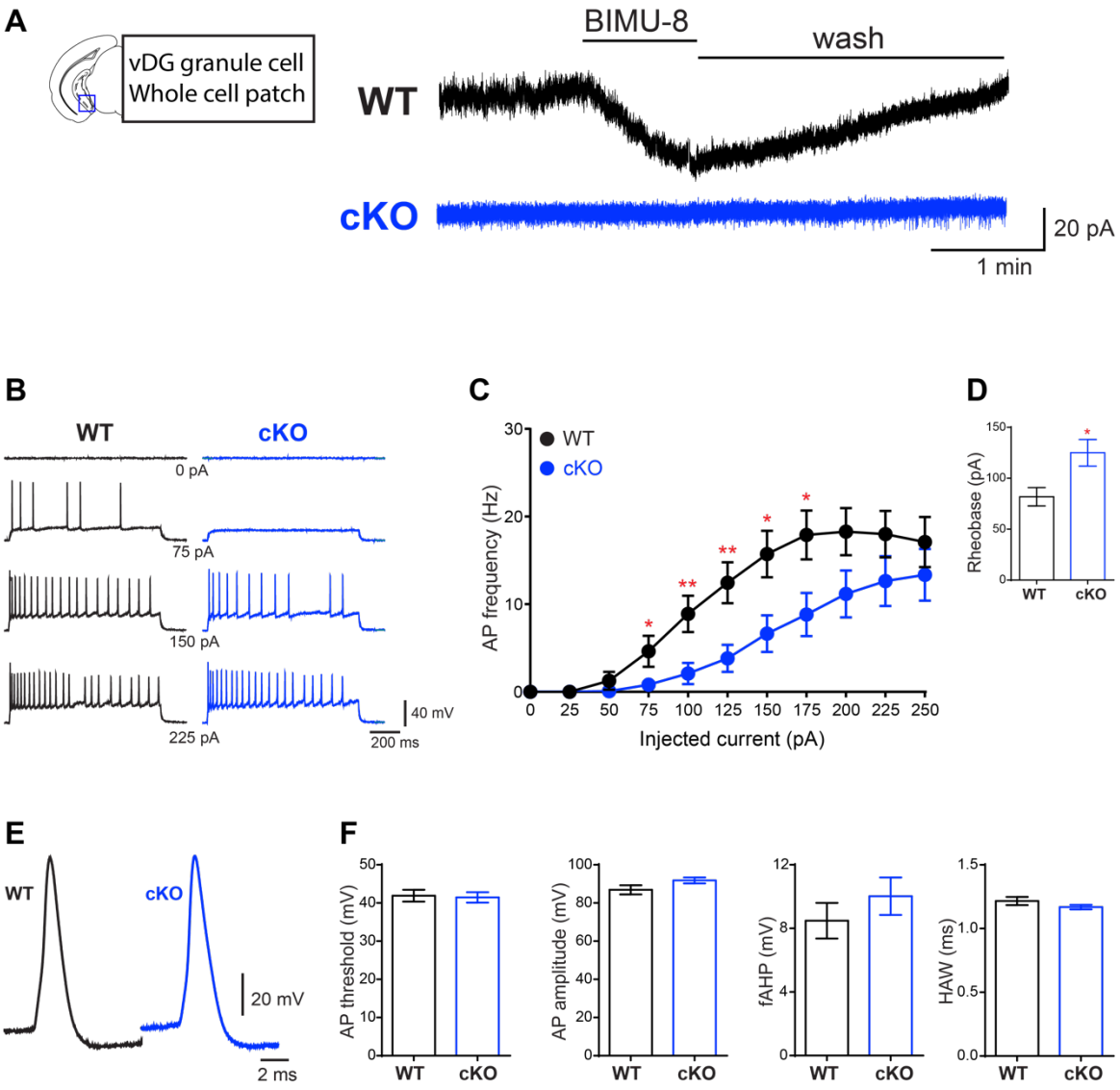

Figure 4.9. DG granule cells showed reduced firing in Drd3-Cre/Htr4 cKO mice.
A. Representative traces of whole-cell recordings in the voltage clamp configuration from DG granule cells (GC) in WT and Drd3-Cre/Htr4 cKO mice. BIMU-8 (10 mM) was added to the bath for 1 minute and subsequently washed.
B. Sample traces from whole-cell current-clamped DG GCs in WT and Drd3-Cre/Htr4 cKO mice showing the action potential (AP) firing of the cells in response to different steps of injected current.
C. Graph of AP frequency of granule neurons in WT and Drd3-Cre/Htr4 cKO mice in response to different steps of injected current.
D. Histogram of the rheobase (minimum amount of injected current necessary to elicit an AP) in WT and Drd3-Cre/Htr4 cKO mice.
E. Representative single APs from WT and Drd3-Cre/Htr4 cKO DG GCs.
F. Action potential properties show no significant difference between genotypes. HAW= half-amplitude width, fAHP = fast afterhyperpolarization potential.
Data are represented as mean ± SEM. For each genotype 11 neurons from 3 mice were used for each experiment. *$p < 0.05$, **$p < 0.01$ two-tailed unpaired t-test.

BIMU-8 (10 mM) was added to the bath for 1 minute and subsequently washed. Tetradotoxin (TTX, 1 mM) was added previously to the bath to avoid activation of neighboring neurons by BIMU-8.

BIMU-8 led to an inward current in WT GCs showing a depolarizing effect of the activation of 5-HT_4R. However, cKO GCs did not respond to BIMU-8, confirming the absence of functional 5-HT_4R in DG GCs in Drd3/Htr4 cKO mice.

Next, to measure the firing of DG GCs, and test whether 5-HT_4R mediates the excitability of DG GCs, we performed whole-cell current-clamp recordings while injecting increasing currents in different steps. Specifically, steps of 25 pA current were injected from a set starting membrane potential of -80mV. The firing frequency (action potential, AP, frequency in Hz) of GCs in Drd3/Htr4 cKO mice was significantly reduced when compared to WT (**Figure 4.9B, C**). We also noticed in GCs from Drd3/Htr4 cKO a significant increase in the rheobase, the amount of current (pA) necessary to be injected to elicit an action potential (**Figure 4.9D**). On the contrary, the properties of a single action potential were not different between GCs from Drd3/Htr4 cKO and WT mice (**Figure 4.9E, F**). Specifically, there were not any difference in the AP threshold (mV), AP amplitude (mV), fast afterhyperpolarization potential (fAHP, mV) and half-amplitude width (HAW, ms) between genotypes. These data show that the loss of 5-HT_4R from DG GCs leads to reduced firing and excitability in DG GCs, indicating discreet and specific physiological changes that may underlie the behavioral phenotype observed in the Drd3/Htr4 cKO mice.

4.4. Cell type specific genome-wide differential gene expression analysis along the dorsoventral axis of the hippocampus

We have shown that 5-HT_4R mediates the expression of neurogenic factor and serotonin receptors, and physiological properties of neuronal activity. It is highly possible that 5-HT_4R regulates these mechanisms, and consequently, anxiety and mood related behaviors, via other intracellular signaling mechanisms. Identification of the novel pathways and the proteins that interact with 5-HT_4R presents a powerful approach to discover unique targets that may contribute to anxiety and depression pathophysiology.

To investigate genome wide molecular neuroadaptations and elucidate candidate mechanisms that might play role in the anxiogenic and antidepressant-like effects of the loss of 5-HT_4R, we used TRAP-Seq method to identify proteins actively transcribed in Drd3-Cre positive cells in the hippocampus. TRAP-Seq combines the isolation of mRNA bound ribosomes from a genetically defined cell type and next-gen genome-wide RNA sequencing to acquire differential expression analyses (see Chapter 1 for details). We used this method to acquire (1) differentially expressed genes between the dorsal and ventral DG in the whole tissue, and specifically in mature excitatory neurons, (2) molecular neuroadaptations in the dorsal and ventral DG upon conditional knockout of Htr4 from mature excitatory neurons of the hippocampus, and (3) changes in the transcriptome of mature excitatory neurons upon the conditional *Htr4* deletion.

For the control samples (WT), we used Drd3-Cre::EGFP-L10a mice, generated by crossing Drd3-Cre mice with Cre-dependent EGFP-L10a reporter mice. These animals expressed the RPL10a-EGFP in the mature excitatory neurons of the hippocampus in a “wildtype” genetic background. The expression of EGFP-RPL10a in Drd3-Cre positive neurons in *Htr4* conditional knockout background was accomplished by two steps. First, we generated Cre dependent EGFP-L10::*Htr4*$^{loxP/loxP}$ by crossing the Cre dependent EGFP-L10a reporter mice with Htr4-floxed mice (*Htr4*$^{loxP/loxP}$) for two generations. Second, Cre-dependent EGFP-L10::*Htr4*$^{loxP/loxP}$ mice were crossed with Drd3-Cre::*Htr4*$^{loxP/loxP}$ (Drd3/Htr4 cKO) to generate Drd3-Cre::EGFP-L10a/Htr4 cKO. Consequently, these animals expressed EGFP-RPL10a in Drd3-Cre cells with Htr4 cKO background, and were used for the cKO samples.

For TRAP, three biological replicate samples were collected from the dDG and vDG of both cKO and WT mice. Bilateral corresponding hippocampal region of age matched (8-to-12 weeks old) one male and one female mice were pooled for each sample, except for the first cKO replicate (cKO1) which used two females, due to the challenging breeding of the cKO animals. The purified mRNA from IP (Drd3-Cre specific TRAP mRNA) and input (whole mRNA) samples of each replicate was sequenced. Normalized values of gene expression from IP and input samples (2) from the dDG and vDG (2) for each of the three (3) replicates of both genotypes (2) were obtained to yield a total of twenty-four (24) RNA-Seq data sets (see Material and Methods for the details).

For the quality control of our TRAP-Seq datasets, the percentage of bases aligned to the genome, and the percentage of aligned bases corresponding to the ribosomal RNA, coding, untranslated (UTR), intronic and intergenic regions were calculated for all samples (**Figure 4.10A**). The analysis of the base alignment data showed consistent percent alignment values for all samples (over 60%), and they were similarly distributed among the genomic regions; except that the input and IP samples from the dDG of cKO1 showed irregularly lower percentage of bases aligned. Furthermore, these datasets had lower percentage of aligned bases to coding regions while higher percentage in intergenic and intronic regions, respectively. Therefore, they (dDG cKO Input/IP 1) were excluded from further differential expression analyses. In order to visualize overall transcriptional variability between different biological replicates and replicate quality, Pearson correlation statistics were performed using normalized expression values between samples with the same origin of preparation (input or IP) and brain region (dDG or vDG). All samples showed minimal variability (r >90), except for the dDG input sample of cKO1 (**Figure 4.10B**).

Next, the visualization of reads from TRAP-Seq datasets mapped to the mouse genome showed that in the cKO samples, there were not any reads mapped to *Htr4* exon 5, confirming the conditional deletion in Drd3/Htr4 cKO mice (**Figure 4.11A**).

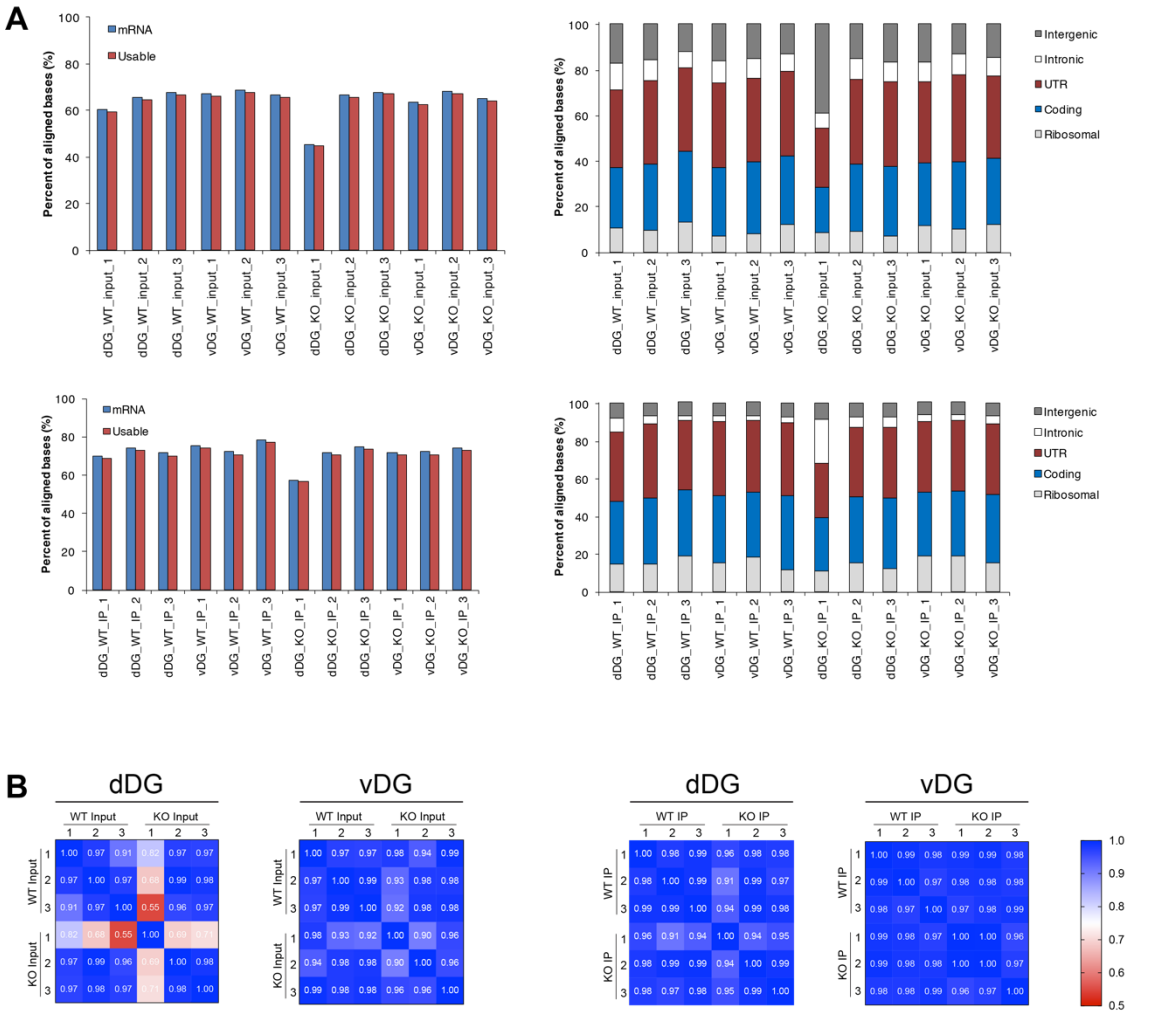

Figure 4.10. Quality control of genome aligned TRAP-Seq replicates.
A. The percentage of alignment of mRNA bases to the genome (left), and the percentage of the aligned bases corresponding to the ribosomal RNA, coding, untranslated (UTR), intronic and intergenic regions (right). Input (above) and IP (below) are shown in separate histograms. Note that “dDG cKO Input/IP 1” showed irregular alignment.
B. Heatmaps showing Pearson correlation statistics performed using normalized expression values between samples with the same preparation (input, left or IP, right) and brain region of origin (dDG or vDG). All samples showed minimal variability (r >90), except for the dDG input sample of cKO1. Legend shows corresponding heatmap colors for r-values between 0.5 (red) and 1 (blue).

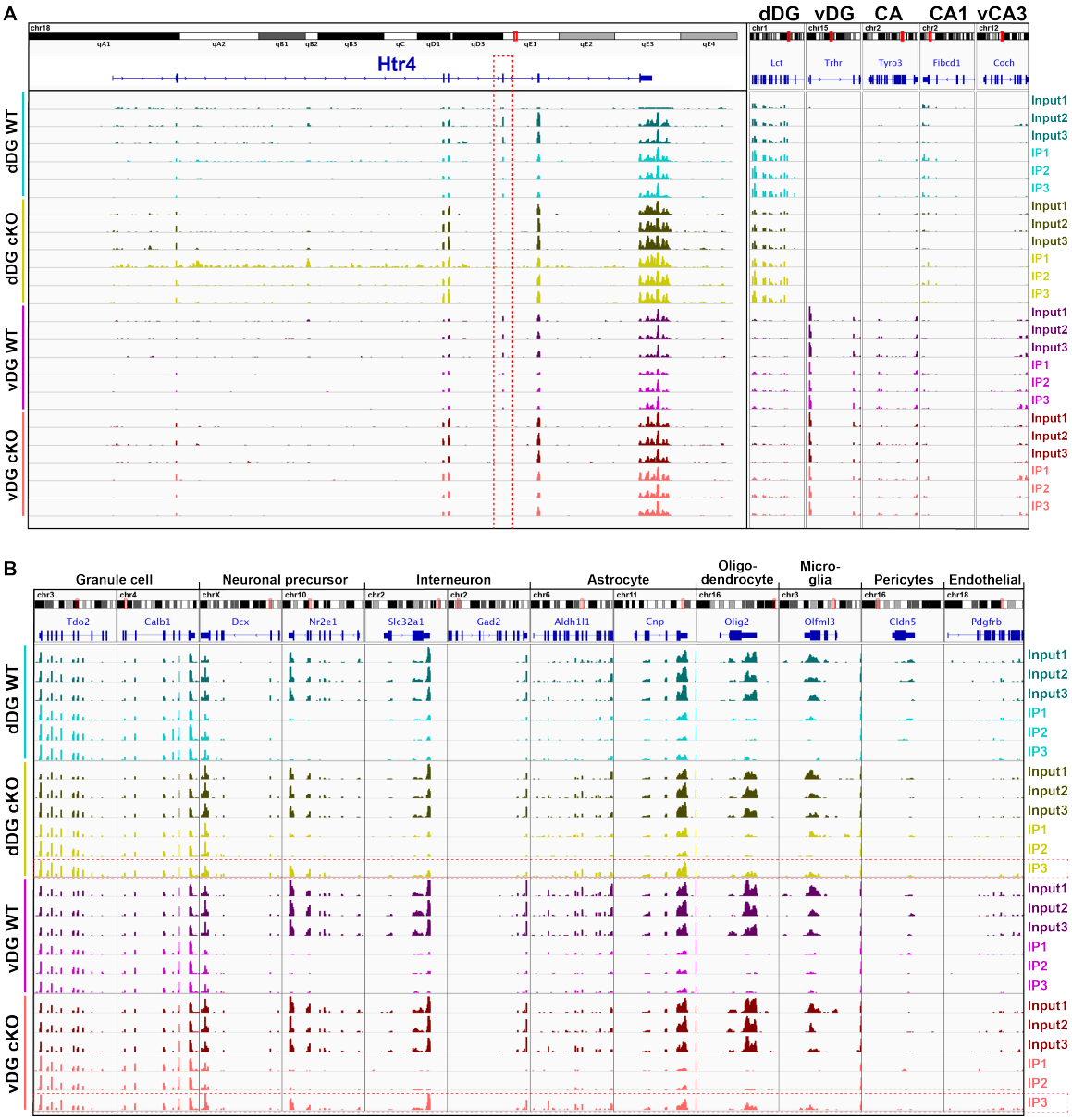

Figure 4.11. Visualization of TRAP-Seq reads mapped to cell type and region marker genes for each sample.

A. There was not any reads mapped to *Htr4* exon 5 (red dotted borders) in samples from Drd3/Htr4 cKO mice. dDG specific *Lct* expression was enriched in dDG samples, and vDG specific *Trhr* expression in vDG samples. Note some CA specific *Tyro3* expression in the vDG. CA1 specific *Fibcd1* expression was not particularly enriched while *Coch* expression (specific to distal tip of vCA3) was observed in vDG samples.

B. Visualization of reads mapped to the cell-type specific marker genes revealed that all IP samples compared to input counterparts were consistently enriched in granule cell specific genes (*Tdo2*, *Calb1*), and depleted for genes specific for neuronal precursors (*Dcx*, *Nr2e1*), interneurons (*Slc32a1*, *Gad2*), astrocytes (*Aldh1l1*, *Cnp*), oligodendrocytes (*Olig2*), microglia (*Olfml3*), pericytes (*Cldn5*) and endothelial cells (*Pdgfrb*), except for dDG cKO IP3 and vDG cKO IP3 (red dotted borderlines).

Reads mapped to other exons of *Htr4* confirmed the expression of exon 5 deleted mRNA (as previously confirmed with qRT-PCR). In addition, dDG specific *Lct* expression was enriched in dDG samples, and vDG specific *Trhr* expression in vDG samples, confirming the quality of our sampling. While some CA specific *Tyro3* expression was observed in vDG, CA1 specific *Fibcd1* expression was not particularly detected. However, similar to *Tyro3*, some *Coch* expression (a gene specific to the distal tip of the vCA3 innervating the vDG) was detected in some of vDG samples, indicating that there may have been a small number of vCA3 cells passed on to these samples. This is possibly due to the anatomical difference between the dDG and vDG, the latter being innervated by the CA3 deeper into the hilus. It would be advisable to keep this in consideration in our analyses.

Further visualization of reads mapped to the cell type specific marker genes revealed that all IP samples compared to their input counterparts were consistently enriched in granule cell specific genes (e.g. *Tdo2, Calb1*), and depleted for genes specific for neuronal precursors (e.g. *Dcx, Nr2e1*), interneurons (e.g. *Slc32a1*, *Gad2*), astrocytes (e.g. *Aldh1l1, Cnp*), oligodendrocytes (e.g. *Olig2*), microglia (e.g.*Olfml3*), pericytes (e.g. *Cldn5*) and endothelial cells (e.g. *Pdgfrb*) (**Figure 4.11B**), except for dDG cKO IP3 and vDG cKO IP3 (red dotted borderlines). We excluded these two IP samples from further analysis because they failed to show a depletion for cell type marker genes which are not expressed in Drd3-Cre cells. In addition, the enrichment/depletion

profile in the IP samples compared to inputs confirmed our previous immunohistological findings indicating that Drd3-Cre cells are mature excitatory neurons.

4.4.1. Differential gene expression between the dorsal and ventral dentate gyrus of the hippocampus

Considering the functional and molecular differences observed along the septotemporal axis of the hippocampus, and our results implying specific ventral DG responses in the loss of 5-HT_4R, we set out to compare the molecular profiles of the dDG and vDG. We performed differential gene expression analysis between samples from these regions that would allow us to identify region enriched genes. In each differential expression analysis between two samples, adjusted p-value (p-adj) <0.05 was considered significant.

The differential expression analysis between input samples from the dorsal and ventral DG of WT animals revealed that 1440 genes were enriched in vDG input versus 1041 genes in dDG input (**Figure 4.12A**), demonstrating the extensive molecular differences between these regions. *Lct* and *Trhr*, two of the previously identified genes enriched in the dDG and vDG respectively, show enrichment in their respective regions confirming our analysis. These data and further mining will serve as a useful reference for variety of analyses using comparative transcriptomics; such as, identification of gene set enrichments, and investigation of a certain cell type marker presence/abundance along the DG.

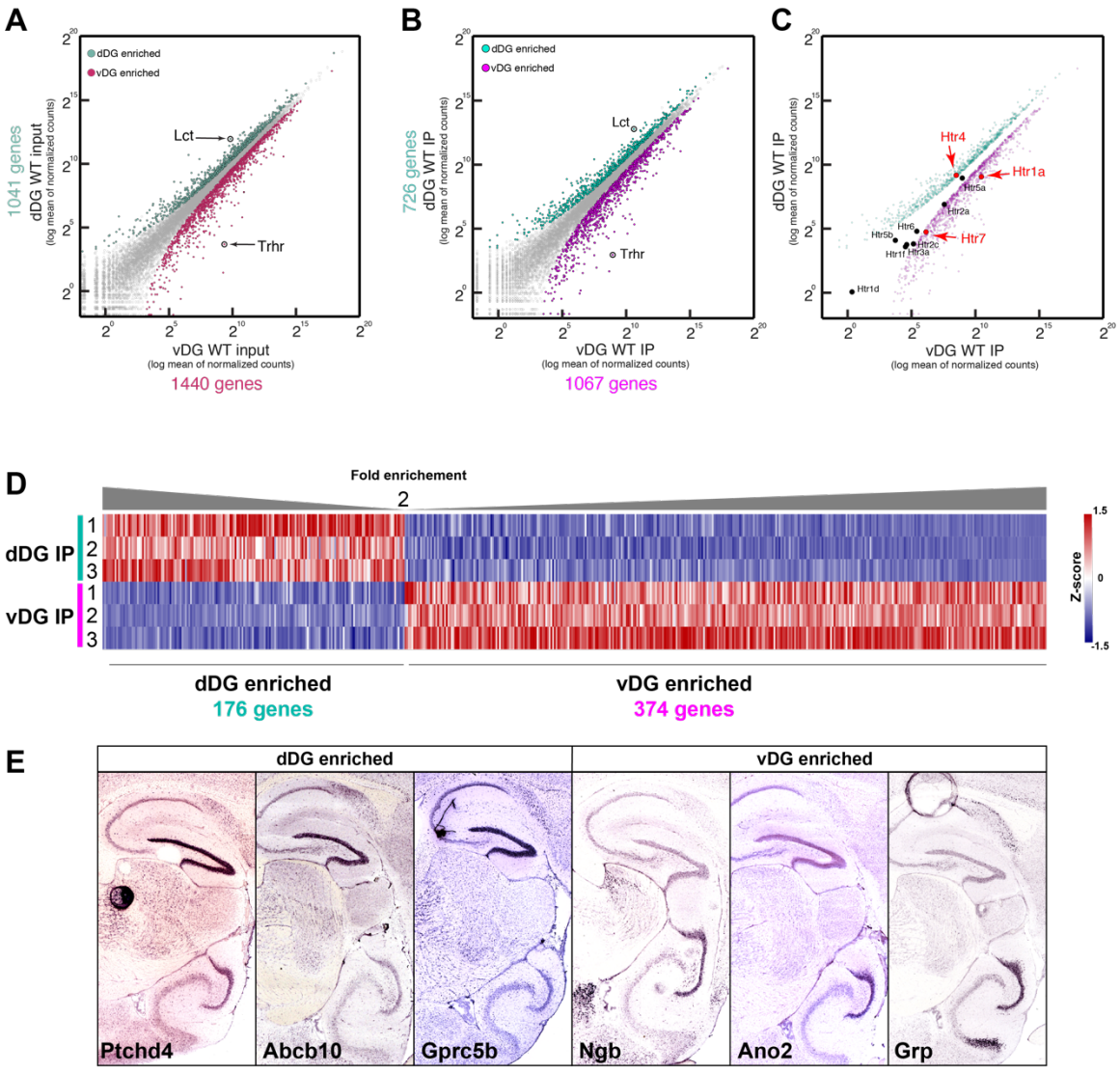

Figure 4.12. Genome-wide gene expression analysis between the dDG and vDG identified differentially expressed genes along the dorsoventral axis of the DG.
A. Scatter plot of normalized gene expression values between input samples from the dDG and vDG of WT mice. Differentially expressed genes (p-adj<0.05) were colored based on region specific enrichment.
B. Scatter plot of normalized gene expression values between IP samples from the dDG and vDG of WT mice. Differentially expressed genes (p-adj<0.05) were colored based on region specific enrichment.
C. Scatter plot of Htr expression and differentially expressed genes between IP samples from the dDG and vDG of WT mice. Differentially expressed Htrs (p-adj<0.05) are shown in red.
D. Heatmap visualizations of differentially expressed genes between IP samples from the dDG and vDG of WT mice with fold changes ≥2.
E. ISH confirmation of dDG and vDG enriched genes. Images from Allen Brain Atlas.

As we are more interested in the Drd3-Cre positive neurons in these regions, we then performed differential gene expression analysis between IP samples from WT animals to specifically enrich for genes expressed in the mature excitatory neurons. There were 1067 genes significantly enriched in vDG Drd3-Cre cells versus 726 genes in the dDG (**Figure 4.12B**). This implies a marked divergence in molecular profiles between the mature excitatory neurons of the dDG and vDG, although IP samples represent the transcriptome of the same cell type - primarily DG granule cells - with only difference being that they reside in spatially distinct parts of the DG. Moreover, the expression of all Htrs were detected in the dDG and vDG, except for *Htr1b*, in IP samples, indicating that mature excitatory neurons of the hippocampus express most of the serotonin receptors to some extent, *Htr1a* and *Htr4* being the highest two. Furthermore, *Htr4* was significantly enriched in the dDG (1.59 fold) while *Htr1a* and *Htr7* were enriched in the vDG (2.69 fold, each), demonstrating the differential expression profile of Htrs in the mature excitatory neurons along the DG dorsoventral axis.

This molecular divergence between dDG and vDG mature excitatory neurons calls for the identification of specific genes that may be expressed in spatially distinct subsets. To this end, we further analyzed the significantly enriched genes in dDG and vDG WT IPs to obtain genes that show >2 fold change in each region compared to the other. We then filtered out those genes that have normalized expression values <100 in their respective IP in order to eliminate very low expressed genes from our analysis. With these criteria, we

found that 176 genes in dDG and 374 genes in vDG were significantly enriched by more than 2 fold in the mature excitatory neurons (**Figure 4.12C**). By mining this gene list, we were able to identify genes expressed in granule cells specifically in the dDG (e.g. *Ptchd4, Abcb10, Gprc5b*) or vDG (e.g. *Ngb, Ano2, Grp*) (**Figure 4.12D**).

4.4.2. Genome-wide molecular neuroadaptations along the dorsoventral axis of the dentate gyrus upon the loss of 5-HT_4R

To assess neuroadaptations in gene expression that may underlie the molecular, cellular and behavioral consequences of the loss of 5-HT_4R from hippocampus, we analyzed the differential gene expression between cKO and WT in the whole dDG and vDG (inputs). As input samples represent the transcriptome of both the granule cells, the major cell type in the DG, and other cell types, we expected to capture any major transcriptional changes that may have occurred in GCs as well as in interneurons and astrocytes in response to the deletion of *Htr4* in Drd3-Cre cells.

In the input samples from the dDG of the cKO compared to WT, there were 185 genes significantly changed by 1.25 fold (84 genes up-regulated, 103 genes downregulated) (**Figure 4.13A**). Similarly, the expression of 186 genes were significantly altered by 1.25 fold in the vDG of cKO (21 genes up-regulated, 165 genes downregulated) (**Figure 4.13B**), indicating a robust molecular response both in the dDG and vDG of Drd3/Htr4 cKO mice.

Figure 4.13. Genome-wide differential gene expression analysis in the dDG and vDG revealed region-specific molecular adaptations in Drd3/Htr4 cKO mice.
A. Scatter plot of normalized gene expression values between WT and Drd3/Htr4 cKO dDG input samples. Differentially expressed genes (p-adj<0.05, fold-change ≥1.25) were colored based on genotype specific enrichment.
B. Scatter plot of normalized gene expression values between WT and Drd3/Htr4 cKO vDG input samples. Differentially expressed genes (p-adj<0.05, fold-change ≥1.25) were colored based on genotype specific enrichment.
C. Heatmap visualizations of differentially expressed genes between WT and cKO in the dDG and vDG.
D. Venn-diagram showing the number of overlapping genes significantly changed in cKOs between two regions.
E. Heatmap visualization of overlapping genes significantly changed in cKOs between two regions. Cell-type specificity based on ISH data from Allen Brain Atlas is indicated for each gene.
(*Figure on next page*)

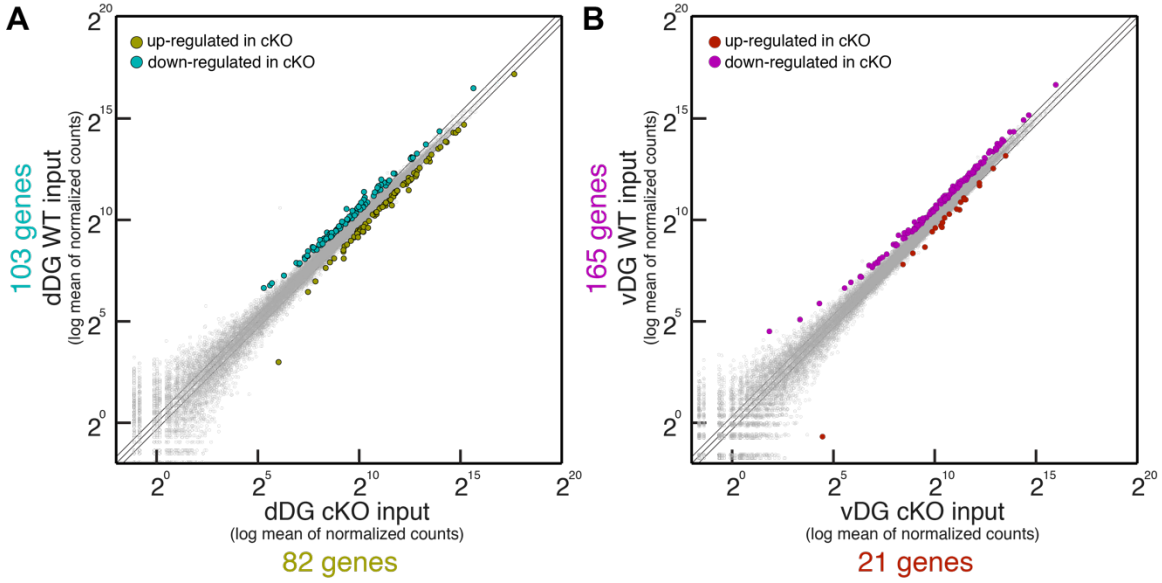
A
up-regulated in cKO
down-regulated in cKO
103 genes
dDG WT input
(log mean of normalized counts)
dDG cKO input
(log mean of normalized counts)
82 genes
B
up-regulated in cKO
down-regulated in cKO
165 genes
vDG WT input
(log mean of normalized counts)
vDG cKO input
(log mean of normalized counts)
21 genes

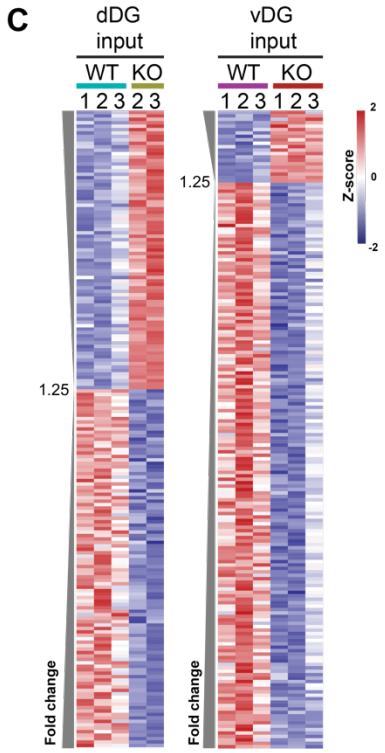
C
dDG input
vDG input
WT KO
1 2 3 2 3
1.25
Fold change
Z-score

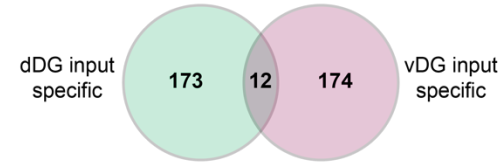
D
Number of significantly changed genes
dDG input specific
173
12
174
vDG input specific

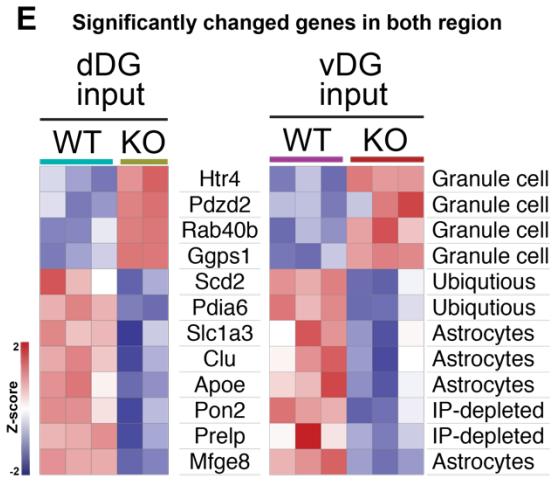
E
Significantly changed genes in both region
dDG input
vDG input
WT KO
Htr4 Granule cell
Pdzd2 Granule cell
Rab40b Granule cell
Ggps1 Granule cell
Scd2 Ubiquitous
Pdia6 Ubiquitous
Slc1a3 Astrocytes
Clu Astrocytes
Apoe Astrocytes
Pon2 IP-depleted
Prelp IP-depleted
Mfge8 Astrocytes
Z-score

Heatmap visualization based on normalized expression values (Z-score, normalization by row) showed that the significant differences in gene expression was consistent across all replicates (**Figure 4.13C**). While the number of genes that was significantly altered in expression was similar in both regions, the discrepancy in the number of up-regulated and down-regulated genes between the dDG and vDG suggested that the molecular response to the loss of *Htr4* were tissue-specific. Indeed, there were only twelve (12) genes commonly altered in response to *Htr4* deletion between the dDG and vDG. On the other hand, the rest of the significant expression changes were specific to each region (173 genes in the dDG versus 174 genes in the vDG). Out of the 12 common genes, four (*Htr4*, *Pdzd2*, *Rab40b* and *Ggps1*) were up-regulated and eight were down-regulated in the cKO in both regions (**Figure 4.13D**), showing agreement also based on the direction of gene regulation. Based on the ISH data from Allen Brain Atlas, all commonly up-regulated genes were expressed in granule cells. On the other hand, commonly down-regulated genes were mostly expressed in genes outside the GCs: ubiquitously expressed (2), astrocytes specific (4), and depleted in our IP samples (2, ISH data not available). Interestingly, *Htr4* expression was commonly upregulated although exon 5 was deleted, suggesting an enhanced transcriptional regulation on *Htr4* trying, but inevitably failing, to compensate for the absence of functional 5-HT_4R. Two other commonly upregulated genes (*Ggps1 and Rab40b*) may be involved in geranylgeranylation, a lipid post-translational modification that facilitate membrane association

(Kainou et al., 1999). Astrocyte-specific genes consisted two apolipoproteins that may be linked to Alzheimer's disease. Significantly dysregulated genes that may be relevant in learning and memory are discussed in Chapter 5.

To identify entire pathways dysregulated in the dDG and vDG in Drd3/Htr4 cKO mice, we performed gene ontology (GO) and gene set enrichment analysis (GSEA) using curated gene sets by Molecular Signature Database (MSigDB, Broad Institute). In both regions, genes with significant changes in expression showed enrichment of numerous and diverse terms (more than a hundred, FDR <0.05). We report five of highly enriched terms for each category; GO Biological Process (BP), GO Cellular Compartment (CC), GO Molecular Function (MF), MSigDB canonical pathways (CP), MSigDB chemical and genetic perturbations gene sets (CGP).

In dDG datasets (**Figure 4.14A**), most notably, the terms with the lowest FDR were consistently related to RNA and protein processing. Note that nuclear transcribed mRNA nonsense mediated decay (BP) and nonsense mediated decay by exon junction complex (CP) related genes were enriched, possibly indicating the transcriptional checkpoint responses to the transcription of the exon 5 deleted *Htr4* mRNA. Other functionally related enriched gene set were related to synapse (CC-cell junction, synapse) and neurogenesis (BP-neurogenesis, CC-neuron projection). Also note that genes enriched in astrocytes (CGP) were detected in our significant gene set, suggesting astrocyte involvement in response to *Htr4* loss from mature excitatory neurons.

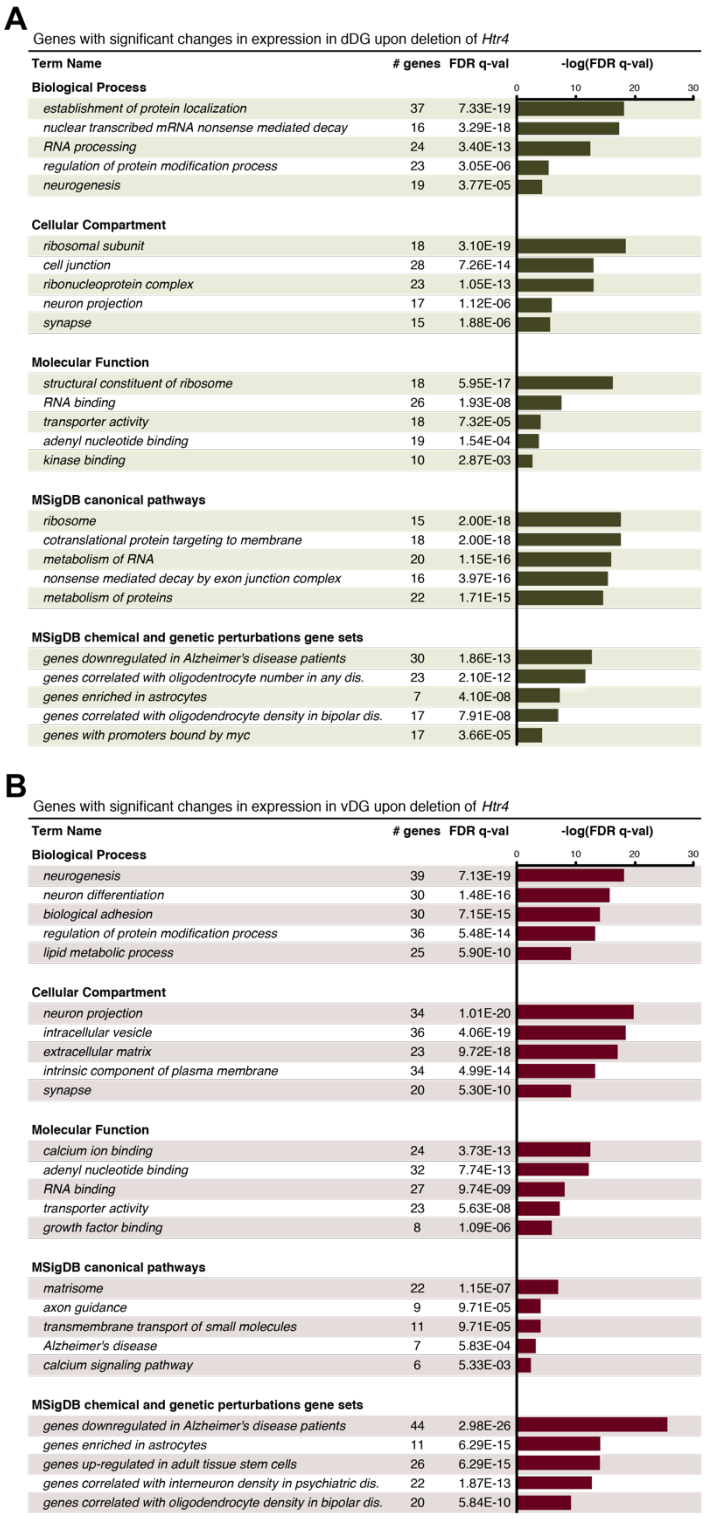

Figure 4.14. Gene set enrichment analysis (GSEA) of significantly regulated genes in Drd3/Htr4 cKO indicated both common and region specific gene sets were altered in the cKO between the dDG and vDG.

A. GSEA of significantly regulated genes in the cKO in the dDG (dark green).

B. GSEA of significantly regulated genes in the cKO in the vDG (dark red).

Finally, genes correlated with Alzheimer's disease and bipolar disorder (CGP) were enriched in our significant gene set.

In vDG datasets (**Figure 4.14B**), the most remarkably enriched terms with the lowest FDR were consistently related to neurogenesis and neuronal connections. Specifically, the terms related to neurogenesis such as neurogenesis (BP), neuron differentiation (BP), neuron projection (CC) and growth factor binding (MF) were among the most significantly associated with genes significantly changed in the vDG upon the deletion of *Htr4.* Although neurogenesis related genes were also significantly altered in the dDG (19 genes), the enrichment FDR was much lower in the vDG with higher number of genes correlated (39), and with only four (4) genes in common, supporting our results showing vDG specific enhanced neurogenesis in Drd3/Htr4 cKO mice. Furthermore, the enrichment in terms related to neuronal connections such as biological adhesion (BP), intracellular vesicle (CC), extracellular matrix (CC) and synapse (CC) may be relevant to a change in synaptic strength. In addition, enrichment in terms such as calcium ion binding (MF) and calcium signaling pathway (CP) may be related to the absence of 5-HT_4R and the decrease in granule cell firing rate. Also note that genes enriched in astrocytes (CGP), and genes correlated with Alzheimer's disease and bipolar disorder (CGP) were also enriched in vDG significant gene set.

Together, our differential expression analysis in input samples between genotypes suggests that the deletion of *Htr4* leads to robust and region specific molecular response in the dorsal and ventral DG. These data provide more insights into molecular processes underlying 5-HT_4R regulation of anxiety and depression related behaviors.

4.4.3. Gene expression changes in mature excitatory neurons in the dentate gyrus upon *Htr4* deletion

To investigate the cell type specific changes within mature excitatory neurons (Drd3-Cre) in the vDG upon the loss of *Htr4*, we performed differential expression analysis in TRAP-Seq datasets between IP samples from the vDG of WT and cKO mice. As IP samples represent the translating mRNA profile specifically in mature excitatory neurons, we expect to identify transcriptional changes that would give insights into the cellular 5-HT_4R pathway, and that may underlie functional cellular consequences of the loss of 5-HT_4R.

In the IP samples from the vDG of the cKO compared to WT, there were 249 genes significantly changed by 1.25 fold (55 genes up-regulated, 194 genes downregulated) (**Figure 4.15A**), indicating a robust molecular response in mature excitatory neurons of the vDG in the cKO. Heatmap visualization based on normalized expression values (Z-score, normalization by row) showed that the significant differences in gene expression were consistent across all replicates (**Figure 4.15B**).

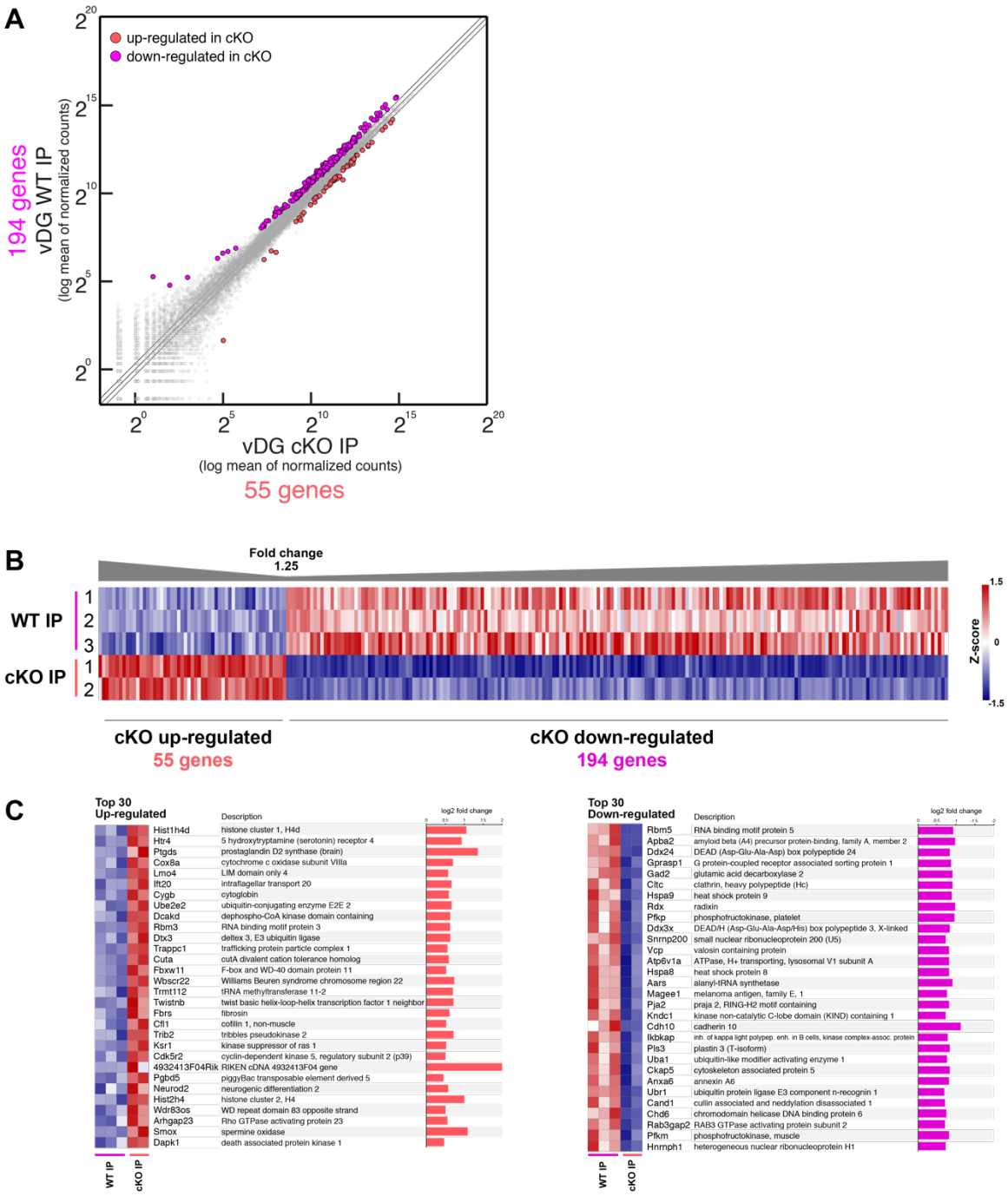

Figure 4.15. TRAP-Seq and differential gene expression analysis reveals a robust molecular change in mature excitatory neurons of the vDG in Drd3/Htr4 cKO mice.
A. Scatter plot of normalized gene expression values between WT and Drd3/Htr4 cKO IP samples from the vDG. Differentially expressed genes (p-adj<0.05, fold-change ≥1.25) were colored based on genotype specific enrichment.
B. Heatmap visualizations of differentially expressed genes between WT and cKO IP samples from the vDG.
C. Heatmap visualizations of top 30 up-regulated and down-regulated genes in cKO IP.

Top 30 up-regulated and down-regulated genes based on p-adj values were also listed (**Figure 4.15C**).

To identify dysregulated pathways in mature excitatory neurons of the vDG in the cKO, we performed GO analysis and GSEA using curated gene sets by MSigDB (Broad Institute). Up-regulated and down-regulated genes were analyzed separately to gain insights into the directionality of a change in a specific pathway. The genes with significant changes in expression showed enrichment of numerous terms (FDR <0.05). Down-regulated genes were consistently correlated with terms related to RNA and protein processing, neurogenesis and neural connection while up-regulated genes were correlated with RNA binding (**Figure 4.16A**). Consistently, both group of genes were correlated with genes dysregulated in Alzheimer's disease and bipolar disorder (**Figure 4.16B**).

In order to categorize and visualize related GO terms and identify more specific pathways, we generated a network of GO terms associated with the genes significantly altered in the cKO using BiNGO (A Biological Network Gene Ontology tool) (Maere et al., 2005). In these networks, each node represents a specific GO term. The size and the color of a node indicate the number of genes associated and the significance (lower FDR, darker; FDR cutoff <0.01), respectively. The nodes located towards the ends of a network represent more specific terms.

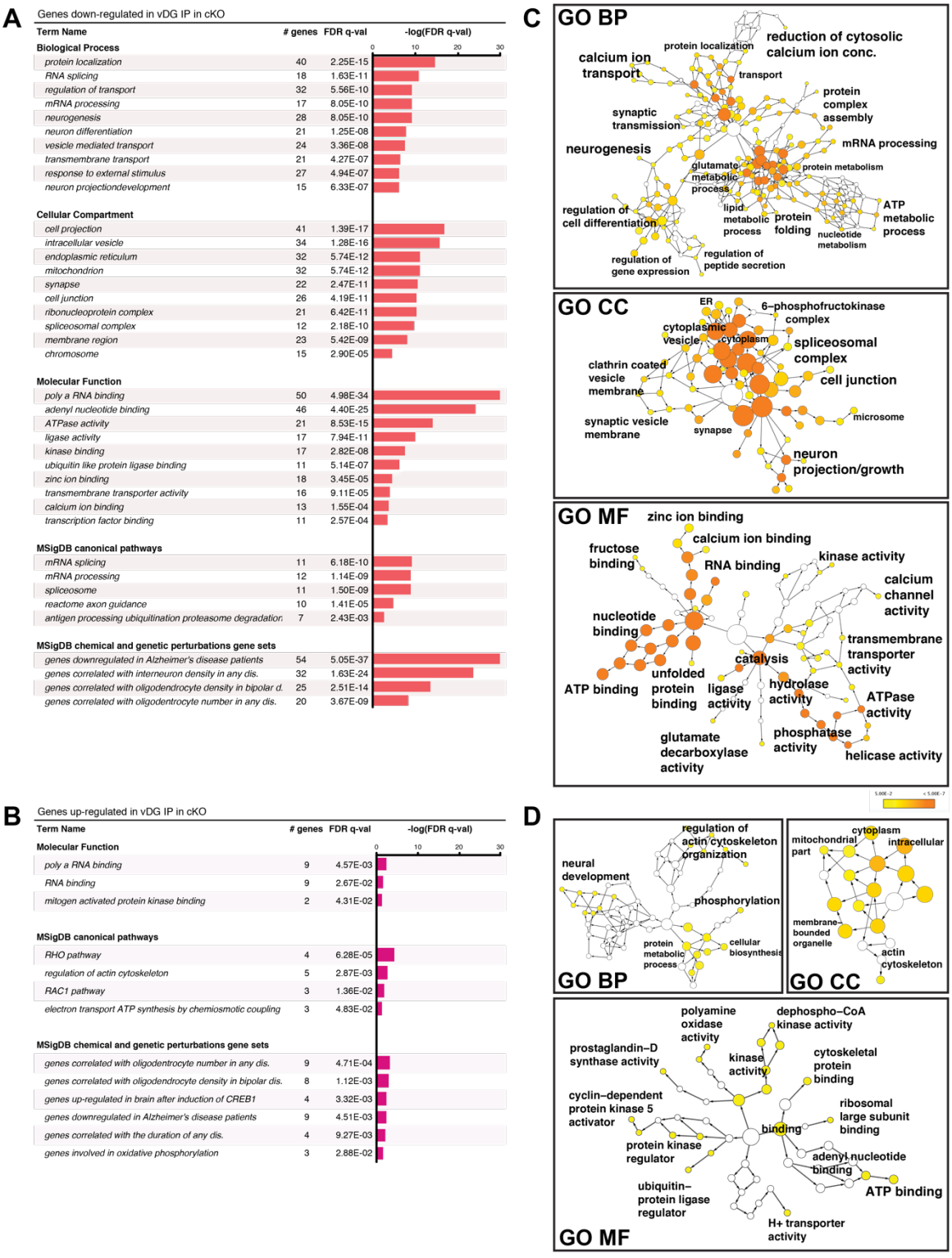

Figure 4.16. Functional interpretation of the gene regulations in Drd3/Htr4 cKO.
A, B. GSEA gene sets list for significantly down-regulated and up-regulated genes in vDG mature excitatory neurons in cKO, respectively.
C, D. Categorization and network of enriched gene ontology (GO) terms using BiNGO for down-regulated and up-regulated genes, respectively.

The most specifically enriched GO BP terms in down-regulated genes were regulation of cell differentiation, neurogenesis, synaptic transmission, glutamate metabolic process, calcium ion transport and reduction of cytosolic calcium ion concentration (**Figure 4.16C**). These terms appeared to be highly relevant for the biological phenotypes observed in the cKO mice. The enriched GO CC and MF terms were also correlated with these biological processes. Moreover, the specific terms such as protein folding (BP), spliceosomal complex (CC) and unfolded protein binding (MF) may be related to the cellular response to transcription and translation of exon 5 deleted *Htr4*.

On the other hand, the most specifically enriched, and functionally related, GO terms by up-regulated genes were neural development (BP), regulation of actin cytoskeleton organization (BP), cyclin-dependent protein kinase 5 activation, a process involved in neuronal maturation and migration (Jessberger et al., 2008) (MF), prostaglandin-D synthase activity, and ATP binding (MF) (**Figure 4.16D**). In addition, the up-regulated genes correlated term ubiquitin protein ligase regulator (MF) may be relevant to the translation of truncated 5-HT_4R in the cKO.

Together, our analysis of differentially expressed genes in IP samples between genotypes suggests that the deletion of *Htr4* leads to a robust molecular response in the mature excitatory neurons of the vDG. These transcriptomic changes in the cKO were strongly associated with the cellular phenotypes observed in the granule cell layer.

4.5. Discussion

In Chapter 4, our findings demonstrate cellular and molecular mechanisms that may underlie the anxiogenic and antidepressant-like behavioral phenotype observed upon the loss of 5-HT_4R in the hippocampus. We identified Drd3-Cre neurons as the mature excitatory neurons of the hippocampus based on established molecular markers. As hippocampus undergo marked cellular, molecular and electrophysiological changes in response to antidepressant treatment, we investigated these responses in the “antidepressant” Drd3/Htr4 cKO mice.

4.5.1. The loss of 5-HT_4R from mature excitatory neurons of the hippocampus led to enhanced neurogenesis

We found increased number of immature neurons specifically in the ventral DG of Drd3/Htr4 cKO mice and elevated gene expression levels of neurotrophic factors (BDNF and VEGF). These data revealed that, in addition to the behavioral antidepressant-like responses, the loss of 5-HT_4R from mature excitatory neurons of the hippocampus led to molecular and cellular antidepressant-like responses as enhanced adult hippocampal neurogenesis in the ventral hippocampus and increased levels of neurogenic factors in the hippocampus. Moreover, especially the increase in neurogenesis was ventral DG specific providing additional information associating the antidepressant-like

behavioral responses and the ventral hippocampus, and suggesting a differential role for 5-HT_4R in mediating anxiety and depression circuitry along the dorsoventral axis of the hippocampus. The mechanism underlying neurogenic effects of antidepressant response are still limited. Nevertheless, our findings showing that Drd3-Cre and Htr4-EGFP-L10a are not expressed in immature neurons suggest that the neurogenic phenotype was not induced directly by intracellular mechanisms in neural precursors, rather possibly by the elevated release of neurotropic factors from hippocampal neurons, or other extrinsic signals.

4.5.2. The loss of 5-HT_4R from mature excitatory neurons of the hippocampus resulted in adaptations in 5-HT receptor expression

Antidepressant treatments affect the serotonergic system in the brain by inducing adaptive changes in various 5-HT receptors subtypes (Adell et al., 2005; Schechter et al., 2005). In our study, 5-HT receptor expression underwent region and receptor type specific alterations when 5-HT_4R was ablated in the mature excitatory neurons of the hippocampus as a decrease in the expression of *Htr1a* (inhibitory) in the ventral hippocampus, an increase in the expression of *Htr2c* (excitatory, expressed prominently in CA3), *Htr6* (excitatory), and *Htr1b* (inhibitory, expressed in DG interneurons). Since 5-HT_4R is an excitatory 5-HT receptor, we suspect that the pattern in the regulation of other 5-HT receptor expression in response to the loss of 5-HT_4R implies compensatory changes to

rebound the levels of serotonergic modulation in the hippocampus. Whether these adaptations resist the functional ablation of 5-HT_4R or underlie some of the cellular and behavioral phenotypes yet to be investigated. Nevertheless, the region- and receptor type specific changes in 5-HT_4R shows the dynamic regulations in the serotonergic system in the hippocampus.

4.5.3. 5-HT_4R was necessary to maintain proper excitability of dentate gyrus granule cells

In addition to the molecular and cellular adaptations, our results showed that 5-HT_4R was necessary to maintain proper granule cell excitability as the loss of 5-HT_4R resulted in decreased firing. The decreased excitability of DG GCs in antidepressant-like action has also been indicated in several recent reports. For example, indirect inhibition of the firing of GCs through PV neurons were observed after acute SSRI administration (Medrihan et al., 2017) while chronic SSRI inhibition of GCs through the 5-HT_{1A}R has been shown to have an antidepressant-like effect (Samuels et al., 2015). Furthermore, chronic SSRI treatment has shown to desensitize 5-HT_4R-dependent signaling and functionality as it decreased the density of 5-HT_4R receptor binding, reduced 5-HT_4R mediated cAMP induction, and attenuated 5-HT_4R-induced excitability in pyramidal cells in the hippocampus (Vidal et al., 2009). The incorporation of young GCs upon neurogenesis has also been shown to inhibit the mature GC activity (Anacker and Hen, 2017). Also note that optogenetic activation of

specifically vDG granule cells resulted in a decrease in innate anxiety (Kheirbek et al., 2013). Considering these reports and our findings together, a decrease in 5-HT_4R-mediated excitability of the hippocampal excitatory neurons seems to be positively correlated to the antidepressant-like cellular and behavioral responses as well as increased anxiety levels.

The molecular mechanisms of 5-HT_4R-mediated excitability of the granule cells are still poorly understood. It is well established that 5-HT_4R is coupled to G_s proteins and positively linked to the adenylate cyclase in the brain ((Bockaert et al., 2004)). The increase in cAMP levels leads to the activation of protein kinase A that mediates closure of calcium (Ca+2) activated potassium (K+) channels mediating afterhyperpolarizing (AHP) current. Thus, evidence suggests that 5-HT_4R contributes to the neuronal excitability of pyramidal neurons via this pathway (Andrade, 2006). Although we did not observe a change in the AHP in DG GCs, previous studies observed the mediating effect of 5-HT_4R following the activation of the receptor in the pyramidal neurons. Hence, cell type and receptor activation may be important to mediate this property. It is possible that our results showing a decreased firing in DG GCs missing 5-HT_4R is mediated by other molecular mechanisms following the long-term loss of 5-HT_4R. Moreover, in addition to its GPCR function, a direct coupling to both voltage-sensitive calcium channels (Hoyer et al., 2002) and extracellular signal-regulated kinase pathway (Barthet et al., 2007) has also been proposed for 5-HT_4R function.

4.5.4. TRAP-Seq may identify novel genes involved in 5-HT_4R signaling, anxiety and depression

Using TRAP-Seq, we performed a cell type and region specific genome-wide differential gene expression analysis to identify the genes and pathways that may underlie the phenotypic changes in the absence of 5-HT_4R from the mature excitatory neurons of DG. Since almost all excitatory neurons of DG are targeted by Drd3-Cre line, and we observed remarkable cellular and molecular adaptations in the vDG after the deletion of 5-HT_4R, we restricted our comparative transcriptomic analysis in the dDG and vDG. Mature excitatory neuron specific differential gene expression analysis between the dDG and vDG in WT animals allowed us to capture previously identified (Cembrowski et al., 2016) and novel region specific GC genes. Therefore, further mining of our TRAP-Seq datasets could be used to identify new genes that are specifically expressed in the GCs and mossy cells in the dorsal or ventral DG. The characterization of these genes that are differentially expressed within the same cell type in a spatial gradient may give further molecular insights into the functional difference between the dDG and vDG as well as distinct susceptibility of these regions to various diseases and treatments.

We also showed that the overall molecular response to the deletion of *Htr4* was robust but distinct between the two poles of the DG, providing further transcriptional evidence into the distinct modulations of the dDG and vDG in anxiety and depression. These changes were observed in genes that are

expressed in excitatory neurons of the DG as well as astrocytes and interneurons, suggesting a possibly involvement of astrocytes and interneurons in response to the loss of 5-HT_4R in the excitatory neurons. Neurogenesis related genes were consistently altered between the two poles, while showing more significance in the vDG, providing further insights into the genes that may be relevant for vDG specific neurogenic regulation. Furthermore, the synaptic and cell junction related gene expression changes may indicate the adaptations in synaptic strength and may be related to decreased firing of GCs after the loss of 5-HT_4R.

Finally, TRAP-Seq analysis made it possible to capture the robust cell-type specific transcriptomic changes in vDG mature excitatory neurons upon the deletion of *Htr4*. Consistent with the function 5-HT_4R as an excitatory GPCR, *Htr4* deletion led to more down-regulation than up-regulation in gene expression. Gene set enrichment analysis showed that neurogenesis and neural differentiation related gene expression was also altered specifically in mature excitatory neurons. Surprisingly, these genes were mostly in down-regulated gene group; nevertheless, it is important to investigate the function of these genes in neurogenesis, that is, whether they are facilitatory or inhibitory. On the other hand, other neural development, maturation and migration related genes were also upregulated. Further exploration of these gene may help understand vDG GC specific modulation of neurogenesis.

More relevant to neuronal function and communication, the genes involved in synaptic transmission including synaptic vesicle formation, transport, and release, glutamate metabolic process, and Ca^{+2} ion transport and binding were down-regulated in the mature excitatory neurons after conditional *Htr4* knockout. The identification of specific genes related to these functions may provide more understanding of the function of 5-HT_4R in granule cell excitability. For example, *Cacna2d3* – calcium channel, voltage-dependent, alpha 2/delta subunit 3 – was among significantly downregulated genes. This gene encodes a protein that is a significant part of many voltage-gated Ca^{+2} channel complexes. It has been shown to regulate Ca^{+2} current density and activation/inactivation kinetics of various voltage-gated calcium channels in neurons upon membrane depolarization as well as synapse formation (Geisler et al., 2015). Another strong candidate for 5-HT_4R pathway may be *Ryr2*, the gene encoding for type 2 ryanodine receptor/calcium release channel, which was found down-regulated following the loss of 5-HT_4R. This channel is responsible for intracellular Ca+2 release from endoplasmic reticulum (ER) and activated by cAMP-PKA pathway (Liu et al., 2012). It is highly expressed in hippocampal excitatory neurons and dysregulation of this receptor has been shown to strongly contribute to stress induced cognitive dysfunction. Together, these two downregulated genes are among the many strong candidates identified in our TRAP-Seq data sets that may be involved in the intracellular 5-HT_4R signaling. The downregulation in the expression of these genes may underlie the decreased excitability of DG GCs.

Further mining of this dataset and gene network analyses may identify more candidate genes that may be involved in 5-HT_4R signaling and its function in the regulation of anxiety and depression related behaviors.

4.5.5. Conclusion

Whether enhanced neurogenesis, or adaptations in serotonergic system, or decreased excitability of GCs is the cause of behavioral antidepressant-like responses to the hippocampal loss of 5-HT_4R is still unknown. Perhaps, these neuroadaptations in the hippocampal circuitry acts synergistically to decrease the hippocampal excitability and overall output to other relevant limbic regions. Further experiments such as non-genetic manipulation of endogenous 5-HT_4R pathway in a region and cell type specific manner, as well as more investigation of neurogenesis, and other serotonin receptors in antidepressant action are needed to understand the exact function of 5-HT_4R in these processes.

Our results strongly indicate ventral dentate gyrus granule cells and 5-HT_4R signaling as striking modulators of anxiety and depression related behaviors. Therefore, a cell type or region specific approach may enable the development of better acting anxiolytics and antidepressants. In this sense, our TRAP-Seq datasets may serve as a reference for identification of specific genes that may be targeted for more efficacious therapeutics with fewer side effects.

CHAPTER 5.

THE ROLE OF 5-HT_4 RECEPTOR IN LEARNING AND MEMORY

5.1. Introduction

Memory is the storage of learned information in the brain and is crucial for adaptive behavior in animals. The study of learning and memory is essential because these processes underpin normal human behavior and they are important abnormal behavioral components of disorders ranging from addiction, anxiety, depression, schizophrenia and neurodegenerative diseases such as Alzheimer's disease (LaBar and Cabeza, 2006). The medial temporal lobe, in particular the hippocampus, has been implicated in the memory of events or episodes by studies in humans and animal models (Strange et al., 1999).

Our studies have indicated 5-HT_4R in the hippocampus as a major regulator for emotive behavior and neuronal activity. Considering the extensive involvement of the hippocampus in memory processes, and growing body of evidence suggesting a role for 5-HT_4R in cognition (discussed below), we investigated whether 5-HT_4R mediates certain learning and memory functions in the hippocampus and neocortex.

5.1.1. Assessment of learning and memory in laboratory mice

The elements regulating learning and memory have been investigated as anatomical structures, physiological processes, neuromodulators, and molecular pathways using behavioral tasks in animal models (Barnhill, 2006). In this chapter, we sought to investigate, the involvement of 5-HT_4R in distinct types of episodic memories with varying emotional valence, such as fear memories

(negative valence), object memory (neutral) and social memory (possibly positive valence).

5.1.1.a. Fear memory

Fear and anxiety are defensive behavioral responses that enable an organism to avoid harm. Fear is evoked upon acute sensory input, whereas anxiety can be evoked by anticipated threats. Innately fearful stimuli or stimuli that are associated with aversive events can induce fear (Peter Curzon, 2008). Associative learning processes can be studied to elucidate the mechanisms involved in learning and memory by the induction and acquisition of fear in laboratory conditions.

In rodents, Pavlovian fear conditioning is the most commonly used paradigm to induce learned fear. In this paradigm, a neutral stimulus, such as a particular context or cue (for example, an auditory tone), is presented sequentially with an aversive event, such as a footshock. In this case, the aversive event, unconditioned stimulus (US), induces fear responses and the neutral stimulus is associated with aversive properties through associative learning, becoming the conditioned stimulus (CS). With successful training, the subject will elicit fear responses even when the CS is presented alone. The fear response in rodents is measured by increased defensive behavior as freezing.

During the fear acquisition phase, the expression of the conditioned fear response gradually increase during the training when multiple CS-US couplings

are presented. If one administers a foot shock paired with an auditory cue in a particular context, fear will be associated with both the cue and the context. Fear memories are consolidated after the training; hence, memory retrieval can be induced by re-exposure to either the conditioning context (contextual fear test) or the auditory cue in a novel context (cued fear test).

Studies using this model have revealed that there is a distributed network of brain regions that are involved in the learning and expression of fear. These include but are not limited to the local microcircuits in the amygdala (Letzkus et al., 2011), and the projections among the amygdala (Fadok et al., 2017; McHugh et al., 2004), hippocampus (Kjelstrup et al., 2002) and frontal cortex (Likhtik et al., 2014). Sensory input from the neocortex and thalamus innervate several amygdala nuclei which are central areas for fear acquisition and expression (Asede et al., 2015). Reciprocal connections between the basal amygdala and the ventral hippocampus as well as the prelimbic cortex modulate the fear related neuronal plasticity (Sotres-Bayon et al., 2012). In addition, central amygdala sends projections to the hypothalamus and brainstem promoting fear (Canteras and Swanson, 1992). Hippocampus-amygdala interactions could be particularly important for contextual fear as the hippocampus is established to encode spatial information. In fact, there is a growing body of evidence demonstrating the contribution of connection between these regions to contextual fear conditioning (Kjelstrup et al., 2002; Sparta et al., 2014).

.

Fear and anxiety are mediated by largely overlapping brain areas and neuromodulatory systems (Davis et al., 2009) while the exact circuits mediating anxiety have been investigated to a lesser extent. Recent developments in optogenetic functional circuit mapping have led to the accumulation of the evidence showing divergent circuits elements for anxiety related behaviors in the brain regions that mediate fear related behaviors (Felix-Ortiz et al., 2013; Tye et al., 2011). Furthermore, neuronal circuits that mediate emotive behavior with a negative valence (for example, fear and anxiety) at least partially overlap with the circuits that regulate positive valence (for example, reward) (Belova et al., 2007; Lammel et al., 2012).

5.1.1.b. Object memory

Object memory is based on recognition and is a type of episodic memory (Pause, 2013). In rodents, the novel object memory test (NORT) has been used to assess non-spatial and object memory in rodents (Leger et al., 2013). The novel object recognition offers advantages over other memory tests for assessing recognition memory because it does not require any external motivation, reward or punishment, dissociating it from emotionality.

The NORT is conducted in a familiar high-walled rectangular arena lacking spatial cues. Subject familiarization with the arena is accomplished before the test by a habituation session typically 24 hours before the test. During the training or sample session, the subject explores two identical novel objects encountered in the familiar arena during which object memory encoding is

putatively occurring. After the sample session, the animal is removed from the arena for a specified amount of time (retention delay), during which the object memory is consolidated. For the subsequent test session, the subject is returned to the same arena, containing the familiar object and a novel object, as a test of object memory retrieval. Mice exhibit a natural proclivity to explore novel objects, and hence, exhibiting a preference for exploring the novel object significantly more than the familiar one. Preference for the novel object, demonstrated by an increase in exploration time, indicates that a memory trace for the familiar object was properly encoded, consolidated and then retrieved to guide the behavior during the test session.

Despite the wide use of the novel object memory test in assessing the memory performances in animal models, underlying neural circuitry have not yet been clearly defined. It has been suggested that the hippocampus is necessary for the retrieval of object recognition memory when a delay greater than 10 min is imposed between the sample and test sessions in the NORT (Cohen and Stackman, 2015). However, at shorter retention delays, perirhinal cortex activity has found to be necessary for the object memory. Essentially, episodic memory for objects emerges from interactions, at least majorly, between the perirhinal cortex and hippocampus.

5.1.1.c. Social recognition memory

Social memory, the ability to recognize and memorize familiar conspecifics is crucial for animals that exhibit social interactions. It is also a form of episodic

memory; however, it involves olfactory cues more than the visual representation of the novel conspecific/object (Gabor et al., 2012). Therefore, the sensory and associative inputs to form the social memory vary compared to the object memory.

The social recognition task that is used to assess social memory in laboratory conditions employs the innate tendency of mice to investigate an unfamiliar conspecific more than a familiar one. Therefore, the three-chamber social recognition test can be run right after the social interaction test during which the subject is familiarized with a confined novel conspecific. For this task, the inanimate object under the container is replaced with a novel, unfamiliar mouse immediately after the social interaction test to assess the short-term social memory. Social memory in a mouse can be quantified by comparing its interaction durations with a novel and a familiar mouse. Ideally, the subject spends more time exploring the unfamiliar mouse compared to the recently familiarized mouse.

Human and non-human primate studies have identified the medial temporal lobe including the hippocampus to be involved in social memory (Viskontas et al., 2009). In rodents, it is also well established that the hippocampus has an essential role in episodic memories including social memory. For example, ventral CA1 pyramidal neurons has been indicated in the storage of the social memory (Okuyama et al., 2016). More evidence from both human and rodent studies suggest that the excitation and inhibition balance in

the neocortex and specifically in the prefrontal cortex is strongly linked with social recognition (Bicks et al., 2015).

5.1.2. Molecular basis of learning and memory

Long-term potentiation (LTP) and depression (LTD) are mechanisms that alters the synaptic strength and mediate the storage of memories. These processes initially involve modifications in intracellular signaling cascades using secondary messengers (calcium-dependent protein kinases such as calcium-calmodulin-dependent kinase II, tyrosine kinase and protein kinase C) (Li et al., 2010). The extend of synaptic plasticity is further mediated by changes in the phosphorylation of key receptors of glutamatergic neurotransmission such as subunits of the AMPA receptor (Malenka and Bear, 2004), the activity of transcription factors (e.g. cyclic AMP response element binding protein, CREB, and early growth response protein 1, Zif268) (Alberini, 2009) and protein expression (e.g. BDNF) (Kovalchuk, 2002) especially in the hippocampus. LTP and LTD play essential roles in memory consolidation and under extensive neuromodulatory control.

5.1.3. Serotonergic modulation of learning and memory

Widespread serotonergic projections in the hippocampus and neocortex underline the anatomical and neurochemical link between the serotonergic system and brain areas associated with learning and memory. The

neuromodulatory action of 5-HT on cognitive functions in both physiological and pathological states largely depend on the specific subtypes of 5-HTRs, and their localization (Seyedabadi et al., 2014). The activity of the 5-HT has been linked with memory and cognitive performance, during aging as well as in many psychiatric (anxiety, depression, addiction) and neurological (Alzheimer's disease, epilepsy) disorders (Meneses, 2015; Rodríguez et al., 2012). As current treatments for learning and memory impairments are very limited, there is an extreme need for developing novel therapeutic approaches, including drugs acting on specific 5-HT receptors.

Several drugs targeting 5-HT receptors, including those specific to 5-HT_4R, have displayed pro-cognitive effects in preclinical behavioral paradigms. For example, various studies reported the beneficial effects of 5-HT_4R activation on cognition in rodents and primates (Lo et al., 2014; Marchetti et al., 2008; Terry et al., 1998). 5-HT_4R agonists improved performance on various learning and memory tests such as social and object recognition, and reversed age related or pharmacologically-induced cognitive deficits (Darcet et al., 2016; Letty et al., 1997; Orsetti et al., 2003). 5-HT_4R have also been implicated in the expression of genes that regulate synaptic plasticity (Vidal et al., 2011). Moreover, 5-HT_4R agonists modulate synaptic plasticity within the hippocampal regions by augmenting LTP, attenuating depotentiation and altering the patterns of LTD (Hagena and Manahan-Vaughan, 2016).

In the human brain, reduced levels of 5-HT_4R have been measured post-mortem in the hippocampus and cortex of Alzheimer's disease (AD) patients (Reynolds et al., 1995). In rodents, 5-HT_4R agonists have been shown to stimulate acetylcholine release (a symptomatic therapeutic approach for AD), enhance memory performance and have neuroprotective and neurotrophic effects in AD models (Cachard-Chastel et al., 2007; Giannoni et al., 2013; Matsumoto et al., 2001). Additionally, they stimulate the non-amyloid-forming metabolism of amyloid precursor protein (APP), therefore, decrease the production of neurotoxic amyloid beta (Aβ), involved in the AD pathology (Tesseur et al., 2013).

Previous reports combined with our findings in Chapter 4 regarding 5-HT_4R-mediated modulation of granule cell firing, and possibly, the regulation of genes associated with synaptic plasticity and Alzheimer's disease, strongly suggest that 5-HT_4R pathway is a promising target for the modulation of synaptic plasticity and memory. In this chapter, we investigated the role of 5-HT_4R in learning and memory both in excitatory neurons in pallial regions (including neocortex, hippocampus, basolateral and lateral amygdala), and specifically in hippocampal excitatory neurons.

5.2. Hippocampus specific 5-HT_4R function in in learning and memory.

Pharmacological studies detailed that the activation of 5-HT_4R enhanced memory performance in various behavioral tasks in rodents (Hagena and Manahan-Vaughan, 2016). Although, there has been an extensive work in the involvement of distinct brain regions, cell types and neuromodulators in various type of learning and memory, the specific cell types and brain regions in which 5-HT_4R may mediate these processes remains unknown. Cre-dependent genetic targeting of 5-HT_4R will help us reveal whether 5-HT_4R in specific cell types and brain regions are involved in the modulation of various types of learning and memory.

We crossed Htr4-floxed mice and two previously described Cre driver lines to ablate 5-HT_4R in excitatory neurons of pallial origin (Emx1/Htr4 cKO) and mature excitatory neurons of the hippocampus (Drd3/Htr4 cKO). These animals and their control littermates (WT) were tested in various assays measuring different learning and memory performances including fear memory, object memory and social memory. Comparison of the performances of these two lines will help us understand the region-specific contributions of 5-HT_4R in these cognitive processes.

5.2.1. The role of 5-HT_4R in behavioral fear responses and fear memory

To investigate whether 5-HT_4R in the excitatory neurons of any pallial region mediate the fear memory and responses, Emx1/Htr4 cKO mice underwent fear conditioning training, and their fear responses to fear-associated context and auditory cue were acquired as freezing behavior. **Figure 5.1A** shows experimental timeline and components for training (fear memory acquisition) and test (fear memory retrieval) stages of contextual and cued fear conditioning (FC) paradigm. Shortly, in day 1, animals were placed in the operant conditioning chamber and an auditory tone was presented for 20 s preceding an electrical footshock for three times at 140, 200 and 260 s in a 300-s training trial. Next day, animals were returned to the operant chamber (same context) for 300 s, and percent freezing was assessed as a measure of contextual fear memory. After a delay in the same day, animals were returned to the operant chamber with different context (altered by novel visual and odorant cues) for 300 s, and conditioned auditory cue was presented in the same way as the training. Percent freezing was assessed as a measure of cued fear memory. During the acquisition phase, Emx1/Htr4 cKO mice showed no difference in freezing compared to their control littermates (WT) (**Figure 5.1B**), indicating that both groups showed similar exploration of the conditioning box before the first footshock (at 140 s), or response to the footshock during the training. Particularly, both groups showed an increase in freezing towards the end of the acquisition phase, indicating a proper fear acquisition. During retrieval phase,

Emx1/Htr4 cKO and WT showed similar context-induced freezing behavior throughout the test and on average (~40%) (**Figure 5.1C**). On the other hand, in the novel context, Emx1/Htr4 cKO displayed significantly lower cue-induced freezing behavior compared to WT during the first and second cue, and on average during all three cues ($p<0.05$, for each). Together, these data indicate that Emx1/Htr4 cKO mice showed attenuated retrieval of cued fear memory.

To test the contribution of 5-HT_4R specifically in the hippocampal excitatory neurons to fear learning, Drd3/Htr4 cKO mice were trained in the same contextual and cued fear conditioning paradigm. Drd3/Htr4 cKO and control showed no difference in exploring the conditioning box before the first footshock during the acquisition phase (0-140 s) (**Figure 5.1D**). Although both groups showed increased freezing after the first footshock towards the end of the training, Drd3/Htr4 cKO displayed blunted freezing response compared to WT, indicating a possible difficulty in the acquisition of fear. Interestingly, during the contextual fear memory retrieval phase, Drd3/Htr4 cKO mice showed significantly low freezing levels compared to control littermates, throughout the test (Two-way RM ANOVA, $p<0.001$) as well as on average (**Figure 5.1E**). When cued memory retrieval was tested in a novel context, Drd3/Htr4 cKO mice also exhibited significantly attenuated cue-induced freezing behavior compared to controls during each cue and on average ($p<0.0001$). Together, these results indicated that Drd3/Htr4 cKO mice showed attenuated retrieval of both contextual and cued memories.

Figure 5.1. Hippocampal 5-HT_4R is necessary for proper retrieval of fear memories.
A. Schematic depicting the fear conditioning experimental design.
B. Emx1/Htr4 cKO mice showed similar freezing during memory acquisition training compared to controls (WT).
C. There was not any difference between freezing between genotypes during contextual fear memory retrieval.
D. Emx1/Htr4 cKO mice displayed attenuated freezing during cued fear memory retrieval.
E. Drd3/Htr4 cKO mice showed slight attenuation in acquisition of freezing during training.
F. Drd3/Htr4 cKO mice froze significantly less during contextual fear memory retrieval.
G. Drd3/Htr4 cKO mice displayed attenuated freezing during cued fear memory retrieval.
Data are represented as mean ± SEM. Two-way RM ANOVA was performed for line graphs showing repeated measurements with 20 s bins, ¥, p<0.5, ¥¥¥, p,0.001; followed by post hoc Fisher's LSD test, *p<0.05, **p<0.01, ***p<0.001, ****p<0.0001. Two-tailed unpaired t-test was performed for bar graphs. *p<0.05, ***p<0.001, ****p<0.0001.
For Emx1/Htr4 cKO mice and their WT littermates, n=22, 22, respectively.
For Drd3/Htr4 cKO mice and their WT littermates, n=18, 17, respectively.
(*Figure on next page*)

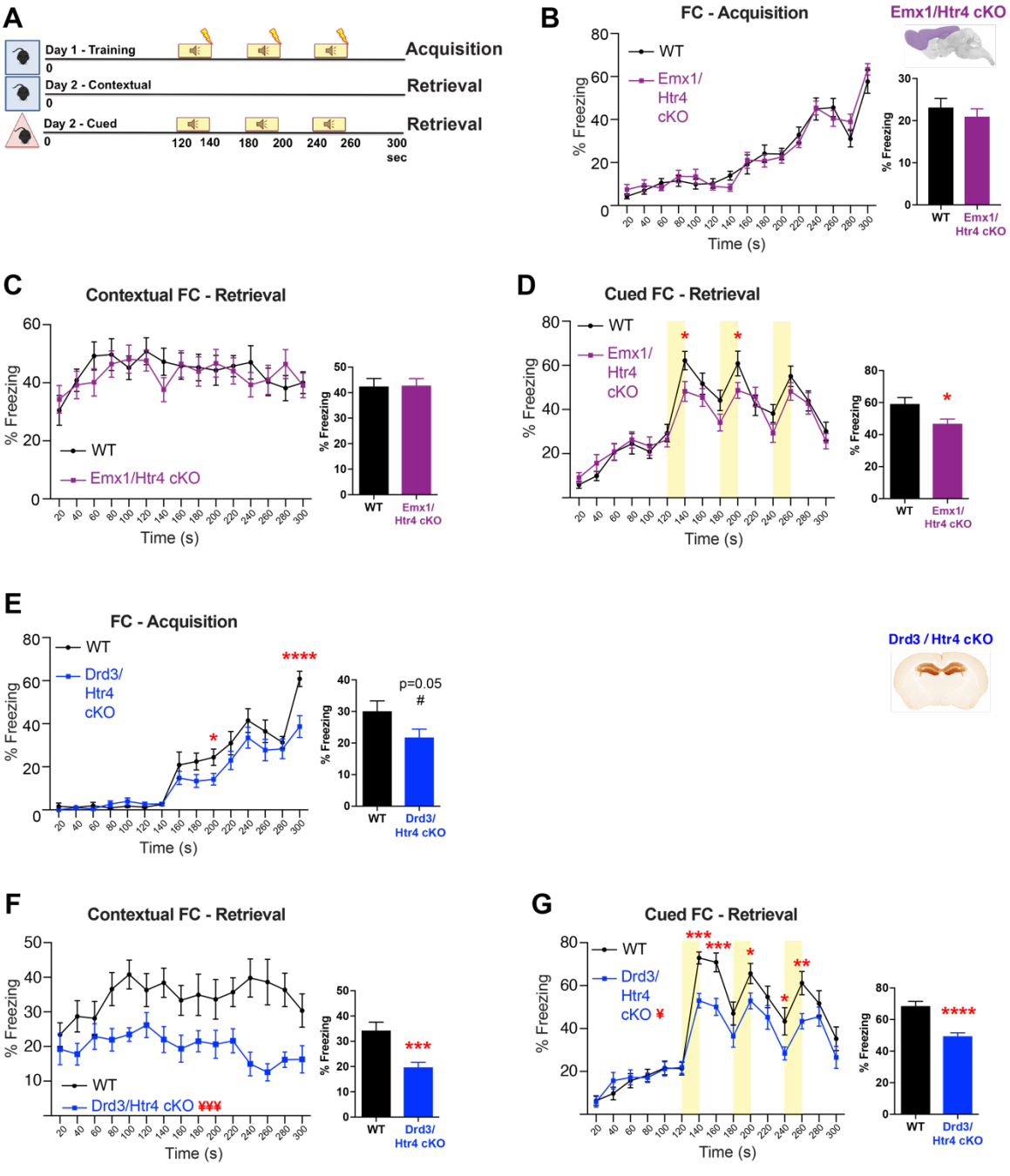
A
Day 1 - Training
0
Acquisition
Day 2 - Contextual
0
Retrieval
Day 2 - Cued
0
120 140 180 200 240 260 300
sec
Retrieval
B
FC - Acquisition
Emx1/Htr4 cKO
WT
Emx1/
Htr4
cKO
% Freezing
Time (s)
WT
Emx1/
Htr4 cKO
C
Contextual FC - Retrieval
WT
Emx1/Htr4 cKO
% Freezing
Time (s)
D
Cued FC - Retrieval
WT
Emx1/
Htr4
cKO
% Freezing
Time (s)
E
FC - Acquisition
WT
Drd3/
Htr4
cKO
****
*
p=0.05
#
% Freezing
Time (s)
WT
Drd3/
Htr4 cKO
Drd3 / Htr4 cKO
F
Contextual FC - Retrieval
WT
Drd3/Htr4 cKO ¥¥¥
***
% Freezing
Time (s)
WT
Drd3/
Htr4 cKO
G
Cued FC - Retrieval
WT
Drd3/
Htr4
cKO ¥
***
***
*
*
**
****
% Freezing
Time (s)
WT
Drd3/
Htr4 cKO

5.2.2. The role of 5-HT_4R in object memory

The novel object recognition is based on memories neutral of emotionality. Therefore, it can be used to discriminate whether changes in memory performance are due to coding of emotional attachment or memory itself.
To investigate whether 5-HT_4R in the excitatory neurons of pallial origin contribute to object memory, Emx1/Htr4 cKO mice were tested in the novel object recognition test (NORT). **Figure 5.2A** shows the NORT timeline. Animals were habituated to the arena 24 hours before the test to eliminate any novelty induced anxiety-like behaviors. During the sampling phase (7 min), each subject was placed in the arena containing two identically object for familiarization. After 1 hour delay, each subject was returned to the arena containing an identical object to the familiarized objects and another novel object. Time spend exploring the objects were measured. While control littermates (WT) spent significantly more time exploring the novel object compared to identical object, Emx1/Htr4 cKO mice did not show difference in exploration time between identical and novel objects (**Figure 5.2B**). Novel object preference was above 50 percent for WT showing positive preference while Emx1/Htr4 cKO showed around 50 percent preference, significantly lower compared to WT ($p<0.001$) (**Figure 5.2C**). Together, these data suggest that Emx1/Htr4 cKO mice displayed impaired object recognition in the NORT.

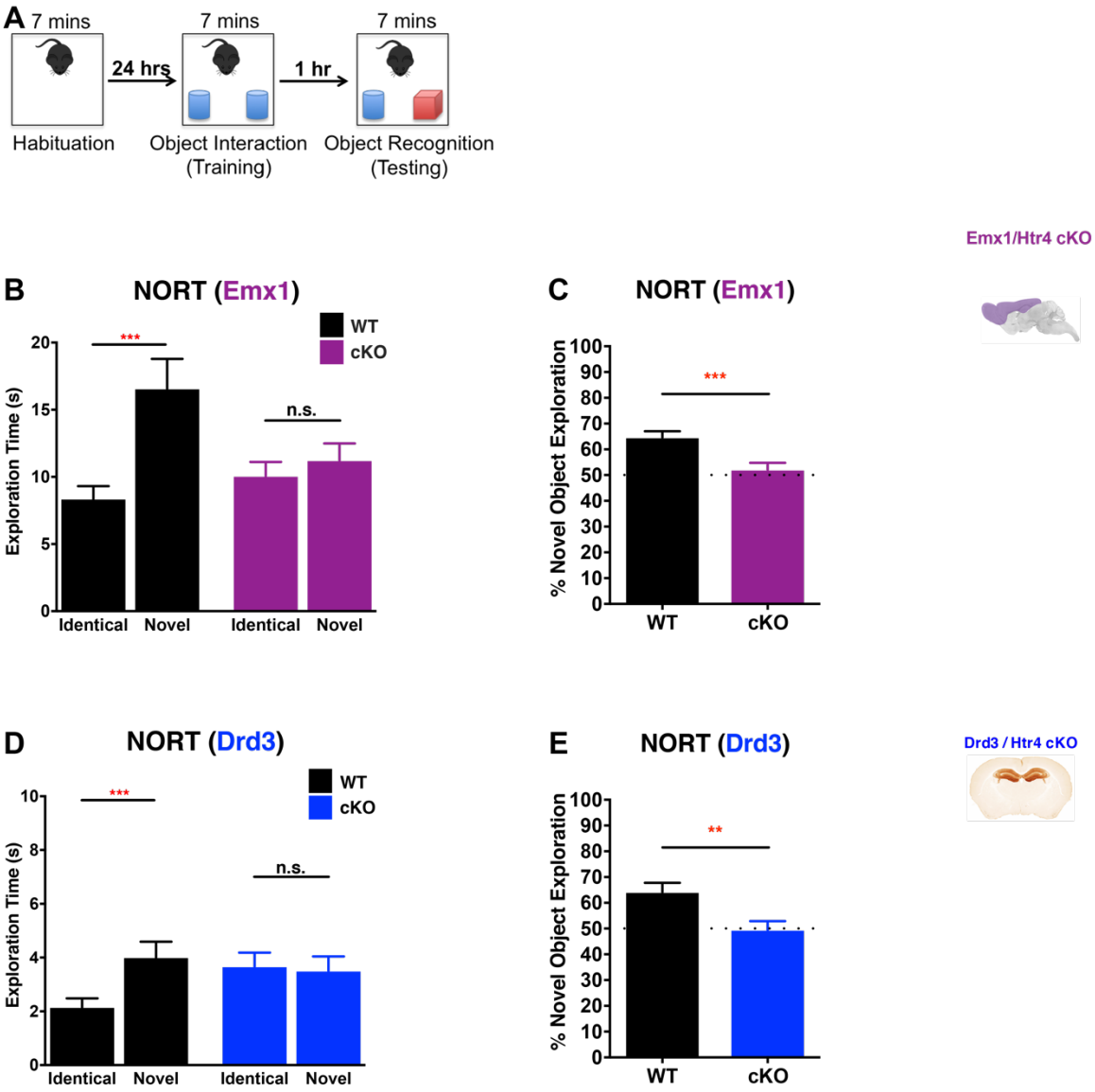

Figure 5.2. Hippocampal 5-HT$_4$R is necessary for object recognition memory.
A. Schematic depicting the novel object recognition test (NORT).
B. Emx1/Htr4 cKO mice did not show a difference in exploration time between the identical and novel objects, compared to controls (WT) showing significantly higher exploration of the novel object. Emx1/Htr4 cKO n=32, WT n=32.
C. Emx1/Htr4 cKO displayed no preference for the novel object compared to WT showing significantly higher percent novel object exploration.
D. Drd3/Htr4 cKO mice did not show a difference in exploration time between the identical and novel objects, compared to controls (WT) showing significantly higher exploration of the novel object. Drd3/Htr4 cKO n=12, WT n=12.
E. Drd3/Htr4 cKO displayed no preference for the novel object compared to WT showing significantly higher percent novel object exploration.
Data are represented as mean ± SEM. Two-way ANOVA followed by post hoc Fisher's LSD test for exploration time (s). Two-tailed unpaired t-test for % novel object exploration. **p<0.01, ***p<0.001.

To delineate the contribution of 5-HT_4R specifically in the hippocampal excitatory neurons to object memory, Drd3/Htr4 cKO mice were tested in the same novel object recognition paradigm. Drd3/Htr4 cKO mice did not show a significant difference in the exploration of the novel and identical objects while WT spent significantly more time exploring the novel object compared to identical object ($p<0.001$) (**Figure 5.2D**). Novel object preference was above 50 percent for WT showing positive preference while Emx1/Htr4 cKO showed around 50 percent preference, significantly lower compared to WT ($p<0.01$) (**Figure 5.2E**). These results indicated that Drd3/Htr4 cKO mice displayed impaired object recognition in the NORT.

5.2.3. The role of 5-HT_4R in social recognition memory

To explore the role of 5-HT_4R in social recognition memory in all excitatory pallial neurons or specifically in the excitatory neurons of the hippocampus, we used the three-chamber social recognition test. **Figure 5.3A** shows the social recognition test timeline. Immediately after the social interaction test (discussed in Chapter 2) during which each subject was familiarized with a previously strange mouse, the inanimate object in one chamber was replaced with a novel strange mouse of same appearance. The percentage of time exploring the novel mouse was used to determine a subject's ability to discriminate between the unfamiliar and familiar mouse as a measure for social memory.

During the recognition phase, Emx1/Htr4 cKO mice showed significantly less percent time exploring the novel mice compared to control littermates ($p<0.05$) (**Figure 5.3B**), indicating an attenuated preference towards exploring the novel mice. On the other hand, both Drd3/Htr4 cKO and WT displayed similar percentage of time exploring the novel mice (**Figure 5.3C**), showing equally high preference towards exploring the novel mice. Together, these data suggested that Emx1/Htr4 cKO mice displayed impaired social memory in the social recognition task while Drd3/Htr4 cKO performed similar to controls.

Since, in mice, social memory relies on olfactory cues, we performed the olfactory habituation/dishabituation test to control for the olfactory performance in the Emx1/Htr4 cKO mice. Naturally, mice are expected to habituate to the same odors when presented consecutively, while the presentation of a novel odor should evoke higher interest (dishabituation) (Yang and Crawley, 2001). In addition, mice's ability to discriminate between social and nonsocial odors as well as between two different social odors are necessary for normal social interaction and recognition. In this test, water was used as a control, almond and mint extracts as non-social cues, and the smell of the bedding from two novel cages previously used by the same sex conspecifics were presented as social olfactory cues. There was not any difference between the habituation and dishabituation responses of Emx1/Htr4 cKO mice compared to WT littermates (**Figure 5.3D**), supporting that the impairment in social recognition in Emx1/Htr4 cKO mice is not due to an olfactory problem.

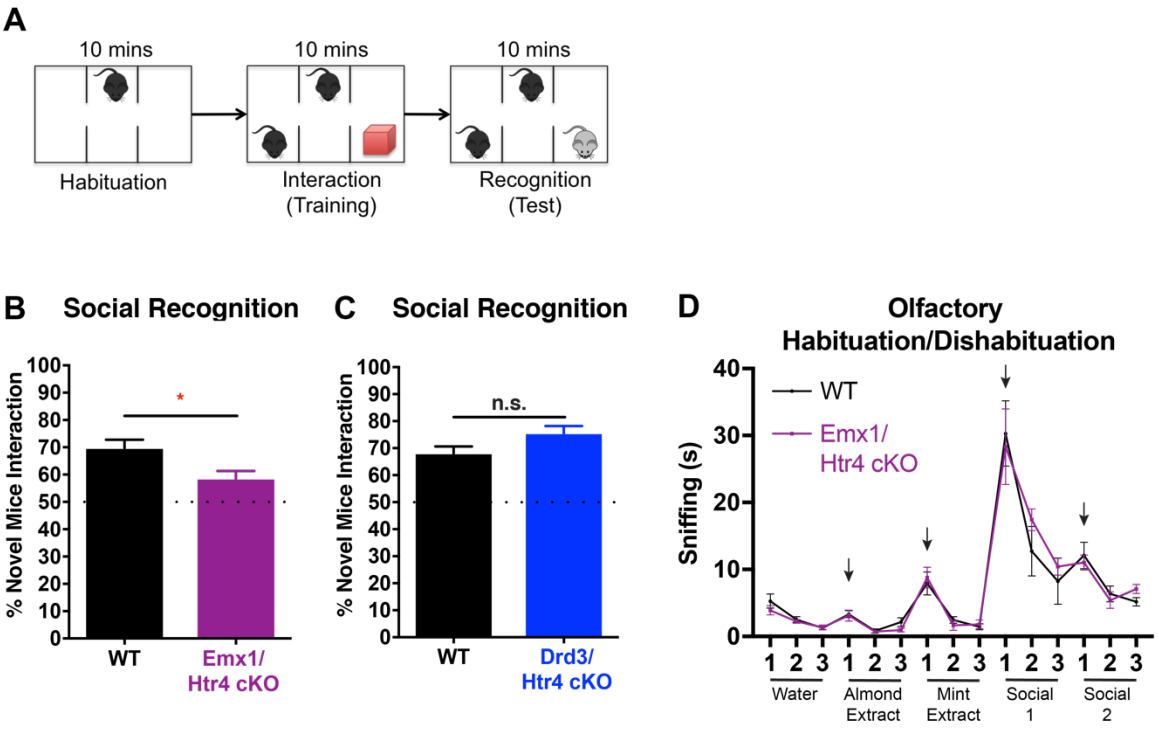

Figure 5.3. Cortical, but not hippocampal, 5-HT$_4$R may mediate social recognition.
A. Schematic depicting the social recognition test.
B. Emx1/Htr4 cKO mice showed attenuated percentage of novel mice interaction during social recognition test compared to controls (WT). Emx1/Htr4 cKO n=25, WT n=29.
C. Drd3/Htr4 cKO and WT animals showed similarly high percentage of novel mice interaction in the social recognition test. Drd3/Htr4 cKO n=12, WT n=12.
D. Emx1/Htr4 cKO did not show any difference in olfactory habituation/dishabituation behavior compared to WT littermates. Arrows indicate the dishabituation when a new type of odor was presented. Emx1/Htr4 cKO n=25, WT n=29.
Data are represented as mean ± SEM. Two-tailed unpaired t-test. *p<0.05, n.s.≥0.5.

5.3. Discussion

Our behavior analysis in two different Emx1/Htr4 cKO and Drd3/Htr4 cKO mice suggested that 5-HT_4R in the excitatory neurons of the hippocampus and neocortex mediates distinct features of learning and memory depending on the brain region and the nature of the memory.

5.3.1. Hippocampal 5-HT_4R mediates fear responses and memories.

We first showed that the loss of 5-HT_4R in all excitatory neurons of brain regions of pallial origin led to attenuation of the retrieval of cued fear conditioning while context-associated fear memory was not affected. However, the ablation of 5-HT_4R exclusively from hippocampal excitatory neurons resulted in impairments in initial fear responses, possibly due to impairments in memory acquisition, as well as the retrieval of contextual and cued fear memories. First, this suggests that 5-HT_4R in hippocampal excitatory neurons mediates both contextual and cued fear memories. Second, the attenuation of fear responses and previously reported increased innate anxiety-like behavior upon the genetic ablation of 5-HT_4R from the hippocampus suggest that innate anxiety and fear responses may be differentially modulated by hippocampal excitatory neurons possibly through 5-HT_4R receptors.

The fact that the specific loss of hippocampal 5-HT_4R resulted in more robust dysregulation of fear memory compared to the pallial deletion promotes the importance of cell type and circuit specific approaches in studying learning and memory mechanisms. In addition, this may indicate that the hippocampal circuits mediating contextual and cued fear conditioning may be distinct. Another possible reason for this observation may be that the loss of 5-HT_4R from the hippocampus and LA/BLA in Emx1/Htr4 cKO mice may have dysregulated the reciprocal connections between these regions in a synergistic way, rendering contextual fear memory unaffected. There may as well be other compensation mechanisms in the Emx1/Htr4 cKO mice since the robust behavioral phenotypes observed in Drd3/Htr4 cKO mice, was either minimal or absent in Emx1/Htr4 cKO mice (Chapter 2 and 3).

5.3.2. Hippocampal 5-HT_4R mediates object memory.

Our findings in the novel object recognition test, showed that 5-HT_4R in the hippocampus was also necessary for emotionally neutral object memory. These findings provide further evidence that hippocampus mediates object memory and that 5-HT_4R is a major regulator in this process. Together with its role in fear memory, it seems possible that 5-HT_4R mediates a relatively general memory process, that may regulate functionally distinct hippocampal circuits responsible for memories with varying valence.

5.3.3. Pallial 5-HT_4R mediates social recognition memory.

Social recognition memory was intact when 5-HT_4R was ablated from most of the hippocampal excitatory neurons while its deletion from almost all pallial neurons blunted this memory. This indicates that 5-HT_4R possibly mediates social memory in pallial neurons, that are not targeted by Drd3-Cre. For example, ventral CA3 pyramidal cells, which are the only neurons in hippocampus that are Drd3-Cre negative, has been shown to store social memory (Okuyama et al., 2016). In addition, the neocortex has been strongly indicated in mediating the social recognition (Bicks et al., 2015). It is possible that 5-HT_4R mediates social memory through these regions since its expression is observed throughout the neocortex and ventral CA1.

5.3.4. Molecular signatures underlying the role of 5-HT_4R in memory

Our electrophysiology and genome-wide TRAP-Seq data may provide further evidence and candidate mechanism underlying the cellular and molecular functions of 5-HT_4R in memory. 5-HT_4R may promote the formation of memory by enhanced synaptic transmission as we found that 5-HT_4R promotes the firing of DG GCs. Indeed, optogenetic inhibition of dorsal DG GCs has shown to impair contextual fear memories (Kheirbek et al., 2013). Our differential expression analysis also support this hypothesis. We have found that many genes dysregulated in the absence of 5-HT_4R were involved in calcium-dependent signaling, synaptic and vesicular transmission, cell adhesion and

phosphorylation, all of which can affect the synaptic plasticity in these neurons. In fact, gene set enrichment analysis (GSEA) in Chapter 4 also identified significantly dysregulated genes that are expressed in GCs and correlated with LTP and LTD, such as, *Ppp2r1a*, *Plcb3*, and *Nos1* (data not shown).

Furthermore, our behavioral findings indicating a role for 5-HT_4R in positive regulation of memory may be correlated with our differential expression data showing the dysregulation of 'genes decreased in Alzheimer's disease patients' (**Figures 4.14 and 4.16**). This may also be supported by the significant changes in the expression of 'genes enriched in astrocytes' (**Figure 4.14**) since astrocytes play a significant role in the processing of extracellular amyloid-beta (Aβ) plaques (Frost and Li, 2017) linked to AD pathology. Furthermore, the genes that are significantly dysregulated both in the dorsal and ventral DG upon the loss of 5-HT_4R (**Figure 4.13E**) include *Apoe* and *Clu*, two of the largest known genetic risk factors for AD (Sadigh-Eteghad et al., 2012). Considering the ameliorating actions of 5-HT_4R agonists in animal models of AD, the analysis and functional confirmation of our RNA-Seq results may bring more insights to the field.

5.4.5. Conclusion

Our results demonstrated that 5-HT_4R in hippocampal excitatory cells is a prominent regulator of hippocampus-dependent memory processing. The identification of cell type specific elements of 5-HT_4R pathway via genome wide

gene expression analyses has presented a powerful resource that will unravel new cellular players for understanding the function of 5-HT_4R in learning and memory. Ultimately, this may provide novel molecular targets for the development of new cognitive enhancers, which will be useful for treatments of cognitive problems observed in many disease.

CONCLUSIONS

Since the discovery of first selective serotonin reuptake inhibitor, fluoxetine, in 1974 (Wong et al., 1974), SSRIs still remain the most prescribed antidepressant as the extensive search for more effective therapeutics continues. Identification and targeting specific cell types and proteins underlying the pathophysiology of the disease presents a powerful approach in this pursuit for developing novel, more efficacious therapies with fewer side effects.

In this study, we generated the first *Htr4* conditional knockout animals. We successfully used this tool to study the role of 5-HT_4R, one of the first putative serotonergic targets for fast acting antidepressants, in different cell populations in the hippocampus and neocortex. This tool will continue to help facilitate our knowledge of the function of this receptor in cell type specific serotonergic modulation in various biological processes.

We found that the loss of 5-HT_4R from mature excitatory neurons of hippocampus led to an extensive antidepressant-like behavioral response along with increased innate anxiety levels. Moreover, these behavioral changes were accompanied by antidepressant-like cellular and molecular changes in the hippocampus; namely enhanced neurogenesis in the ventral dentate gyrus and elevated neurotropic factors in the hippocampus. Slice electrophysiology experiments revealed that the excitability of dentate gyrus granule cells was decreased when 5-HT_4R was absent, a regulation that is also observed in response to SSRI treatments. Together, our results strongly indicate that 5-HT_4R in the hippocampus mediates anxiety and mood related behaviors differentially,

and the ablation of functional 5-HT_4R specifically in the hippocampus leads to antidepressant-like actions.

The ventral dentate gyrus specific changes in neurogenesis as well as the differential regulation of gene expression between ventral and dorsal dentate gyrus in response to the loss of 5-HT_4R provide further evidence that these regions are under distinct control in modulating emotive behaviors. These results support the hypothesis that 5-HT_4R mediate anxiety and mood related behaviors through ventral hippocampus.

Our results provide further insights in the circuit modulation underlying antidepressant-like behavioral changes. The inhibition of dentate gyrus granule cell activity seems to be a common and necessary factor in this process. Our data and previous reports strongly suggest that antidepressant action may be accomplished by increasing serotonergic inhibition directly on dentate gyrus granule cells and recruiting GABAergic inhibition on the granule cells through interneurons via increased number of young adult born neurons. As dentate gyrus is the “main gate” to the hippocampus and mediates the neural transmission to the rest of the region along the dorsoventral axis, an approach targeting functionally distinct granule cell populations may be necessary. Teasing apart the circuit elements that are sufficient to mediate emotive behavior may lead to more specific anxiolytic and antidepressant targets.

Our TRAP-Seq approach identified excitatory cell specific 5-HT_4R regulations in the dentate gyrus. The analysis of gene set enrichment in

dysregulated genes suggests that 5-HT_4R is necessary for homeostasis of intracellular calcium signaling which may be essential for the excitability of these neurons and synaptic signaling. Further investigation and functional confirmation of candidate genes identified in this study will unravel the exact intracellular mechanisms of 5-HT_4R signaling, especially that mediate granule cell excitability. Further identification of ventral dentate gyrus specific genes in this pathway will be especially valuable since it may lead to more specific targets for novel therapeutics against anxiety and mood disorders.

Pharmacological activation of 5-HT_4R shows fast acting anxiolytic and antidepressant properties however the underlying mechanism of this action is poorly understood. Our results showing that the ablation of 5-HT_4R from the hippocampus was sufficient to produce antidepressant-like responses support the previously generated hypothesis that the desensitization of hippocampal 5-HT_4R may mediate the fast acting antidepressant effects of the 5-HT_4R agonist and the action of chronic SSRIs. On the other hand, it is also possible that the agonist may achieve its fast actions via other brain regions such as the mPFC. The administration of the 5-HT_4R agonist in cell type specific or spatially restricted Htr4 conditional knockout animals may point out a specific path of action.

One of the questions regarding the function of 5-HT_4R was whether it mediates the SSRI responses in the neocortex. We tackled this question by deleting 5-HT_4R from all excitatory cells of pallial origin, and showed that 5-HT_4R

was not necessary for behavioral responses to chronic SSRIs in the neocortex. This hypothesis was also tested with a more specific approach that directs the conditional 5-HT_4R targeting to the cortical cell population that mediates the chronic SSRI actions. Although these cells had shown an increase in Htr4 mRNA levels in response to chronic SSRI treatment, our results suggested that 5-HT_4R was not required for the behavioral antidepressant responses. However, what would be the biological relevance of elevated 5-HT_4R levels in these cells? It is possible that neocortical 5-HT_4R mediates the strength or side effects of the SSRI action. Due to the limitations of behavioral tests in mice, the strength of the SSRIs would be challenging to interpret. However, our results may support the latter provocative hypothesis by indicating that pallial 5-HT_4R was necessary for some of the anxiogenic effects of SSRIs and its specific loss in corticostriatal neurons may be anxiolytic. Regardless, these results suggest distinct functions for 5-HT_4R in the hippocampus and neocortex.

In addition to emotive behavior, hippocampal 5-HT_4R was necessary for maintaining some episodic memories involving hippocampal function, such as contextual and cued fear memory and object memory. These results shed light into the function of hippocampal 5-HT_4R in mediating memory, as well as differential regulation of innate anxiety and fear responses. Further electrophysiological studies and the analysis of potential intracellular targets identified by TRAP-Seq will elucidate its role in synaptic plasticity and may help identify targets for cognitive enhancers.

Furthermore, the differential regulation of anxiety, mood and memory related behaviors by a single 5-HT receptor in the excitatory neurons of hippocampus points out the importance of targeting functionally distinct circuit elements to study emotive and cognitive processes. In this regard, our analysis of multidimensional transcriptomics data that identified region and cell type specific genes mediated by 5-HT_4R will facilitate the discovery of such cell type markers or direct molecular targets.

Overall, the behavioral and neural adaptations following hippocampal loss of 5-HT_4R were similar to the effects of SSRIs, considering our findings and others showing SSRIs yield antidepressant-like responses while also elevating anxiety levels in naïve animals of some mouse strains. Moreover, in patients, chronic SSRIs achieve improved mood while acute SSRIs sometimes exacerbate anxiety symptoms, resulting in poor therapeutic compliance. In this context, this study will help elucidate the cellular and molecular mechanisms underlying 5-HT_4R function that may lead to novel targets for the treatment of anxiety and mood disorders.

Closing remarks

As affective disorders show a change in the balance of the activity of various limbic regions, teasing apart the distinct elements of the emotive circuitry in the brain is essential to understand the disease. The source of the problem may differ in each patient; however, the pathophysiology and symptoms show

convergence to a great extent. Therefore, targeting a specific circuit component could compensate for possible failures in other parts of the circuitry and recover the emotive homeostasis. The circuit specific targeting may be achieved by the identification of disturbances in the molecular profiles of specific cell types within. The promise of the 5-HT_4 receptor as a therapeutic target have led us to study its function in distinct parts of the emotive circuit. This study identified specific roles of this major neuromodulatory receptor in the limbic system, and provided strong evidence in favor of the current hypothesis of hippocampal and serotonergic modulation of emotive behavior. Furthermore, it provided new insights into the divergent regulation of anxiety and mood as well as how a faster acting antidepressant response may be achieved. Future investigation should focus on confirming new targets in the hippocampus that is specific to a functional circuit mediating a particular aspect of emotive behavior. This approach may lead to more efficacious therapies and bring a balance to the extended circuitry. Discreet targeting may also have a higher chance to challenge the behavioral and physiological side effects of a more generalized therapy. While a discovery of an effective and circuit specific target may not alleviate every symptom, it may hopefully fix convergent problems. Further combinatorial pharmacological approaches with the right dose adjustments based on a particular affective disorder or even an individual patient will extend the scope of the therapeutics.

MATERIALS AND METHODS

M.1. Generation of *Htr4*-floxed mouse line

Targeting vector (TV) was designed by inGenious Targeting Laboratory Inc., Ronkonkoma, NY. Annotated TV sequence (in full) can be found in the **Appendix**. A 7.92 Kb region used to construct the targeting vector was first subcloned from a positively identified C57BL/6 BAC clone (RP23:358G18). The region was designed such that the short homology arm (SA) extends 2347 base pairs (bp) 3' to the Neo cassette. The long homology arm (LA) ends 5' to the target region, and is 4820 bp long. The loxP/FRT flanked Neo cassette is inserted 252 bp downstream of exon 5. The single loxP site, containing engineered MfeI and ApaI sites for southern blot analysis, is inserted 347 bp upstream of exon 5. The target region is 752 bp and includes exon 5.

The targeting vector is confirmed by restriction analysis after each modification step, and finally, by sequencing with the following primers. P6 (5'-GAG TGC ACC ATA TGG ACA TAT TGT C -3') and T73 (5'- TAA TGC AGG TTA ACC TGG CTT ATC G -3') primers anneal to the backbone vector sequence and read into the 5' and 3' ends of the BAC sub-clone. N1 (5'- TGC GAG GCC AGA GGC CAC TTG TGT AGC -3') and N2 (5'- TGC GAG GCC AGA GGC CAC TTG TGT AGC -3') primers anneal to the 5' and 3' ends of the loxP/FRT flanked Neo cassette and sequence the 5' side of SA and 3' side of the target region, respectively.

The BAC was sub cloned into a ~2.4kb backbone vector (pSP72, Promega) containing an ampicillin selection cassette for retransformation of the construct prior to electroporation. A pGK-gb2 loxP/FRT Neo cassette was inserted into the gene as depicted in **Figure 2.1** and **Appendix**. The targeting construct was linearized using NotI prior to electroporation into ES cells. The total size of the targeting construct (including vector backbone and Neo cassette) is 13.69 Kb.

Three lines of chimeric mice using C57BL/6 ES cells were generated at the Janelia Research Campus Gene Targeting and Transgenic Facility; and one of these lines, ROXY *Htr4* 1G12, showed germline transmission of the mutation. We have established a colony of mice from the 1G12 line in our laboratory referred as *Htr4*$^{loxP/loxP}$ or *Htr4*-floxed mice.

M.2. Animals

All procedures involving animals were approved by The Rockefeller University Institutional Animal Care and Use Committee and were in accordance with National Institutes of Health guidelines. Emx1-Cre mice were purchased from The Jackson Laboratories (Stock #005628). Tlx3-Cre (Tlx3-Cre PL56) and Drd3-Cre (Drd3-Cre KI198) mice were generated by the GENSAT Project (Gong et al., 2007). Tlx3-Cre mice were maintained at The Rockefeller University and Drd3-Cre were purchased from the Mutant Mouse Regional Resource Center

(MMRRC: 031741-UCD). Cre-dependent EGFP-L10a expressing mice, Rosa26^{fsTRAP}, were purchased from the Jackson Laboratories (Stock #022367). All mice were bred on a C57BL/6J background, maintained on a 12-hour light-dark cycle (light cycle, 7 am to 7 pm) and given ad libitum access to food and water. Animals used in the study were male and female.

M.3. Breeding and Genotyping

To generate enough number of age-matched littermates for behavior cohorts, accelerated breeding by in vitro fertilization (IVF) was employed in collaboration with Transgenic Services Laboratory in Comparative Bioscience Center (CBC) at The Rockefeller University. For IVF, eggs from *Htr4*$^{loxP/loxP}$ females and spermatozoa from Emx1/Tlx3/Drd3-Cre::*Htr4*$^{loxP/loxP}$ male mice. Animals for other lines and experiments were generated by duo (one male, one female) or trio (one male, two females) breeding. Breeding for each specific experiment was discussed in the corresponding Chapter.

For genotyping, at age 15-18 days, pups were marked with an ear punch for identification and tail biopsies were performed. Each tail sample was lysed for DNA extraction in 200 μl tail lysis buffer (100 mM Tris.HCl-pH8.8, 1 mM EDTA, 0.5% Tween20) at 56 °C for at least 24 hours. The tail DNA samples were analyzed via PCR using 1-2 μl of lysis solution, GoTaq DNA Polymerase (Promega) and corresponding primer pairs (**Table M.1**).

Table M.1. Genotyping primers.

Primer*	Sequence	Expected results (bp)
Htr4 loxP F	TCGAGGCATTCCTCGATTCA	WT: 172 loxP: 239
Htr4 loxP R	TAACACCTGGCCGAAACGTT	
Cre F	CCGGGCTGCCACGACCAA	WT: n/a Cre: 150
Cre R	GGCGCGGCAACACCATTTTT	
EGFP F	GCACGACTTCTTCAAGTCCGCCATGCC	WT: n/a EGFP: 265
EGFP R	GCGGATCTTGAAGTTCACCTTGATGCC	
Rosa WT F	AAGGGAGCTGCAGTGGAGTA	WT: 297
Rosa WT R	GAGCGGGAGAAATGGATA G	

*F: forward, R: reverse

M.4. Drug treatments and behavioral assays

Behavioral assays were performed on male mice starting from 8 weeks and up to 4 months old. Mice were housed 2-3 per cage. Each experiment was performed using only aged matched mice, and control groups always consisted of littermates. All experiments, scoring and analysis were performed blinded to the experimental groups. For every behavioral experiment, animals were brought into the procedure room in their home cages and habituated to the room for one hour. Assays were performed within the light cycle of the animals unless otherwise is noted. The number of animals per group (n) and the statistical analyses used for the result of each experiment were detailed in the corresponding chapter. For behavioral analysis, data points outside 90% confidence interval (conventionally, SD= ±1.644854) of the estimated Gaussian

curve for each group were determined as “outliers” and excluded from analyses. Statistical analyses were performed using GraphPad Prism 7 software, and $p<0.05$ was considered significant.

For chronic fluoxetine (FLX) treatments, 8-week old mice were given either 0.167 mg/ml FLX (Fluoxetine hydrochloride, Sigma F132, Sigma-Aldrich) in vehicle (VEH, 1% saccharine in drinking water to mask the taste of FLX) or only VEH for control. Drugs were administered by drinking via 50 ml canonical tubes with sipper caps composed of 2.5 cm straight stainless steel sipper tubes ball-point sipper tubes (Ancare), inserted into rubber stoppers. Behavioral assays stared after 18 days of drug treatment. The treatment continued throughout the behavior assessment period until mice were sacrificed. Every 2-3 days, fresh FLX and VEH solutions were replaced.

M.4.1. Open field

Open field behavior was assayed in eight identical square arenas (50x50x22.5 cm, acrylic) with white floor and clear walls, equipped with two rows of infrared photocells placed 20 and 50 mm above the floor, spaced 31 mm apart. The procedure room was brightly and homogenously lit with fluorescent ceiling lamps and the arenas were placed on tables. Each animal was placed in the open field arena for 60 min. Photocell beam interruptions were recorded on a computer using the Superflex software (Accuscan Instruments). The floors and the walls of the arenas were cleaned with Clidox sterilizer and water in between

trials. The data was exported as time spent and distance traveled in total, peripheral and center areas in 5 min bins. Thigmotaxis was calculated by dividing time spend in the peripheral area by total time spent.

M.4.2. Elevated Plus Maze

The plus maze consisted of two opposite open arms without sidewalls (35x5 cm) and two enclosed arms with 14 cm high sidewalls (35x5x14 cm). The arms extended from a common central square (5 cm^2) perpendicular to each other, completing the shape of a plus sign. The entire plus-maze apparatus was elevated to a height of 30 cm. The experimental area was isolated from the experimenter with black curtains running down from the ceiling to the floor on four-sides and homogenously lit by ceiling mounted LED lamps on four sides, ensuring minimal shadows. The illumination at the middle of each open arm was set to 30-lux. Testing began by placing an animal on the central platform of the maze facing the same open arm. Trials were 5 min and recorded by a ceiling mounted camera connected to a computer. EthoVision XT 7.0 software (Noldus) was used to operate the camera, track the subject and record the total time spent in each arm, total distance moved and velocity. The maze was wiped with 30% Ethanol in between trials. Mice that fell off the open arms were excluded from the analysis.

M.4.3. Novelty Suppressed Feeding

Mice were food deprived for 24-hour before the test. The efficiency of food deprivation was measured as the decrease in body weight (data is not reported as none of the animals were excluded from the analysis by this measure). Testing was performed in a brightly lit arena similar to the open field (50x50x22.5 cm) where a food pellet (1.8 cm length of 1.58x0.95 cm diameter oval pellets) was placed in the middle on a circular filter paper (20 cm diameter, Fisherbrand). A white noise source was active throughout the habituation and testing. Four subjects were tested at the same time in adjacent arenas. The observer in the room measured the latency to bite the food in 15 min trials. To record homecage feeding, each animal was put in a clean cage similar to their home cage for 30 min with food ad libidum after each trial.

M.4.4. Tail suspension test

Mice were suspended by their tails using adhesive tape (1-2 cm from the tip of the tail) to the end of a piece of flexible plastic tubing hanging from the top center of one of the four compartments of the white acrylic box setup (101x55x26 cm). Four mice were tested at the same time in four adjacent compartments separated by white acrylic walls. While suspending, mice were about 30 cm above the floor of the box. Test sessions lasted 6 min and were videotaped. Mice that held on to their bodies by their front limbs or started climbing up their tails were gently repositioned using a long stick without distracting other subjects. The

floors and the walls of the box were cleaned with Clidox sterilizer and water in between trials. At a later date, the amount of time spent immobile in the last 4 min of the test was measured, which was estimated by scoring as mobile or immobile in every 5 s. In case of body holding or climbing, scoring was not applicable. If more than four time points were missed, mice were excluded from the analysis.

M.4.5. Forced swim test

Mice were individually placed into the glass cylinders (15 cm diameter, 35 cm height) filled with tap water (23-25 °C) to a height of 15.7 cm. Four mice were tested at the same time in separate cylinders placed as 2x2 adjacently. The cylinders were visually separated by white acrylic sheets. To start a trial, mice were gently placed into the cylinders keeping their head above the water surface. Test sessions lasted 6 min and were videotaped from above. At a later date, the amount of time spent immobile, defined as the absence of all motions except floating and those required to keep a mouse's head above the surface, was measured, which was estimated by scoring as mobile or immobile in every 5 s.

M.4.6. Splash test

These experiments were performed in the dark cycle of the mice to observe higher amount of activity. The procedure room was illuminated with red light. Mice were squirted with 10% sucrose (in tap water) enough to soak the fur

on their back by a small spray bottle (for results discussed in Chapter 2), or 200 μl per animal on their lower back by a 1 ml syringe with a needle tip attached (for results discussed in Chapter 3). Immediately after, mice were placed in clean small mouse cages (22.2x30.80x16.24 cm) with bedding and filter top (no wire top). Four mice were tested at the same time in adjacent cages visually separated by white acrylic sheets. Test sessions lasted 5 min and were videotaped from the side. At a later date, grooming time was measured in total 5 min, which was estimated by scoring as grooming in every 5 s.

M.4.7. Sucrose preference test

Mice were water deprived for 24 h. Each mouse was then placed in a clean cage with bedding, containing a 1% sucrose filled bottle and a tap water filled bottle (50 ml canonical tubes with sipper caps composed of 2.5 cm straight stainless steel sipper tubes ball-point sipper tubes (Ancare), inserted into rubber stoppers). Sucrose and water consumption for 6 hours was measured by the decrease in the weight of the bottles. At the 3-hour mark, bottles were switched to avoid side preference. Sucrose preference was calculated as the ratio of the amount of 1% sucrose consumed to the amount of total drinking.

M.4.8. Sucrose consumption test

Each mouse was placed in a clean cage with bedding and food, containing a 1% sucrose filled bottle and a tap water filled bottle (as described in

sucrose preference test). Sucrose and water consumption for 72 h was measured by the decrease in the weight of the bottles. At the each 12 h mark, the bottles were weighted and switched to avoid side preference. At the end of the test, animals were weighted. The amount of 1% sucrose or water consumed (g or ml) was normalized per animal to the weight of the animals (g).

M.4.9. Marble burying

Equally spaced 12 black marbles (4x3) were placed on a deep woodchip bedding (Sani-Chips) filled 3:4 of a small mouse cage (22.2 x 30.80 x 16.24 cm) with open top. The number of marbles buried in 15 min was counted as a measure of spontaneous digging. Marbles submerged at least 2:3 way into the bedding was counted as buried.

M.4.10. Acoustic startle response and pre-pulse inhibition

Startle and PPI testing were performed in four identical startle response systems (39×38×58 cm, SR-LAB system, San Diego Instruments), each consisting of a non-restrictive clear Plexiglas cylinders (inner diameter 4 cm, length 13 cm), resting on a white Plexiglas platform, placed in a ventilated, sound-attenuated chamber. High frequency speakers mounted 33 cm above the cylinders presented all acoustic stimuli, which were controlled by SR-LAB software. Piezoelectric accelerometers mounted under the cylinders transduced movements of the animals which were digitized and stored by an interface and

computer assembly. A dynamic calibration system was used to ensure comparable sensitivities across chambers.

The animal was placed into the startle chamber and allowed to acclimatize for 5 min. The time between each trial was 7-23 s. The measurement was performed in four blocks. All intensities were presented in a pseudo-random order within a block. Beginning at startling stimulus onset, 65 consecutive 1-ms readings were recorded to obtain the peak amplitude of the animal's startle response (Vmax). 5 s after each stimulus, another 65 ms were measured which constitutes the no-stimulus trials. Background noise was 65 dB.

In the first block (pre-test), mice were presented with 120 dB acoustic stimuli (65 ms) for five trials. Maximum startle responses (Vmax) were recorded per trial and averaged per subject.

In the second block (ASR), acoustic stimuli were presented in five different intensities (120, 110, 100, 90 and 80 dB, 65 ms), each for four trials. Maximum startle responses (Vmax) were recorded for each trial and averaged for each stimulus intensity per subject.

In the third block (PPI), 120 dB acoustic stimuli (40 ms) preceded by four different pre-pulse (PP) intensities (0, 3, 6, 12 dB, 20 ms) were presented, each for ten trials. The time between the prepulse and the pulse were 100 ms. Maximum startle responses (Vmax) were recorded for each trial and averaged for each prepulse intensity per subject. PPI was calculated as the percent

decrease in startle response in PP3, PP6 and PP12 compared to PP0 per subject.

Lastly, in the fourth block (post-test), 120 dB stimuli (65 ms) were presented for five trials. Maximum startle responses (Vmax) were recorded per trial, averaged per subject, and compared to the pre-test responses to assess the habituation of ASR during the testing.

M.4.11. Fear Conditioning

Coulbourn Instruments Shuttle Cage for mouse (H10-11M-SC) was converted into the operant conditioning chamber for fear conditioning experiments as following: The Shuttle Cage was placed into a sound and light proof isolation cubicle. Mice were only placed in the chamber on the right. A USB camera (Coulbourn Instruments, ACT-VP-02) was mounted on the ceiling of the right chamber to record the behavior of mice. The sound and shock generation, control and delivery were accomplished by configuring the appropriate accessories and modules (Coulbourn Instruments) with the chamber. The FreezeFrame 3 Software (Coulbourn Instruments) was used to program the test, operate the setup, record the videos and analyze the freezing behavior.

In day 1, mice were placed in the operant conditioning chamber for 300 s, and an auditory tone (70 Db) was presented for 20 s preceding an electrical footshock (0.75 mA, 1 s) for three times at 140, 200 and 260 s in a 300-s training trial. In day 2 (24 h later), first, animals were returned to the operant chamber

(same context) for 300 s to induce contextual freezing behavior. After all animals in a given cohort were tested for context, in the same day, animals were returned to the operant chamber with altered context for 300 s: bottom and sides of the camber was covered with colored and patterned plastic layering, and cotton balls sprayed with 1% mint extract (in 30% ethanol) was placed in a separate compartment at the bottom of chamber. Conditioned auditory tone was presented in the same way as the training to induce cued freezing behavior. Percent freezing was calculated by FreezeFrame 3 Software using the recorded videos and the freezing detection threshold was set to 10 (default).

M.4.12. Novel object recognition

These experiments were performed in the dark cycle of the mice to observe higher amount of activity. However, the fluorescent ceiling lamps in the room were kept on, illuminating the room and arena similar to the light cycle. Animals were habituated to the square arena (58x58x40 cm, clear acrylic) 24 h before the test for 7 min. During the sampling phase (7 min), each subject was placed in the arena containing two identical objects placed at 10 cm distances from the two opposite corners of the same side. After 1 hour delay, each subject was returned to the arena containing an identical object at one corner, and another novel object at the other corner replacing the familiar object. This recognition phase also lasted for 7 min. The arena was videotaped from above

and the interactions with each object were manually scored by two stopwatches. The sniffing behavior was considered as interaction.

M.4.13. Social interaction and recognition

Social behavior was measured using the three-chamber social interaction setup. The arena is a rectangular box (58.5x43x22.7 cm) made of white acrylic, two inner walls dividing it equally into three chambers. Each inner wall has an open middle section with a removable sliding door, allowing free access between the middle and the two side chambers when the doors are removed. The social interaction test comprised two parts: a habituation session and a trial session. During the habituation session, two empty wire cups were placed in the left and right chambers. The test mouse was placed in the middle chamber and allowed to explore all three chambers for 10 min. Next, the doors to the side chambers were closed, the test mouse was placed in the middle chamber for the trial session. A stranger mouse of the same sex/appearance and a novel Lego® piece were placed inside the left and right wire cups in a random order to balance for side preference. Doors between chambers were opened to allow the test mouse to explore the three chambers freely for 10 min.

For social recognition, immediately following the social interaction test, the doors were closed once again and the test mouse was placed in the middle chamber. A novel stranger mouse of the same sex was replaced with the Lego®

piece. Immediately, doors between chambers were opened to allow the test mouse to explore the three chambers freely for 10 min.

During all sessions, the arena was videotaped from above. Stranger mice were habituated to the wire cups for 10 min each day for three days before the testing to minimize movement and stress responses such as defecation and urination. The arena and the wire cups were thoroughly cleaned with Clidox sterilizer and water between subjects. At a later date, the interaction time with each cup were manually measured by two stopwatches on the recorded videos. The sniffing behavior was considered as interaction.

M.4.14. Olfactory habituation/dishabituation

The procedure was performed as described previously (Yang and Crawley, 2001). Cotton swabs dipped into water (control), two nonsocial odors (almond and mint extracts) and two social odors (bedding from two separate cages of same sex) were presented as olfactory stimuli. Sniffing behavior was recorded by stopwatches in real time.

M.5. shRNA construct generation and screening

Five shRNA sequences against *Htr4* were designed by The RNAi Consortium, Broad Institute (https://portals.broadinstitute.org/gpp/public). The single-stranded DNA (ssDNA) oligonucleotides for shRNA (sense) and

complementary (antisense) sequences were commercially synthesized and purchased from e-oligos (Gene Link) (**Table M.2**). Overhang sequences were added to allow for cloning (SapI: 5'- TTT -3' for the sense, and XbaI: 3'- GATC -5' to the antisense sequences). These oligonucleotides were annealed to generate double-stranded DNA oligonucleotides with overhangs, and cloned into the pGFP-shRNA vector (pAAV-CMV-EGFP-hGH-PA-mU6-shRNA-PA) as described previously (Hommel et al., 2003). Briefly, ssDNA oligonucleotides were resuspended at 0.25 nM/μl in water. Complementary ssDNA oligonucleotides were annealed as following: 20 μl sense-oligo, 20 μl antisense-oligo, 5 μl water and 5 μl 10X annealing buffer (10X = 1M NaCl, 100mM Tris pH7.4) for a total of 50 μl annealing reaction was mixed, rapidly heated to 95°C, and slowly cooled down to room temperature in a PCR machine. Annealed templates were diluted 1:1000 in 0.5X annealing buffer. 1 μl of the dilution to 30-50 ng of the SapI/XbaI restriction digested/gel purified pGFP-shRNA was used for each ligation reaction in a total 10 μl volume. Sequencing primers, pGFP-shRNA-forward (5'- CAC AGA CTT GTG GGA GAA GC -3', 270 bp from hairpin) and pGFP-shRNA-reverse (5'- CCC CTG AAC CTG AAA CAT AAA -3', 190 bp from hairpin), were used to select and confirm the positive clones.

Table M.2. shRNA oligonucleotide sequences.

Name	Strand	Hairpin Sequence 5'-to-3'	TRC Clone ID
shControl	sense	**TTT**GGATCTTAGCCCCAAGGTACCGCAGGA TTGCCCGTATAGGTGACGTCTCATATTTTT	
shControl	anti	**CTAG**AAAAATATGAGACGTCACCTATACGGG CAATCCTGCGGTACCTTGGGGCTAAGATCC	
sh249	sense	**TTT**CCGGCCCTTCTTTGTCACCAATATTCTC GAGAATATTGGTGACAAAGAAGGGTTTTT	TRCN0000026249
sh249	anti	**CTAG**AAAAACCCTTCTTTGTCACCAATATTCT CGAGAATATTGGTGACAAAGAAGGGCCGG	
sh261	sense	**TTT**CCGGCCTTCCCATGTTTATATCTTTCTC GAGAAAGATATAAACATGGGAAGGTTTTT	TRCN0000026261
sh261	anti	**CTAG**AAAAACCTTCCCATGTTTATATCTTTCT CGAGAAAGATATAAACATGGGAAGGCCGG	
sh270	sense	**TTT**CCGGCCTCACAGCAACTTCTCCTTTCTC GAGAAAGGAGAAGTTGCTGTGAGGTTTTT	TRCN0000026270
sh270	anti	**CTAG**AAAAACCTCACAGCAACTTCTCCTTTCT CGAGAAAGGAGAAGTTGCTGTGAGGCCGG	
sh284	sense	**TTT**CCGGGCCTTTGGTTTATAGGAACAACTC GAGTTGTTCCTATAAACCAAAGGCTTTTT	TRCN0000026284
sh284	anti	**CTAG**AAAAAGCCTTTGGTTTATAGGAACAAC TCGAGTTGTTCCTATAAACCAAAGGCCCGG	
sh304	sense	**TTT**CCGGGCTGGCCTATTACCGAATCTACTC GAGTAGATTCGGTAATAGGCCAGCTTTTT	TRCN0000026304
sh304	anti	**CTAG**AAAAAGCTGGCCTATTACCGAATCTAC TCGAGTAGATTCGGTAATAGGCCAGCCCGG	

For in vitro screening of the knockdown efficiency of shRNAs, HEK293T cells (ATCC) cultured in 24-well plates (1.9 cm^2 culture area, Corning) in Dulbecco's Modified Eagle's Medium (DMEM) (Gibco) supplemented with 10% fetal bovine serum (FBS) (Gibco) were cotransfected with pCMV6-Htr4-Myc-DDK (Origene) and each of the pGFP-shRNA vectors via FuGENE 6 transfection reagent (Promega). Four replicates per each shRNA construct were prepared. 48 hours after the transfection, total RNA samples were isolated using Qiagen RNeasy Mini Kit with on-column DNase digestion. Total cDNA samples were generated using qScript cDNA SuperMix (QuantaBio). qRT-PCR was employed using the cDNA samples and TaqMan probes for *Htr4* and *Gapdh* (**Table M.3**) to measure relative *Htr4* expression and calculate knockdown efficiency.

M.6. Total RNA isolation and quantitative RT-PCR

Total RNA was isolated from cultured cells or dissected tissue using Qiagen RNeasy Mini Kit for whole cortex and hippocampus, and RNeasy Micro Kit for DG and CA fields. For tissue dissection, mice were sacrificed, followed by rapid dissection of desired brain region with fine tip forceps in ice-cold HBSS containing 2.5 mM HEPES-KOH (pH 7.4), 35 mM glucose, 4 mM $NaHCO_3$. RNA quantity was measured with a Nanodrop 1000 spectrophotometer (Thermo Scientific). cDNA samples were generated from 300-1000 ng of total RNA using qScript cDNA SuperMix (QuantaBio) (see Chapter 6.13 for polysome-bound RNA isolation and cDNA amplification for TRAP-Seq).

All qRT-PCR experiments were performed on the LightCycler® 480 System (Roche), using TaqMan assays (Applied Biosystems) and LightCycler® 480 Probes Master mix (Roche). A list of Taqman assays used in this study was given in **Table 6.3**. Default cycling conditions were followed (pre-incubation: one cycle, 95°C, 5 min; amplification: 45 cycles, 95°C for 10 s, 60°C for 30 s, 72°C for 1 s; ramp rate: 4.4°C/s). 10-20 ng of cDNA were used for each qRT-PCR reaction and three technical triplicates were run for every sample. The mean CT for technical replicates was used for the quantification. Data were normalized to *Gapdh* as the endogenous control by the comparative CT (2-ΔΔCT) method (Schmittgen and Livak, 2008).

Table M.3. TaqMan Gene Expression Assays used for qRT-PCR.

Gene Symbol	Assay ID	Dye
Htr4 (3-4)	Mm00434129_m1	FAM
Htr4 (4-5)	Mm01258807_m1	FAM
Htr4 (5-6)	Mm01258808_m1	FAM
Htr4 (6-7)	Mm01258809_m1	FAM
Gapdh	Mm99999915_g1	FAM
Htr1a	Mm00434106_s1	FAM
Htr1b	Mm00439377_s1	FAM
Htr1d	Mm00434115_s1	FAM
Htr1f	Mm02619863_s1	FAM
Htr2a	Mm00555764_m1	FAM
Htr2c	Mm00434127_m1	FAM
Htr3a	Mm00442874_m1	FAM
Htr5a	Mm00434132_m1	FAM
Htr5b	Mm00439389_m1	FAM
Htr6	Mm00445320_m1	FAM
Htr7	Mm00434133_m1	FAM
S100a10	Mm00501457_m1	FAM
Bdnf	Mm04230607_s1	FAM
Vegfa	Mm00437306_m1	FAM
Gad1	Mm00725661_s1	FAM
Tyro3	Mm00444547_m1	FAM
Lct	Mm01285112_m1	FAM
Dsp	Mm01351876_m1	FAM
Meis2	Mm00487748_m1	FAM
Trhr	Mm00443262_m1	FAM
Tdo2	Mm00451269_m1	FAM
EGFP	Mr04097229_mr	FAM
Colgalt2	Mm01290012_m1	FAM
Actb	Mm02619580_g1	FAM

M.7. Generation of *Htr4* cKO and WT expression vectors

Total RNA samples from the hippocampi of Emx1/*Htr4* cKO mice or *Htr4*-floxed (WT) littermates were isolated using Qiagen RNeasy Mini Kit with on-column DNase digestion. Htr4 cKO and WT cDNA was generated using qScript cDNA SuperMix (QuantaBio). *Htr4* cKO and WT cDNA coding sequences (CDSs) (inserts) were cloned into pCMV6-Entry-Myc-DDK tagged mammalian expression vector (OriGene) by homologous recombination-based In-fusion HD cloning kit (Clontech). Specifically, the vector was linearized using AsiSI and MluI restriction sites. The inserts were amplified from the cDNA samples by PCR using CloneAmp HiFi PCR Premix (Clontech) and primers “Htr4 infusion forward” (5’- AGA TCT GCC GCC GCG ATC GCC ATG GAC AAA CTT GAT GCT AAT GTG -3’) and “Htr4 infusion reverse” (5’- GCG GCC GCG TAC GCG TAG TAT CAC TGG GCT GAG CAG -3’). The primers were designed using “Online In-Fusion Tools” (https://bit.ly/1eFKzsP) to include 5’ and 3’ homologous sequences to the ends of the linearized vector for In-Fusion HD cloning, and the *Htr4* CDS start codon, yet exclude the stop codon to allow for the expression of the Myc-DDK tag sequences and following stop codon and polyA tail in the backbone. The resulted expression vectors were called *Htr4* cKO and WT plasmids.

M.8. cAMP induction assay

HEK293T cells (ATCC) cultured in 24-well plates (1.9 cm^2 culture area, Corning) in Dulbecco's Modified Eagle's Medium (DMEM) (Gibco) supplemented with 10% fetal bovine serum (FBS) (Gibco) were transfected with the *Htr4* cKO and WT plasmids via FuGENE 6 transfection reagent (Promega). 48 hours after the transfection, all cells were incubated in stimulation buffer (DMEM + 0.5mM IBMX (Sigma Aldrich)) for 30 min. For cAMP induction, cells were incubated in either stimulation buffer (Basal) or 100μM Zacopride (Tocris Bioscience) in stimulation buffer (Zacopride) for 45 min. The cells were lysed with lysis buffer (0.1 M HCl, 0.1%Triton-X) for 20 min, and the lysates were centrifuged for 10 min at 21,500 x g. cAMP levels in the supernatants were measured by monoclonal anti-cAMP antibody based direct cAMP ELISA kit (Non-acetylated version, NewEast Biosciences). Four biological replicates and two technical replicates were performed for each experimental group. The cAMP level of each biological replicate was normalized to its protein concentration measured by Qubit protein assay kit (Invitrogen) and Qubit 3.0 Fluorometer (Invitrogen). Statistical analysis of normalized cAMP levels was performed in GraphPad Prism 7 by two-way ANOVA followed by Fisher's LSD.

M.9. Generation of AAV-DIO-Htr4-Myc

The mouse Htr4-Myc-DDK transgene was PCR amplified from pCMV6-Htr4-Myc-DDK (Origene) using Phusion High-Fidelity DNA Polymerase (New England Biolabs) and primers Htr4-inverted-AscI-forward (5'- GGC GCG CCC TAT TAA ACC TTA TCG TCG TCA TCC T -3') and Htr4-inverted-NheI-reverse (5'- GCT AGC CAC CAT GGA CAA ACT TGA TGC TAA TGT -3'), adding 5' AscI and 3' NheI restriction sites to the inverted Htr4-Myc-DDK sequence (insert). For the vector backbone, pAAV-EF1a-DIO-EYFP (Addgene, plasmid #27056) was linearized using AscI and NheI restriction sites removing the inverted EYFP sequence. The insert was then cloned into the backbone in reverse orientation by Quick Ligation Kit (New England Biolabs), to generate pAAV-DIO-Htr4-Myc. For the confirmation of the Cre-dependent expression of the plasmid in HEK cells in vitro (detailed in Chapter 3), AAV-Cre-GFP (AAV-CMV-Cre-GFP, Stereotype:2) were purchased from University of North Carolina (UNC) Vector Core. Following the confirmation of expression in vivo, the plasmids were packaged into AAV2.9 stereotype viral vectors at the University of Pennsylvania Vector Core at the titer 4.782 $x10^{13}$ gc/ml (gc: genome copy).

M.10. Stereotactic surgeries

Mice were anesthetized with a mixture of ketamine (100 mg/kg) and xylazine (10 mg/kg) in 0.9% sterile saline solution by intraperitoneal injection. Once deeply anesthetized, mice were immobilized in a Kopf stereotactic apparatus using intra-aural positioning studs and a tooth bar to immobilize the skull. Bilateral holes were drilled on the surface of the skull at the injection sites. Each AAV injections was performed using a glass needle (thinly pulled glass capillary) attached to a Hamilton Microliter syringe (5 μl syringe with 0.05 μl increments). The syringe was held and controlled by a Kopf Microinjection Unit (Modell 5000) for a precise volume delivery (0.05 μl every 5 min). If an injection was performed at multiple point on the same dorsoventral (DV) axis, it was completed with a single needle insertion, starting at the most ventral coordinate and retracting to the following dorsal point of injection. After an injection was completed at a coordinate, the needle was left in place for an additional 5 min before slowly being retracted. The injection coordinates and volumes for different brain regions were as follows: dorsal DG (A-P: -1.58, M-L: 0.8, D-V: 1.87 [0.1 μl]; and A-P: -2.06, M-L: 1.13, D-V: 1.75 [0.1 μl]), ventral DG (A-P: -3.52, M-L: 2.50, D-V: 3.25 [0.05 μl], 2.25 [0.05 μl]; and A-P: -3.80, M-L: 2.50, D-V: 3.50 [0.05 μl], 2.88 [0.1 μl], 2.25 [0.05 μl]). A-P and M-L are distances (mm) from bregma, D-V is from dura.

After the needle removal, the incision sites were closed by surgical sutures or wound staples. Antibiotic powder (Neo-Predef with Tetracaine, Pharmacia and Upjohn) was placed on the wounds, and 0.5 ml sterile 0.9% saline solution was administered subcutaneously to prevent dehydration. Animals were allowed to recover in a clean cage set on a heating blanket 37°C until achieving ambulatory recovery. Ibuprofen (0.1 mg/ml) was administered in the drinking water for 2-7 days following surgery, and all surgical sutures or wound staples were removed after 7-10 days.

M.11. Electrophysiological recordings

Mice of 8 weeks of age were euthanized with CO_2. After decapitation and removal of the brains, transversal slices (400 µm thickness) were cut using a Vibratome 1000 Plus (Leica Microsystems) at 2 °C in a NMDG-containing cutting solution (in mM): 105 NMDG (N-Methyl-D-glucamine), 105 HCl, 2.5 KCl, 1.2 NaH_2PO_4, 26 $NaHCO_3$, 25 Glucose, 10 $MgSO_4$, 0.5 $CaCl_2$, 5 L-Ascorbic Acid, 3 Sodium Pyruvate, 2 Thiourea (pH was around 7.4, with osmolarity of 295–305 mOsm). After cutting, slices were left to recover for 15 min in the same cutting solution at 35 °C and for 1 h at room temperature (RT) in recording solution (see below). Whole-cell patch-clamp recordings were performed with a Multiclamp 700B/Digidata1550A system (Molecular Devices). Dentate gyrus granule neurons were selected for recording based on their size, shape and position in the granular

layer using an upright Olympus BX51WI microscope. The extracellular solution used for recordings contained (in mM): 125 NaCl, 25 $NaHCO_3$, 2.5 KCl, 1.25 NaH_2PO_4, 2 $CaCl_2$, 1 $MgCl_2$ and 25 glucose (bubbled with 95% O_2 and 5% CO_2). The slice was placed in a recording chamber (RC-27L, Warner Instruments) and constantly perfused with oxygenated aCSF at 24 °C (TC-324B, Warner Instruments) at a rate of 1.5–2.0 ml/min. Whole-cell patch-clamp recordings were obtained from granule neurons using recording pipettes (King Precision Glass, Inc, Glass type 8250) pulled in a horizontal pipette puller (Narishige) to a resistance of 3–4 MΩ, filled with an internal solution containing (in mM): 126 K-gluconate, 4 NaCl, 1 $MgSO_4$, 0.02 $CaCl_2$, 0.1 BAPTA, 15 glucose, 5 HEPES, 3 ATP, 0.1 GTP (pH 7.3). For whole-cell recordings in the voltage clamp configuration, BIMU-8 (10 mM, Tocris Bioscience) was added to the bath for 1 minute and subsequently washed. Tetradotoxin (TTX, 1 mM, Tocris Bioscience) was added previously to the bath to avoid activation of neighboring neurons by BIMU-8. To measure the firing of the DG granule neurons, steps of 10 pA current were injected from a set starting membrane potential of -80mV.

Data were acquired at a sampling frequency of 50 kHz and filtered at 1 kHz and analyzed offline using pClamp10 software (Molecular Devices). All electrophysiological data are expressed as means ± SEM. Statistical analysis was performed using the two-tailed unpaired Student's t-test in GraphPad Prism 7 software. $p<0.05$ was considered significant.

M.12. Histology

For fixed brain serial slice preparations, mice were deeply anesthetized by ketamine/xylazine intraperitoneal (IP) injections and transcardially perfused with 10 ml of phosphate buffered saline (PBS) followed by 30 ml of 4% paraformaldehyde (PFA) in PBS. Brains were post-fixed in 4% PFA overnight at 4°C and cryoprotected by 30% sucrose in PBS. Coronal sections (40 μm) were acquired by a freezing microtome (Leica SM2010 R Sliding Microtome). The sections were then transferred to PBS, or cryoprotection buffer (25% glycerol and 25% ethylene glycol in PBS, pH 7.4) for long term storage at -20°C.

For both 3,3′-Diaminobenzidine (DAB) immunohistochemistry (IHC) and all immunofluorescence (IFC) procedures, serial sections were blocked for 60 min in PBS containing 3-5% normal donkey serum (NDS, Jackson ImmunoResearch) or normal goat serum (NGS, Vector Laboratories) and 0.1% Triton X-100 or 0.1% Saponin; and then incubated in the same blocking buffer overnight at 4°C with primary antibodies on **Table M.4** at listed dilutions. On the next day, the sections were washed 3 times with PBS for 5 min, and then incubated for 2 h at room temperature with the appropriate Alexa dye-conjugated (for IFC) or horseradish peroxidase (HRP)- conjugated (for DAB IHC) secondary antibodies (Invitrogen) diluted 1:500 in the blocking buffer. The sections were then washed 3 times with PBS, and counterstained with DAPI for nuclear staining at 1:10,000 dilution (for IFC). For DAB IHC, the staining was developed using

SIGMAFAST™ DAB tablets (Sigma-Aldrich) following the manufacturers' protocol. The sections were mounted on the Superfrost slides (VWR) and sealed with Prolong Gold mounting reagent (Invitrogen). The slides were imaged on a Zeiss LSM700 confocal microscope or a Zeiss Axiosko2 microscope. Brightness and contrast adjustments were made on ImageJ post-acquisition.

Table M.4. Primary antibodies used in this study.

Antibody Name	Source	Catalog #	Dilution
rbxHtr4_C'	Abcam	ab101910	1:500
rbxHtr4_N'	Millipore	SAB4501480	1:500
rbxHtr4_Ala361	Cell Signaling	#13690	1:1000
rbxHtr4_3rdCYTloop	Sigma	S0195	1:150
rbxHtr4_31-70	Abcam	ab60359	1:500
rbxHtr4_presige	Sigma	HPA040591	1:200
SR-4 (C-18)	Santa Cruz	sc-32566	1:50
SR-4 (K-19)	Santa Cruz	sc-19155	1:50
SR-4 (N-18)	Santa Cruz	sc-32564	1:50
SR-4 (N-16)	Santa Cruz	sc-19154	1:50
SR-4 (G-3)	Santa Cruz	sc-376158	1:50
rbxHtr4_C'_NL	Novus Bio	NLS656	1:500
DDK, clone 4C5	OriGene	TA50011	1:1000
GAD67, clone 1G10.2	Millipore	MAB5406	1:500
GFP	Abcam	ab13970	1:1000
Myc tag, clone 9E10	Sigma	SAB4700447	1:500
NeuN, clone A60	Millipore	MAB377	1:1000
Calbindin-D-28K	Sigma	C7354	1:500
Calretinin	Swant	6B3	1:500
ChAT	Millipore	AB144P	1:500
Parvalbumin	SWANT	McAB325	1:500
Doublecortin (C-18)	Santa Cruz	sc-8066	1:200

M.13. Translating ribosome affinity purification and RNA isolation

Affinity purification of EGFP-tagged polysomes was performed as previously described (Heiman et al., 2014), with minor modifications. Three biological replicates consisting of brain tissue pooled from one male and one female mice were used for each condition (except for KO1 replicate which was pooled from two females). Mice were sacrificed, followed by rapid microdissection of dorsal and ventral dentate gyrus with fine tip forceps in ice-cold HBSS containing 2.5 mM HEPES-KOH (pH 7.4), 35 mM glucose, 4 mM $NaHCO_3$, and 100 µg/ml cycloheximide. Each pooled dentate gyrus tissue sample was then homogenized in 1 ml extraction buffer containing 10 mM HEPES-KOH (pH 7.4), 150 mM KCl, 5 mM $MgCl_2$, 0.5 mM DTT, 100 µg/ml cycloheximide, RNasin (Promega) and SUPERas-In™ (Life Technologies) RNase inhibitors, and Complete-EDTA-free protease inhibitors (Roche), and then cleared by centrifugation at 2000 x g at 4 °C. IGEPAL CA-630 (NP-40, Sigma) and DHPC (Avanti Polar Lipids) were both added to the S2 supernatant to a final concentration of 1% for each, followed by centrifugation at 20,000 x g. Polysomes were immunoprecipitated from the S20 supernatant using 100 µg monoclonal anti-EGFP antibodies (50 µg each of clones 19C8 and 19F7; see (Heiman et al., 2008)) bound to biotinylated-Protein L (Pierce, Thermo Scientific) coated streptavidin-conjugated magnetic beads (Life Technologies), and washed in high salt buffer containing 10 mM HEPES-KOH (pH7.4), 350 mM KCl, 5 mM

$MgCl_2$, 1% IGEPAL CA-630, 0.5 mM DTT, 100 µg/ml cycloheximide, and RNasin RNase inhibitors (Promega). IPs were carried out overnight at 4°C. Bound RNA was purified using the RNeasy Micro Kit (Qiagen) with on-column DNase digestion. RNA was also purified from a fraction of the pre-IP S20 supernatant to serve as whole-tissue "input" samples. RNA quantity was determined using the Qubit RNA HS Assay kit (Invitrogen) and RNA quality was determined using Agilent 2100 Bioanalyzer with RNA 6000 Pico chips. Only samples with RNA integrity values >7.0 were used for RNA-seq.

M.14. RNA sequencing (RNA-Seq)

For each sample, 15 ng of purified RNA was converted to cDNA and amplified using the Ovation RNA-Seq System V2 Kit (NuGEN). cDNA was fragmented to an average size of 250 bp using a Covaris C2 sonicator with the following parameters: intensity 5, duty cycle 10%, cycles per burst 200, treatment time 120 seconds. RNA-Seq libraries were prepared from 10 µg amplified RNA using the TruSeq RNA Sample Preparation Kit v2 (Illumina) following manufacturer's protocols. The quality of the libraries was assessed using the Agilent 2200 TapeStation system with D1000 High Sensitivity ScreenTapes. Libraries were sequenced at The Rockefeller University Genomics Resource Center on the Illumina NextSeq 500 platform to obtain 75 bp paired-end reads. 12 samples were multiplexed per sequencing lane (**Table M.5)**.

Table M.5. Overview of RNA-Seq datasets.[¥]

Sample*	FastQ Name	RNA-Seq Pool	Truseq Adapter Index
dDG_WT_IP_1	2128_Drd3_dDG_WT_IP Rep1	A	AR002
dDG_WT_IP_2	2129_Drd3_dDG_WT_IP Rep2	A	AR005
dDG_WT_IP_3	2130_Drd3_dDG_WT_IP Rep3	A	AR007
vDG_WT_IP_1	2131_Drd3_vDG_WT_IP Rep1	A	AR004
vDG_WT_IP_2	2132_Drd3_vDG_WT_IP Rep2	A	AR006
vDG_WT_IP_3	2133_Drd3_vDG_WT_IP Rep3	A	AR012
dDG_KO_IP_1	2134_Drd3_dDG_Htr4_KO_IP Rep1	A	AR013
dDG_KO_IP_2	2135_Drd3_dDG_Htr4_KO_IP Rep2	A	AR015
dDG_KO_IP_3	2136_Drd3_dDG_Htr4_KO_IP Rep3	A	AR018
vDG_KO_IP_1	2137_Drd3_vDG_Htr4_KO_IP Rep1	A	AR014
vDG_KO_IP_2	2138_Drd3_vDG_Htr4_KO_IP Rep2	A	AR016
vDG_KO_IP_3	2139_Drd3_vDG_Htr4_KO_IP Rep3	A	AR019
dDG_WT_Input_1	2140_Drd3_dDG_WT_input Rep1	B	AR002
dDG_WT_Input_2	2141_Drd3_dDG_WT_input Rep2	B	AR005
dDG_WT_Input_3	2142_Drd3_dDG_WT_input Rep3	B	AR007
vDG_WT_Input_1	2143_Drd3_vDG_WT_input Rep1	B	AR004
vDG_WT_Input_2	2144_Drd3_vDG_WT_input Rep2	B	AR006
vDG_WT_Input_3	2145_Drd3_vDG_WT_input Rep3	B	AR012
dDG_KO_Input_1	2146_Drd3_dDG_Htr4_KO_input Rep1	B	AR013
dDG_KO_Input_2	2147_Drd3_dDG_Htr4_KO_input Rep2	B	AR015
dDG_KO_Input_3	2148_Drd3_dDG_Htr4_KO_input Rep3	B	AR018
vDG_KO_Input_1	2149_Drd3_vDG_Htr4_KO_input Rep1	B	AR014
vDG_KO_Input_2	2150_Drd3_vDG_Htr4_KO_input Rep2	B	AR016
vDG_KO_Input_3	2151_Drd3_vDG_Htr4_KO_input Rep3	B	AR019

* brain region_genotype_RNA source_replicate

[¥] All data sets have been deposited in NCBI's Gene Expression Omnibus (GEO) (Barrett et al., 2013): accession-numbers-pending.

M.15. RNA-Seq read mapping, analysis, and visualization

RNA-Seq read quality was assessed by FastQC (0.11.4). Sequences were trimmed for trailing adaptors from the Illumina sequencing process by Trim Galor (0.4.1). The trimmed reads were then aligned to annotated exons using the mm10 mouse reference genome (UCSC) with STAR (2.4.2a) (Dobin et al., 2013) using default settings. SAMtools (v0.1.19-444) was used for indexing and removal of duplicates. The numbers of raw and mapped reads (bases), and the percentage of mapping for each sample were calculated via Picard (1.123) using the CollectRNASeqMetrics program (**Table M.6**).

The quantification of aligned, sorted and indexed reads was done using the htseq-count module of the HTSeq framework (0.6.0) (Anders et al., 2015), using the “union” mode with default settings to generate raw counts for each sample. Aligned bam files were converted to tdf format using igvtools (2.3.61) for Integrative Genomics Viewer (IGV) visualization. Differential expression was calculated by DESeq2 (Love et al., 2014), R-package version 1.4.5. Significant p values were corrected to control the false discovery rate (FDR) of multiple testing at 0.05 threshold. Fold change cutoff ± 1.25 ($|\log_2|$ fold change >0.3219) was applied unless otherwise noted. For scatter plots and heatmap visualizations, raw counts normalized to sample size for each sample (“normalized counts”) were used as calculated by DESeq2. Morpheus software (Broad Institute) was used to generate the heatmaps. Significant differentially expressed genes were split into

up- and down-regulated for Gene set enrichment analysis (GSEA) and gene ontology (GO) analysis. GSEA was performed using Molecular Signature Database (MSigDB, Broad Institute) (FDR<0.05). GO network and visualization was generated using BiNGO (A Biological Network Gene Ontology tool, 3.0.3) (Maere et al., 2005) as a Cytoscape (3.6.0) plugin.

Table M.6. Quality control of RNA-Seq alignments.

Sample	Raw Reads	Mapped Reads	Riboso-mal %	Coding %	UTR %	Intro-nic %	Interge-nic %	mRNA* %
dDG_WT_IP_1	5389296447	5287301402	15.10	33.07	37.00	7.52	7.95	70.07
dDG_WT_IP_2	5211282117	5115099172	15.04	34.80	39.34	4.30	7.20	74.13
dDG_WT_IP_3	4532219275	4440093124	19.30	35.14	36.49	2.95	6.96	71.64
vDG_WT_IP_1	5055676715	4963214738	15.25	35.93	39.45	3.22	6.83	75.37
vDG_WT_IP_2	5200875692	5096531166	18.77	34.24	37.98	2.97	6.88	72.22
vDG_WT_IP_3	5176647321	5088146609	11.74	39.38	38.93	3.07	7.41	78.31
dDG_KO_IP_1	5097724216	5010604143	10.87	28.77	28.77	23.42	8.65	57.54
dDG_KO_IP_2	4873024410	4780034112	15.55	34.78	37.09	5.73	7.53	71.87
dDG_KO_IP_3	4279892247	4200940083	12.57	37.37	37.59	5.45	7.58	74.96
vDG_KO_IP_1	4386834142	4294720920	18.98	33.93	37.81	3.40	6.72	71.74
vDG_KO_IP_2	5041820503	4938661168	18.97	34.77	37.26	3.27	6.56	72.04
vDG_KO_IP_3	4351693105	4268363380	15.35	36.19	37.92	3.98	7.24	74.11
dDG_WT_input_1	4976974951	4898777541	11.00	26.15	34.18	11.65	17.48	60.33
dDG_WT_input_2	4114194145	4048376030	9.60	28.97	36.85	9.12	15.87	65.82
dDG_WT_input_3	6348807839	6241867530	13.52	30.73	36.91	7.14	12.29	67.64
vDG_WT_input_1	5274266386	5200347558	7.32	29.76	37.30	9.69	16.25	67.07
vDG_WT_input_2	5908160994	5817160131	8.02	31.64	36.97	8.64	15.09	68.61
vDG_WT_input_3	5200024888	5110416182	12.45	30.12	36.81	7.70	13.47	66.93
dDG_KO_input_1	5030052258	4951122004	8.97	19.82	25.71	6.90	38.97	45.54
dDG_KO_input_2	5318465410	5237452256	9.40	29.55	37.17	8.97	15.33	66.72
dDG_KO_input_3	4494618359	4433172922	7.08	30.48	37.47	8.40	16.89	67.95
vDG_KO_input_1	5390357255	5295752262	11.57	27.52	35.93	8.45	17.04	63.45
vDG_KO_input_2	5347253361	5264487834	10.03	29.78	38.46	8.79	13.38	68.24
vDG_KO_input_3	4711433994	4633197615	12.18	29.09	36.28	8.18	14.81	65.37

* mRNA is the percentage of total bases mapping to Coding + UTR.

M.16. Statistical Analysis

All data analysis was performed in GraphPad Prism 7, Microsoft Excel or R (R Core Team, 2013). Statistical parameters including the exact value of n, precision measures (mean ± SEM) and statistical significance are reported within the corresponding Chapter in the text, the figures and/or the figure legends. Data were judged to be statistically significant when $p<0.05$ by two-way ANOVA (regular or repeated measures-RM) followed by post hoc Fisher's LSD test, or two-tailed unpaired t-test. '¥' symbol indicates significance by Two-way ANOVA, and asterisk indicates significance by Fisher's LSD test or two-tailed t-test.

For RNA-Seq analysis, Pearson correlation coefficients were calculated with GraphPad Prism 7 using normalized expression values and statistical significance was based upon the assumption that values exhibit a Gaussian distribution. Differential expression was calculated by DESeq2 (Love et al., 2014), R-package version 1.4.5. DESeq2 corrected the p values to control the false discovery rate (FDR) of multiple testing, generating adjusted p values (p-adj). p-adj<0.05 was considered significant. For GSEA, FDR<0.05 was used. For BiNGO, hypergeometric statistical test with Benjamini & Hochberg FDR correction was applied with a significance level 0.01 using Cytoscape.

APPENDIX

Construction of Conditional Targeting Vector for Htr4-floxed

1. Vector Design Outline

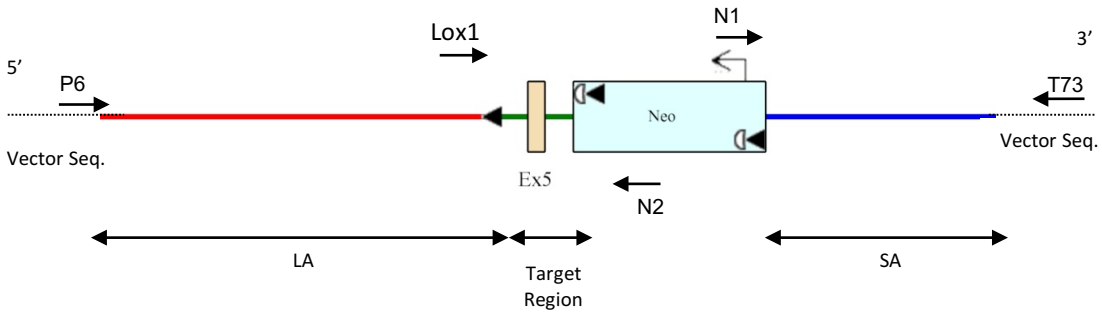

Ex5: Htr4 exon 5
LA: Long arm
SA: Short arm
Neo: Neomycin resistance cassette
Black triangles: LoxP sites
White semicircles: FRT sites

2. Sequencing Data Analysis

PCR primers used for sequencing:

```
Primer P6:  5'- GAG TGC ACC ATA TGG ACA TAT TGT C   -3'
Primer T73: 5'- TAA TGC AGG TTA ACC TGG CTT ATC G   -3'
Primer N1:  5'- TGC GAG GCC AGA GGC CAC TTG TGT AGC -3'
Primer N2:  5'- TTC CTC GTG CTT TAC GGT ATC G       -3'
Primer lox1:5'- GGA CAG CAA TCT AAG GAG CAC AG      -3'
```

3. Assembled ROXY Htr4 targeting vector

1. Vector backbone: Blue text (e.g., ATCG)
2. LA (4820 bp): Bold and italic text (e.g., ***ATCG***)
3. Distal loxP (67 bp): Lightgray text, highlighted in yellow (e.g., ATCG)
4. MA (752 bp): Green text (e.g., ATCG)
5. Neo (1713 bp): Red text (e.g., ATCG)
6. SA (2347 bp): Underlined text (e.g., ATCG)
7. LoxP: Red text, highlighted in yellow (e.g., ATCG)
8. FRT: Red and underlined text, highlighted in gray (e.g., ATCG)
9. Exon: Highlighted in pink (e.g., ATCG)
10. Genotyping forward primer – Htr4 loxP F (**TCGAGGCATTCCTCGATTCA**)
11. Genotyping reverse primer – Htr4 loxP R (**TAACACCTGGCCGAAACGTT**, reverse transposed)

3'end of BAC subclone joins here.

CGATGATATCAGATCTGCCGGTCTCCCTATAGTGAGTCGTATTAATTTCGATAAGCCAGGTTAACCTGCAT
TAATGAATCGGCCAACGCGCGGGGAGAGGCGGTTTGCGTATTGGGCGCTCTTCCGCTTCCTCGCTCACTGA
CTCGCTGCGCTCGGTCGTTCGGCTGCGGCGAGCGGTATCAGCTCACTCAAAGGCGGTAATACGGTTATCCA
CAGAATCAGGGGATAACGCAGGAAAGAACATGTGAGCAAAAGGCCAGCAAAAGGCCAGGAACCGTAAAAAG
GCCGCGTTGCTGGCGTTTTTCCATAGGCTCCGCCCCCCTGACGAGCATCACAAAAATCGACGCTCAAGTCA
GAGGTGGCGAAACCCGACAGGACTATAAAGATACCAGGCGTTTCCCCCTGGAAGCTCCCTCGTGCGCTCTC
CTGTTCCGACCCTGCCGCTTACCGGATACCTGTCCGCCTTTCTCCCTTCGGGAAGCGTGGCGCTTTCTCAT
AGCTCACGCTGTAGGTATCTCAGTTCGGTGTAGGTCGTTCGCTCCAAGCTGGGCTGTGTGCACGAACCCCC
CGTTCAGCCCGACCGCTGCGCCTTATCCGGTAACTATCGTCTTGAGTCCAACCCGGTAAGACACGACTTAT
CGCCACTGGCAGCAGCCACTGGTAACAGGATTAGCAGAGCGAGGTATGTAGGCGGTGCTACAGAGTTCTTG
AAGTGGTGGCCTAACTACGGCTACACTAGAAGAACAGTATTTGGTATCTGCGCTCTGCTGAAGCCAGTTAC
CTTCGGAAAAAGAGTTGGTAGCTCTTGATCCGGCAAACAAACCACCGCTGGTAGCGGTGGTTTTTTTGTTT
GCAAGCAGCAGATTACGCGCAGAAAAAAAGGATCTCAAGAAGATCCTTTGATCTTTTCTACGGGGTCTGAC
GCTCAGTGGAACGAAAACTCACGTTAAGGGATTTTGGTCATGAGATTATCAAAAAGGATCTTCACCTAGAT
CCTTTTAAATTAAAAATGAAGTTTTAAATCAATCTAAAGTATATATGAGTAAACTTGGTCTGACAGTTACC
AATGCTTAATCAGTGAGGCACCTATCTCAGCGATCTGTCTATTTCGTTCATCCATAGTTGCCTGACTCCCC
GTCGTGTAGATAACTACGATACGGGAGGGCTTACCATCTGGCCCCAGTGCTGCAATGATACCGCGAGACCC
ACGCTCACCGGCTCCAGATTTATCAGCAATAAACCAGCCAGCCGGAAGGGCCGAGCGCAGAAGTGGTCCTG
CAACTTTATCCGCCTCCATCCAGTCTATTAATTGTTGCCGGGAAGCTAGAGTAAGTAGTTCGCCAGTTAAT
AGTTTGCGCAACGTTGTTGCCATTGCTACAGGCATCGTGGTGTCACGCTCGTCGTTTGGTATGGCTTCATT
CAGCTCCGGTTCCCAACGATCAAGGCGAGTTACATGATCCCCCATGTTGTGCAAAAAAGCGGTTAGCTCCT
TCGGTCCTCCGATCGTTGTCAGAAGTAAGTTGGCCGCAGTGTTATCACTCATGGTTATGGCAGCACTGCAT
AATTCTCTTACTGTCATGCCATCCGTAAGATGCTTTTCTGTGACTGGTGAGTACTCAACCAAGTCATTCTG
AGAATAGTGTATGCGGCGACCGAGTTGCTCTTGCCCGGCGTCAATACGGGATAATACCGCGCCACATAGCA
GAACTTTAAAAGTGCTCATCATTGGAAAACGTTCTTCGGGGCGAAAACTCTCAAGGATCTTACCGCTGTTG
AGATCCAGTTCGATGTAACCCACTCGTGCACCCAACTGATCTTCAGCATCTTTTACTTTCACCAGCGTTTC
TGGGTGAGCAAAAACAGGAAGGCAAAATGCCGCAAAAAAGGGAATAAGGGCGACACGGAAATGTTGAATAC
TCATACTCTTCCTTTTTCAATATTATTGAAGCATTTATCAGGGTTATTGTCTCATGAGCGGATACATATTT
GAATGTATTTAGAAAAATAAACAAATAGGGGTTCCGCGCACATTTCCCCGAAAAGTGCCACCTGACGTCTA
AGAAACCATTATTATCATGACATTAACCTATAAAAATAGGCGTATCACGAGGCCCTTTCGTCTCGCGCGTT
TCGGTGATGACGGTGAAAACCTCTGACACATGCAGCTCCCGGAGACGGTCACAGCTTGTCTGTAAGCGGAT
GCCGGGAGCAGACAAGCCCGTCAGGGCGCGTCAGCGGGTGTTGGCGGGTGTCGGGGCTGGCTTAACTATGC
GGCATCAGAGCAGATTGTACTGAGAGTGCACCATATGGACATATTGTCGTTAGAACGCGGCTACAATTAAT
ACATAACCTTATGTATCATACACATACGATTTAGGTGACACTATACCTGCAGGCGCGCCATTTAAATGCGG

CCGCTTAATTAACTCGA***CAAAAGCTGTTGGGATATGCCACTCCCCATGACAGGGAGGGTCTTCAGAGGGTA***
AGACTAAAACTAAGCCCTGAATCATTAATTATGAACTAATGCATTTCAGCCTTTGATTTTCATTGTATATG
TTTTGTGTCTGTGTGGACCATTCATTACCTATAAGCATGGTAGCTCATCTTGGTCTGTTTTTTGGCCAGTT
TCTCCCTAATTAAGAATGCCAAAAGAACCAATCTGACCTCATCAACTTTGTGCTCTTGCTACAGACAAACA
AAGGAGCTGTCCCATACGTGTTTACATGAACATAGGCTGCTCTGAGATGTGCCTTGTTTTTTTATTACAAT
TTTGGTGTTAATTTTTCTTCTCTTCTGATAAATTTGACATAAGAAAAAAATGGGTAAGAGTGTGGCCTGGG
GTATTAGACTGCCTAGGTGCATTCTCACTTGAACAAATATGAGTTTCATCATCTTGAAAAAGCTACTTGAA
TTTTCTGGAGCTCACCTAGTTTGTAGAATTATGTTAATGACAGAAGCTTTCTCTGAGAGACTAAGGGAGTG
ACATAAATGAAGTGTGTGTGTGTGTGTGTGTGTGTGTGTGTGTGTGTGTGTGATGTATAAGCAGGTGCC
GCATACCTAATTCATCTCACTGATTTTAACCATTTGCCTTGGGAATTTTCCAAATACAAAGTGGCTTCTGC
AGGTGACTTCCTCGGCCTGACTCTTCAGCCTGATGAGCATCTGTTGTTGGAGAGTTAAGAGATTTCTCAGC
CTTGTGTGAAGCCTCCCCTTCCTTTGAAGAACTTACTTATCTGGTGGCTCACTTGAACCTTTCTTTTTGTT
CTCTCAGTTTACTTCTAGGCTCCAAGGTCCTCTCTCTATCTGTCTCTTATGAGGAGTACCTTCAGCATCTT
TCCTTTTCTCTCAAACCCAATAGGTTCAAAGTGGAAAATGTCCATCATACCTTAATAATCTTTTCTAGTTG
TTACATCAAAGGATTCCAAGTGTTGCCTTGTAGTTGCAGACATTGATACAAAATAGGACTTGCTTCTTGCC
ACAAAAGGTACTTCAATTAGCATGTGGCATATGCTGTAGATAATTGAAGTATCAGAGAAGAAAGCAGCAAT
TACAATGTAGTTGGAGAAACACCATGGAAACAGCAATGATACAGTGTGCTGAAGTGGGAAGCACATCCTTG
ATCTGGAGAGAAGGACACATTCAGAGAGCTGACCTAAAATATGGCTACTCCACAGCCTGGAGGAAGGGCTA
CTTCACTGCCCAGCTACACACACACACACACACACACACACACACACACACACACACACAAATGTATAGGTAAAG
ATATAGGTATTGATATAGATGATATCTCTGTTTATCCTGTTGTAATTATGTGTGAGTATGGAAATTGACCC
CAAAATGTGTAAGCAATAGTATCTATTACATCTTATATGCAATGAACTCCATCATTCGCAGCCATTTACCT
AGAGGGAACAGCTTATTTGACGTTTTGTGTCTTAGACTCTCTAAGTACTAGGAGAGATGCTGATCCAGGCA
TTTTCATATGATGTATGTGCCAGGATCTTCCTATGTTTTCAACATATTATCTCATCTGTTCTCACAGCAAG
TGCATGGCGTAGCATCATTATCCCACTTTACAACTGAAGAAACTGTCTCGAAGAGGGTCAATAGCTAGCTC
TAAGTCTAGAGGGTATAAGAGTAAGGTAAAGGAAGTCAGTGGCCAACTGTGAGGGCACATGAGGTTGACTG
CTAGGTCTGCTAATTGTGAAAATCCAGGATTCCTGGTTGGTCTGGATGCTTCTCCTTTACCTATGGTTAGA
GAGCAGGGAATGAAAAGGTAAAATTTTCCTTAATGGCAGGAGTGGTGAAGACATTAGCTTGGGGCTTAAAA
TATACTGCTCTCTTCTAAGACTTGTCAAAGTAAATTGTGTCCCTGGAGACATTTAAAAGCAATTATGTCCC
TCATTTGCATGTGGCTGTGGTTGGAGAAGCTGCAGGTTGTCTACCAAAGGGGACTTTTATGGAGTTTTGTG
AGCAAACTTTGAAATGTTCAAAATAAGAACTTACTTTGTAAATTCCTTTGCTACATTCTAGCTAATCCTGG
CCATCTGGAACCAAATTTGCCATTACATTTATTGATTCATTTTGTAAAAGTATTTTTGCTTAACTAGAAAA
TGTCCTAGGAATGTCTAAAGAACAGAACTTATATAGTAGTATACTCCCAAGATAAACCACAGTTCTGTTTG
CTAAACAGCATCCTCTAGCCTGAGAATCAACAGCCCTCCTCTTTATTGGTTGTAATCCTCTCTGTTAGAAG
GGCATGCTGCAGGATTGACCTAGATGGGCATGTTCAAGTTCTGTGACCTCTTCTACATTAATAAACTCTTT
TAGAAGAATTACACCACTCCTTCTTTTCCTGCCTTGCATCTTTAGTTTTTGAGATGAGACTACCTTGAAAC
AGATGTCCTGGTCCTCTGGCTCTTACAATCTTTCTGGTGTCTCTTCCCCTGTGTCCCCTGAGCCTTAGATA
CAGGAATTGTGTTGTAGACCTATCCACTGGGGCTGGCACCCATGGCCAGCTCTTCTCTACAGTTTGAGCAG
TTGTTGTTTTGTGTTGGTCTCTATCTACTGAAAAAATGAAGCTCCTTCGATTCAGGGCAAAAACTACTCTT
ATCTGTAGGTGTAGGAACAGTACTTAGAATGCAGTTAGAAACCACACTGCTTTGAGAATGTGACAGTAAAT
TCTATGTCCCATGGCCTCGCCAGTTCTTATTTTTTCATCTTGAGACAGATACATGTGTGTATTTTGCCTTT
TAAAAAACTCAGGAGGGGCTGCTAGAAAGATATTCCAGTCACTAAAGTGACATGTTGTGCTCGTACAAGGA
CTTAAGTTCAAGCTTTAGAACTCATGTGAAAAGCTGGGCATTGTGGCACACACCTGTAATCTCAGGGTTGG
TGTTGGGTGTGGGGGTGGGAAGTGAGTAGACACAGGCAGGCCCCAGGGCTTGCCAGCCAGCCAGCTGAGAA
TATTTGATGAGTTCCTTTCCCATGAAAGACTCCTTTTCAAAAAAAAAAAAAAAAAACAGGTGAATGGCAATC
AAGATTGACCTCTGGCCGCCTCTGCACACATATAAACACAGGCTTGCCTACAAAACACACACACACACACA
CACACACACACACACACACTAGTTATGAGTGTTGTATATTCTAAGTACAGCCTTTAGTAAGGAAATCAGTG
GTAACGGTTACAATCAACTCTGTCAGTATATGTTAGGTGATCTCAGAACACTTGCCAATTTGACTTGCAAC
TTCTCACTAATGATGCTACCGTGCATATTTTAGAGGAAGGTCACAATACCATAAGGAAATTTTCTTAAAAA
CAAAACATACACAAAAAAACGTTTCTAGAATTTTTGCTTGAAATTGAAGATTTTATGATATGAGGAAAGGT
ACTCAAAACACATAGGTGGCTTTTTGAGAGTTCTGCCTTGAGAATACCAAAATCCTCAAAAGGAACCTTCA
GCATTTATGTCAATGTTGTGAGTTTTAGCTAAGAATCTCATATTTTGCCAGGCAGTGAGGCCAGTTTGGTC
TATAGACTGAATTTCAAGGCTACACAGAAAAACCCTGCCTTGAAATACAAAATACACAAACAAAAGCAAAA
ACCCTAATATTCTTTGTCCCATGCTACCAGTTAAAAATATTGTTATGTTTATTGTAGAATAAAGACAGAAT
TTAAGTCAAATATGAATCTGGGCATAATCACATATTTTCATTATATCTAAGCTAATCTAGCACTCCGGGTT
TCACCAACCTAGTTTAAAATTAAATAAAATAATCTCCTCCTCTTTTCTATTGCTAATGTTTTAAAGATGAG
GAAGAATTTTCCTATCTTCCTTAATAATTCATGTCTATGCAAGTTCAAATGTCCATAATTGTCTATACAGT
GGGCATCCCTGCCTCCCACACTAGCCCCTGACAACATCTTCAGTTACCCATTCCCCAGGATACTGACTGTA

TCCAGAATATTTCCATTTGTTTCTCTGAATCAGCATCCTATACTAGTCTAGAGCAGTACCAATCAAGGCAT
AGAACATCTGGATAGACTGGAATAACATGGAGGATCACGTCTGGGAGTTGGAACTGAGGCCATTTGTGGAG
GAACAAGAAATTTAATACTTCAGGCAGAATATAAGAGGGTGAACAGTAAATTCCAAGAAAGGCTCCTATCA
CAGCAAATAAGGGAAGAGTACTTTCAACAAGCTGGCAAAATAACTAAGAGTAAGATGTTGGCAATTTTATA
TTCTTAGCTTTAGAGAAACAATTAAGCAATCACTGTCAGAAACAATGTATGTGAATTCTACTTGCCACATT
TCAGCTTGAGCATCTCATGTGCATGTACCCCTAGCCGGGAAATAAATAAGTGGTACTTCCTGGAGGTAGTG
TTGACTCAGGGGTGGACATGTACAGTCCAGGTGGCTGCCCGGCAAGCCGTGATACAGAAGACCCTCAGAAT
CTATGCTCTTCTCAGCTAAGTCTGTTGAGGGAGAAGAGAGGAGAAAGGGTAAGCCGGGACAGCAATCTAAG
GAGCACAGAAGTACACACAACATCTCAGCACCACCCTCAAGAAGAAGAGGACAAATCTGTGATAGTTCAAA
TTATCGTCACAGAAGCTAAAGGTGCCTGTGTGTAAGGGTCTGGAGAGCTCGAGGCATTCCTCGATTCACAG
AAAATGGGACTGTGTCCGAGGCAGAGTAGACCTTCATGCTACTTAAGACTTTGGGAATGAAGAGGGAAGTG
GAGCCAATTGTATCACGCGTATAACTTCGTATAGCATACATTATACGAAGTTATGCCACTAGAGGATCCCC
GGGCCCGAGGCAATGTCCTTCACATGCACTATAAACGTATTTTATATAGTAACAAACGTTTCGGCCAGGTG
TTAATGTTTTTATTGTATAATTGCCTTTATTATTCTCTCTGTTCTCTGCCCTCATCCCCTTCCTTTTCATT
TCCCTCCTCTGCCATCTCCTTCCCCACTTATTCCCAATTTTGTTTTCCCATTTTACTCTCCTCCTCTGATT
CTCCTTTTCTCAATATTTCCTCCTTCTTTCCATTTTTTTTTTACTCTTCTTGTCCTTCTCTCCCTTGTCCA
CTGTGGTCTTTCCCCTCTCCTTCTCATGTCCCCCTGCCTGTGGCCCCACCCTTAATTGTCTCTCCAGGTAT
TACGCCATCTGCTGCCAGCCTTTGGTTTATAGGAACAAGATGACCCCTCTACGCATCGCATTAATGTTGGG
AGGCTGCTGGGTCCTTCCCATGTTTATATCTTTTCTCCCCATAATGCAAGGCTGGAACAACATCGGCATAG
TTGATGTGGTAAGTATGCATACAAAGCCATGGGATTATTATCCACTCGGTTTTGTTAGGCATTTTAGATAA
GCAGACACTCTTAGCTAGGTAGCTATTTTAATAGATATTATAATAGTGGTCTGAGCAACATATTTAAATGT
CCTATTGATGCCTTGGTCAAATGTTAGTCAAGATCCTCTGAATTATCTTCCCAATGAGAACTTGTGTTCTT
AGAGTTCATTTATTTATTATTTGAAAATCTCATGCATAAGTGCAATCGTACGCCGGCTTAAGTGTACACGC
GTACTAGTCTAGCGAAGTTCCTATACTTTCTAGAGAATAGGAACTTCCCGCGGATAACTTCGTATAGCATA
CATTATACGAAGTTATGTAGATCTGATATCAGGGAGCTCTCAGACGTCGCTTGGTCGGTCTTTATTCGAAC
CCCAGAGTCCCGCTCAGAAGAACTCGTCAAGAAGGCGATAGAAGGCGATGCGCTGCGAATCGGGAGCGGCG
ATACCGTAAAGCACGAGGAAGCGGTCAGCCCATTCGCCGCCAAGCTCTTCAGCAATATCACGGGTAGCCAA
CGCTATGTCCTGATAGCGGTCCGCCACACCCAGCCGGCCACAGTCGATGAATCCAGAAAAGCGGCCATTTT
CCACCATGATATTCGGCAAGCAGGCATCGCCATGGGTCACGACGAGATCCTCGCCGTCGGGCATGCGCGCC
TTGAGCCTGGCGAACAGTTCGGCTGGCGCGAGCCCCTGATGCTCTTCGTCCAGATCATCCTGATCGACAAG
ACCGGCTTCCATCCGAGTACGTGCTCGCTCGATGCGATGTTTCGCTTGGTGGTCGAATGGGCAGGTAGCCG
GATCAAGCGTATGCAGCCGCCGCATTGCATCAGCCATGATGGATACTTTCTCGGCAGGAGCAAGGTGAGAT
GACAGGAGATCCTGCCCCGGCACTTCGCCCAATAGCAGCCAGTCCCTTCCCGCTTCAGTGACAACGTCGAG
CACAGCTGCGCAAGGAACGCCCGTCGTGGCCAGCCACGATAGCCGCGCTGCCTCGTCCTGCAGTTCATTCA
GGGCACCGGACAGGTCGGTCTTGACAAAAAGAACCGGGCGCCCCTGCGCTGACAGCCGGAACACGGCGGCA
TCAGAGCAGCCGATCGTCTGTTGTGCCCAGTCATAGCCGAATAGCCTCTCCACCCAAGCGGCCGGAGAACC
TGCGTGCAATCCATCTTGTTCAATGGCCGATCCCATGGTTTAGTTCCTCACCTTGTCGTATTATACTATGC
CGATATACTATGCCGATGATTAATTGTCAACACGTGCTGCTGCAGGTCGAAAGGCTCGGAGATGAGGAAGA
GGAGAACAGCGCGGCAGACGTGCGCTTTTGAAGCGTGCAGAATGCCGGGCCTCCGGAGGACCTTCGGGCGC
CCGCCCCGCCCCTGAGCCCGCCCCTGAGCCCGCCCCCGGACCCACCCCTTCCCAGCCTCTGAGCCCAGAAA
GCGAAGGAGCAAAGCTGCTATTGGCCGCTGCCCCAAAGGCCTACCCGCTTCCATTGCTCAGCGGTGCTGTC
CATCTGCACGAGACTAGTGAGACGTGCTACTTCCATTTGTCACGTCCTGCACGACGCGAGCTGCGGGGCGG
GGGGGAACTTCCTGACTAGGGGAGGAGTGGAAGGTGGCGCGAAGGGGCCACCAAAGAACGGAGCCGGTTGG
CGCCTACCGGTGGATGTGGAATGTGTGCGAGGCCAGAGGCCACTTGTGTAGCGCCAAGTGCCCAGCGGGGC
TGCTAAAGCGCATGCTCCAGACTGCCTTGGGAAAAGCGCCTCCCCTACCCGGTAGAATGAAGTTCCTATAC
TTTCTAGAGAATAGGAACTTCGTTCGAACATAACTTCGTATAGCATACATTATACGAAGTTATGGTACCTG
CAGAATTCATGCATAAGCTTGGATCCGTTCTTCGGACGCCTCGTCAACACCGTACGAATGTATTTAGATCA
CATGAAACCCTAAACAAGAAGTTACATTTCTGTGTCTGTCTTAGATTCTTTTCCTGTGCAATAATAAAATG
CCCTGACAGAAACAACTTAAGGGAGAAATGGCTTATTTTAGCTCACAGTTTAAGATATCCATCATGGCAGA
GATGTCAAGAGAGCAGGGACCTGCAGCAGTGAGTCCCTTAATGTCCATAGTCAGAAGACAATTAAACTGCT
CAGTTTGGGGTTTGTTTGTTTGTTTGTTTGTTTTGGGTTTGTTTGTTTTGGCTTCTACATTCTAGAACCCC
GTGTTAGGGTAAGGTCCTACCCACAACTAAGATGGATCTTCCCACACCAATTACCATACACAAGATAATCT
TCCCCGCTATACCCAGTGGCACTTCTTGTAGGTGATTCAGACTCTGTCAAGTTGACAATTCCCTCTAACCA
ACACAATGTCCAACTTTGCATTGCTCAGTTTCAGCAAGGATGCTGATGAGTCGGTTTATCTTGAATCCCCC
AGGACCAGGCACTTCATCCTTCACCTTTCCCATGAGATGTCTGATTGCCCTGGCTTGTCTTCAGCAAGAAT
CCTGCTAAGTTGACTTTCCCACTTTCTCTTCCCATTTACTCTGAATAGTTTTCTGTTCACTGACCCTCATC
CATCAATTCCTTGGCTATACATTCCCCACCACCACCACCACCTTTTTTTCCCTTTGGTGTTTTAGAGTTGA

ATCTAATCTCTTTGTGAAAAAAATCACAGTATTTTCTCTTATGAAAATAATGTGAAATATGTGGAATAAAG
GCTCCTTAGCAGGTGTTTCAAATATTTTTTTAACATTACAGTGAATCAGACATTACAATAAGGAATGACAT
TACAATAAGGAATTATACTTTTGGAAAGAGTATAATTATGGCAGTTTAAAGATGTGCAGGTTAATTTGCAC
TTCCCATGACACATAGTTTTCCTATAAAAAGAGTTTTAATTTCATTTATTTTATATATTTATTAAATATTT
ATTGATATTTATAAATCAGTTTCCAGAACTTGAGGCATATCATGTCCCAAGAAGTCTTCGTTATATTTCAT
ATTGAGTCTATAAGGATTACAGTGCCTATGGAAAGGCATACCAAGTAAATGGACAATGCCAAGGAATATGA
AAATCCTGGGCCAGAAGTCAGGAACTAAGCTGTGAGCCCAGCTCTGCTAATGCCCAACTTCCTGAAGAACT
GTATTAAGAAGGGAAGTTGGTGCTGAGTGAAAAATTGTCTAGTGTGAGTCTAAGGGGACCCATGCCACATA
GGCCATACATTGTCCAAACTCTGGATATTGTTTTCCAGAGACATAGAACTAATAGGATGTTTGTGTGCATA
TGTTCATCTATCTGTCTATCCATCTATATGTCTATCCACCTATCTGTCCATGAATCTATCTGTCATCTATC
TGTCTGTCTGTCTAACCATCTATCTACTATCTATTATCTATCTAACTATCTATCTGTCTGTCTGTCTGTCT
AACCAACCATCTATCTACTATCTATTATCTATATATCTACATTTCTATTTATCTTCTAATCTATCTAATCT
ATCTATCTATCTATCTATCTATCTATCTATCTATCTATCTATCATCTTTTCCTTGTCATGTATCTCTTTAT
CTATTTACCTATACACTTAGAAAAAGAAAAAGAGAAACAGAGGCAGACATATAGACATATTGTAACTGGTC
CTCCTGGTTGTGGAAGTTGATAATTCTCAGCAAACTAGAGACTGAGGAAAGGCAATATTTCAACTCAAGTC
CAAATATAGGAAAAAACTGATGGCCTTCATTAAGTCAATAGAGCAGTTCCCTCTTATTCGGTTATTTTGTT
CTATTTGGGCCTTTAATAGAGTTAGATGCAGTGCTAAATCGGAAGAGAAAATGGATTTATACAATCTGCCA
GTACAGAGCTTAATCTCAATCCCAAATGTTGTCGTACACAAAATTGGGTTTTACCAATTATCTGGATACCT
ATGACTTGGTTACACTGGCACATAACATTAACCATCTTGCTGTCAAAATCATCTACTCTGGCACACCAAAT
TATAATGATGATTAAAACTGATAGTCCAGATTCATTGTCAGGGCTATACATTTCTAAAGGAATATGGCATG
CAGTCACTTATAGCCAGTCCTAAGATCTTGCTAGATGTGGAGAAGGGGGCAGAAAGAAGAGGTTGAGAATG
AAGAATGAGTTCTGACCCAAGTGGATCAGAAAAAAAGAGAATTTGCCTTCTTTTCTGCACACCTAAGGACT
TTAATTTTATTTTCAAATGAGTCCCATGGCCAGGACATTTCTGAGTA

5’ end of BAC subclone joins here.

REFERENCES

Adell, A., Castro, E., Celada, P., Bortolozzi, A., Pazos, Á., and Artigas, F. (2005). Strategies for producing faster acting antidepressants. Drug Discov. Today *10*, 578–585.

Alberini, C.M. (2009). Transcription factors in long-term memory and synaptic plasticity. Physiol. Rev. *89*, 121–145.

Alexander, G.E., DeLong, M.R., and Strick, P.L. (1986). Parallel organization of functionally segregated circuits linking basal ganglia and cortex. Annu. Rev. Neurosci. *9*, 357–381.

Amaral, D.G., and Witter, M.P. (1989). The three-dimensional organization of the hippocampal formation: a review of anatomical data. Nsc *31*, 571–591.

Amaral, D.G., Scharfman, H.E., and Lavenex, P. (2007). The dentate gyrus: fundamental neuroanatomical organization (dentate gyrus for dummies). In The Dentate Gyrus: a Comprehensive Guide to Structure, Function, and Clinical Implications, (Elsevier), pp. 3–790.

Anacker, C., and Hen, R. (2017). Adult hippocampal neurogenesis and cognitive flexibility — linking memory and mood. Nature Publishing Group *18*, 335–346.

Anacker, C., Scholz, J., O'Donnell, K.J., Allemang-Grand, R., Diorio, J., Bagot, R.C., Nestler, E.J., Hen, R., Lerch, J.P., and Meaney, M.J. (2016). Neuroanatomic Differences Associated With Stress Susceptibility and Resilience. Biological Psychiatry *79*, 840–849.

Anders, S., Pyl, P.T., and Huber, W. (2015). HTSeq--a Python framework to work with high-throughput sequencing data. Bioinformatics *31*, 166–169.

Andrade, R. (2006). Electrophysiological Properties of Gαs-Coupled 5-HT Receptors (5-HT4, 5-HT6, 5-HT7). In The Serotonin Receptors, (Totowa, NJ: Humana Press), pp. 481–494.

Artigas, F., Romero, L., de Montigny, C., and Blier, P. (1996). Acceleration of the effect of selected antidepressant drugs in major depression by 5-HT1A antagonists. Trends in Neurosciences *19*, 378–383.

Asede, D., Bosch, D., Lüthi, A., Ferraguti, F., and Ehrlich, I. (2015). Sensory inputs to intercalated cells provide fear-learning modulated inhibition to the basolateral amygdala. Neuron *86*, 541–554.

Auer, D.P., Pütz, B., Kraft, E., Lipinski, B., Schill, J., and Holsboer, F. (2000). Reduced glutamate in the anterior cingulate cortex in depression: an in vivo proton magnetic resonance spectroscopy study. Biological Psychiatry *47*, 305–313.

Avesar, D., and Gulledge, A.T. (2012). Selective serotonergic excitation of callosal projection neurons. Front Neural Circuits *6*, 12.

Åsberg, M. (1976). 5-HIAA in the Cerebrospinal Fluid. Arch. Gen. Psychiatry *33*, 1193–1197.

Baek, I.-S., Park, J.-Y., and Han, P.-L. (2015). Chronic Antidepressant Treatment in Normal Mice Induces Anxiety and Impairs Stress-coping Ability. Exp Neurobiol *24*, 156.

Bagot, R.C., Parise, E.M., Peña, C.J., Zhang, H.-X., Maze, I., Chaudhury, D., Persaud, B., Cachope, R., Bolaños-Guzmán, C.A., Cheer, J.F., et al. (2015). Ventral hippocampal afferents to the nucleus accumbens regulate susceptibility to depression. Nature Communications *6*, 7062.

Banasr, M., Soumier, A., Hery, M., Mocaër, E., and Daszuta, A. (2006). Agomelatine, a new antidepressant, induces regional changes in hippocampal neurogenesis. Bps *59*, 1087–1096.

Barnhill, R. (2006). Animal Models of Cognitive Impairment. 1–395.

Barrett, T., Wilhite, S.E., Ledoux, P., Evangelista, C., Kim, I.F., Tomashevsky, M., Marshall, K.A., Phillippy, K.H., Sherman, P.M., Holko, M., et al. (2013). NCBI GEO: archive for functional genomics data sets--update. Nucleic Acids Res. *41*, D991–D995.

Barthet, G., Framery, B., Gaven, F., Pellissier, L., Reiter, E., Claeysen, S., Bockaert, J., and Dumuis, A. (2007). 5-hydroxytryptamine 4 receptor activation of the extracellular signal-regulated kinase pathway depends on Src activation but not on G protein or beta-arrestin signaling. Mol. Biol. Cell *18*, 1979–1991.

Belova, M.A., Paton, J.J., Morrison, S.E., and Salzman, C.D. (2007). Expectation modulates neural responses to pleasant and aversive stimuli in primate amygdala. Neuron *55*, 970–984.

Berger, M., Gray, J.A., and Roth, B.L. (2009). The Expanded Biology of Serotonin. Annu. Rev. Med. *60*, 355–366.

Bicks, L.K., Koike, H., Akbarian, S., and Morishita, H. (2015). Prefrontal Cortex and Social Cognition in Mouse and Man. Frontiers in Psychology *6*, 693.

Birn, R.M., Shackman, A.J., Oler, J.A., Williams, L.E., McFarlin, D.R., Rogers, G.M., Shelton, S.E., Alexander, A.L., Pine, D.S., Slattery, M.J., et al. (2014). Evolutionarily conserved prefrontal-amygdalar dysfunction in early-life anxiety. Molecular Psychiatry *19*, 915–922.

Blier, P., Piñeyro, G., Mansari, el, M., Bergeron, R., and de Montigny, C. (1998). Role of somatodendritic 5-HT autoreceptors in modulating 5-HT neurotransmission. Annals of the New York Academy of Sciences *861*, 204–216.

Bockaert, J., Claeysen, S., Compan, V., and Dumuis, A. (2004). 5-HT4 receptors. Curr Drug Targets CNS Neurol Disord *3*, 39–51.

Bockaert, J., Perroy, J., Bécamel, C., Marin, P., and Fagni, L. (2010). GPCR interacting proteins (GIPs) in the nervous system: Roles in physiology and pathologies. Annu. Rev. Pharmacol. Toxicol. *50*, 89–109.

Boldrini, M., Butt, T.H., Santiago, A.N., Tamir, H., Dwork, A.J., Rosoklija, G.B., Arango, V., Hen, R., and Mann, J.J. (2014). Benzodiazepines and the potential trophic effect of antidepressants on dentate gyrus cells in mood disorders. Int. J. Neuropsychopharm. *17*, 1923–1933.

Boldrini, M., Santiago, A.N., Hen, R.E., Dwork, A.J., Rosoklija, G.B., Tamir, H., Arango, V., and Mann, J.J. (2013). Hippocampal Granule Neuron Number and Dentate Gyrus Volume in Antidepressant-Treated and Untreated Major Depression. Neuropsychopharmacology *38*, 1068–1077.

Bonaventure, P., Hall, H., Gommeren, W., Cras, P., Langlois, X., Jurzak, M., and Leysen, J.E. (2000). Mapping of serotonin 5-HT(4) receptor mRNA and ligand binding sites in the post-mortem human brain. Synapse *36*, 35–46.

Bradwejn, J., Koszycki, D., and Shriqui, C. (1991). Enhanced sensitivity to cholecystokinin tetrapeptide in panic disorder. Clinical and behavioral findings. Arch. Gen. Psychiatry *48*, 603–610.

Britt, J.P., Benaliouad, F., McDevitt, R.A., Stuber, G.D., Wise, R.A., and Bonci, A. (2012). Synaptic and behavioral profile of multiple glutamatergic inputs to the nucleus accumbens. Neuron *76*, 790–803.

Buckmaster, P.S., Strowbridge, B.W., Kunkel, D.D., Schmiege, D.L., and Schwartzkroin, P.A. (1992). Mossy cell axonal projections to the dentate gyrus molecular layer in the rat hippocampal slice. Hippocampus *2*, 349–362.

Cachard-Chastel, M., Lezoualc'h, F., Dewachter, I., Deloménie, C., Croes, S., Devijver, H., Langlois, M., Van Leuven, F., Sicsic, S., and Gardier, A.M. (2007). 5-HT4 receptor agonists increase sAPPalpha levels in the cortex and hippocampus of male C57BL/6j mice. Br. J. Pharmacol. *150*, 883–892.

Campbell, S., and Macqueen, G. (2004). The role of the hippocampus in the pathophysiology of major depression. J Psychiatry Neurosci *29*, 417–426.

Canteras, N.S., and Swanson, L.W. (1992). Projections of the ventral subiculum to the amygdala, septum, and hypothalamus: a PHAL anterograde tract-tracing study in the rat. J. Comp. Neurol. *324*, 180–194.

Carreno, F.R., Donegan, J.J., Boley, A.M., Shah, A., DeGuzman, M., Frazer, A., and Lodge, D.J. (2015). Activation of a ventral hippocampus & medial prefrontal cortex pathway is both necessary and sufficient for an antidepressant response to ketamine. *21*, 1298–1308.

Castello, J., LeFrancois, B., Flajolet, M., Greengard, P., Friedman, E., and Rebholz, H. (2017). CK2 regulates 5-HT4 receptor signaling and modulates depressive-like behavior. Molecular Psychiatry 1–11.

Cembrowski, M.S., Wang, L., Sugino, K., Shields, B.C., and Spruston, N. (2016). Hipposeq: a comprehensive RNA-seq database of gene expression in hippocampal principal neurons. Elife *5*, e14997.

Challis, C., Boulden, J., Veerakumar, A., Espallergues, J., Vassoler, F.M., Pierce, R.C., Beck, S.G., and Berton, O. (2013). Raphe GABAergic neurons mediate the acquisition of avoidance after social defeat. Journal of Neuroscience *33*, 13978–88–13988a.

Chen, A., Kelley, L.D.S., and Janušonis, S. (2012). Effects of prenatal stress and monoaminergic perturbations on the expression of serotonin 5-HT_4 and adrenergic β_2 receptors in the embryonic mouse telencephalon. Brain Research *1459*, 27–34.

Chen, B., Dowlatshahi, D., MacQueen, G.M., Wang, J.-F., and Young, L.T. (2001). Increased hippocampal bdnf immunoreactivity in subjects treated with antidepressant medication. Biological Psychiatry *50*, 260–265.

Claeysen, S., Sebben, M., Becamel, C., Bockaert, J., and Dumuis, A. (1999). Novel brain-specific 5-HT4 receptor splice variants show marked constitutive activity: role of the C-terminal intracellular domain. Mol. Pharmacol. *55*, 910–920.

Cohen, S.J., and Stackman, R.W., Jr (2015). Assessing rodent hippocampal involvement in the novel object recognition task. A review. Behavioural Brain Research *285*, 105–117.

Compan, V. (2004). Attenuated Response to Stress and Novelty and Hypersensitivity to Seizures in 5-HT4 Receptor Knock-Out Mice. Journal of Neuroscience *24*, 412–419.

Coryell, W., Nopoulos, P., Drevets, W., Wilson, T., and Andreasen, N.C. (2005). Subgenual prefrontal cortex volumes in major depressive disorder and schizophrenia: diagnostic specificity and prognostic implications. Am J Psychiatry *162*, 1706–1712.

Covington, H.E., Lobo, M.K., Maze, I., Vialou, V., Hyman, J.M., Zaman, S., LaPlant, Q., Mouzon, E., Ghose, S., Tamminga, C.A., et al. (2010). Antidepressant Effect of Optogenetic Stimulation of the Medial Prefrontal Cortex. Journal of Neuroscience *30*, 16082–16090.

Cowen, P.J. (2008). Serotonin and depression: pathophysiological mechanism or marketing myth? Trends Pharmacol. Sci. *29*, 433–436.

Cryan, J.F., and Lucki, I. (2000). 5-HT4 receptors do not mediate the antidepressant-like behavioral effects of fluoxetine in a modified forced swim test. European Journal of Pharmacology *409*, 295–299.

Daitz, H.M., and Powell, T.P. (1954). Studies of the connexions of the fornix system. J. Neurol. Neurosurg. Psychiatry *17*, 75–82.

Darcet, F., Gardier, A.M., David, D.J., and Guilloux, J.-P. (2016). Chronic 5-HT4 receptor agonist treatment restores learning and memory deficits in a neuroendocrine mouse model of anxiety/depression. Neurosci. Lett. *616*, 197–203.

David, D.J., Samuels, B.A., Rainer, Q., Wang, J.-W., Marsteller, D., Mendez, I., Drew, M., Craig, D.A., Guiard, B.P., Guilloux, J.-P., et al. (2009). Neurogenesis-Dependent and -Independent Effects of Fluoxetine in anAnimal Model of Anxiety/Depression. Neuron *62*, 479–493.

David, D.J.P., Renard, C.E., Jolliet, P., Hascoët, M., and Bourin, M. (2003). Antidepressant-like effects in various mice strains in the forced swimming test. Psychopharmacology *166*, 373–382.

Davis, M., Walker, D.L., Miles, L., and Grillon, C. (2009). Phasic vs Sustained Fear in Rats and Humans: Role of the Extended Amygdala in Fear vs Anxiety. Neuropsychopharmacology *35*, 105–135.

Delgado, M.R. (2007). Reward-related responses in the human striatum. Annals of the New York Academy of Sciences *1104*, 70–88.

Delgado, P.L., and Moreno, F.A. (2000). Role of norepinephrine in depression. J Clin Psychiatry *61 Suppl 1*, 5–12.

Deller, T., Frotscher, M., and Nitsch, R. (1996). Sprouting of crossed entorhinodentate fibers after a unilateral entorhinal lesion: Anterograde tracing of fiber reorganization withPhaseolus vulgaris-leucoagglutinin (PHAL). J. Comp. Neurol. *365*, 42–55.

Deng, W., Aimone, J.B., and Gage, F.H. (2010). New neurons and new memories: how does adult hippocampal neurogenesis affect learning and memory? Nat. Rev. Neurosci. *11*, 339–350.

Dias, B.G., Banerjee, S.B., Duman, R.S., and Vaidya, V.A. (2003). Differential regulation of brain derived neurotrophic factor transcripts by antidepressant treatments in the adult rat brain. Neuropharmacology *45*, 553–563.

Dobin, A., Davis, C.A., Schlesinger, F., Drenkow, J., Zaleski, C., Jha, S., Batut, P., Chaisson, M., and Gingeras, T.R. (2013). STAR: ultrafast universal RNA-seq aligner. Bioinformatics *29*, 15–21.

Doetsch, F. (2003). A niche for adult neural stem cells. Curr. Opin. Genet. Dev. *13*, 543–550.

Dougherty, K.A., Islam, T., and Johnston, D. (2012). Intrinsic excitability of CA1 pyramidal neurones from the rat dorsal and ventral hippocampus. J. Physiol. (Lond.) *590*, 5707–5722.

Dougherty, K.A., Nicholson, D.A., Diaz, L., Buss, E.W., Neuman, K.M., Chetkovich, D.M., and Johnston, D. (2013). Differential expression of HCN subunits alters voltage-dependent gating of h-channels in CA1 pyramidal neurons from dorsal and ventral hippocampus. Journal of Neurophysiology *109*, 1940–1953.

Drevets, W.C., Price, J.L., and Furey, M.L. (2008). Brain structural and functional abnormalities in mood disorders: implications for neurocircuitry models of depression. Brain Struct Funct *213*, 93–118.

Dulawa, S.C., and Hen, R. (2005). Recent advances in animal models of chronic antidepressant effects: the novelty-induced hypophagia test. Neurosci Biobehav Rev *29*, 771–783.

Dulawa, S.C., Holick, K.A., Gundersen, B., and Hen, R. (2004). Effects of Chronic Fluoxetine in Animal Models of Anxiety and Depression. Neuropsychopharmacology *29*, 1321–1330.

Duman, R.S. (1997). A Molecular and Cellular Theory of Depression. Arch. Gen. Psychiatry *54*, 597–606.

Duman, R.S. (2004). Depression: a case of neuronal life and death? Bps *56*, 140–145.

Dunlop, B.W., and Nemeroff, C.B. (2007). The role of dopamine in the pathophysiology of depression. Arch. Gen. Psychiatry *64*, 327–337.

Egeland, M., Warner-Schmidt, J., Greengard, P., and Svenningsson, P. (2011a). Neuropharmacology. Neuropharmacology *61*, 442–450.

Egeland, M., Warner-Schmidt, J., Greengard, P., and Svenningsson, P. (2011b). Co-expression of serotonin 5-HT1B and 5-HT4 receptors in p11 containing cells in cerebral cortex, hippocampus, caudate-putamen and cerebellum. Neuropharmacology *61*, 442–450.

Fadok, J.P., Krabbe, S., Markovic, M., Courtin, J., Xu, C., Massi, L., Botta, P., Bylund, K., Müller, C., Kovacevic, A., et al. (2017). A competitive inhibitory circuit for selection of active and passive fear responses. Nature *542*, 96–100.

Fagni, L., Dumuis, A., Sebben, M., and Bockaert, J. (1992). The 5-HT4 receptor subtype inhibits K+ current in colliculi neurones via activation of a cyclic AMP-dependent protein kinase. Br. J. Pharmacol. *105*, 973–979.

Felix-Ortiz, A.C., and Tye, K.M. (2014). Amygdala Inputs to the Ventral Hippocampus Bidirectionally Modulate Social Behavior. J. Neurosci. *34*, 586–595.

Felix-Ortiz, A.C., Beyeler, A., Seo, C., Leppla, C.A., Wildes, C.P., and Tye, K.M. (2013). BLA to vHPC inputs modulate anxiety-related behaviors. Neuron *79*, 658–664.

File, S.E. (1985). Animal models for predicting clinical efficacy of anxiolytic drugs: social behaviour. Neuropsychobiology *13*, 55–62.

File, S.E., and Hyde, J.R. (1979). A test of anxiety that distinguishes between the actions of benzodiazepines and those of other minor tranquilisers and of stimulants. Pharmacol. Biochem. Behav. *11*, 65–69.

Freund, T.F., and Buzsáki, G. (1996). Interneurons of the hippocampus. Hippocampus *6*, 347–470.

Frost, G.R., and Li, Y.-M. (2017). The role of astrocytes in amyloid production and Alzheimer's disease. Open Biol *7*, 170228.

Gabor, C.S., Phan, A., Clipperton-Allen, A.E., Kavaliers, M., and Choleris, E. (2012). Interplay of oxytocin, vasopressin, and sex hormones in the regulation of social recognition. Behavioral Neuroscience *126*, 97–109.

Gage, F.H., and Thompson, R.G. (1980). Differential distribution of norepinephrine and serotonin along the dorsal-ventral axis of the hippocampal formation. Brain Research Bulletin *5*, 771–773.

Gardier, A.M., Trillat, A.C., Malagié, I., David, D., Hascoët, M., Colombel, M.C., Jolliet, P., Jacquot, C., Hen, R., and BOURIN, M. (2001). [5-HT1B serotonin receptors and antidepressant effects of selective serotonin reuptake inhibitors]. C. R. Acad. Sci. III, Sci. Vie *324*, 433–441.

Geisler, S., Schöpf, C.L., and Obermair, G.J. (2015). Emerging evidence for specific neuronal functions of auxiliary calcium channel α2δ subunits. General Physiology and Biophysics *34*, 105–118.

Geyer, M.A., and Swerdlow, N.R. (2001). Measurement of startle response, prepulse inhibition, and habituation. Curr Protoc Neurosci *Chapter 8*, Unit8.7–8.7.15.

Giakoumaki, S.G., Bitsios, P., Frangou, S., Roussos, P., Aasen, I., Galea, A., and Kumari, V. (2010). Low baseline startle and deficient affective startle modulation in remitted bipolar disorder patients and their unaffected siblings. Psychophysiology *85*, 231–668.

Giannoni, P., Gaven, F., de Bundel, D., Baranger, K., Marchetti-Gauthier, E., Roman, F.S., Valjent, E., Marin, P., Bockaert, J., Rivera, S., et al. (2013). Early administration of RS 67333, a specific 5-HT4 receptor agonist, prevents amyloidogenesis and behavioral deficits in the 5XFAD mouse model of Alzheimer's disease. Front Aging Neurosci *5*, 1–12.

Gong, S., Doughty, M., Harbaugh, C.R., Cummins, A., Hatten, M.E., Heintz, N., and Gerfen, C.R. (2007). Targeting Cre recombinase to specific neuron populations with bacterial artificial chromosome constructs. Journal of Neuroscience *27*, 9817–9823.

Gorman, J.M. (1996). Comorbid depression and anxiety spectrum disorders. Depress Anxiety *4*, 160–168.

Gorski, J.A., Talley, T., Qiu, M., Puelles, L., Rubenstein, J.L.R., and Jones, K.R. (2002). Cortical excitatory neurons and glia, but not GABAergic neurons, are produced in the Emx1-expressing lineage. Journal of Neuroscience *22*, 6309–6314.

Gould, T.D., Dao, D.T., and Kovacsics, C.E. (2009). The Open Field Test. In Mood and Anxiety Related Phenotypes in Mice: Characterization Using Behavioral Tests, T.D. Gould, ed. (Totowa, NJ: Humana Press), pp. 1–20.

Gray, T.S., Carney, M.E., and Magnuson, D.J. (1989). Direct Projections from the Central Amygdaloid Nucleus to the Hypothalamic Paraventricular Nucleus: Possible Role in Stress-Induced Adrenocorticotropin Release. Neuroendocrinology *50*, 433–446.

Greene-Schloesser, D.M., Van der Zee, E.A., Sheppard, D.K., Castillo, M.R., Gregg, K.A., Burrow, T., Foltz, H., Slater, M., and Bult-Ito, A. (2011). Predictive validity of a non-induced mouse model of compulsive-like behavior. Behavioural Brain Research *221*, 55–62.

Griebel, G., Simiand, J., Serradeil-Le Gal, C., Wagnon, J., Pascal, M., Scatton, B., Maffrand, J.-P., and Soubrie, P. (2002). Anxiolytic- and antidepressant-like effects of the non-peptide vasopressin V1b receptor antagonist, SSR149415, suggest an innovative approach for the treatment of stress-related disorders. Proc. Natl. Acad. Sci. U.S.a. *99*, 6370–6375.

Hagena, H., and Manahan-Vaughan, D. (2016). Neurobiology of Learning and Memory. Neurobiology of Learning and Memory 1–9.

Hannon, J., and Hoyer, D. (2008). Molecular biology of 5-HT receptors. Behavioural Brain Research *195*, 198–213.

Hashimoto, K., Sawa, A., and Iyo, M. (2007). Increased Levels of Glutamate in Brains from Patients with Mood Disorders. Biological Psychiatry *62*, 1310–1316.

Hegde, S.S., and Eglen, R.M. (1996). Peripheral 5-HT4 receptors. Faseb J. *10*, 1398–1407.

Heiman, M., Kulicke, R., Fenster, R.J., Greengard, P., and Heintz, N. (2014). Cell type-specific mRNA purification by translating ribosome affinity purification (TRAP). Nature Protocols *9*, 1282–1291.

Heiman, M., Schaefer, A., Gong, S., Peterson, J.D., Day, M., Ramsey, K.E., Suárez-Fariñas, M., Schwarz, C., Stephan, D.A., Surmeier, D.J., et al. (2008). A Translational Profiling Approach for the Molecular Characterization of CNS Cell Types. Cell *135*, 738–748.

Henke, P.G. (1990). Hippocampal pathway to the amygdala and stress ulcer development. Brain Research Bulletin *25*, 691–695.

Herman, J.P., Figueiredo, H., Mueller, N.K., Ulrich-Lai, Y., Ostrander, M.M., Choi, D.C., and Cullinan, W.E. (2003). Central mechanisms of stress integration: hierarchical circuitry controlling hypothalamo-pituitary-adrenocortical responsiveness. Front Neuroendocrinol *24*, 151–180.

Hirschfeld, R.M. (2000). History and evolution of the monoamine hypothesis of depression. J Clin Psychiatry *61 Suppl 6*, 4–6.

Hommel, J.D., Sears, R.M., Georgescu, D., Simmons, D.L., and DiLeone, R.J. (2003). Local gene knockdown in the brain using viral-mediated RNA interference. *9*, 1539–1544.

Hoyer, D., Hannon, J.P., and Martin, G.R. (2002). Molecular, pharmacological and functional diversity of 5-HT receptors. Pharmacol. Biochem. Behav. *71*, 533–554.

Hu, H., Gan, J., and Jonas, P. (2014). Interneurons. Fast-spiking, parvalbumin^{+} GABAergic interneurons: from cellular design to microcircuit function. Science *345*, 1255263–1255263.

Huang, X., Yang, J., Yang, S., Cao, S., Qin, D., Zhou, Y., Li, X., Ye, Y., and Wu, J. (2017). Role of tandospirone, a 5-HT1A receptor partial agonist, in the treatment of central nervous system disorders and the underlying mechanisms. Oncotarget *8*, 102705–102720.

Jankord, R., and Herman, J.P. (2008). Limbic regulation of hypothalamo-pituitary-adrenocortical function during acute and chronic stress. Annals of the New York Academy of Sciences *1148*, 64–73.

Jayatissa, M.N., Bisgaard, C., Tingström, A., Papp, M., and Wiborg, O. (2006). Hippocampal cytogenesis correlates to escitalopram-mediated recovery in a chronic mild stress rat model of depression. Neuropsychopharmacology *31*, 2395–2404.

Je, K.-H., Ryu, W.-S., Lee, S.-K., Kim, E.J., Kim, J.-Y., Jang, H.J., Park, J.E., Nahrendorf, M., Schellingerhout, D., and Kim, D.-E. (2017). Green-channel autofluorescence imaging: A novel and sensitive technique to delineate infarcts. J. Neurosci. Methods *279*, 22–32.

Jessberger, S., Aigner, S., Clemenson, G.D., Toni, N., Lie, D.C., Karalay, O., Overall, R., Kempermann, G., and Gage, F.H. (2008). Cdk5 regulates accurate maturation of newborn granule cells in the adult hippocampus. PLoS Biol *6*, e272.

Kaidanovich-Beilin, O., Lipina, T., Vukobradovic, I., Roder, J., and Woodgett, J.R. (2011). Assessment of social interaction behaviors. JoVE e2473–e2473.

Kainou, T., Kawamura, K., Tanaka, K., Matsuda, H., and Kawamukai, M. (1999). Identification of the GGPS1 genes encoding geranylgeranyl diphosphate synthases from mouse and human. Biochim. Biophys. Acta *1437*, 333–340.

Karege, F., Perret, G., Bondolfi, G., Schwald, M., Bertschy, G., and Aubry, J.-M. (2002). Decreased serum brain-derived neurotrophic factor levels in major depressed patients. Psychiatry Research *109*, 143–148.

Katsuragi, S., Kunugi, H., Sano, A., Tsutsumi, T., Isogawa, K., Nanko, S., and Akiyoshi, J. (1999). Association between serotonin transporter gene polymorphism and anxiety-related traits. Biological Psychiatry *45*, 368–370.

Kaviani, H., Gray, J.A., Checkley, S.A., Raven, P.W., Wilson, G.D., and Kumari, V. (2004). Affective modulation of the startle response in depression: influence of the severity of depression, anhedonia, and anxiety. J Affect Disord *83*, 21–31.

Kessler, R.C., Aguilar-Gaxiola, S., Alonso, J., Chatterji, S., Lee, S., Ormel, J., Ustün, T.B., and Wang, P.S. (2009). The global burden of mental disorders: an update from the WHO World Mental Health (WMH) surveys. Epidemiol Psichiatr Soc *18*, 23–33.

Kessler, R.C., Berglund, P., Demler, O., Jin, R., Merikangas, K.R., and Walters, E.E. (2005). Lifetime prevalence and age-of-onset distributions of DSM-IV disorders in the National Comorbidity Survey Replication. Arch. Gen. Psychiatry *62*, 593–602.

Kheirbek, M.A., Drew, L.J., Burghardt, N.S., Costantini, D.O., Tannenholz, L., Ahmari, S.E., Zeng, H., Fenton, A.A., and Hen, R. (2013). Differential Control of Learning and Anxiety along the Dorsoventral Axis of the Dentate Gyrus. Neuron *77*, 955–968.

Kim, E.J., Juavinett, A.L., Kyubwa, E.M., Jacobs, M.W., and Callaway, E.M. (2015). Three Types of Cortical Layer 5 Neurons That Differ in Brain-wide Connectivity and Function. Neuron *88*, 1253–1267.

Kjelstrup, K.B., Solstad, T., Brun, V.H., Hafting, T., Leutgeb, S., Witter, M.P., Moser, E.I., and Moser, M.-B. (2008). Finite scale of spatial representation in the hippocampus. Science *321*, 140–143.

Kjelstrup, K.G., Tuvnes, F.A., Steffenach, H.-A., Murison, R., Moser, E.I., and Moser, M.-B. (2002). Reduced fear expression after lesions of the ventral hippocampus. Proc. Natl. Acad. Sci. U.S.a. *99*, 10825–10830.

Kovalchuk, Y. (2002). Postsynaptic Induction of BDNF-Mediated Long-Term Potentiation. Science *295*, 1729–1734.

Krishnan, V., and Nestler, E.J. (2008). The molecular neurobiology of depression. Nature *455*, 894–902.

Krishnan, V., and Nestler, E.J. (2011). Animal models of depression: molecular perspectives. Curr Top Behav Neurosci *7*, 121–147.

Kühn, R., and Torres, R.M. (2002). Cre/loxP recombination system and gene targeting. Methods Mol. Biol. *180*, 175–204.

LaBar, K.S., and Cabeza, R. (2006). Cognitive neuroscience of emotional memory. Nat. Rev. Neurosci. *7*, 54–64.

Lammel, S., Lim, B.K., Ran, C., Huang, K.W., Betley, M.J., Tye, K.M., Deisseroth, K., and Malenka, R.C. (2012). Input-specific control of reward and aversion in the ventral tegmental area. Nature *491*, 212–217.

Langen, M., Leemans, A., Johnston, P., Ecker, C., Daly, E., Murphy, C.M., dell'Acqua, F., Durston, S., and Murphy, D.G.M. (2012). Fronto-striatal circuitry and inhibitory control in autism: Findings from diffusion tensor imaging tractography. Cortex *48*, 183–193.

Laryea, G., Arnett, M.G., and Muglia, L.J. (2012). Behavioral Studies and Genetic Alterations in Corticotropin-Releasing Hormone (CRH) Neurocircuitry: Insights into Human Psychiatric Disorders. Behavioral Sciences *2*, 135–171.

Laurberg, S. (1979). Commissural and intrinsic connections of the rat hippocampus. J. Comp. Neurol. *184*, 685–708.

Lee, Y., and Davis, M. (1997). Role of the Hippocampus, the Bed Nucleus of the Stria Terminalis, and the Amygdala in the Excitatory Effect of Corticotropin-Releasing Hormone on the Acoustic Startle Reflex. J. Neurosci. *17*, 6434–6446.

Leger, M., Quiedeville, A., Bouet, V., Haelewyn, B.I.T., Boulouard, M., Schumann-Bard, P., and Freret, T. (2013). Object recognition test in mice. Nature Protocols *8*, 2531–2537.

Lein, E.S., Hawrylycz, M.J., Ao, N., Ayres, M., Bensinger, A., Bernard, A., Boe, A.F., Boguski, M.S., Brockway, K.S., Byrnes, E.J., et al. (2007). Genome-wide atlas of gene expression in the adult mouse brain. Nature *445*, 168–176.

Letty, S., Child, R., Dumuis, A., Pantaloni, A., Bockaert, J., and Rondouin, G. (1997). 5-HT4 receptors improve social olfactory memory in the rat. Neuropharmacology *36*, 681–687.

Letzkus, J.J., Wolff, S.B.E., Meyer, E.M.M., Tovote, P., Courtin, J., Herry, C., and Lüthi, A. (2011). A disinhibitory microcircuit for associative fear learning in the auditory cortex. Nature *480*, 331–335.

Li, Z., Jo, J., Jia, J.-M., Lo, S.-C., Whitcomb, D.J., Jiao, S., Cho, K., and Sheng, M. (2010). Caspase-3 Activation via Mitochondria Is Required for Long-Term Depression and AMPA Receptor Internalization. Cell *141*, 859–871.

Licht, C.L., Kirkegaard, L., Zueger, M., Chourbaji, S., Gass, P., Aznar, S., and Knudsen, G.M. (2010). Changes in 5-HT4 receptor and 5-HT transporter binding in olfactory bulbectomized and glucocorticoid receptor heterozygous mice. Neurochemistry International *56*, 603–610.

Licht, C.L., Marcussen, A.B., Wegener, G., Overstreet, D.H., Aznar, S., and Knudsen, G.M. (2009). The brain 5-HT4 receptor binding is down-regulated in the Flinders Sensitive Line depression model and in response to paroxetine administration. J. Neurochem. *109*, 1363–1374.

Likhtik, E., Stujenske, J.M., Topiwala, M.A., Harris, A.Z., and Gordon, J.A. (2014). Prefrontal entrainment of amygdala activity signals safety in learned fear and innate anxiety. Nature Publishing Group *17*, 106–113.

Lindseth, G., Helland, B., and Caspers, J. (2015). The effects of dietary tryptophan on affective disorders. Arch Psychiatr Nurs *29*, 102–107.

Liu, M. (2005). Expression and function of 5-HT4 receptors in the mouse enteric nervous system. Am. J. Physiol. Gastrointest. Liver Physiol. *289*, G1148–G1163.

Liu, X., Betzenhauser, M.J., Reiken, S., Meli, A.C., Xie, W., Chen, B.-X., Arancio, O., and Marks, A.R. (2012). Role of leaky neuronal ryanodine receptors in stress-induced cognitive dysfunction. Cell *150*, 1055–1067.

Lo, A.C., De Maeyer, J.H., Vermaercke, B., Callaerts-Vegh, Z., Schuurkes, J.A.J., and D'Hooge, R. (2014). SSP-002392, a new 5-HT4 receptor agonist, dose-dependently reverses scopolamine-induced learning and memory impairments in C57Bl/6 mice. Neuropharmacology *85*, 178–189.

Love, M.I., Huber, W., and Anders, S. (2014). Moderated estimation of fold change and dispersion for RNA-seq data with DESeq2. Genome Biol. *15*, 550.

Lucas, G., Compan, V., Charnay, Y., Neve, R.L., Nestler, E.J., Bockaert, J., Barrot, M., and Debonnel, G. (2005). Frontocortical 5-HT4 receptors exert positive feedback on serotonergic activity: Viral transfections, subacute and chronic treatments with 5-HT4 agonists. Biological Psychiatry *57*, 918–925.

Lucas, G., Rymar, V.V., Du, J., Mnie-Filali, O., Bisgaard, C., Manta, S., Lambas-Senas, L., Wiborg, O., Haddjeri, N., Piñeyro, G., et al. (2007). Serotonin4 (5-HT4) Receptor Agonists Are Putative Antidepressants with a Rapid Onset of Action. Neuron *55*, 712–725.

Lucki, I., Dalvi, A., and Mayorga, A. (2001). Sensitivity to the effects of pharmacologically selective antidepressants in different strains of mice. Psychopharmacology *155*, 315–322.

Maere, S., Heymans, K., and Kuiper, M. (2005). BiNGO: a Cytoscape plugin to assess overrepresentation of Gene Ontology categories in Biological Networks. Bioinformatics *21*, 3448–3449.

Magdaleno, S., Jensen, P., Brumwell, C.L., Seal, A., Lehman, K., Asbury, A., Cheung, T., Cornelius, T., Batten, D.M., Eden, C., et al. (2006). BGEM: an in situ hybridization database of gene expression in the embryonic and adult mouse nervous system. PLoS Biol *4*, e86.

Maggio, N., and Segal, M. (2007). Striking variations in corticosteroid modulation of long-term potentiation along the septotemporal axis of the hippocampus. Journal of Neuroscience *27*, 5757–5765.

Malenka, R.C., and Bear, M.F. (2004). LTP and LTD: an embarrassment of riches. Neuron *44*, 5–21.

Mann, J.J. (1999). Role of the Serotonergic System in the Pathogenesis of Major Depression and Suicidal Behavior. Neuropsychopharmacology *21*, S99–S105.

Manzke, T. (2003). 5-HT4(a) Receptors Avert Opioid-Induced Breathing Depression Without Loss of Analgesia. Science *301*, 226–229.

Marchetti, E., Jacquet, M., Jeltsch, H., Migliorati, M., Nivet, E., Cassel, J.C., and Roman, F.S. (2008). Complete recovery of olfactory associative learning by activation of 5-HT4 receptors after dentate granule cell damage in rats. Neurobiology of Learning and Memory *90*, 185–191.

Marner, L., Gillings, N., Madsen, K., Erritzoe, D., Baaré, W.F.C., Svarer, C., Hasselbalch, S.G., and Knudsen, G.M. (2010). Brain imaging of serotonin 4 receptors in humans with [11C]SB207145-PET. Neuroimage *50*, 855–861.

Matsumoto, M., Togashi, H., Mori, K., Ueno, K., Ohashi, S., Kojima, T., and Yoshioka, M. (2001). Evidence for involvement of central 5-HT(4) receptors in cholinergic function associated with cognitive processes: behavioral, electrophysiological, and neurochemical studies. J. Pharmacol. Exp. Ther. *296*, 676–682.

Mayberg, H.S., Lozano, A.M., Voon, V., McNeely, H.E., Seminowicz, D., Hamani, C., Schwalb, J.M., and Kennedy, S.H. (2005). Deep brain stimulation for treatment-resistant depression. Neuron *45*, 651–660.

McHugh, S.B., Deacon, R.M.J., Rawlins, J.N.P., and Bannerman, D.M. (2004). Amygdala and Ventral Hippocampus Contribute Differentially to Mechanisms of Fear and Anxiety. Behavioral Neuroscience *118*, 63–78.

McQuade, R., and Sharp, T. (1997). Functional mapping of dorsal and median raphe 5-hydroxytryptamine pathways in forebrain of the rat using microdialysis. J. Neurochem. *69*, 791–796.

Medrihan, L., Sagi, Y., Inde, Z., Krupa, O., Daniels, C., Peyrache, A., and Greengard, P. (2017). Initiation of Behavioral Response to Antidepressants by Cholecystokinin Neurons of the Dentate Gyrus. Neuron *95*, 564–576.e564.

Mendez-David, I., David, D.J., Darcet, F., Wu, M.V., mer, S.K.-R.O., Gardier, A.M., and Hen, R.E. (2014). Rapid Anxiolytic Effects of a 5-HT. Neuropsychopharmacology *39*, 1366–1378.

Meneses, A. (2015). Serotonin, neural markers, and memory. Front. Pharmacol. *6*.

Miller, M.W., and Gronfier, C. (2006). Diurnal variation of the startle reflex in relation to HPA-axis activity in humans. Psychophysiology *43*, 297–301.

Mnie-Filali, O., Amraei, M.G., Benmbarek, S., Archer-Lahlou, E., Peñas-Cazorla, R., Vilaró, M.T., Boye, S.M., and Piñeyro, G. (2010). Cellular Signalling. Cellular Signalling *22*, 501–509.

Morris, R.G., Garrud, P., Rawlins, J.N., and O'Keefe, J. (1982). Place navigation impaired in rats with hippocampal lesions. Nature *297*, 681–683.

Moser, E., Moser, M.B., and Andersen, P. (1993). Spatial learning impairment parallels the magnitude of dorsal hippocampal lesions, but is hardly present following ventral lesions. J. Neurosci. *13*, 3916–3925.

Nahas, Z., Anderson, B.S., Borckardt, J., Arana, A.B., George, M.S., Reeves, S.T., and Takacs, I. (2010). Bilateral epidural prefrontal cortical stimulation for treatment-resistant depression. Biological Psychiatry *67*, 101–109.

Nestler, E.J., Barrot, M., DiLeone, R.J., Eisch, A.J., Gold, S.J., and Monteggia, L.M. (2002). Neurobiology of depression. Neuron *34*, 13–25.

Neumann, I.D., and Slattery, D.A. (2016). Oxytocin in General Anxiety and Social Fear: A Translational Approach. Biological Psychiatry *79*, 213–221.

Nichols, D.E., and Nichols, C.D. (2008). Serotonin receptors. Chem. Rev. *108*, 1614–1641.

O'Leary, O.F., and Cryan, J.F. (2009). The Tail-Suspension Test: A Model for Characterizing Antidepressant Activity in Mice. In Mood and Anxiety Related Phenotypes in Mice: Characterization Using Behavioral Tests, T.D. Gould, ed. (Totowa, NJ: Humana Press), pp. 119–137.

O'Leary, O.F., and Cryan, J.F. (2014). A ventral view on antidepressant action: roles for adult hippocampal neurogenesis along the dorsoventral axis. Trends Pharmacol. Sci. *35*, 675–687.

Ogawa, S.K., Cohen, J.Y., Hwang, D., Uchida, N., and Watabe-Uchida, M. (2014). Organization of Monosynaptic Inputs to the Serotonin and Dopamine Neuromodulatory Systems. Cell Rep *8*, 1105–1118.

Ohtsuki, T., Ishiguro, H., Detera-Wadleigh, S.D., Toyota, T., Shimizu, H., Yamada, K., Yoshitsugu, K., Hattori, E., Yoshikawa, T., and Arinami, T. (2002). Association between serotonin 4 receptor gene polymorphisms and bipolar disorder in Japanese case-control samples and the NIMH Genetics Initiative Bipolar Pedigrees. Molecular Psychiatry *7*, 954–961.

Okuyama, T., Kitamura, T., Roy, D.S., Itohara, S., and Tonegawa, S. (2016). Ventral CA1 neurons store social memory. Science *353*, 1536–1541.

Ongür, D., and Price, J.L. (2000). The organization of networks within the orbital and medial prefrontal cortex of rats, monkeys and humans. Cereb. Cortex *10*, 206–219.

Orsetti, M., Dellarole, A., Ferri, S., and Ghi, P. (2003). Acquisition, retention, and recall of memory after injection of RS67333, a 5-HT(4) receptor agonist, into the nucleus basalis magnocellularis of the rat. Learn. Mem. *10*, 420–426.

Padilla-Coreano, N., Bolkan, S.S., Pierce, G.M., Blackman, D.R., Hardin, W.D., Garcia-Garcia, A.L., Spellman, T.J., and Gordon, J.A. (2016). Direct Ventral Hippocampal-Prefrontal Input Is Required for Anxiety-Related Neural Activity and Behavior. Neuron *89*, 857–866.

Pariante, C.M., and Lightman, S.L. (2008). The HPA axis in major depression: classical theories and new developments. Trends in Neurosciences *31*, 464–468.

Pause, B.M. (2013). Perspectives on episodic-like and episodic memory. 1–12.

Penttonen, M., Kamondi, A., Sik, A., Acsády, L., and Buzsáki, G. (1997). Feed-forward and feed-back activation of the dentate gyrus in vivo during dentate spikes and sharp wave bursts. Hippocampus *7*, 437–450.

Peñas-Cazorla, R., and Vilaró, M.T. (2014). Serotonin 5-HT4 receptors and forebrain cholinergic system: receptor expression in identified cell populations. Brain Struct Funct.

Peter Curzon, N.R.R.A.K.E.B. (2008). Chapter 2: Cued and Contextual Fear Conditioning for Rodents. 1–19.

Petit-Demouliere, B., Chenu, F., and Bourin, M. (2005). Forced swimming test in mice: a review of antidepressant activity. Psychopharmacology *177*, 245–255.

Phelps, E.A. (2004). Human emotion and memory: interactions of the amygdala and hippocampal complex. Curr. Opin. Neurobiol. *14*, 198–202.

Piguet, P., and Galvan, M. (1994). Transient and long-lasting actions of 5-HT on rat dentate gyrus neurones in vitro. J. Physiol. (Lond.) *481*, 629–639.

Pizzagalli, D.A., Holmes, A.J., Dillon, D.G., Goetz, E.L., Birk, J.L., Bogdan, R., Dougherty, D.D., Iosifescu, D.V., Rauch, S.L., and Fava, M. (2009). Reduced caudate and nucleus accumbens response to rewards in unmedicated individuals with major depressive disorder. Am J Psychiatry *166*, 702–710.

Price, J.L., and Drevets, W.C. (2009). Neurocircuitry of Mood Disorders. Neuropsychopharmacology *35*, 192–216.

Price, J.L., and Drevets, W.C. (2012). Neural circuits underlying the pathophysiology of mood disorders. Trends Cogn. Sci. (Regul. Ed.) *16*, 61–71.

Quitkin, F.M. (1984). Identification of True Drug Response to Antidepressants. Arch. Gen. Psychiatry *41*, 782–786.

Radley, J.J., and Sawchenko, P.E. (2011). A common substrate for prefrontal and hippocampal inhibition of the neuroendocrine stress response. Journal of Neuroscience *31*, 9683–9695.

Radley, J.J., Arias, C.M., and Sawchenko, P.E. (2006). Regional differentiation of the medial prefrontal cortex in regulating adaptive responses to acute emotional stress. Journal of Neuroscience *26*, 12967–12976.

Ramos, A. (2008). Animal models of anxiety: do I need multiple tests? Trends Pharmacol. Sci. *29*, 493–498.

Raoul, C., Barker, S.D., and Aebischer, P. (2005). Viral-based modelling and correction of neurodegenerative diseases by RNA interference. Gene Ther *13*, 487–495.

Ressler, K.J., Pine, D.S., and Olasov Rothbaum, B. (2015). Anxiety Disorders.

Reynolds, G.P., Mason, S.L., Meldrum, A., De Keczer, S., Parnes, H., Eglen, R.M., and Wong, E.H. (1995). 5-Hydroxytryptamine (5-HT)4 receptors in post mortem human brain tissue: distribution, pharmacology and effects of neurodegenerative diseases. Br. J. Pharmacol. *114*, 993–998.

Richardson, M.P., Strange, B.A., and Dolan, R.J. (2004). Encoding of emotional memories depends on amygdala and hippocampus and their interactions. Nat Neurosci *7*, 278–285.

Rodríguez, J.J., Noristani, H.N., and Verkhratsky, A. (2012). The serotonergic system in ageing and Alzheimer's disease. Prog. Neurobiol. *99*, 15–41.

Rosel, P., Arranz, B., Urretavizcaya, M., Oros, M., San, L., and Navarro, M.A. (2004). Altered 5-HT2A and 5-HT4 Postsynaptic Receptors and Their Intracellular Signalling Systems IP_3 and cAMP in Brains from Depressed Violent Suicide Victims. Neuropsychobiology *49*, 189–195.

Rubin, R.T., Mandell, A.J., and Crandall, P.H. (1966). Corticosteroid responses to limbic stimulation in man: localization of stimulus sites. Science *153*, 767–768.

Rudnick, G., and Clark, J. (1993). From synapse to vesicle: the reuptake and storage of biogenic amine neurotransmitters. Biochim. Biophys. Acta *1144*, 249–263.

Ruhé, H.G., Mason, N.S., and Schene, A.H. (2007). Mood is indirectly related to serotonin, norepinephrine and dopamine levels in humans: a meta-analysis of monoamine depletion studies. Molecular Psychiatry *12*, 331–359.

Rush, A.J., Trivedi, M.H., Wisniewski, S.R., Nierenberg, A.A., Stewart, J.W., Warden, D., Niederehe, G., Thase, M.E., Lavori, P.W., Lebowitz, B.D., et al. (2006). Acute and Longer-Term Outcomes in Depressed Outpatients Requiring One or Several Treatment Steps: A STAR*D Report. American Journal of Psychiatry *163*, 1905–1917.

Sadigh-Eteghad, S., Talebi, M., and Farhoudi, M. (2012). Association of apolipoprotein E epsilon 4 allele with sporadic late onset Alzheimer`s disease. A meta-analysis. Neurosciences (Riyadh) *17*, 321–326.

Sahay, A., and Hen, R. (2007). Adult hippocampal neurogenesis in depression. Nat Neurosci *10*, 1110–1115.

Sahay, A., Scobie, K.N., Hill, A.S., O'Carroll, C.M., Kheirbek, M.A., Burghardt, N.S., Fenton, A.A., Dranovsky, A., and Hen, R. (2011). Increasing adult hippocampal neurogenesis is sufficient to improve pattern separation. Nature *472*, 466–470.

Sairanen, M., Lucas, G., Ernfors, P., Castrén, M., and Castrén, E. (2005). Brain-derived neurotrophic factor and antidepressant drugs have different but coordinated effects on neuronal turnover, proliferation, and survival in the adult dentate gyrus. Journal of Neuroscience *25*, 1089–1094.

Samuels, B.A., Anacker, C., Hu, A., Levinstein, M.R., Pickenhagen, A., Tsetsenis, T., al, N.M.N., Donaldson, Z.R., Drew, L.J., Dranovsky, A., et al. (2015). 5-HT1A receptors on mature dentate gyrus granule cells are critical for the antidepressant response. Nature Publishing Group 1–13.

Sanacora, G., Gueorguieva, R., Epperson, C.N., Wu, Y.-T., Appel, M., Rothman, D.L., Krystal, J.H., and Mason, G.F. (2004). Subtype-Specific Alterations of γ-Aminobutyric Acid and Glutamatein Patients With Major Depression. Arch. Gen. Psychiatry *61*, 705.

Sanchez, C., Asin, K.E., and Artigas, F. (2015). Vortioxetine, a novel antidepressant with multimodal activity: review of preclinical and clinical data. Pharmacology and Therapeutics *145*, 43–57.

Santarelli, L., Saxe, M., Gross, C., Surget, A., Battaglia, F., Dulawa, S., Weisstaub, N., Lee, J., Duman, R., Arancio, O., et al. (2003). Requirement of hippocampal neurogenesis for the behavioral effects of antidepressants. Science *301*, 805–809.

Scharfman, H.E., and Schwartzkroin, P.A. (1988). Electrophysiology of morphologically identified mossy cells of the dentate hilus recorded in guinea pig hippocampal slices. J. Neurosci. *8*, 3812–3821.

Scharfman, H.E. (2013). Hilar mossy cells of the dentate gyrus: a historical perspective. 1–17.

Schechter, L.E., Ring, R.H., Beyer, C.E., Hughes, Z.A., Khawaja, X., Malberg, J.E., and Rosenzweig-Lipson, S. (2005). Innovative approaches for the development of antidepressant drugs: current and future strategies. NeuroRx *2*, 590–611.

Schmidt, E.F., Kus, L., Gong, S., and Heintz, N. (2013). BAC transgenic mice and the GENSAT database of engineered mouse strains. Cold Spring Harbor Protocols *2013*, pdb.top073692–pdb.top073692.

Schmidt, E.F., Warner-Schmidt, J.L., Otopalik, B.G., Pickett, S.B., Greengard, P., and Heintz, N. (2012). Identification of the cortical neurons that mediate antidepressant responses. Cell *149*, 1152–1163.

Schmittgen, T.D., and Livak, K.J. (2008). Analyzing real-time PCR data by the comparative CT method. Nature Protocols *3*, 1101–1108.

Schoenfeld, T.J., Rada, P., Pieruzzini, P.R., Hsueh, B., and Gould, E. (2013). Physical exercise prevents stress-induced activation of granule neurons and enhances local inhibitory mechanisms in the dentate gyrus. Journal of Neuroscience *33*, 7770–7777.

Segu, L., Lecomte, M.-J., Wolff, M., Santamaria, J., Hen, R., Dumuis, A., Berrard, S., Bockaert, J., Buhot, M.-C., and Compan, V. (2010). Hyperfunction of Muscarinic Receptor Maintains Long-Term Memory in 5-HT4 Receptor Knock-Out Mice. PLoS ONE *5*, e9529.

Seyedabadi, M., Fakhfouri, G., Ramezani, V., Mehr, S.E., and Rahimian, R. (2014). The role of serotonin in memory: interactions with neurotransmitters and downstream signaling. Exp Brain Res *232*, 723–738.

Shackman, A.J., Fox, A.S., Oler, J.A., Shelton, S.E., Davidson, R.J., and Kalin, N.H. (2013). Neural mechanisms underlying heterogeneity in the presentation of anxious temperament. Proc. Natl. Acad. Sci. U.S.a. *110*, 6145–6150.

Sharp, P.A. (2001). RNA interference—2001. Genes & Development *15*, 485–490.

Shepherd, G.M.G. (2013). Corticostriatal connectivity and itsrole in disease. 1–14.

Shimizu, E., Hashimoto, K., Okamura, N., Koike, K., Komatsu, N., Kumakiri, C., Nakazato, M., Watanabe, H., Shinoda, N., Okada, S.-I., et al. (2003). Alterations of serum levels of brain-derived neurotrophic factor (BDNF) in depressed patients with or without antidepressants. Biological Psychiatry *54*, 70–75.

Singh, S.P., Singh, V., Kar, N., and Chan, K. (2018). Efficacy of antidepressants in treating the negative symptoms of chronic schizophrenia: meta-analysis. British Journal of Psychiatry *197*, 174–179.

Sinha, P., Shetty, D.J., Bairy, L.K., and Andrade, C. (2017). Antidepressant-related jitteriness syndrome in anxiety and depressive disorders: Incidence and risk factors. Asian Journal of Psychiatry *29*, 148–153.

Smythies, J. (2005). Section V. Serotonin system. Int. Rev. Neurobiol. *64*, 217–268.

Sotres-Bayon, F., Sierra-Mercado, D., Pardilla-Delgado, E., and Quirk, G.J. (2012). Gating of fear in prelimbic cortex by hippocampal and amygdala inputs. Neuron *76*, 804–812.

Sparta, D.R., Smithuis, J., Stamatakis, A.M., Jennings, J.H., Kantak, P.A., Ung, R.L., and Stuber, G.D. (2014). Inhibition of projections from the basolateral amygdala to the entorhinal cortex disrupts the acquisition of contextual fear. Front Behav Neurosci *8*, 129.

Strange, B.A., Fletcher, P.C., Henson, R.N., Friston, K.J., and Dolan, R.J. (1999). Segregating the functions of human hippocampus. Proc. Natl. Acad. Sci. U.S.a. *96*, 4034–4039.

Strange, B.A., Witter, M.P., Lein, E.S., and Moser, E.I. (2014). Functional organization of the hippocampal longitudinal axis. Nature Publishing Group *15*, 655–669.

Strekalova, T., Couch, Y., Kholod, N., Boyks, M., Malin, D., Leprince, P., and Steinbusch, H.M. (2011). Update in the methodology of the chronic stress paradigm: internal control matters. Behavioral and Brain Functions *7*, 9.

Strekalova, T., Spanagel, R., Bartsch, D., Henn, F.A., and Gass, P. (2004). Stress-Induced Anhedonia in Mice is Associated with Deficits in Forced Swimming and Exploration. Neuropsychopharmacology *29*, 2007–2017.

Sullivan, G.M., Oquendo, M.A., Huang, Y.-Y., and Mann, J.J. (2006). Elevated cerebrospinal fluid 5-hydroxyindoleacetic acid levels in women with comorbid depression and panic disorder. International Journal of Neuropsychopharmacology *9*, 547–556.

Suwa, B., Bock, N., Preusse, S., Rothenberger, A., and Manzke, T. (2014). Distribution of serotonin 4(a) receptors in the juvenile rat brain and. Journal of Chemical Neuroanatomy 1–11.

Swanson, L.W. (1987). The limbic region. I. The septohippocampal system. Integrated Systems of the CNS 125–277.

Tanaka, K.F., Samuels, B.A., and Hen, R. (2012). Serotonin receptor expression along the dorsal-ventral axis of mouse hippocampus. Philosophical Transactions of the Royal Society B: Biological Sciences *367*, 2395–2401.

Terry, A.V., Buccafusco, J.J., Jackson, W.J., Prendergast, M.A., Fontana, D.J., Wong, E.H., Bonhaus, D.W., Weller, P., and Eglen, R.M. (1998). Enhanced delayed matching performance in younger and older macaques administered the 5-HT4 receptor agonist, RS 17017. Psychopharmacology *135*, 407–415.

Tesseur, I., Pimenova, A.A., Lo, A.C., Ciesielska, M., Lichtenthaler, S.F., De Maeyer, J.H., Schuurkes, J.A.J., D'Hooge, R., and De Strooper, B. (2013). Neurobiology of Aging. Neurobiology of Aging *34*, 1779–1789.

The Hippocampus Book (2007). The Hippocampus Book. 1–853.

Tokarski, K., Zahorodna, A., Bobula, B., and Hess, G. (2002). Comparison of the effects of 5-HT 1A and 5-HT 4 receptor activation on field potentials and epileptiform activity in rat hippocampus. Exp Brain Res *147*, 505–510.

Toni, N., and Schinder, A.F. (2015). Maturation and Functional Integration of New Granule Cells into the Adult Hippocampus. Cold Spring Harbor Perspectives in Biology *8*, a018903.

Tonini, M., and Pace, F. (2006). Drugs acting on serotonin receptors for the treatment of functional GI disorders. Dig Dis *24*, 59–69.

Torres, G.E., Chaput, Y., and Andrade, R. (1995). Cyclic AMP and protein kinase A mediate 5-hydroxytryptamine type 4 receptor regulation of calcium-activated potassium current in adult hippocampal neurons. Mol. Pharmacol. *47*, 191–197.

Torres, G.E., Holt, I.L., and Andrade, R. (1994). Antagon ists of 5- HT4 Receptor-M ed iated Responses in Adult Hippocampal Neurons1. J. Pharmacol. Exp. Ther. *271*, 255–261.

Tovote, P., Fadok, J.P., and Lüthi, A. (2015). Neuronal circuits for fear and anxiety. Nature Publishing Group *16*, 317–331.

Treadway, M.T., Grant, M.M., Ding, Z., Hollon, S.D., Gore, J.C., and Shelton, R.C. (2009). Early adverse events, HPA activity and rostral anterior cingulate volume in MDD. PLoS ONE *4*, e4887.

Tye, K.M., Prakash, R., Kim, S.-Y., Fenno, L.E., Grosenick, L., Zarabi, H., Thompson, K.R., Gradinaru, V., Ramakrishnan, C., and Deisseroth, K. (2011). Amygdala circuitry mediating reversible and bidirectional control of anxiety. Nature *471*, 358–362.

Valsamis, B., and Schmid, S. (2011a). Habituation and Prepulse Inhibition of Acoustic Startle in Rodents. JoVE 1–10.

Valsamis, B., and Schmid, S. (2011b). Habituation and Prepulse Inhibition of Acoustic Startle in Rodents. JoVE 1–10.

van Groen, T., Miettinen, P., and Kadish, I. (2003). The entorhinal cortex of the mouse: organization of the projection to the hippocampal formation. Hippocampus *13*, 133–149.

Varnäs, K., Halldin, C., Pike, V.W., and Hall, H. (2003). Distribution of 5-HT4 receptors in the postmortem human brain--an autoradiographic study using [125I]SB 207710. Eur Neuropsychopharmacol *13*, 228–234.

Vidal, R., Pilar-Cuéllar, F., Anjos, dos, S., Linge, R., Treceño, B., Vargas, V.I., Rodriguez-Gaztelumendi, A., Mostany, R., Castro, E., Díaz, Á., et al. (2011). New strategies in the development of antidepressants: towards the modulation of neuroplasticity pathways. Curr. Pharm. Des. *17*, 521–533.

Vidal, R., Valdizán, E.M., Mostany, R., Pazos, Á., and Castro, E. (2009). Long-term treatment with fluoxetine induces desensitization of 5-HT4 receptor-dependent signalling and functionality in rat brain. J. Neurochem. *110*, 1120–1127.

Videbech, P., and Ravnkilde, B. (2004). Hippocampal volume and depression: a meta-analysis of MRI studies. Am J Psychiatry *161*, 1957–1966.

Vilaro, M.T., Cort s, R., and Mengod, G. (2005). Serotonin 5-HT4 receptors and their mRNAs in rat and guinea pig brain: Distribution and effects of neurotoxic lesions. J. Comp. Neurol. *484*, 418–439.

Viskontas, I.V., Quiroga, R.Q., and Fried, I. (2009). Human medial temporal lobe neurons respond preferentially to personally relevant images. Proc. Natl. Acad. Sci. U.S.a. *106*, 21329–21334.

Voorn, P., Vanderschuren, L.J.M.J., Groenewegen, H.J., Robbins, T.W., and Pennartz, C.M.A. (2004). Putting a spin on the dorsal-ventral divide of the striatum. Trends in Neurosciences *27*, 468–474.

Vorhees, C.V., Morford, L.R., Graham, D.L., Skelton, M.R., and Williams, M.T. (2011). Effects of periadolescent fluoxetine and paroxetine on elevated plus-maze, acoustic startle, and swimming immobility in rats while on and off-drug. Behavioral and Brain Functions *7*, 41.

Võikar, V., Kõks, S., Vasar, E., and Rauvala, H. (2001). Strain and gender differences in the behavior of mouse lines commonly used in transgenic studies. Physiology & Behavior *72*, 271–281.

Walf, A.A., and Frye, C.A. (2007). The use of the elevated plus maze as an assay of anxiety-related behavior in rodents. Nature Protocols *2*, 322–328.

Wang, P.S., Aguilar-Gaxiola, S., Alonso, J., Angermeyer, M.C., Borges, G., Bromet, E.J., Bruffaerts, R., de Girolamo, G., de Graaf, R., Gureje, O., et al. (2007). Use of mental health services for anxiety, mood, and substance disorders in 17 countries in the WHO world mental health surveys. Lancet *370*, 841–850.

Warner-Schmidt, J.L., Flajolet, M., Maller, A., Chen, E.Y., Qi, H., Svenningsson, P., and Greengard, P. (2009). Role of p11 in Cellular and Behavioral Effects of 5-HT4 Receptor Stimulation. Journal of Neuroscience *29*, 1937–1946.

Warner-Schmidt, J.L., and Duman, R.S. (2006). Hippocampal neurogenesis: Opposing effects of stress and antidepressant treatment. Hippocampus *16*, 239–249.

Watanabe, Y., Gould, E., and McEwen, B.S. (1992). Stress induces atrophy of apical dendrites of hippocampal CA3 pyramidal neurons. Brain Research *588*, 341–345.

Weber, E.T., and Andrade, R. (2010). Htr2a Gene and 5-HT(2A) Receptor Expression in the Cerebral Cortex Studied Using Genetically Modified Mice. Front Neurosci *4*.

Wong, D.T., Horng, J.S., Bymaster, F.P., Hauser, K.L., and Molloy, B.B. (1974). A selective inhibitor of serotonin uptake: Lilly 110140, 3-(p-Trifluoromethylphenoxy)-n-methyl-3-phenylpropylamine. Life Sciences *15*, 471–479.

Yang, M., and Crawley, J.N. (2001). Simple Behavioral Assessment of Mouse Olfaction (Hoboken, NJ, USA: John Wiley & Sons, Inc.).

Yohn, C.N., Gergues, M.M., and Samuels, B.A. (2017). The role of 5-HT receptors in depression. 1–12.

Zhou, L., Liu, M.-Z., Li, Q., Deng, J., Mu, D., and Sun, Y.-G. (2017). Organization of Functional Long-Range Circuits Controlling the Activity of Serotonergic Neurons in the Dorsal Raphe Nucleus. Cell Rep *20*, 1991–1993.